WESTERN SYDNEY
UNIVERSITY

Molecular Mechanism for the Regulation of Zinc Transport by Protein Kinase CK2

Mohammad Sear Zaman

Primary supervisor: Dr Ming J. Wu

Co-Supervisor: Dr Chandra S. Malladi

In fulfilments of the requirements for the Degree of Doctor of Philosophy

School of Science

Western Sydney University

Mohammad S. Zaman

6th January 2021

To my loved ones and parents

Dr Mohammad Zaman and Nadera Zaman

Statement of authenticity

This thesis is submitted in fulfilment of the requirements for the degree of Doctor of Philosophy at Western Sydney University, School of Science. The work presented in this thesis is, to the best of my knowledge and belief, original except as acknowledged in the text. I hereby declare that I have not submitted this material, either in full or in part, for any other degree at this or any other institution.

.....

Mohammad Sear Zaman

6th January 2021

Declaration of COVID-19 Impacts to Research

The disruption to my research caused by COVID-19 from March 2020 was limited due to the fact that majority of my experimental studies were completed before the pandemic. I have completed all experiments required for my PhD. Therefore, no major impact is declared.

.....

Mohammad Sear Zaman

6th January 2021

Statement of support by the Principal Supervisor

.....

Dr Ming J. Wu

6th January 2021

Acknowledgements

This PhD research project would not have been possible without the guidance and support of my supervisors Dr Ming J. Wu and Dr Chandra S. Malladi. Their guidance and support were key to the collection of the meaningful results in this PhD project. Dr Ming J. Wu, you have been an absolute blessing and your scrupulous training in the lab is the foundation to my knowledge and experience which I will forever value. You have been more like a father figure than a primary supervisor who has always believed in me and inspired me to push through the challenges of this project. Dr Ming J. Wu, your humbleness and tireless work ethic is truly inspirational, I believe you are the hardest working academic and I hope your admirable characteristics will be ingrained in me. Likewise, Dr Chandra S. Malladi, your valued assistance, expertise, advice and support were crucial for the completion of this PhD project. You have been extremely helpful and your meticulous nature in the lab is inspirational. Dr Chandra S. Malladi, I appreciate you providing valuable resources and equipment for this PhD project. Thank you both for your support and consistent feedback! My gratitude also extends to Associate Professor Qihan Dong. Thank you for your help and your cell lines.

To Dr Ming J. Wu's lab group and everyone else who was part of this PhD project; thank you for all your support and assistance, I have learnt a great deal from everyone. You all have made me feel welcome and constantly helped me throughout all my scientific endeavours. A special thanks goes to Dr Adam J. Johnson and Dr Gayani Petersingham, your valued assistance, support and guidance have been a miracle. Dr Adam J. Johnson, I have spent countless hours in the lab with you conducting experiments. You have taught me many scientific techniques, crucial scientific advice, humbleness, creativity and have always supported me. Dr Gayani Petersingham, you have always encouraged me, provided me critical scientific feedback, heard my concerns and assisted me in finalising my thesis. The

amount of respect and admiration I have for you both cannot be put into words. Without both your contributions and help this PhD project would not have been possible. To both of you, thank you kindly!

I would also like to thank the technical support from Dr Sindy Kueh and Sonja Starkovska from School of Medicine, Dr Chun Ho and Julie Witcombe from School of Science, Western Sydney University. You all have always provided generous technical assistance.

To my loved ones, thank you for all your support throughout this PhD project. Your love and belief in me kept me motivated to strive for my best. It was their constant support, advice and motivation which inspired me to work as hard as I did to make them proud.

Finally, I would like to dedicate the work of this PhD thesis to cancer suffers and their families, I want you to know that there are researchers out there trying to make a difference!

Table of contents

DEDICATION ..... **I**

STATEMENT OF AUTHENTICITY ..... **II**

DECLARATION OF COVID-19 IMPACTS TO RESEARCH ..... **III**

STATEMENT OF SUPPORT BY THE PRINCIPAL SUPERVISOR ..... **III**

ACKNOWLEDGEMENTS ..... **IV**

TABLE OF CONTENTS ..... **VI**

LIST OF TABLES ..... **XII**

LISTS OF FIGURES ..... **XIII**

PUBLICATIONS ..... **XV**

CONFERENCE PRESENTATION ..... **XVI**

THESIS ABSTRACT ..... **XVIII**

LIST OF ABBREVIATIONS ..... **XXI**

1 LITERATURE REVIEW **1**

1.1 GENERAL INTRODUCTION 1

1.2 CHEMISTRY OF ZINC 3

1.3 ZINC ION HOMEOSTASIS 4

1.4 REGULATION OF ZINC TRANSPORT IN THE CELL 9

1.4.1 Transporters involved in zinc uptake 9

1.4.2 TRANSPORTERS ASSOCIATED WITH THE DECREASE OF INTRACELLULAR ZINC 12

1.4.3 Metallothioneins and zinc homeostasis 16

1.4.4 Zinc ion dyshomeostasis and its role in cancer 18

1.4.5 Zinc and metal-regulatory transcription factor 1 (MTF-1) 19

1.5 POTENTIAL REGULATION OF ZINC HOMEOSTASIS IN THE CELL BY PROTEIN KINASE CK2 21
1.6 PROTEIN KINASE CK2 24
1.6.1 The structure of CK2 24
1.6.2 Biological roles of CK2 28
1.7 BREAST ANATOMY AND BREAST CANCER 30
1.7.1 Anatomy and function of adult female breast 30
1.7.2 Breast cancers 31
1.8 PROSTATE GLAND ANATOMY AND PROSTATE CANCER 34
1.8.1 Anatomy and function of the prostate gland 34
1.8.2 Prostate cancer 35
1.9 EXPERIMENTAL APPROACH 37
1.9.1 Utility of breast and prostate cancer cell lines 37
1.9.2 Utility of normal breast and prostate cell lines 39
1.9.3 The relevance of breast and prostate cancer cell lines to clinical cancers 42
1.9.4 Inhibition of CK2 activity 42
1.9.5 Manipulation of CK2 expression by siRNA 44
1.9.6 Next-generation RNA sequencing for identification of genes involved in zinc homeostasis 46
1.9.7 qRT-PCR validation 47
1.9.8 Confocal microscopy visualising the zinc ion 49
1.9.9 Quantifying cellular zinc ion uptake by ICP-MS 50
1.10 SIGNIFICANCE OF THIS STUDY 51
1.11 HYPOTHESIS 52
1.12 AIMS 52

2 MATERIALS AND METHODS 53

2.1 GENERAL MATERIALS 53

2.2 MODUS OPERANDI OF GENERAL EXPERIMENTAL PRACTICE THROUGHOUT THIS STUDY 53

2.3 GROWTH AND MAINTENANCE OF MAMMALIAN CELL LINES 54

2.3.1 Maintaining and passaging conditions 54

2.3.2 Cryopreservation of mammalian cells 57

2.3.3 Thawing mammalian cells from cryopreservation 57

2.4 EXPERIMENTAL WORK USING THE MAMMALIAN CELLS 58

2.4.1 MTT assay and cell enumeration 58

2.4.2 Inhibition of CK2 activity and zinc treatment 59

2.4.3 Knockdown of CK2 gene expression by siRNA 60

2.4.4 Purification of RNA for quantitative reverse transcription-polymerase chain reaction (qRT-PCR) 63

2.4.5 cDNA synthesis by reverse transcriptase 64

2.4.6 Real time quantitative reverse transcriptase polymerase chain reaction (qRT-PCR) 64

2.4.7 Comparison of gene expression in cancerous against normal cells via qRT-PCR 66

2.4.8 Next-generation RNA sequencing 66

2.4.9 Quantification of gene expression levels and differential expression analysis in MCF-7 breast cancer cells 67

2.4.10 Imaging of intracellular zinc ion by confocal microscopy 68

2.4.11 Quantification of zinc ion content in mammalian cells by inductively coupled plasma-mass spectrometry (ICP-MS) 69

2.4.12 Data analysis 70

3 PROTEIN KINASE CK2 IS INVOLVED IN ZINC HOMEOSTASIS IN BREAST AND PROSTATE CANCER CELLS 71

3.1 INTRODUCTION 71

3.2 RESULTS 73

3.2.1 IC_{50} of $ZnSO_4$ in the cancer cell lines 73

3.2.2 Effect of CK2 inhibitors on Zn^{2+} homeostasis under exposure of IC_{50} $ZnSO_4$ 74

3.2.3 Efficacy of CK2 gene expression knockdown by siRNA 76

3.2.4 Effect of CK2 siRNA knockdown on cell viability under zinc exposure 78

3.2.5 Visualisation of intracellular Zn^{2+} in $ZnSO_4$ treated cells under CK2 inhibition and siRNA knockdown 80

3.3 DISCUSSION 84

3.4 CONCLUSION 86

4 TRANSCRIPTOMIC INSIGHTS INTO THE ZINC HOMEOSTASIS IN MCF-7 BREAST CANCER CELLS VIA NEXT-GENERATION RNA SEQUENCING 88

4.1 INTRODUCTION 88

4.2 RESULTS 90

4.2.1 Determination of IC_{50} of $ZnSO_4$ for MCF-7 and MDA-MB-231 breast cancer cells 90

4.2.2 Overview of differentially expressed genes in MCF-7 cells in the time course under zinc treatment 91

4.2.3 Top differentially expressed genes in response to zinc exposure 93

4.3 DISCUSSION 105

4.4 CONCLUSION 112

5 VALIDATION OF THE DIFFERENTIALLY EXPRESSED GENES AND EXPLORATION OF THE ROLE OF CK2 IN ZINC HOMEOSTASIS VIA QRT-PCR AND ICP-MS ANALYSIS 113

5.1 INTRODUCTION 113

5.2 RESULTS 114

5.2.1 Determination of inhibitory concentration IC_{50} of the six cell lines 114

5.2.2 Validation of the differentially expressed genes involved in zinc homeostasis by qRT-PCR 116

5.2.3 Comparison of the gene expression in cancerous and normal cells by qRT-PCR 124

5.2.3 Quantification of the genes of CK2 subunits under zinc treatment by qRT-PCR expression 128

5.2.4 Comparison of the genes of CK2 subunits without any treatment by qRT-PCR expression 130

5.2.5 Quantification of cellular zinc content under zinc IC_{50} treatment and CK2 inhibition by ICP-MS analysis 132

5.3 DISCUSSION 134

5.4 CONCLUSION 138

6 FINAL DISCUSSION 139

6.1 INVOLVEMENT OF CK2 IN ZINC HOMEOSTASIS OF BREAST AND PROSTATE CANCER CELLS 139

6.2 HOLISTIC VIEW OF ZINC HOMEOSTASIS IN MCF-7 BREAST CANCER CELLS 141

6.3 UNDERSTANDING ZINC HOMEOSTASIS IN BREAST CANCER CELLS 143

6.4 UNDERSTANDING ZINC HOMEOSTASIS IN PROSTATE CANCER CELLS 144

6.5 PROPOSED MOLECULAR MECHANISMS OF ZINC HOMEOSTASIS 146

6.6 THE SIGNIFICANCE OF THIS STUDY AND FUTURE WORK 149

7 REFERENCES 151

8 APPENDICES.....169

8.1 UP-REGULATED GENES AT T_{30} ZINC TREATMENT 169

8.2 DOWN-REGULATED GENES IN T_{30} ZINC TREATMENT.....172

8.3 UP-REGULATED GENES AT T_{120} ZINC TREATMENT.....173

8.4 DOWN-REGULATED GENES IN T_{120} ZINC TREATMENT 184

List of Tables

Table 1.1 Comparison of zinc level in cancer and normal tissue 8

Table 1.2 Family of ZIP transporters and known localisation in mammalian cells 10

Table 1.3 Family of ZnT transporters and known localisation in mammalian cells 14

Table 2.1 List of mammalian cell lines used in this study.....56

Table 2.2 siRNA targets and sequences for human CK2 subunits 62

Table 2.3 Run parameters for the qRT-PCR thermal cycler 65

Table 4.1 Significantly up or down-regulated genes at T_{30} zinc treatment 95

Table 4.2 Significantly up or down-regulated genes at T_{120} zinc treatment. 96

Lists of Figures

Fig 1.1 Diagram of general mechanisms of zinc uptake, storage and export 6

Fig 1.2 Zinc transport and zinc-binding proteins in the cell 17

Fig 1.3 Schematic of the mechanisms in response to extracellular zinc 20

Fig 1.4 Tetrameric isoforms and monomeric subunits of CK2 in mammalian cells 25

Fig 1.5 Structural illustration of CK2 tetrameric holoenzyme 27

Fig 1.6 Anatomy of female breast 30

Fig 1.7 Anatomy of the male prostate 34

Fig 1.8 Structure of CK2 inhibitor TBB and CX-4945 43

Fig 1.9 siRNA mechanism of knockdown expression.....45

Fig 3.1 Determination of IC_{50} of $ZnSO_4$ by MTT assay.....73

Fig 3.2 Effect of CK2 inhibitors on cancer cell viability under exposure of IC_{50} $ZnSO_4$ 75

Fig 3.3 Efficacy of CK2 gene expression knockdown by the specific siRNA.....77

Fig 3.4 Effect of CK2 siRNA knockdown on cell viability under zinc exposure 79

Fig 3.5 Visualisation of Zn^{2+} in $ZnSO_4$ treated cells under CK2 inhibition.....82

Fig 3.6 Visualisation of Zn^{2+} under siRNA knockdown of CK2 subunit genes.....83

Fig 4.1 Zinc dose responsive curves of MCF-7 and MDA-MB-231 breast cancer cells 90

Fig 4.2 Volcano plots for T_{30} and T_{120} zinc treatment versus control 92

Fig 4.3 Log_2FC of differentially expressed genes shared by T_{30} and T_{120} 102

Fig 4.4 Quantification of gene expression in MCF-7 breast cancer cells by qRT-PCR.....103

Fig 4.5 Quantification of gene expression in MDA-MB-231 breast cancer cells by qRT-PCR.....104

Fig 5.1 Zinc dose responsive curves of the six cell lines.....115

Fig 5.2 Validation of *GAPDH* expression in the cell lines of this study via qRT-PCR 117

Fig 5.3 Validation of the differentially expressed genes in MCF-7 cells via qRT-PCR 118

Fig 5.4 Quantification of the differentially expressed genes in MDA-MB-231 cells via qRT-PCR.....119
Fig 5.5 Quantification of the differentially expressed genes in MCF10A cells via qRT-PCR 120
Fig 5.6 Quantification of the differentially expressed genes in PC3 cells via qRT-PCR....121
Fig 5.7 Quantification of the differentially expressed genes in DU145 cells via qRT-PCR 122
Fig 5.8 Quantification of the differentially expressed genes in RWPE-1 cells via qRT-PCR 123
Fig 5.9 Comparison of gene expression in MCF-7 against MCF10A cells via qRT-PCR..124
Fig 5.10 Comparison of gene expression MDA-MB-231 against MCF10A cells via qRT-PCR.....125
Fig 5.11 Comparison of gene expression in PC3 against RWPE-1 cells via qRT-PCR 126
Fig 5.12 Comparison of gene expression in DU154 against RWPE-1 cells via qRT-PCR.127
Fig 5.13 CK2 subunit expression profile under zinc IC_{50} treatment 129
Fig 5.14 Comparison of CK2 subunit gene expression between cancerous and normal cells 131
Fig 5.15 Determination of cellular zinc content through ICP-MS analysis 133
Fig 6.1 Schematic description for molecular details in zinc homeostasis 147

Publications

Zaman, M. S., Barman, S. K., Corley, S. M., Wilkins, M. R., Malladi, C. S and Wu, M. (2021), *'Transcriptomic insights into the zinc homeostasis of MCF-7 breast cancer cells via next-generation RNA sequencing'*, Metallomics, vol 13, Issue 6, Accepted manuscript https://doi.org/10.1039/c6mt00230g.

Zaman, M. S., Johnson, A. J., Petersingham, G., Muench, G. A. and Wu, M. (2019), *'Protein kinase CK2 is involved in zinc homeostasis in breast and prostate cancer cells'*, BioMetals, vol 32, no 6, pp 861-873.

Johnson, A. J., **Zaman, M. S.**, Veljanoski, F., Phrakaysone, A., Li, S., O'Doherty, P., Petersingham, G., Perrone, G., Molloy, M. and Wu, M. (2017), *'Unravelling the role of protein kinase CK2 in metal toxicity using gene deletion mutants'*, Metallomics, vol 9, no 3, pp 301 - 308.

Johnson, A. J., Veljanoski, F., O'Doherty, P., **Zaman, M. S.**, Petersingham, G., Bailey, T., Muench, G. A., Kersaitis, C. and Wu, M. (2016), *'Revelation of molecular basis for chromium toxicity by phenotypes of Saccharomyces cerevisiae gene deletion mutants'*, Metallomics, vol 8, no 5, pp 542 - 550.

Johnson, A. J., Veljanoski, F., O'Doherty, P., **Zaman, M. S.**, Petersingham, G., Bailey, T., Muench, G. A., Kersaitis, C. and Wu, M. (2016), *'Molecular insight into arsenic toxicity via the genome-wide deletion mutant screening of Saccharomyces cerevisiae'*, Metallomics, vol 8, no 2, pp 228 - 235.

Conference presentation

Zaman, M. S., Barman, S. K., Malladi, C. and Wu, M. *Protein kinase CK2 regulates zinc homeostasis in breast and prostate cancer cells*. Research Continuity Student Council (RCSC), Western Sydney University, Australia, March 2020.

Barman, S. K., **Zaman, M. S.,** Malladi, S. C., Mahns, A. D. and Wu, M. *Molecular insights into Zn^{2+} homeostasis of breast and prostate cancer cells.* Research Continuity Student Council (RCSC), Western Sydney University, Australia, March 2020.

Gupta, A., Wijesekera, D., **Zaman, M. S.** and Price, W. S. *Visualising tumour hypoxia: advanced MRI contrast agents.* In 3rd Translational Cancer Research Workshop, Austinmer, Australia, October 2018.

Petersingham, G., **Zaman, M. S.,** Johnson, A. J., Reddy, N., Torres, A. and Wu, M. *Characterisation of metal-ligand interactions and the effect of metal ions on the gene expression of amyloid precursor protein.* Gordon Research Conference, Metals in Biology, California, United States of America, January 2018.

Wijesekera, D., Gupta, A., **Zaman, M. S.**, Willis, S.A. and Price W.S., *Evaluation of Hypoxia Using MRI*, Australian MRI-LINAC Collaborators Meeting, Newcastle, Australia, December 2017.

Johnson, A. J., **Zaman, M. S.**, Veljanoski, F. and Wu, M. *Protein kinase CK2 regulates metal uptake and toxicity*. Lecture delivered at the 8th international conference on Protein Kinase CK2, Saarland University, Homburg, Germany, November 2016.

Johnson, A. J., **Zaman, M. S.**, Veljanoski, F. and Wu, M. *Protein kinase CK2 regulates metal uptake and toxicity*. Poster presentation delivered at the 8th international conference on Protein Kinase CK2, Saarland University, Homburg, Germany, November 2016.

Zaman, M. S., Johnson, A., Bobek, G., Kueh, S., Kersaitis, C., Baily, T., Buskila, Y. and Wu, M. *Protein kinase CK2 regulates metal toxicity in neuronal cells*. Presented at the Molecular Medicine Research Group annual meeting (MMRG), Western Sydney University, November 2015.

Thesis abstract

Breast and prostate cancers are the most common cancers in Australian women and men, respectively. The dysregulation of zinc (Zn^{2+}) homeostasis is an intriguing hallmark for both cancers, e.g., hyper-accumulation of Zn^{2+} in breast cancer compared to normal breast tissue and low level of cellular Zn^{2+} in prostate cancer in comparison to normal prostate tissue. Such opposite profiles of zinc in breast and prostate cancer cells point to the potential involvement of zinc in cancer development. This study takes advantage of such characteristic feature between breast and prostate cancer cells to explore their molecular details in zinc homeostasis.

In this study, protein kinase CK2 (CK2) was firstly analysed in breast and prostate cancer cells, by dissecting the distinct roles of CK2 subunits (CK2α, CK2α' and CK2β) in zinc homeostasis. Using CK2 inhibitors 4,5,6,7-tetrabromobenzotriazole (TBB) and CX-4945, siRNA-mediated knockdown and zinc ion specific fluorophores (FluoZin-3 AM), this study demonstrated that zinc accumulation was elevated in PC3 and DU145 prostate cancer cells due to knockdown of the gene expression for CK2α', while the opposite was observed in MCF-7 and MDA-MB-231 breast cancer cells. Furthermore, siRNA knockdown of individual CK2 subunits showed that individual subunits of CK2 have distinct roles in zinc homeostasis in breast and prostate cancer cells. These findings demonstrated that CK2 is indeed involved in zinc homeostasis in breast and prostate cancer cells, as well as that of individual CK2 subunits play distinct roles.

To gain a holistic view of the molecular details of zinc homeostasis, I carried out the transcriptomic analysis by the means of high throughput next-generation RNA sequencing (RNA-seq). Breast cancer cells (MCF-7) were subjected to extracellular zinc exposure (320 μM) and then analysed by RNA-seq at three time points (T_0, T_{30} and T_{120}) in the time course.

The findings revealed a significant increase in gene expression, up to 869-fold, for metallothioneins (*MT1B*, *MT1F*, *MT1X* and *MT2A*) and the zinc exporter ZnT1 (*SLC30A1*) at T_{30}, continuingly through to T_{120}. Similarly, the dynamic expression pattern was also found for the autophagy-related gene (*VMP1*) and numerous genes for zinc finger proteins (e.g., *RNF165*, *ZNF365*, *ZBTB2*, *SNAI1*, *ZNF442*, *ZNF547*, *ZNF563* and *ZNF296*). These findings point to the all-hands-on-deck strategy adopted by the cancer cells for maintaining zinc homeostasis. The stress-responsive genes encoding heat shock proteins (*HSPA1A*, *HSPA1B*, *HSPA1L*, *HSPA4L*, *HSPA6*, *HSPA8*, *HSPH1*, *HSP90AA1* and *HSP90AB1*) were also differentially up-regulated at T_{120}, suggesting the critical role of heat shock proteins in dealing with zinc exposure. Furthermore, the genes encoding protein kinase CK2 subunits (*CSNK2A1*, *CSNK2A2* and *CSNK2B*) were found unchanged. These results provide significant molecular clues which contributes to our understanding of zinc homeostasis and cancer development.

The transcriptomic findings were validated by quantitative reverse transcription polymerase chain reaction (qRT-PCR) and further extended to a panel of breast and prostate cancer cells as well as normal breast and prostate epithelial cells. The top differentially expressed genes from RNA-seq (*MT1B*, *MT1F*, *MT1X*, *MT2A*, *SLC30A1*, *VMP1*, *ZNF850*, *HSPA6* and *HSPA90AA1*) were quantified via qRT-PCR. The results revealed that the expression of metallothionein genes (*MT1B*, *MT1F*, *MT1X* and *MT2A*) was increased at T_{30} and T_{120} following IC_{50} $ZnSO_4$ treatment, which agrees with the transcriptomic RNA-seq dataset.

The gene for ZnT1 (*SLC30A1*) was expressed higher in the basal type of breast cancer cells (MDA-MB-231) compared to the luminal MCF-7 cells. As ZnT1 is the sole zinc efflux transporter residing in the plasma membrane and is functionally non-redundant in the maintenance of zinc homeostasis. Its higher expression in MDA-MB-231 cells than MCF-7

may relate to the degree of their malignancy. Additionally, the expression of CK2 subunit genes was elevated in breast cancer cells compared to the normal breast epithelial cells, indicating its intrinsic role in the zinc homeostasis of the cancer cells. Furthermore, the expression of the zinc-related genes in prostate cancers is not as robust as the breast cancer cells, indicating that prostate cancer cells are naturally programmed to inhabit in low-zinc environment compared to breast cancer cells.

Taken together, the results of this study demonstrated the involvement of CK2 in zinc homeostasis in breast and prostate cancer cells. The RNA-seq dataset confers a holistic view at the molecular level on how the cancer cell responds to the extracellular zinc exposure. The findings of this study provide molecular insights into zinc homeostasis of breast and prostate cancer cells. As zinc is critical for the structure and function of ~3000 human proteins, the molecular details described in this thesis should open multitudes of avenues for cancer research and anti-cancer drug development.

List of abbreviations

Abbreviation	Definition
%	Percentage
°C	Degrees celsius
µg	Microgram
µL	Microliter
µM	Micro molar
3'	Three prime end of DNA
5'	Five prime end of DNA
A_{600}	Absorbance at 600nm
Al^{3+}	Trivalent aluminium cation
As^{3+}	Trivalent arsenic cation
ATP	Adenosine triphosphate
bp	Base pair
BPE	Bovine pituitary extract
BPH	Benign prostate hyperplasia
BY4743	S288C-derivative laboratory strain of *S. cerevisiae*
Ca^{2+}	Divalent calcium cation
$CaCl_2$	Calcium chloride
Cat	Catalogue
$CdCl_2$	Cadmium chloride
cDNA	Complementary deoxyribonucleic acid
CK2	Protein kinase CK2 (formerly known as Casein kinase 2)
CK2α	α catalytic subunit of mammalian protein kinase CK2
CK2α'	α' catalytic subunit of mammalian protein kinase CK2
CK2β	β regulatory subunit of mammalian protein kinase CK2
CKA1	Yeast gene encoding the Cka1p catalytic subunit of yeast protein kinase CK2
CKA2	Yeast gene encoding the Cka2p catalytic subunit of yeast protein kinase CK2
CKB1	Yeast gene encoding the Ckb1p regulatory subunit of yeast protein kinase CK2
CKB2	Yeast gene encoding the Ckb2p regulatory subunit of yeast protein kinase CK2
cm	Centimetre
Co^{2+}	Divalent cobalt cation
$CoCl_2$	Cobalt chloride
Cr^{6+}	Chromium hexavalent ion
CT	Cycle threshold
CX-4945	Small-molecule inhibitor of protein kinase CK2

DEPC	Diethyl pyrocarbonate treated water
DMEM	Dulbecco's modified eagle medium
DMSO	Dimethyl sulfoxide
DNA	Deoxyribonucleic acid
dNTP	Deoxyribonucleotide triphosphate
dsRNA	Double-strand RNA
DU145	Prostate cancer cell line
EDTA	Ethylenediaminetetraacetic acid
EGFR	Epidermal growth factor receptor
ER	Endoplasmic reticulum
EUROSCARF	European *Saccharomyces Cerevisiae* archive for functional analysis
FBS	Foetal bovine serum
FC	Fold change
FluoZin-3 AM	Zinc ion specific fluorophore
g	Relative centrifugal force
GAPDH	Glyceraldehyde 3-phosphate dehydrogenase
GTP	Guanosine triphosphate
h	Hour
H_2O	Water
HCl	Hydrochloric acid
HEPES	4-(2-hydroxyethyl)-1-piperazineethanesulfonic acid
HER	Human epidermal growth factor receptor
HPV	Human papillomavirus
HSP	Heat shock proteins
IC_{50}	Inhibitory concentration 50%
ICP-MS	Inductively coupled plasma mass spectrometry
KCl	Potassium chloride
kDa	Kilodalton
KH_2PO_4	Potassium dihydrogenphosphate
L-15	Leibovitz's L-15 medium
LNCaP	Androgen-sensitive human prostate adenocarcinoma
Log_2FC	Logarithm of fold change
M	Million
MAPK	Mitogen-activated protein kinase
MCF10A	Non-tumuorigenic breast epithelial cell line
MCF-7	Human breast cancer cell line
MDA-MB-231	Human breast cancer cell line
mg	Milligram
$MgCl_2$	Magnesium chloride
MilliQ water	Water purified using a Milli-Q system

min	Minute
mL	Millilitre
mM	Millimolar
MRE	Metal responsive element
mRNA	Messenger ribonucleic acid
MT	Metallothionein
MTF-1	Metal regulatory transcription factor 1
MTT	3-(4,5-Dimethylthiazol-2-yl)-2,5-Diphenyltetrazolium Bromide
Na^+	Sodium cation
Na_2HPO_2	Sodium hypophosphite
NaCl	Sodium chloride
Neuro-2a	Murine neuroblastoma cell line
$NF_k\beta$	Nuclear Factor Kappa Beta
ng	Nanogram
nM	Nanomolar
No	Number
OPTI-MEM	Modified Eagle's Minimum Essential Media used for transfection
p53	Gene that codes for a protein that regulates cell cycle
PAP	Prostatic acid phosphatase
PBS	Phosphate buffered saline
PC3	Human prostate cancer cell line
PCR	Polymerase chain reaction
pH	Acidic or basic a substance
PML	Promyelocytic leukemia protein
PR	Progesterone receptor
PSA	Prostate-specific antigen
qRT-PCR	Quantitative polymerase chain reaction
RNA	Ribonucleic acid
RNA-seq	RNA-sequencing
RNF	Zinc finger proteins
ROS	Reactive oxygen species
rpm	Revolutions per minute
RWPE-1	Non-tumuorigenic prostate epithelial cell line
SD	Standard deviation
sec	Second
SEM	Standard error of the mean
siRNA	Small interfering ribonucleic acid
ssRNA	Single-stranded RNA
T_0	0-hour time point
T_{120}	2-hour time point
T_{30}	30-minute time point

TBB	4,5,6,7-Tetrabromo-2-azabenzimidazole
TRIzol™	Solution used in RNA/DNA/protein extraction
UNSW	University of New South Wales
UV	Ultraviolet
VMP	Vacuolar membrane protein
Vs	Verses
x	Times
ZIP	ZRT, IRT-like Protein
Zn^{2+}	Divalent zinc cation
ZNF	Zinc finger proteins
$ZnSO_4$	Zinc sulfate
ZnT	Zinc transporter
ZRT	Zinc regulated transporter
α	Alpha
α'	Alpha prime
β	Beta
Δ	Delta (Used as a suffix after a gene to signify a deletion strain in yeast)

1 LITERATURE REVIEW

1.1 General introduction

This thesis seeks to investigate the involvement of zinc and protein kinase CK2 (CK2) in breast and prostate cancer cells, by dissecting the distinct roles of CK2 subunits (CK2α, CK2α' and CK2β) in zinc homeostasis of breast and prostate cancer cells. Furthermore, revealing the rounded molecular details for zinc in breast cancer cells by the means of next-generation RNA sequencing and extending the discovery in breast cancer cells to prostate cancer cells.

The basis of this project comes from previous studies in our lab, with the model organism *Saccharomyces cerevisiae*. Deletion of the *CKA2* gene (the yeast equivalent of mammalian *CSNK2A2* encoding CK2α') was found to render the deletion mutant (*cka2*Δ) resistant to zinc toxicity, suggesting that CK2α' is involved in regulating zinc uptake and such a process is interrupted in *cka2*Δ hence resulting in resistance to zinc exposure. Moreover, the latter finding by inductively-coupled plasma mass spectrometry (ICP-MS) confirmed CK2α' indeed plays a role in zinc uptake (Johnson et al., 2017).

Further work in mouse neuroblastoma cells (Neuro-2a) extends our previous finding in yeast to mammalian cells. I found that CK2α' was the predominant CK2 subunit in regulating zinc uptake of neuronal cells (Zaman et al., 2016). The knockdown of CK2α' gene (*CSNK2A2*) by its specific small interfering RNA (siRNA) leads to increased tolerance to the zinc level. With the aid of the confocal microscope, I discovered that Neuro-2a cells treated with individual specific siRNA targeting the genes encoding CK2 subunits α, α' and β respectively exhibited a significant reduction of intracellular zinc,

whilst the knockdown of CK2α' was the most prominent. Such a decrease of intracellular zinc correlated with the healthy morphology of the neuronal cells treated with CK2α' siRNA as compared to the cells treated with zinc sulfate alone (Zaman et al., 2016). These findings demonstrate the involvement of CK2 in zinc homeostasis.

Altered zinc profiles are linked to the development and progression of breast and prostate cancers (Margalioth et al., 1983; Rizk and Sky-Peck, 1984; Costello and Franklin, 2006). Studies have determined that zinc levels differ in various cancer types. It has been demonstrated that the zinc level in cancers of the breast is distinctly increased compared to normal breast epithelial cells (Margalioth et al., 1983; Rizk and Sky-Peck, 1984). In contrast, the zinc level in cancers of the prostate has been shown to be lower when compared to normal prostate epithelial cells (Costello and Franklin, 2006; Franklin and Costello, 2007; Franklin and Costello, 2009). Hence, dysregulation of zinc homeostasis is an intriguing hallmark for breast and prostate cancers, e.g., hyper-accumulation of Zn^{2+} in breast cancer and low levels in prostate cancer. Such diametrical opposite profiles of zinc in breast and prostate cancer cells provide an ideal tool to explore the role of protein kinase CK2 and zinc in these two types of cancer cells.

Both CK2 and the zinc ion are key players in cell biology and oncogenesis (Vallee, 1983; Vallee and Auld, 1990; Litchfield, 2003) and this study demonstrates that CK2 and Zn^{2+} are intricately linked to breast and prostate cancer cells. Herein, a systematic experimental approach was employed, including experiments using CK2 inhibitors 4,5,6,7-tetrabromobenzotriazole (TBB) and CX-4945, siRNA-mediated knockdown and zinc ion specific fluorophores (FluoZin-3 AM) were carried out to identify CK2's involvement in regulating zinc toxicity of breast and prostate cancer cells. Next-generation RNA sequencing was conducted on the MCF-7 breast cancer cell line, followed-up by qRT-

PCR, to determine the main genes involved in regulating zinc ion homeostasis. ICP-MS allowed me to determine the cellular content of zinc upon IC_{50} $ZnSO_4$ treatment alone and in the presence of the CK2 inhibitor TBB, allowing me to explore the role of CK2 in zinc uptake. Prominent genes found to be involved in zinc ion homeostasis were further investigated via qRT-PCR. In this study the role of CK2 in zinc homeostasis was investigated in the breast (MCF-7 and MDA-MB-231) and prostate (PC3 and DU145) cancer cells, along with normal breast (MCF10A) and prostate (RWPE-1) epithelial cells. The findings of this study should have a direct bearing on cancer research.

1.2 Chemistry of zinc

Zinc is a transitional metal in the *d* block of the periodic table, with an atomic number of *30*. The underlying chemistry for the versatility of zinc, when compared to other metal ions like copper, iron and calcium, is found in its properties such as the completely filled *d*-shell and its ability to have different coordination numbers and a variety of coordinating ligands including the amino acid residues histidine and cysteine (Colvin et al., 2003; Cousins et al., 2006). The coordination chemistry of zinc permits its binding to a range of biological proteins due to its property as a Lewis acid, which makes it structurally suitable to preform protein-protein interactions (Vallee and Auld, 1990; Yamasaki et al., 2007). Lack of unpaired electrons in zinc means it is stable and does not participate in redox reactions, in contrast to the redox-active transition metal ions such as copper and iron (Laity et al., 2001).

The stability of zinc is beneficial to the biological environment, intracellularly and extracellularly. As is known, the internal milieu of the cell is dynamic, containing both reducing and oxidative chemicals or metabolites (Koh and Choi, 1994; Hershfinkel et al., 2001). A redox-inert metal ion like zinc provides stability, whether in enzymatic reactions

or in maintaining protein structures (Laity et al., 2001). Its versatility in coordination is also a valuable trait utilised by the cell for its role in regulating protein functions (Vallee and Auld, 1990; Ebert and Altman, 2008; Maret, 2012). With respect to its catalytic functions, zinc has been found to serve as a cofactor in numerous enzymes, with carbonic anhydrase being the first enzyme discovered in 1940 for using zinc as cofactor (Keilin and Mann, 1940; Ho and Ames, 2002). Studies have determined intracellular free zinc ion concentration at picomolar (pM) levels ranging from 60-500 pM, with pancreatic β-cell lines 110-250 pM (Qin et al., 2013; Chabosseau et al., 2014) and 400 pM in INS-1 rat pancreatic β-cells (Vinkenborg et al., 2009).

1.3 Zinc ion homeostasis

Arguably, zinc is one of the most important trace metal ions in organisms ranging from the single-celled *S. cerevisiae* to humans. Chronologically, zinc was first found essential to living organisms in 1869, by Jules Raulin, a student of Louis Pasteur (Raulin, 1869). Over the ensuing years, zinc has been found to be involved in multitudes of biological functions, including catalysis as a cofactor for enzymes, as a structural component in proteins and in signal transduction as a second messenger (Hershfinkel et al., 2001; Laity et al., 2001; Maret, 2001; Taylor et al., 2012). As mentioned previously, the first zinc-binding enzyme discovered was carbonic anhydrase (Keilin and Mann, 1940). It is estimated that, in the cell's proteome, there are at least 3000 zinc-binding proteins (Maret, 2012). About 40% of these proteins are transcription factors, which often contain the famous zinc-finger motifs, allowing the proteins to bind DNA (Vallee and Auld, 1990; Ebert and Altman, 2008). The other 60% of zinc-binding proteins are mainly enzymes, structural proteins and ion transporters (Ebert and Altman, 2008).

Consequently, zinc is required for life on earth (Vallee and Auld, 1990). When compared against other micronutrients (e.g., iron, manganese and copper), zinc is quite distinctive in its functional diversity (Laity et al., 2001; Yamasaki et al., 2007; Prasad et al., 2009). Studies have catalogued the cellular functions which requires zinc such as gene expression (Vallee, 1983), the stabilisation of protein and nucleic acid structure (Vallee and Auld, 1990), subcellular organelle integrity (Vallee, 1983; Vallee and Auld, 1990; Guerra and Issinger, 1999) and involvement in the activity of numerous enzymes (Grummt et al., 1986; Vallee and Auld, 1990; Franklin and Costello, 2007). Zinc ion homeostasis in the cell is maintained through three highly regulated processes. They include zinc uptake by a family of ZRT/IRT-like protein transporters (ZIP), zinc storage in metallothioneins (MT) and subcellular compartments and zinc export to the extracellular space or into the subcellular organelle via a family of zinc transporters (ZnT) (Fig. 1.1) (Nelson, 1999; Guerinot, 2000; Colvin et al., 2003; Kirschke and Huang, 2003; Maret, 2003; Desoize, 2004; Cousins et al., 2006; Kagara et al., 2007; Lopez et al., 2011; Choi and Bird, 2014).

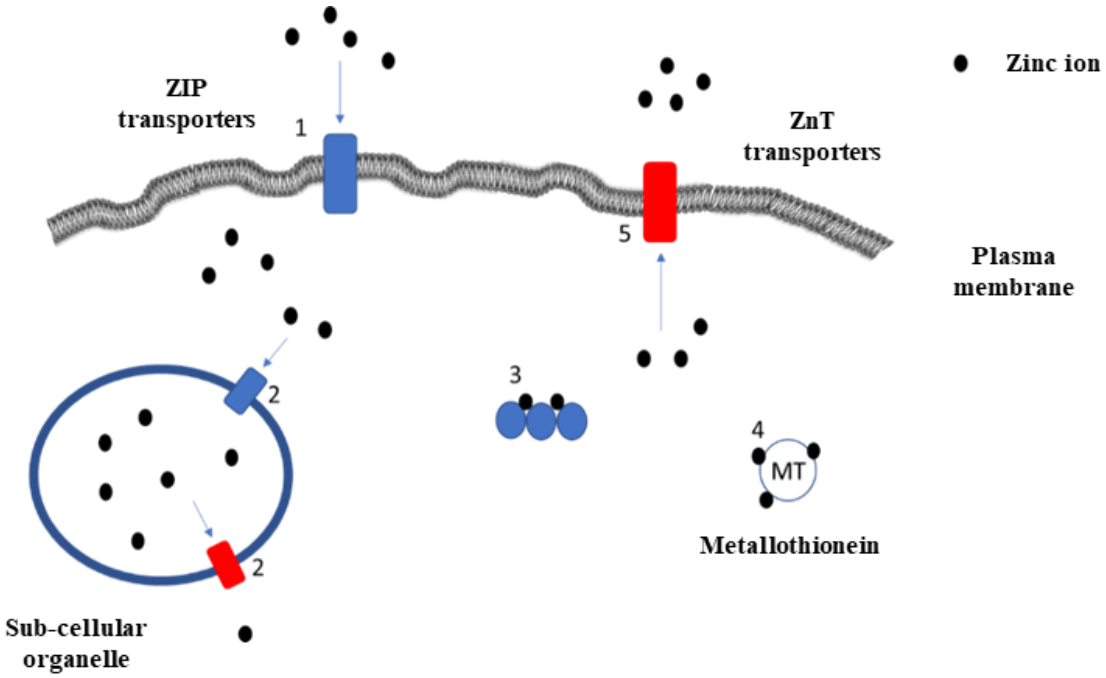

Fig 1.1 Diagram of general mechanisms of zinc uptake, storage and export

Zinc ions enter the cell through ZIP transporters (denoted by 1), their sub-cellular location is controlled by zinc transporters embedded in organelles (2). They may form structural components of enzymes or participate as co-factors in metabolic processes (3). Specific proteins, such as metallothioneins may sequester zinc if concentrations are too high (4). Efflux of zinc is facilitated by ZnT transporters (5).

A specific set of transporters functions in the plasma and subcellular organellar membranes to provide a delicate balance of transport activities for maintaining zinc ion homeostasis (Nelson, 1999). As previously asserted, intracellular zinc is critical for the functioning of biological processes including DNA transcription, cellular proliferation, cell signaling and apoptosis (Cousins et al., 2006; Kambe et al., 2014). Hence, the tight control of intracellular zinc, or maintaining its homeostasis, is essential for cell survival (Vallee and Auld, 1990; Choi and Bird, 2014). Mounting evidence implicates the dyshomeostasis of cellular zinc in cancers of the breast, prostate, liver, ovaries and pancreas, as zinc concentration in cancer tissues being disparate from the surrounding normal tissues (Table

1.1) (Colvin et al., 2003; Desoize, 2004; Franklin et al., 2005; Cousins et al., 2006; Kagara et al., 2007; Prasad et al., 2009; Lopez et al., 2011; Grattan and Freake, 2012). Understanding the molecular mechanisms for zinc homeostasis, an objective for this thesis, is critical in understanding the relationship between the dyshomeostasis of zinc and diseases such as cancers.

Table 1.1 Comparison of zinc level in cancer and normal tissue

Tissue/cells	Zinc level comparison	References
Breast cancer cells	Higher intracellular zinc level compared to normal breast epithelial cells	(Margalioth et al., 1983; Rizk and Sky-Peck, 1984)
Prostate cancer cells	Lower intracellular zinc level compared to normal prostate epithelial cells	(Liang et al., 1999; Costello and Franklin, 2006)
Hepatocellular cancer tissue	Lower intracellular zinc level compared to benign liver tissue	(Ebara et al., 2000)
Ovarian cancer tissue	Lower intracellular zinc level compared to benign ovarian tissue	(Costello and Franklin, 2006)
Pancreatic cancer cells	Higher intracellular zinc level compared to normal pancreatic epithelial cells	(Li et al., 2007)

1.4 Regulation of zinc transport in the cell

1.4.1 Transporters involved in zinc uptake

For zinc to fulfil the myriad of roles in enzymatic activities, protein structures and signal transduction, nutrient zinc has to be transported into the cell (Cousins et al., 2006). As a charged cation, zinc itself cannot cross the plasma membrane by simple diffusion (Nelson, 1999). As a result, there are numerous transporters involved in zinc uptake. They include the (ZIP1-14 family) which are represented in Table. 1.2 (Guerinot, 2000). Herein, ZRT is an abbreviation for zinc-regulated transporter, whilst IRT is for iron-regulated transporters. ZIP proteins are predicted to have eight transmembrane domains with extracellular N- and C- termini (Kagara et al., 2007). ZIP transporters increase intracellular zinc concentrations, $[Zn^{2+}]_i$, by promoting zinc uptake from extracellular space and vesicular zinc release into the cytoplasm.

Zinc is tightly controlled in the cell by the 14 ZIP proteins as well as the other transporters such as ZnTs, which are to be described in the following section (Vallee and Auld, 1990; Mackay and Crossley, 1998; Kagara et al., 2007). As mentioned previously, it is essential for cells to regulate zinc influx, storage/sequestration and efflux to maintain homeostasis and prevent the onset of diseases such as cancers (Vallee and Auld, 1990; Mackay and Crossley, 1998; Kagara et al., 2007). Over-expression of several zinc transporters (ZIP6, ZIP7 and ZIP10) is associated with zinc hyper-accumulation in breast tumours and several breast cancer cell lines (Mackay and Crossley, 1998; Kirschke and Huang, 2003; Kagara et al., 2007; Prasad et al., 2009; Song and Ho, 2009; Lopez et al., 2011). Comparatively, ZIP6 over-expression has been noted in estrogen-responsive subtypes and is associated with less aggressive breast tumours (Vallee and Auld, 1990; Mackay and Crossley, 1998; Kagara et al., 2007).

Table 1.2 Family of ZIP transporters and known localisation in mammalian cells

ZIP Family (*SLC39*)	Gene expression	Cellular location	Molecular function	Reference
ZIP1 (*SLC39A1*)	Widespread	Plasma membrane	Zinc uptake	(Song and Ho, 2009)
ZIP2 (*SLC39A2*)	Prostate, uterus, cervical epithelium, optic nerve and monocytes	Plasma membrane	Zinc uptake	(Song and Ho, 2009)
ZIP3 (*SLC39A3*)	Widespread	Plasma membrane	Zinc uptake	(Guerinot, 2000; Prasad et al., 2009)
ZIP4 (*SLC39A4*)	Small intestine, stomach, colon, cecum and kidney	Apical membrane	Zinc uptake	(Guerinot, 2000)
ZIP5 (*SLC39A5*)	Kidney, liver, spleen, colon, stomach and pancreas	Basolateral membrane of polarised cells	Zinc uptake	(Guerinot, 2000; Song and Ho, 2009)
ZIP6 (*SLC39A6*)	Widespread	Plasma membrane	Zinc uptake	(Song and Ho, 2009; Grattan and Freake, 2012)
ZIP7 (*SLC39A7*)	Widespread	Endoplasmic reticulum and Golgi	Zinc into cytosol	(Taylor et al., 2008)
ZIP8 (*SLC39A8*)	Widespread	Plasma membrane, vesicles and mitochondria	Zinc, cadmium and manganese uptake	(Guerinot, 2000; Prasad et al., 2009)

ZIP9 (*SLC39A9*)	Widespread	Unknown	Unknown	(Vallee and Auld, 1990)
ZIP10 (*SLC39A10*)	Widespread	Plasma membrane	Zinc uptake	(Guerinot, 2000; Prasad et al., 2009)
ZIP11 (*SLC39A11*)	Widespread	Unknown	Unknown	(Guerinot, 2000)
ZIP12 (*SLC39A12*)	Brian, lungs, testis and retina	Plasma membrane	Zinc uptake	(Guerinot, 2000; Song and Ho, 2009)
ZIP13 (*SLC39A13*)	Widespread	Golgi apparatus	Zinc into cytosol	(Vallee and Auld, 1990)
ZIP14 (*SLC39A14*)	Widespread	Golgi apparatus	Zinc and iron uptake	(Vallee and Auld, 1990)

*SLC denotes solute carrier. ZIP 1-14 belongs to family 39 of SLC superfamily of membrane-bound transport proteins.

1.4.2 Transporters associated with the decrease of intracellular zinc

Zinc transporters (ZnT1-10) function in the opposite direction to ZIP, being responsible for decreasing $[Zn^{2+}]_i$ by promoting zinc efflux from the cytoplasm to the extracellular space or into subcellular compartments (Colvin et al., 2003; Huang and Tepaamorndech, 2013). The first ZnT to be discovered is ZnT1, which is located in the plasma membrane and its gene expression is mapped to chromosome 1 in both humans and mice (Guerinot, 2000). Most ZnT proteins have six transmembrane domains (TMDs) and are predicted to have cytoplasmic amino and carboxyl termini. Furthermore, a classic characteristic of ZnT proteins is the long histidine rich loop between TMDs IV and V, which could potentially represent a metal binding domain (Vallee and Auld, 1990). The main ZnT transporters that have been studied are ZnT1 and ZnT2, while the other members of ZnTs are yet to be fully investigated.

ZnT1 displays a ubiquitous tissue distribution, although it is highly expressed in tissues involved in zinc acquisition and transport such as within the basolateral surface of enterocytes lining the villi of the small intestine (Guerinot, 2000). It is important to take a big-picture view here, regarding this particular characteristic for ZnT1 expressed in basolateral face of enterocytes. The zinc ions absorbed into the enterocytes are transported out of these enterocytes via ZnT1 into the tissue and eventually into the blood stream. Therefore, ZnT1 is in fact involved in zinc acquisition in humans. In terms of the cancer cells, ZnT1 is responsible for transporting intracellular zinc out of the cells, hence decreasing $[Zn^{2+}]_i$. While ZnT2 is localised on vesicles and allows the storage and sequestration of zinc when the cytoplasm is replete with zinc (Kelleher and Lönnerdal, 2003; Lopez et al., 2011). There is evidence to suggest ZnT2 is involved in mammary gland zinc metabolism where an abundance of ZnT2 at the basolateral surface appears to

remain the same, whilst the expression of ZnT2 at the apical membrane of the mammary gland decreases through lactation (Kelleher and Lönnerdal, 2003). In breast cancer cells, zinc accumulation coincides with ZnT2 overexpression and an increase in vesicular zinc pools (Mackay and Crossley, 1998; Guerinot, 2000; Kagara et al., 2007; Prasad et al., 2009). In contrast to the elevated ZnT2 expression level in breast cancer cells, its expression level is decreased in prostate cancer cells (Song and Ho, 2009; Lopez et al., 2011). Currently, there is a lack of evidence for the mechanistic roles of ZnTs in the maintenance and regulation of zinc homeostasis, hence it is necessary for further research to elucidate the role of ZnT transporters in zinc homeostasis.

Table 1.3 Family of ZnT transporters and known localisation in mammalian cells

ZnT Family (*SLC30*)	Gene expression	Subcellular location	Molecular function	Reference
ZnT1 (*SLC30A1*)	Widespread	Plasma membrane, vesicles	Cytoplasmic zinc removal	(Lopez et al., 2011)
ZnT2 (*SLC30A2*)	Small intestine, kidney, pancreas, testis, seminal vesicles, mammary gland, prostate gland and epithelial cells	Vesicles and lysosomes	Zinc transport into vesicles and lysosomes	(Lopez et al., 2011)
ZnT3 (*SLC30A3*)	Brain and testis	Synaptic vesicles and endosomes	Zinc transport into synaptic vesicles	(Song and Ho, 2009; Lopez et al., 2011)
ZnT4 (*SLC30A4*)	Mammary gland, brain, small intestine, mast cell, placenta, blood and epithelial cells	Endosomes and Golgi	Zinc transport into milk and mast cell vesicles	(Kelleher and Lönnerdal, 2003)
ZnT5 (*SLC30A5*)	Pancreatic β-cells, intestine, heart, brain, liver, kidney, blood and epithelial cells	Golgi, insulin granules and plasma membrane	Zinc transport into Golgi and vesicles	(Kirschke and Huang, 2003; Prasad et al., 2009)

ZnT6 (*SLC30A6*)	Small intestine, brain, liver, blood and adipose tissue	Golgi and expressed and plasma membrane	Zinc transport into Golgi and vesicles	(Song and Ho, 2009)
ZnT7 (*SLC30A7*)	Small intestine, liver, retina, heart, kidney, spleen, blood, epithelial cells	Golgi apparatus, vesicular compartments	Zinc transport into Golgi	(Kirschke and Huang, 2003)
ZnT8 (*SLC30A8*)	Pancreatic β-cells	Islets of Langerhans and insulin granules	Zinc transport	(Yamasaki et al., 2007)
ZnT9 (*SLC30A9*)	Widespread	Cytoplasm and nucleus	Unknown	(Vallee and Auld, 1990)
ZnT10 (*SLC30A10*)	Widespread	Plasma membrane	Zinc uptake	(Song and Ho, 2009)

*SLC denotes solute carrier. ZnTs 1-10 belongs to family 30 of SLC superfamily of membrane-bound transport proteins.

1.4.3 Metallothioneins and zinc homeostasis

Apart from ZIP and ZnT, another player in maintaining zinc homeostasis is the cytosolic metallothioneins (MTs) (Maret, 2003). MTs are a class of small, cysteine-rich, metal binding proteins that play a role in essential metal ion homeostasis, detoxification of non-essential metal ions and protect against intracellular oxidative stress (Adams et al., 2002). There are eight functional isoforms of MTs identified in humans (*MT1A, MT1B, MT1E, MT1F, MT1G, MT1H, MT1X* and *MT2A*) (Werynska et al., 2013). The cysteine residues in MTs are involved in zinc-binding, thereby allowing metallothioneins to serve as zinc buffering proteins (Vallee and Auld, 1990; Nelson, 1999). MT expression is positively regulated by zinc exposure through the activation of metal responsive elements (MREs) in the promoter of metallothionein genes (*MT1A*, *MT1B*, *MT1E*, *MT1F*, *MT1G*, *MT1H*, *MT1L*, *MT1M*, *MT1X*, *MT2*, *MT3* and *MT4*) (Suhy et al., 1999). MRE is the binding site for the DNA transcription factor metal-responsive transcription factor 1 (MTF-1) (Nelson, 1999). MTF-1 responds to changes in zinc metal ion concentration by coordinating the expression of genes involved in uptake, distribution and storage of zinc such as ZIP, ZnT and MTs (Fig. 1.2) (Nelson, 1999; Rutherford and Bird, 2004). Not only do MTs bind and sequestrate Zn^{2+}, they also bind and detoxify a variety of heavy metals such as lead and copper (Suhy et al., 1999).

In relation to cancer, both MTs and MTF-1 are over-expressed in radiation-resistant tumours, suggesting their possible role in zinc homeostasis for cancer development (Suhy et al., 1999). Despite the importance of MTs for cell survival, their expression in varying cell types, normal and cancerous, differs by upwards of 400-fold (Suhy et al., 1999; Achary et al., 2001; Rutherford and Bird, 2004; Song and Ho, 2009). Like zinc transport proteins

(ZIP and ZnT), MTs and MTF-1 were also known to be involved in the dysregulation of zinc in cancer cells (Suhy et al., 1999; Rutherford and Bird, 2004; Song and Ho, 2009).

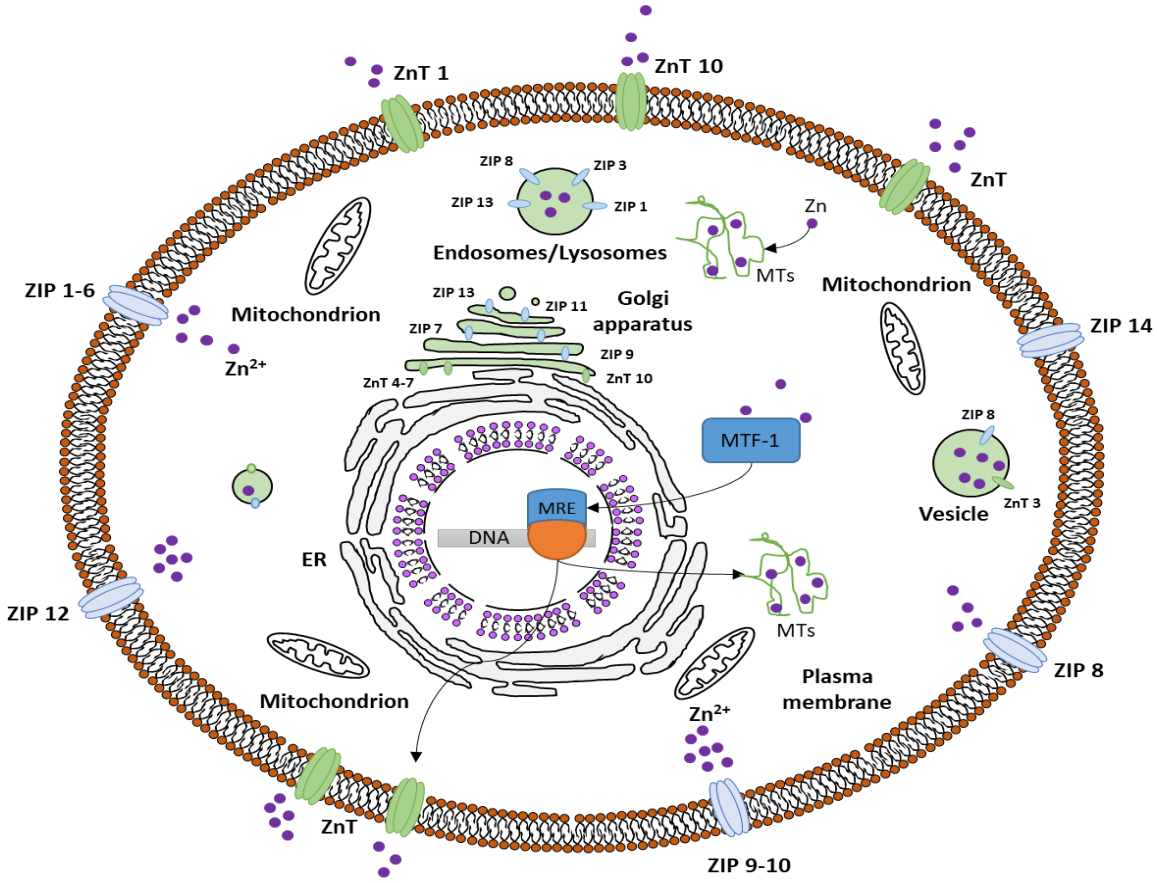

Fig 1.2 Zinc transport and zinc-binding proteins in the cell

As is shown, the function of the ZnT and ZIP transporter families is to reduce and increase the cytoplasmic zinc concentration, respectively. The diagram also depicts other zinc related transporters and their relative locations. Such diverse distributions of these proteins suggest individual roles in executing the catalytic, structural and regulatory roles of zinc. Also shown is the mechanism of sequestration facilitated by metallothioneins. Metal transcription factor 1 (MTF-1) binds the metal responsive element (MRE), resulting in the production of metallothioneins (MTs) which bind excess Zn^{2+}.

1.4.4 Zinc ion dyshomeostasis and its role in cancer

Dysregulation of zinc homeostasis is detrimental to the cell. A considerably higher zinc level is found in breast cancer cells compared to normal breast cells (Alam and Kelleher, 2012). Higher $[Zn^{2+}]_i$ correlates with high malignancy for breast cancer (Margalioth et al., 1983; Rizk and Sky-Peck, 1984; Kagara et al., 2007). Its accumulation is concomitant with abnormal expression of ZIP6, ZIP7, ZIP10, ZnT1 and ZnT2 (Kagara et al., 2007; Taylor et al., 2008; Lopez et al., 2011). In clear contrast, $[Zn^{2+}]_i$ is lower in prostate cancer cells compared to normal prostate cells and down-regulation of transporter expression such as ZIP1 in malignant prostate tissue correlates with marked depletion of intracellular zinc levels (Franklin et al., 2005; Song and Ho, 2009). In normal prostate, zinc is thought to be involved in reproductive functions by aiding in the accumulation of citrate, a component of semen (Chyan et al., 2014). Within mitochondria of epithelial prostate cells, the high concentration of zinc has been shown to inhibit the metabolic enzyme aconitase which catalyses the isomerisation of citrate to isocitrate in citric acid cycle. By blocking the activity of aconitase, the citric acid cycle is impeded and citrate is accumulated (Vallee and Auld, 1990; Suhy et al., 1999; Rutherford and Bird, 2004; Prasad et al., 2009; Song and Ho, 2009). However, when prostate cells become cancerous, zinc concentration is lowered in mitochondria (Song and Ho, 2009). Consequently, the citric acid cycle is no longer inhibited. As a result, more ATP molecules are produced and cancer cells proliferate faster with the availability of energy.

In this study, four cancer cell lines including breast (MCF-7 and MDA-MB-231) and prostate (PC3 and DU145) along with normal breast (MCF10A) and prostate (RWPE-1) epithelial cells were studied to gain a better understanding of zinc homeostasis and CK2

in these two types of cancer cells, which have diametrically opposite zinc profiles as described earlier.

1.4.5 Zinc and metal-regulatory transcription factor 1 (MTF-1)

Zinc homeostasis can be regulated at the level of gene expression. In this regard, MTF-1, a nucleocytoplasmic shuttling transcription factor, is the critical regulator (Choi and Bird, 2014). It is basically a zinc sensor and it can sense the intracellular zinc level. When $[Zn^{2+}]_i$ is high, MTF-1 is phosphorylated and then translocated into the nucleus where it binds to the promoters containing an MRE and activates the gene expression relevant to zinc export and sequestration such as the ZnT and MT genes (Fig. 1.3). Interestingly, it has been shown that in the presence of increased zinc metal ions the transcription factor MTF-1 can be phosphorylated by CK2 (Adams et al., 2002). Upon phosphorylation by CK2, cytoplasmic MTF-1 translocates to the nucleus where it activates genes such as metallothioneins (Adams et al., 2002). This phosphorylation of MTF-1 ultimately leads to the activation of metallothionein transcription (Adams et al., 2002). Metallothioneins are a class of cysteine-rich metal binding protein that play a role in metal ion homeostasis and detoxification of toxic metal ions (Nelson, 1999; Adams et al., 2002). At the gene level, CK2 may be influencing metal ion uptake through phosphorylation and activation of the metal transcription factor, which then regulates genes that are involved in metal ion uptake, storage and/or binding or it may be directly activating zinc transporters such as ZIP/ZnTs (Fig. 1.3). Evidence has shown that the phosphorylation of endoplasmic reticulum (ER) zinc channel ZIP7 is due to the action of CK2. This phosphorylation results in the gated release of Zn^{2+} from intracellular stores (Taylor et al., 2012).

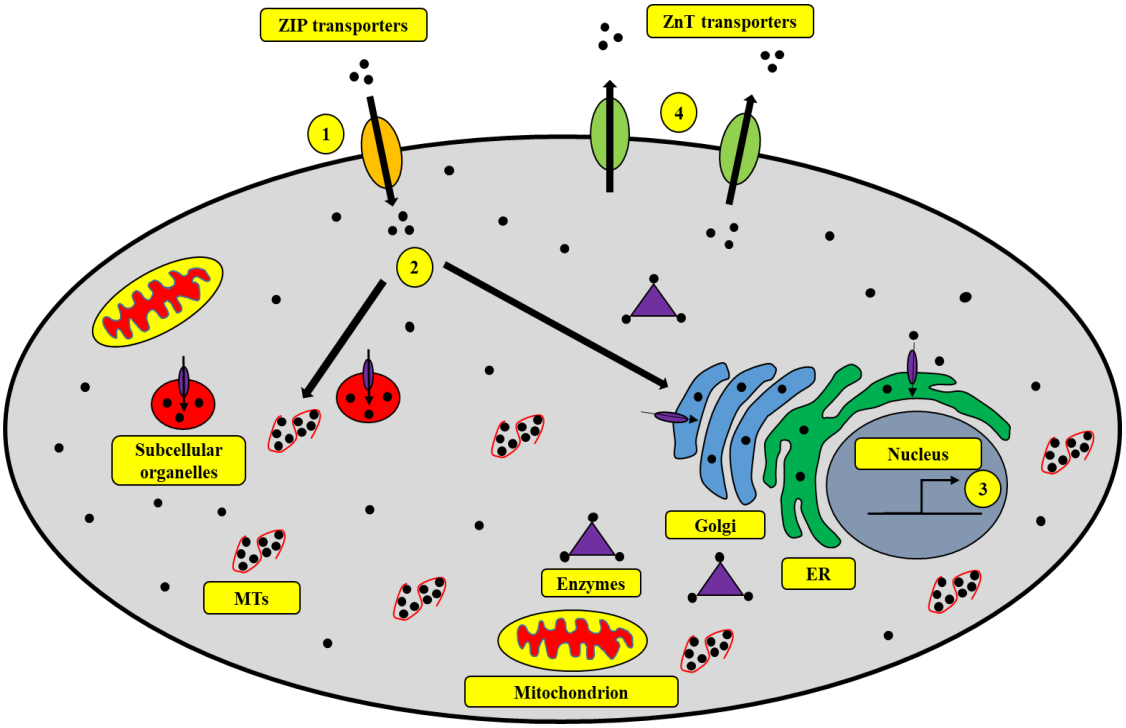

Fig 1.3 Schematic of the mechanisms in response to extracellular zinc

Zinc ions enter the cell through ZIP ion transporters (1). The increase of $[Zn^{2+}]_i$ leads to sequestration via metallothioneins in the cytoplasm and ZnT in organelles to reduce cytosolic zinc concentrations (2). The cell undergoes up-regulation of metallothionein and ZnTs that sequester zinc ions into organelles for detoxification (3). Up-regulation of ZnT transporters allow efflux of excess intracellular zinc (4).

1.5 Potential regulation of zinc homeostasis in the cell by protein kinase CK2

As alluded previously, zinc homeostasis can also be regulated at the protein level (Hershfinkel et al., 2001; Laity et al., 2001). In response to the extracellular stimuli such as hormones or growth factors, CK2 was found to phosphorylate the zinc channel, ZIP7, which is located in the membrane of the endoplasmic reticulum (Taylor et al., 2012). Consequently, zinc ions in ER store were released and intracellular concentration of zinc increased, triggering a cascade of downstream signal transduction. This finding demonstrates that CK2 is involved in regulating zinc homeostasis. However, further investigation is necessary to unravel CK2's potential role in regulating other zinc transport proteins.

The emerging evidence from our laboratory and that of others, demonstrates that CK2 regulates the cell's response to other metal or metalloid ions such as aluminium (Adams et al., 2002; Becaria et al., 2002), arsenic (Johnson et al., 2016) and chromium (Johnson, 2016). By employing the non-biased high throughput functional genomics platform – genome-wide deletion mutant screening of *S. cerevisiae,* my lab has screened a panel of metal ions (Al^{3+}, As^{3+} and Cr^{6+}) with 4873 gene deletion mutants in the past years. A striking finding from these three datasets is that CK2 deletion mutants (*cka1*Δ, *cka2*Δ, *ckb1*Δ and *ckb2*Δ) showed diverse phenotypes against the metal ions. The deletion of the *CKA2* gene (the yeast equivalent to the mammalian *CSNK2A2* which encodes CK2α') leads to a significant resistance to Al^{3+}, whilst the deletion of *CKB1* or *CKB2* (the yeast counterpart of mammalian *CSNK2B* encoding for CK2β) renders the yeast tolerant to As^{3+} and Cr^{6+} (Johnson et al., 2016). *CKA2* was found to be involved in regulating zinc transport in *S. cerevisiae* (Tun et al., 2014; Johnson et al., 2016). Biochemical analysis by ICP-MS

demonstrates that the resistant phenotype of these CK2 subunit deletion mutants is due to the significantly reduced intracellular accumulation of Al^{3+}, As^{3+}, Cr^{6+} and Zn^{2+} (Johnson et al., 2016). Therefore, all these findings demonstrate that CK2 regulates metal ion uptake and toxicity. Furthermore, as mentioned earlier, in Neuro-2a cells, CK2α' is shown to regulate zinc uptake (Zaman et al., 2016). Consequently, this study seeks to investigate the role of CK2 and zinc in breast and prostate cancer cells.

The characteristics of Al^{3+}, As^{3+}, Cr^{6+} and Zn^{2+} are diverse, which offers no clue to the underlying reason shared by all of these metals in regards to their regulation by CK2 in the cell. For example, aluminium is a post-transition metal belonging to the *P* block of the periodic table, with an atomic number of 13. Al^{3+} is toxic and has no proven biological roles. Trace quantities of aluminium are present in drinking water and foods (de Paiva et al., 2020; Edzwald, 2020). Aluminium can accumulate in the body through ingestion and is linked to multiple neurological disorders such as Alzheimer's disease (Exley and Clarkson, 2020; Van Dyke et al., 2021). Arsenic is a metalloid that also belongs to the *P* block of the periodic table, with an atomic number of 33. As^{3+} is very toxic and can be present in the contaminated ground and drinking water, air and foods (Medunić et al., 2020). Its mining and industrial usage lead to the increased contamination of water and crops (McCarty et al., 2011; Sohn, 2014).

Chromium is a transition metal belonging to the *d* block of the periodic table, with an atomic number of 24. It has adverse effects on living organisms such as lung cancer amongst chromate-exposed workers (Coyle et al., 2006; Beveridge et al., 2010; Poonia et al., 2021). Chromium's biological roles are complicated due to the properties of its two prominent oxidation variants, the hexavalent Cr^{6+} and the trivalent Cr^{3+}. Cr^{6+} is found to be highly toxic whilst Cr^{3+} is considered as a micronutrient and commonly used in health

supplements (Urbano et al., 2012; Liu et al., 2015; Wu et al., 2016). In contrast, zinc is a transitional metal in the *d* block of the periodic table, with an atomic number of 30. Zn^{2+} is the most crucial trace metal ion after iron ($Fe^{2+/3+}$) to all living organisms (Tang et al., 2017; He et al., 2018; Zeng et al., 2019). The biological functions of Zn^{2+} have been known for a long period of time, such as its involvement in gene expression (Vallee, 1983; Chasapis et al., 2020), the stabilisation of proteins and nucleic acids structure (Vallee and Auld, 1990; Bafaro et al., 2017), subcellular organelle (Vallee and Auld, 1990; Bafaro et al., 2017), the activity of numerous enzymes (Eide, 1998; Bafaro et al., 2017) and signal transduction as a second messenger (Grummt et al., 1986; Bafaro et al., 2017). It has been projected that roughly 10% of all proteins in eukaryotic cells bind zinc, which suggests there are roughly 3000 zinc proteins in humans (Andreini et al., 2006; Maret, 2012; Bafaro et al., 2017).

The role of CK2 in regulating metal ions in the cell requires more research, and this is exactly what this project is about. I have focused on zinc because of its prominence in cellular functions and cancer development.

1.6 Protein kinase CK2

1.6.1 The structure of CK2

In mammalian cells, CK2 is a heterotetramer comprised of dual catalytic (α and/or α') subunits bound to a central homodimer of non-catalytic regulatory (β) subunits (Fig. 1.4) (Meggio and Pinna, 2003). Zinc plays an essential role here to hold the two β subunits together. The two catalytic isoforms are designated as CK2α and CK2α' (Litchfield, 2003). In contrast to mammalian CK2β, two β subunits of CK2, designated as *CKB1* and *CKB2*, have been found in *S. cerevisiae* (Litchfield, 2003). As shown in Fig. 1.4, with mammalian CK2, tetrameric CK2 complexes may exist in three different tetramers (ααββ, αα'ββ and α'α'ββ) (Litchfield, 2003). In *S. cerevisiae*, CK2 can also be in three different quaternary makeups (ααβ1β2, αα'β1β2 and α'α'β1β2) (Meggio and Pinna, 2003). For mammalian cells, the size of catalytic subunits varies between 36 and 44 kDa, whereas the size of the beta subunits is 25kDa (Schnitzler et al., 2014).

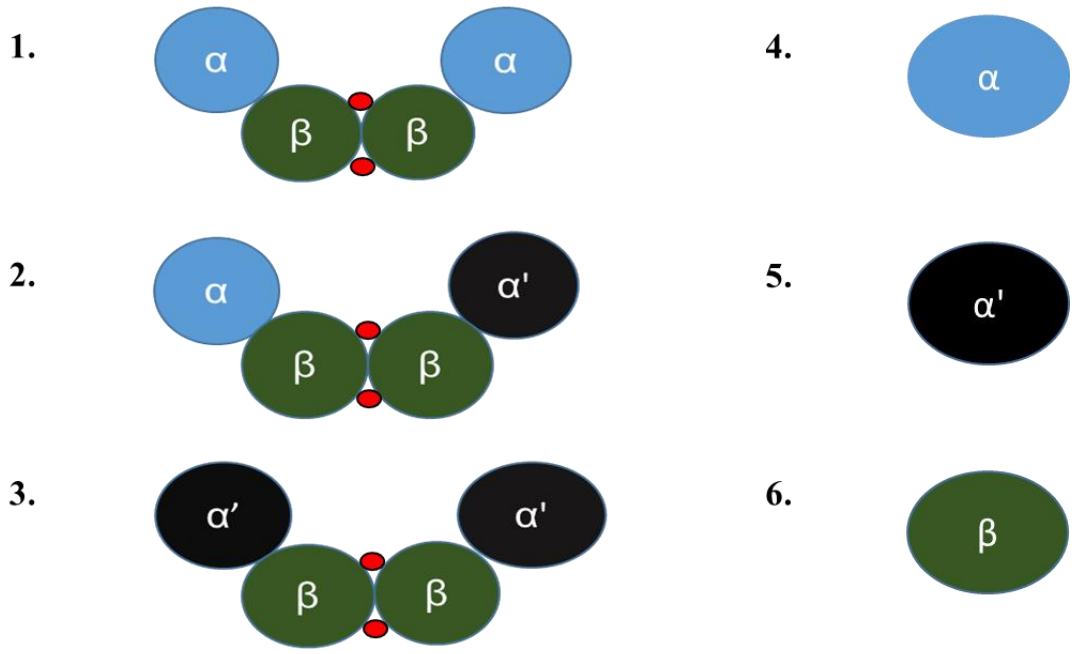

Fig 1.4 Tetrameric isoforms and monomeric subunits of CK2 in mammalian cells

In mammalian cells the CK2 tetramer has three potential isoforms ααββ (1), αα'ββ (2) and α'α'ββ (3). The preliminary step in tetramer formation is the development of a β homodimer to which the catalytic subunits α or α' affix. The various combinations of catalytic subunits α (4) and α' (5) attach to the β regulatory subunit (6) which accounts for the different isoforms of the CK2 tetramer. The red dot denotes zinc atom.

Through crystallographic studies it has been shown that the enzyme CK2 consists of a fold formed by two domains; β-sheet based N-terminal domain and a C-terminal domain that contains several α-helices, as can be seen in Fig. 1.5 (Pechkova et al., 2003; Bischoff et al., 2011). Moreover, the active site of CK2 is located in a cleft between the two domains (Bischoff et al., 2011). The differences in the α and α' subunits give rise to different three dimensional configurations (Bischoff et al., 2011). The characteristics of CK2β subunits include four cysteines in a zinc finger-like arrangement (Allende and Allende, 1995). The zinc finger motif plays a role in dimerisation of β subunits which mediate interactions between CK2 and its substrate proteins (Mackay and Crossley, 1998).

Like any other protein kinase involved in signal transduction, the reversible phosphorylation of protein substrates is a major mechanism for the regulation of a broad spectrum of fundamental cellular processes such as the cell cycle and gene expression (Meggio and Pinna, 2003). As is known, the human genome encodes several hundred distinct protein kinases, hence it is not surprising that a third of all cellular proteins appear to be phosphorylated and that many proteins appear to be phosphorylated at several specific sites or signature sequences (Litchfield, 2003). Accordingly, on average, each protein kinase may phosphorylate a few dozen proteins within the cell (Litchfield, 2003; Meggio and Pinna, 2003). Intriguingly, at present, well over 300 potential physiological protein targets of CK2 have been identified (Meggio and Pinna, 2003). Why can CK2 phosphorylate such a large quantity of proteins? The possible reason behind it could be due to the shared signature sequence amongst protein substrates (Meggio and Pinna, 2003). As the list of likely protein targets of CK2 continues to accumulate, it becomes increasingly evident that CK2 has the potential to participate in the regulation of a diverse selection of cellular processes such as cell proliferation or apoptosis. Along this line of

reasoning, CK2 could potentially phosphorylate certain ZIP and ZnT proteins apart from ZIP7 which has already been demonstrated (Taylor et al., 2012).

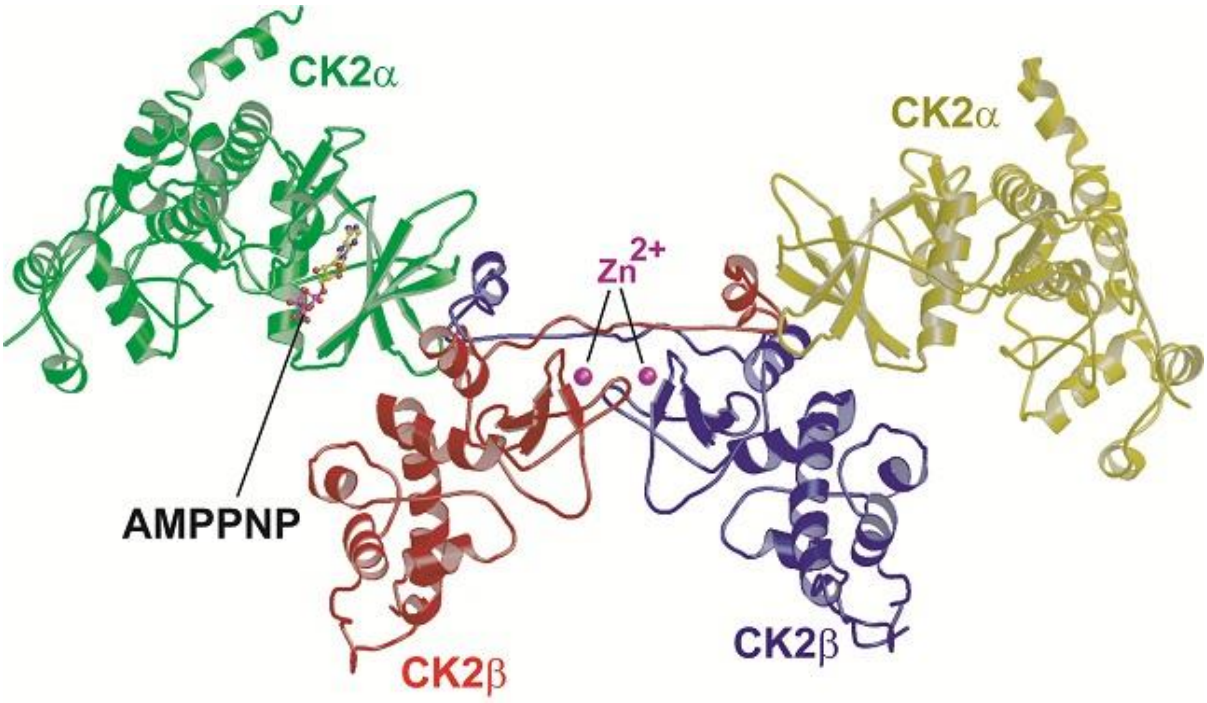

Fig 1.5 Structural illustration of CK2 tetrameric holoenzyme

A ribbon diagram representation of the crystal structure of tetrameric CK2 (ααββ) obtained from Protein Data Bank (PDB ID 4DGL). The catalytic α subunits flank the central homodimer of regulatory CK2β subunit. AMPPNP is the competitive inhibitor of ATP, which binds to the active site of CK2.

1.6.2 Biological roles of CK2

Studies in the past decades indicate that CK2 plays multiple roles in regulating cellular functions, including cell proliferation (Guerra and Issinger, 1999; Meggio and Pinna, 2003; Kappes et al., 2004). CK2 is required for progression through both the G1/S and G/M transition (Zatta et al., 2009). Additional evidence for the role of CK2 in the G2/M transition and mitosis comes from the observation that CK2 is associated with the mitotic spindle and with centrosomes (Litchfield, 2003). The demonstration that CK2α and CK2β are phosphorylated in mitotic cells provides a further indication that CK2 is a regulatory participant in the life of a cell (Zatta et al., 2009). The fact that CK2 is constitutively active demonstrates its prominence and necessity to cell survival (Schnitzler et al., 2014). Since its discovery, CK2 has been implicated in the phosphorylation of DNA and RNA polymerase, DNA topoisomerase, the oncogene products of *fas*, *myc* and SV-40 large T and of the p53 tumour suppressor gene (Pinna, 1990; Meggio and Pinna, 2003). In addition, several reports have presented evidence linking CK2 with the regulation of the cell cycle and with the induction of cell growth (Allende and Allende, 1995). Interestingly, it has been proposed that the proteins phosphorylated by CK2 may make up one quarter of the eukaryotic phosphoproteome (Meggio and Pinna, 2003). Despite the many years of research however, several aspects of CK2 are yet to be elucidated such as regulatory mechanisms involving the role of CK2 in metal ion uptake and toxicity. Within this study, the focus will be on the role of CK2 subunits in modulating zinc homeostasis in the cancer cells.

As of 1984 it has been identified that the function of CK2 is intensified in rapidly proliferating tissue (Guerra et al., 1999). Studies have established that CK2 expression is up-regulated in all cancers examined and this correlation has prompted studies on CK2's

role in oncogenesis (Trembley et al., 2009). Interestingly, it has been demonstrated that elevated levels of CK2 in cancer tissue is an indicator of dysplasia instead of implying increased proliferation (Faust et al., 1999). Dysregulation of CK2 invokes unwarranted oncogenic capability on cells even though CK2 is not officially classed as an oncogene (Trembley et al., 2009). It has been discovered that over-expression of CK2α coupled with TAL1, a transcription factor, resulted in accelerated leukemogenesis in mice (Kelliher et al., 1996). CK2 over-expression has been linked to the development of lymphoma and this is synergistic with co-expression of the c-myc oncogene (Seldin and Leder, 1995). Moreover, over-expression of CK2α and loss of p53, a tumour suppressor gene, resulted in marked increase of lymphoma in mice (Landesman-Bollag et al., 1998). Furthermore, it has been discovered that CK2 can phosphorylate β-catenin and is a progressive regulator of the Wnt signaling pathway (Seldin et al., 2005). Interestingly, it has been revealed that CK2 regulates the basal $NF_{\kappa}B$ through phosphorylation of IKB (Landesman-Bollag et al., 2001).

Regarding cancer development, changes in cellular zinc concentration are likely the result of alterations in the activation and/or expression of zinc transporters ZIPs and ZnTs, which may involve CK2. In prostate cancer, a potential mechanism for the dramatically diminished concentration of zinc in malignant tissue is found with the down-regulation of ZIP1 (Guerinot, 2000; Prasad et al., 2009; Song and Ho, 2009). Conversely, it has been reported that zinc accumulation experimentally induced through over-expression of ZIP4, leads to enhanced progression of established pancreatic cancer (Grattan and Freake, 2012). Similarly, ZIP6 overexpression and/or activation has been observed to be of importance for breast, pancreatic, cervical and prostate cancer (Guerinot, 2000; Kagara et al., 2007; Song and Ho, 2009; Grattan and Freake, 2012). It is unclear if CK2 is involved in the expression of ZIP1, ZIP4 and ZIP6.

1.7 Breast anatomy and breast cancer

1.7.1 Anatomy and function of adult female breast

Adult female breasts are made up of fatty, lymph nodes, connective and glandular tissues. It is comprised of approximately 15-20 lobules (glands) which are arranged in clusters (Fig. 1.6). Each lobule is made up of alveoli. All lobules are linked by a network of ducts (Stone and Wheeler, 2015). For lactation to occur, hormones such as estrogen, prolactin and progesterone are involved for milk production and secretion to occur (Geddes, 2007).

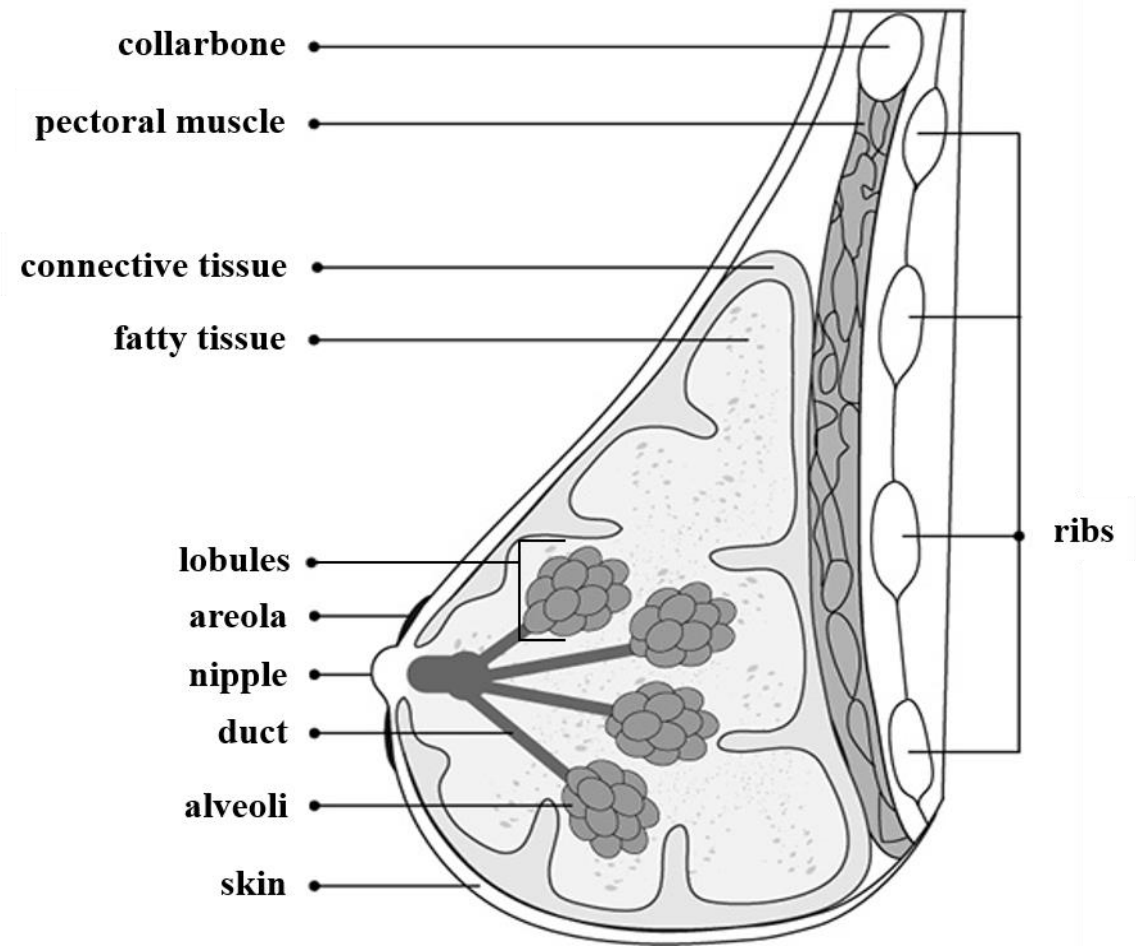

Fig 1.6 Anatomy of female breast

The adult female breast has lobules that branch out from the nipple. Each lobule holds tiny hollow sacs referred to as alveoli. The lobules are linked together by a network of thin ducts.

1.7.2 Breast cancers

Breast cancers often initiate in the ducts (ductal carcinoma) or within the lobules (lobular carcinoma) due to uncontrolled cellular growth under various carcinogenic influences (Kelsey et al., 1993). Studies have classified breast cancer as the second highest in terms of incidence (2,088,849 cases) and the fifth highest mortality rate (626,679 deaths) amongst the ten most prominent cancers in humans worldwide (Bray et al., 2018). There are various risk factors such as genetic alteration/mutations, aging, estrogen, family history and unhealthy lifestyle (Grattan and Freake, 2012). Molecularly, breast cancer is a heterogeneous disease and through gene expression analysis, four subtypes of breast cancer are classified based on markers such as estrogen receptors (ERs), progesterone receptors (PR), human epidermal growth factor receptor 2 (HER2), including Luminal A ($ER^+/PR^+/HER2^-$), Luminal B ($ER^+/PR^+/HER2^+$), Basal ($ER^-/PR^-/HER2^-$) and HER2-enriched ($ER^-/PR^-/HER2^+$) (Ambion; Ebara et al., 2000; Desoize, 2004; Grattan and Freake, 2012). These terms, "luminal" and "basal", refers to the outer basal cells and inner luminal cells in the epithelial glandular network (lobules) of breast. These different breast cancer subtypes vary in incidence, aggressiveness and response to treatment. Studies have shown that basal breast cancer tumours express higher levels of metallothioneins, *ZIP4*, *ZIP14* genes and lower levels of *ZIP6*, *ZIP9*, *ZIP11* compared to luminal and HER2 overexpression tumours (Chandler et al., 2016). However, the underlying molecular mechanism for such findings was not clear then and remains to be investigated.

It is important to note that Zn^{2+} accumulation in breast cancer cells directly correlates with abnormal expression of *ZIP6*, *ZIP7*, *ZIP10* and *SLC30A2* (Kagara et al., 2007; Taylor et al., 2007; Taylor et al., 2008; Lopez et al., 2011; Taylor et al., 2012; Taylor et al., 2016). This implies that various types of breast cancers might have their unique signature of genes

for zinc homeostasis. MCF-7 luminal breast cancer cell line is less aggressive and categorised as non-invasive compared to the MDA-MB-231 breast cancer cell line, categorised as aggressive, invasive and a poorly differentiated form of triple-negative breast cancer (Chandler et al., 2016). Triple-negative breast cancer is a type of breast cancer that is negative to the hormones estrogen and progesterone along with a protein receptor called HER2 (Foulkes et al., 2010; Garrido-Castro et al., 2019). Clinically, triple-negative breast cancer patients have limited treatment options with a high possibility of relapse (Chandler et al., 2016; Reddy et al., 2018). More research is required to understand the involvement of zinc homeostasis in breast cancer progression and malignancies.

Not surprisingly, many genes are strongly linked with breast cancer development such as breast cancer type 1 (*BRCA1*) and 2 (*BRCA2*), human epidermal growth factor 2 (*HER2*), epidermal growth factor receptor (*EGFR*), *Ras* gene family (H-ras, K-ras and N-ras), *p53*, retinoblastoma protein 1 (*RB1*), phosphatase and tensin homolog (*PTEN*), ataxia-telangiectasia mutated (*ATM*), cyclin D1 (*CCND1*), cadherin-1 (*CDH1*), nucleoside diphosphate kinase A (*NME1*), phosphatidylinositol-4,5-bisphosphate 3-kinase, catalytic subunit alpha (*PIK3CA*), fragile histidine triad protein (*FHIT*) etc. have been linked to breast tumour initiation and development (Kagara et al., 2007; Prasad et al., 2009; Grattan and Freake, 2012; Stephens et al., 2012).

As previously mentioned, studies have determined that zinc levels are substantially increased in breast cancer tissue compared with normal breast tissue (Costello and Franklin, 2006). A study by Rizk and Sky-Peck (1984) also showed elevated zinc levels in neoplastic human breast tissue compared to normal breast tissue. Studies utilising invasive basal-like breast cancer cell lines MDA-MB-231 and MDA-MB-435S confirmed higher expression of ZIP10 and increased zinc level compared to less invasive luminal-

like breast cancer cells such as MCF-7, T47D, ZR75-1 and ZR75-30 (Costello and Franklin, 2006; Kagara et al., 2007; Franklin and Costello, 2009). Consistent with this notion, it has been discovered that increased ZIP10 and ZIP6 (LIV1) expression correlates with increased aggressiveness, progression and metastasis of breast cancer (Grattan and Freake, 2012).

1.8 Prostate gland anatomy and prostate cancer

1.8.1 Anatomy and function of the prostate gland

The adult prostate is a walnut-sized exocrine gland of the male reproductive system which consists of four zones: anterior, transition/periurethral (making up 5%), peripheral (making up 70%) and central (making up 25%) zones (Fig. 1.7) (McNeal et al., 1988; Kumar and Majumder, 1995). Histologically, the prostate gland is mainly divided into central and peripheral zones (Kumar and Majumder, 1995). The unique metabolic and functional activity of the prostate is the accumulation of higher concentration of zinc and citrate (Kumar and Majumder, 1995; Yamasaki et al., 2007; Song and Ho, 2009). The prostate is responsible for the secretion of prostatic fluid (pH 6.4) comprising 20% volume in semen containing lipids, metal ions, amines and enzymes (e.g., fibrinolysin, coagulum lysing enzymes, coagulase etc.) essential for ensuring the homeostatic environment for spermatozoa (Kumar and Majumder, 1995; Grattan and Freake, 2012; Kambe et al., 2015).

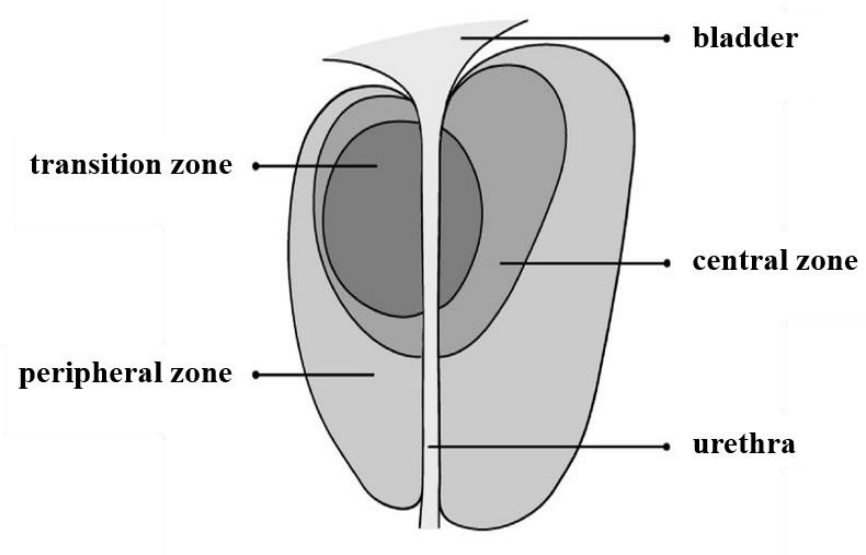

Fig 1.7 Anatomy of the male prostate

The male prostate is a walnut-sized exocrine gland of the male reproductive system. It is comprised of distinct regions, transition zone, central zone and peripheral zone.

1.8.2 Prostate cancer

Prostate cancer develops when cells of the prostate gland grow in an abnormal and uncontrolled manner (Ferlay et al., 2018). Strikingly, epidemiological studies have demonstrated that prostate cancer is the second highest diagnosed type of cancer after lung cancer among 10 commonly occurring cancers in men worldwide (Torre et al., 2015). It has been estimated that one in six men will be diagnosed with prostate cancer over the age of 85, with 63% of cases diagnosed in men over the age of 65 (Costello and Franklin, 2006; Bray et al., 2018; Ferlay et al., 2018). Prostate carcinoma commonly arises in the peripheral zone whilst benign prostate hyperplasia (BPH) usually arises in central and transitional zones of the prostate gland (Ferlay et al., 2018). Adenocarcinoma type of prostate cancer accounts for approximately 80% of all cancers of the prostate, which is developed from the secretory epithelial cells of the peripheral zone (Song and Ho, 2009; Torre et al., 2015; Ferlay et al., 2018). The malignant cells commonly grow and spread to the bladder, bone, lymph nodes and other organs of the body via the blood-stream (Torre et al., 2015; Ferlay et al., 2018).

Interestingly, studies have demonstrated that normal prostate epithelial cells are zinc accumulating cells and contain elevated zinc level in comparison to malignant cells of the prostate (Franklin et al., 2005; Costello and Franklin, 2006; Cousins et al., 2006). ZIP1 is down-regulated in human malignant prostate cancer cells derived from metastatic prostate cancer tissue (PC3, DU145 and LNCaP) (Franklin et al., 2005; Zou et al., 2011; Kambe et al., 2014). Similarly, it has been determined that zinc importers ZIP2, ZIP3, ZIP4 and ZIP9 transporters are down-regulated in prostate cancer cells, while up-regulated in normal epithelial cells of the prostate (Rishi et al., 2003; Franklin et al., 2005; Costello and Franklin, 2006; Franklin and Costello, 2009; Huang and Tepaamorndech, 2013). This

indicates that prostate cancer cells evade the tumour suppression effects of zinc, such as suppression of abnormal cell proliferation and apoptosis induction in cells by maintaining low cellular zinc levels (Franklin et al., 2005; Costello and Franklin, 2006; Cousins et al., 2006; Franklin and Costello, 2009).

1.9 Experimental approach

1.9.1 Utility of breast and prostate cancer cell lines

Cell lines are a workhorse in research and play an invaluable role as *in vitro* models in cancer research. In order to identify the roles of zinc and CK2 in cancer cells, this study employs breast (MCF-7 and MDA-MB-231) and prostate (PC3 and DU145) cancer cell lines and normal breast (MCF10A) and prostate (RWPE-1) epithelial cell lines (Table 1.4). The two cancer types are of opposite zinc profiles as described previously, which should serve as an effective tool for this project.

The MCF-7 cell line was initially isolated from a 69-year-old Caucasian woman named Frances Mallon who died in 1970 from a malignant luminal breast cancer. Dr. Soule and colleagues established the MCF-7 cell line in 1973 from the pleural effusion of Frances Mallon with metastatic cancer (Soule et al., 1973). In the 1970's, a major focus was directed towards finding definitive proof that estrogen directly stimulated tumour growth (Levenson and Jordan, 1997). There was a major breakthrough in breast cancer research when it was discovered that certain types of breast cancer were estrogen receptor positive (ER^+) and that the anti-estrogen drug Tamoxifen was found to inhibit the growth of MCF-7 breast cancer cells (Soule et al., 1973; Levenson and Jordan, 1997). In relative recency, it was revealed that the MCF-7 breast cancer cell line was ER^+, progesterone receptor (PR^+) and belonged to the Luminal A molecular subtype of breast cancer (Baguley and Leung, 2011; Shirazi et al., 2011). The MCF-7 cell line is a less aggressive and non-invasive cell line compared to the MDA-MB-231 breast cancer cell line.

The MDA-MB-231 cell line was established from a pleural effusion of a 51-year-old Caucasian female with metastatic mammary basal adenocarcinoma (Cailleau et al., 1978). The cell line is extremely aggressive, invasive and a poorly differentiated form of triple-

negative breast cancer, as the cell line is ER^-, PR^- and $HER2^-$ (Liu et al., 2003; Chavez et al., 2010). Initially, the MDA-MB-231 cell line was classed as a form of basal breast cancer due to being ER^-, PR^- and $HER2^-$. It was later discovered to also exhibit down-regulation of Claudin-3 and Claudin-4, low expression of the Ki-67 proliferation, markers for epithelial-mesenchymal transition and expression features associated with mammary cancer stem cells, such as the $CD44^+CD24^-$/low phenotype (Holliday and Speirs, 2011). Moreover, it was demonstrated to be E-cadherin negative and express mutated p53 (Liu et al., 2003; Chavez et al., 2010). Clinically, triple-negative breast cancer patients have limited treatment options with a high possibility of relapse. For this reason, many studies utilise the MDA-MD-231 breast cancer cell line in their research.

The PC3 prostate cancer cell line was established in 1979 from a 62-year-old Caucasian male from a lumbar vertebral (bone) metastasis stage four prostate cancer (Kaighn et al., 1979). Studies thereafter have revealed that PC3 cells do not respond to androgens, fibroblast growth factors or glucocorticoids, but rather are influenced by epidermal growth factors (Ching et al., 1993; Tai et al., 2011). It has been discovered that PC3 cells express low levels of testosterone-5-alpha reductase and do not express prostate-specific antigens (PSA) (Tai et al., 2011). Overall, PC3 cells are hormone insensitive and do not show androgen receptor nor expression of PSA mRNA, however, the cells show high levels of transforming growth factor-alpha (TGF-α) and epidermal growth factor receptor mRNA expression (Ching et al., 1993). Considering the expression profile and morphological characteristics, PC3 cells can be classified as a poorly differentiated adenocarcinoma (Ching et al., 1993; Tai et al., 2011). The PC3 prostate cancer cell line has been identified to have a higher metastatic potential compared to the DU145 prostate cancer cell line (Pulukuri et al., 2005).

The DU145 prostate cancer cell line was derived in 1975 from a 69-year-old male with a metastatic brain tumour (Stone et al., 1978). It has been identified that prostatic acid phosphatase (PAP) expression is modestly expressed in DU145 cells, but androgen receptor, PSA mRNA and protein expression are non-existent in DU145 cells (Sherwood et al., 1990). However, the cells do express cytokeratin-7 (CK-7), CK-8, CK-18 and CK-19 (Stone et al., 1978; Sherwood et al., 1990). Studies have demonstrated that subcutaneous injection of DU145 cells into nude mice have produced tumours that maintained their phenotype and genotype (Mickey et al., 1977; Bastide et al., 2002).

1.9.2 Utility of normal breast and prostate cell lines

The MCF10A cell line was isolated from the mammary gland of a 36-year-old Caucasian woman with extensive fibrocystic disease, comprising of increased mammary fibrous stroma containing numerous dilated mammary ducts (Soule et al., 1990). Furthermore, MCF10A cells are a non-tumuorigenic mammary epithelial cell line derived from benign proliferative breast tissue that is widely used as *in vitro* model for studying normal breast cell function and transformation (Soule et al., 1990; Tait et al., 1990). Studies have determined that MCF10A cells do not express the estrogen receptor, but is responsive to insulin, glucocorticoids, cholera endotoxin and epidermal growth factor (EGF) (Keller et al., 2010). Morphologically, MCF10A cells display characteristics of luminal cells but not of myoepithelial cells (Neve et al., 2006).

The RWPE-1 cell line was derived from a 54-year-old Caucasian male, with epithelial cells isolated from the peripheral zone of the prostate (Webber, 1979). RWPE-1 cells are a great model to investigate the molecular mechanisms underlying the proliferation of benign prostatic epithelial cells. RWPE-1 cells express androgen receptor, cytokeratin 18, cytokeratin 8 tumour suppressor gene p53 (Bello et al., 1997). The RWPE-1 cell line was

immortalised with the human papillomavirus (HPV) with subsequent isolation and propagation (Ambion; Webber, 1979; Webber et al., 1999). Moreover, RWPE-1 cells typically respond to EGF, TGF-β treatment and do not form tumours in mice (Webber, 1979; Bello et al., 1997; Webber et al., 1999).

Table 1.4 The cell lines utilised in this study

Cell line	Cancer type	Chromosomal profile	References
MCF-7	Luminal breast cancer	The chromosome numbers of MCF-7 breast cancer cell line range from hypertriploidy to hypotetraploidy (modal number = 82; range = 66 to 87).	(Rondón-Lagos et al., 2014).
MDA-MB-231	Basal breast cancer	The MDA-MB-231 breast cancer cell line has been derived from aneuploid female (modal number = 64, range = 52 to 68), with chromosome counts in the near-triploid range.	(Cailleau et al., 1976)
PC3	Prostate cancer with high metastatic potential	The PC3 cell line has a near-triploid characteristic with a modal number of 62 chromosomes.	(Ohnuki et al., 1980; Chen, 1993)
DU145	Prostate cancer with moderate metastatic potential	The DU145 cell line has a hypotriploid karyotype with 62 chromosomes.	(Pan et al., 1999)
MCF10A	Normal breast epithelial cell	The MCF10A normal breast cell line has a diploid karyotype.	(Soule et al., 1990; Yoon et al., 2002)
RWPE-1	Normal prostate epithelial cell	The RWPE-1 normal prostate cell line has a diploid karyotype.	(Webber, 1979; Bello et al., 1997)

1.9.3 The relevance of breast and prostate cancer cell lines to clinical cancers

Cancer cell lines play a significant role in the field of cancer research. Researchers in multiple prestigious institutes worldwide have utilised both breast (MCF-7 and MDA-MB-231) and prostate (PC3 and DU145) cancer cell lines in their research. For example, the use of breast cancer cell lines along with the use of mouse models was essential in the discovery of the drug Tamoxifen which has played a pivotal role in the treatment of all stages of oestrogen-receptor-positive breast cancer (Clemons et al., 2002; Jordan, 2003; Meiser et al., 2017). Millions of breast cancer patients worldwide have benefited from using Tamoxifen for the treatment of their breast cancer. Similarly, by employing the cancer cell lines, the anticancer drug, Cisplatin, was developed. It was the first FDA-approved platinum compound for cancer treatment in 1978 (Kelland, 2007; Frezza et al., 2010).

Cancer cell lines and their normal counterparts are routinely used in studying the molecular mechanisms of cancer development (Sakallı Çetin et al., 2017; Nguyen et al., 2018; Sun et al., 2018; Zhu et al., 2018; Kim et al., 2020). Therefore, this study employed MCF-7 and MDA-MB-231 breast cancer cell lines and PC3 and DU145 prostate cancer cell lines, as well as the MCF10A normal breast and RWPE-1 normal prostate cell lines. The findings to be obtained from these cell lines should contribute to our knowledge and understanding of zinc homeostasis in breast and prostate cancer cells and provide avenues for future studies on breast and prostate cancers.

1.9.4 Inhibition of CK2 activity

In order to unravel the role of CK2 in regulating zinc homeostasis, breast and prostate cancer cell lines were treated biochemically with CK2-specific inhibitors 4,5,6,7-

tetrabromobenzotriazole (TBB) (Calbiochem-Millipore) or CX-4945 (Adooq bioscience) (Fig. 1.8) TBB and CX-4945 block the ATP-binding site in CK2 kinase (Duncan et al., 2008; Cozza et al., 2009). CK2 inhibition has been the subject of intensive study (Duncan and Litchfield, 2008; Jacob P. T., 2013). Studies of CK2 structure have revealed the ATP binding domains are highly conserved between monomeric subunits and the tetrameric holoenzyme (Chantalat et al., 1999; Litchfield, 2003). By using CK2 inhibitors TBB and CX-4945 and zinc treatment, it was expected that we could determine valuable information about CK2's involvement in zinc homeostasis.

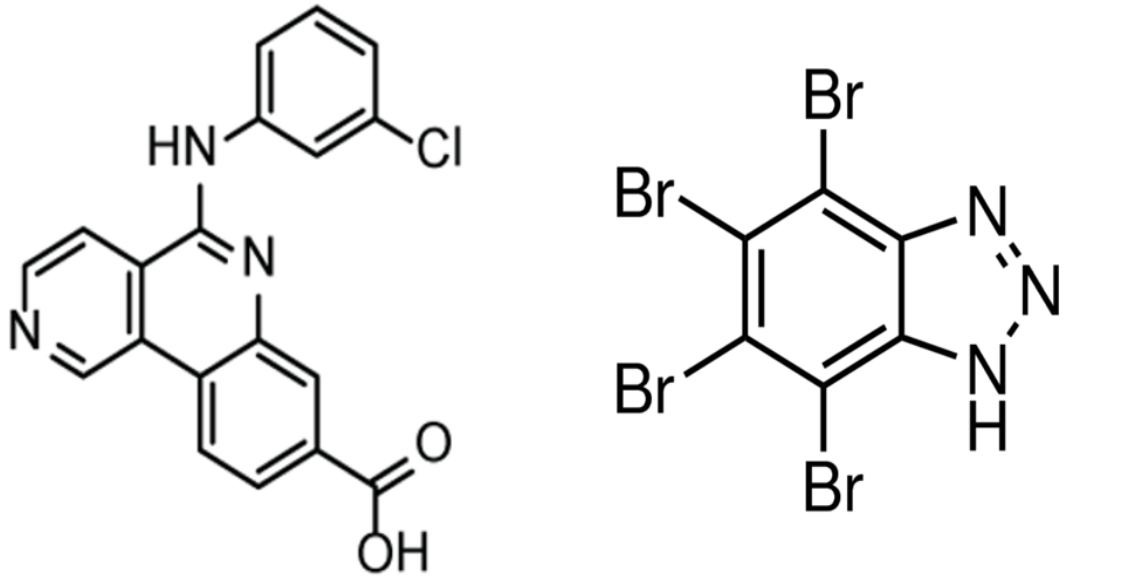

CX-4945 (Silmitasertib) TBB (4,5,6,7-tetrabromobenzotriazole)

Fig 1.8 Structure of CK2 inhibitor TBB and CX-4945

1.9.5 Manipulation of CK2 expression by siRNA

To determine the role of specific CK2 subunits in zinc homeostasis, I utilised subunit-specific siRNA to manipulate the expression of CK2 subunits. siRNA is a powerful tool for gene knockdown. In 1998, Andrew Fire, Craig Mello and colleagues discovered a way to turn off specific genes in the organism, *Caenorhabditis elegans* (Kumar. D. L, 2007). This was achieved via injecting double-stranded RNA interference (RNAi) in the embryos and was found to block the synthesis of the target proteins (Mello. C, 2004). Further studies confirmed that it is double-strand RNA (dsRNA) and not single-stranded RNA (ssRNA) that was responsible for gene silencing, however exact molecular mechanisms were yet to be uncovered at the time of discovery (Kumar. D. L, 2007).

Since its discovery, siRNAs have been found to be comprised of short segments of dsRNA, about 21-24 nucleotides long, with phosphorylated 5' ends and hydroxylated 3' end overhangs (Mello. C, 2004). The endonuclease dicer enzyme (RNase III) has been found to interfere with the translation of proteins by binding to and promoting the degradation of messenger RNA (mRNA) at specifically desired sequences (Aagaard. L, 2007). Once dicer is complexed with the TAR-RNA binding protein (TRBP), it positions the siRNA to the RNA-induced silencing complex (RISC) which contains the slicing protein Argonaute2 (Ago2). Ago2 cleaves the target mRNA molecule amongst bases 10-11, in accordance to the 5' end of the antisense siRNA strand (Kumar. D. L, 2007). The degraded mRNA can no longer be translated into a functional polypeptide. Consequently, siRNAs prevent the expression of the targeted gene due to the silencing of their corresponding mRNA (Fig. 1.9).

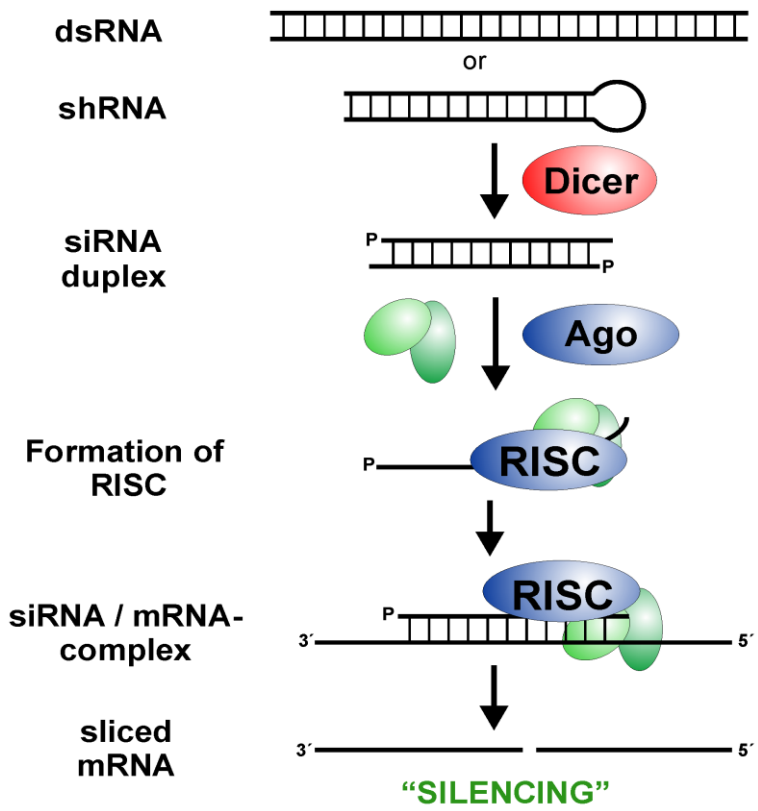

Fig 1.9 siRNA mechanism of knockdown expression

Illustration of siRNA where the Dicer enzyme cuts large double-stranded molecules or RNA into smaller sections of small interfering RNA, which through enzymatic actions of Ago2, cleaves mRNA and has a silencing effect.

Provided that the target mRNA sequences are known, researchers can utilise siRNAs to silence gene expression in mammalian somatic cells as a research tool (Mello. C, 2004). Currently, several oncogenic and mutant tumour suppressor genes present potential targets for the siRNA interference approach. For instance, the p53 protein is mutated in over 50% of human malignancies and specific elimination of p53 mutant protein by siRNA has been shown to result in the restoration of wild-type function (Aagaard. L, 2007). Additionally, siRNA techniques have been widely implemented in studies as a method to reduce the expression of individual genes in order to establish a link between the gene and the gene function (Almedia. R, 2005; Aagaard. L, 2007). By observing the effects of blocking a

gene through siRNA, further insights into the role of the gene in biological pathways can be established.

There are many companies such as Dharmacon (USA) and Sigma-Aldrich (Australia) which provide predesigned and tested siRNA for experimental application. A study by Yamane and Kinsella utilised three specific siRNA's to specifically knockdown expression of CK2 catalytic subunits. These siRNAs were purchased from Dharmacon (USA) (Yamane and Kinsella, 2005). Within this project, the knockdown of CK2 subunit expression (CK2α, CK2α' and CK2β) by their specific siRNA was pursued to dissect the role of individual CK2 subunits in zinc homeostasis.

1.9.6 Next-generation RNA sequencing for identification of genes involved in zinc homeostasis

Next-generation RNA sequencing (RNA-seq) is a high throughput technology, increasingly being used in transcriptomic analysis for discovering differentially expressed genes in varieties of biological contexts. The procedure of RNA-seq involves RNA being extracted from samples of interest, then conversion of pure RNA into cDNA fragments and finally performing sequencing which results in millions of reads mapped to the transcriptome (Ozsolak and Milos, 2011). Once reads are determined and analysed, one needs to identify the differentially expressed genes between samples e.g., controls versus treatments. In this study RNA-seq is employed on the MCF-7 breast cancer cell line to identify the key genes involved in zinc homeostasis. In doing so, we will gain valuable insight into how the MCF-7 breast cancer cells respond to zinc exposure.

1.9.7 qRT-PCR validation

Quantitative reverse transcription polymerase chain reaction (qRT-PCR) is a frequently used biological technique for quantification of nucleic acid molecules in samples (Fleige and Pfaffl, 2006). The technique relies on the detection of a fluorescent reporter signal that is generated equivalent to the amplification of the PCR product. This in turn allows the visualisation of the exponential part of the PCR reaction (Bustin, 2002). Accurate quantification of the fluorescent signal is reliant on the capacity to obtain cycle threshold (CT) values. When the PCR achieves the exponential amplification phase, concentration of PCR target is essentially doubling at each cycle (Fig. 2.1) (Freeman et al., 1999).

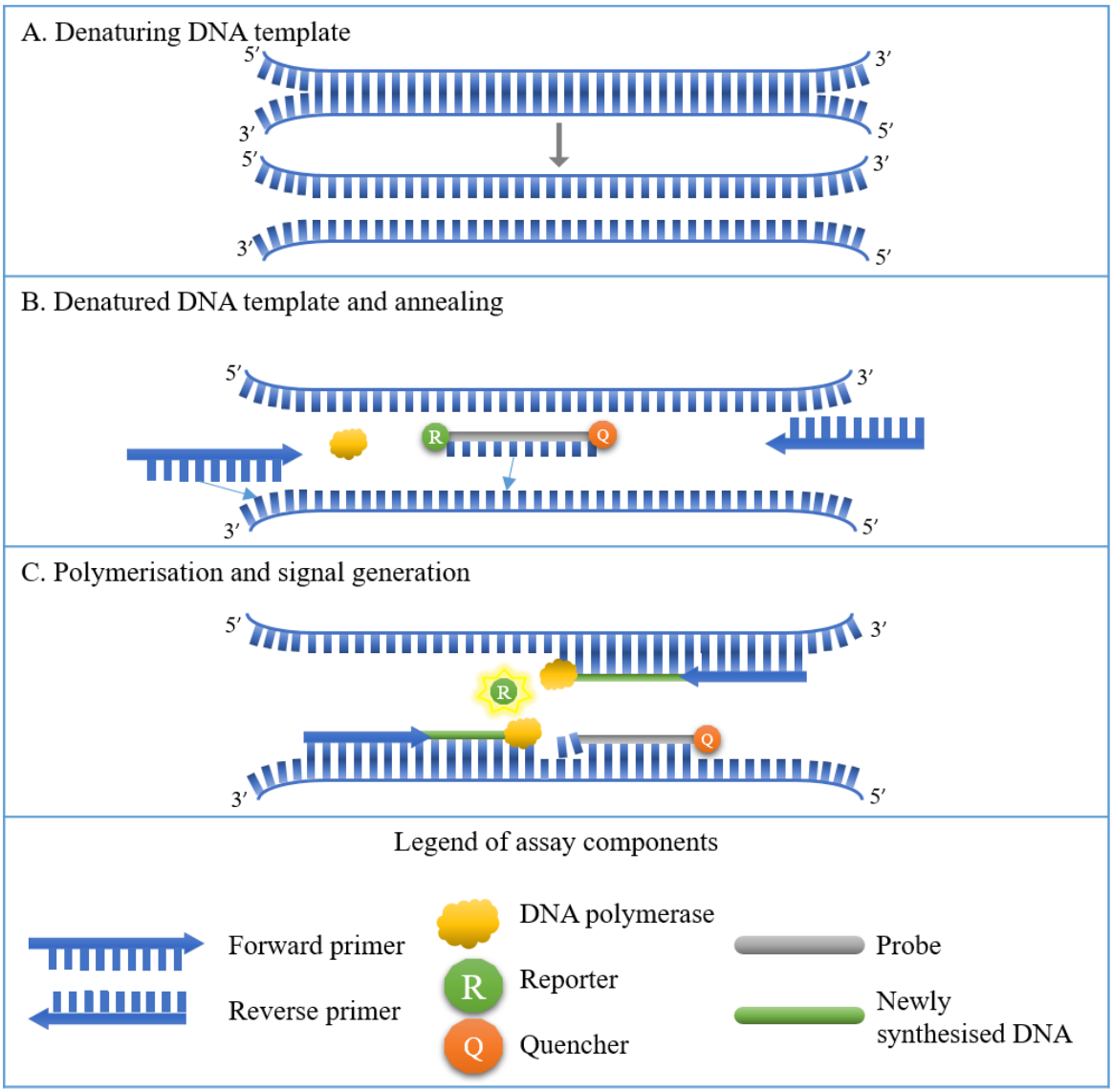

Fig. 2.1 Depiction of the fundamental principle of TaqMan technology

Once double-stranded DNA melts at 95°C, the reaction is cooled to the annealing temperature (60°C) where the primers and probe bind to the target sequences in the cDNA template. Taq polymerase then catalyses the extension of the primer along the template strand. Upon reaching the probe, it relocates the reporter. After the reporter is no longer close to the quencher, it can fluoresce. During each consecutive cycle, higher levels of reporter are released from their vicinity to the quencher and therefore each cycle is characterised by an increase in fluorescence.

1.9.8 Confocal microscopy visualising the zinc ion

Fluorescence confocal microscopy is widely utilised in the research of *in vitro* studies. In essence, fluorescence microscopy uses synthetic fluorophores that are specific for the target molecules and are able to fluoresce when bound to the target and stimulated by light (Patel and McGhee, 2007). The technology can provide details of subcellular location of the target molecules in nuclei, cytoplasm, endoplasmic reticulum or mitochondria (Brelje and Sorenson, 1992). The excitation of light that stimulates the fluorophores for confocal microscopy is usually provided by a laser that is set at a specific wavelength for excitation (Levoy et al., 2004). The fluorophores emission and excitation wavelength of light pass through the same objective but the emission of light eventually hits the light detector. A pinhole is utilised to eliminate scattered light which commonly occurs when conducting fluorescence microscopy. The result is that light is collected from a highly focused point, forming high resolution images of specimens (White et al., 1987).

In this study fluorescent imaging using a confocal microscope was employed to quantify zinc ion uptake using a fluorophore specific for zinc. The intracellular localisation of zinc can be accomplished through the use of fluorophores such as Zinquin and FluoZin-3 AM (Colvin. R et al., 2006). The FluoZin-3 AM probe specific for Zn^{2+} detection was performed in this study to visualise intracellular zinc ions and elucidate the involvement of specific CK2 subunits in zinc ion homeostasis.

1.9.9 Quantifying cellular zinc ion uptake by ICP-MS

Inductively coupled plasma mass spectrometry (ICP-MS) is an analytical technique utilised to quantify elements like metal ions. It is widely used for the quantification of essential biological elements such as iodine, manganese, iron, copper, selenium, calcium, zinc etc. (Geldmacher-von Mallinckrodt and Meissner, 1994). Even though the first developed and functional ICP-MS machine was established close to 40-years ago, current ICP-MS machines are more advanced and can offer high sample through-put, precision and short analysis time of samples (Houk et al., 1980). Essentially, the ICP-MS analyser is made up of six distinct segments which include the sample introduction system, inductively coupled plasma (ICP), interface, ion optics, mass analyser and finally the sensitive detector (Montaser, 1998).

Samples are usually dissolved in a low percentage of nitric acid and are first nebulised in the sample introduction system, generating a delicate aerosol that is later transported to the argon plasma. The high temperature of the plasma (approximately 6000 °C) atomises and ionises the sample, producing ions that are then separated through the interface segment and into a set of electrostatic lenses referred to as ion optics (Wilschefski and Baxter, 2019). The ion optics then directs the ion beam into the quadrupole mass analyser. Then the mass analyser divides ions according to their mass-charge ratio (m/z) and finally, these ions are measured via the detector which can accurately detect ions in parts per billion (ppb) (Houk et al., 1980; Montaser, 1998). ICP-MS analysis will be employed in this study to precisely determine the intracellular zinc levels in the cell lines under control condition and IC_{50} zinc treatment. This would provide insight into the zinc levels in breast and prostate cancer cells.

1.10 Significance of this study

From the above account, it is evident that zinc homeostasis is linked to breast and prostate cancers and that CK2 is related to zinc homeostasis as well as cancers. This study investigates the role of zinc and CK2 in breast and prostate cancer cells. The findings reported here should have a pronounced bearing to basic biology and cancer research. By utilising breast (MCF-7 and MDA-MB-231) and prostate (PC3 and DU145) cancer cell lines and normal breast (MCF10A) and prostate (RWPE-1) epithelial cell lines, the two cancer types with opposite zinc profiles, the molecular details on the roles of zinc and CK2 in cancer cells are obtained, providing meaningful insights and understanding of these two major cancers.

The novelty of this study involves the use of six well established cell lines mentioned above which to date have not been used side by side in any study to better understand the role of zinc homeostasis in breast and prostate cancer cells. Deployment of CK2 inhibitors TBB and CX-4945, siRNA-mediated knockdown and zinc ion specific fluorophores demonstrate the thoroughness of the experimental approach in this project.

In this study, I investigated the transcriptomic response of the breast cancer cells (MCF-7) to the exposure of extracellular zinc using the high throughput next-generation RNA sequencing. The dataset was collected for three time points (T_0, T_{30} and T_{120}) in the time course of zinc treatment. The comprehensive approach, in combination with the time course, is novel for the study of zinc homeostasis in cancer cells. The dataset acquired should provide in-depth molecular details in zinc homeostasis and contribute to the future cancer research.

1.11 Hypothesis

- It is hypothesised that CK2 is involved in zinc ion homeostasis.
- It is also hypothesised that the contrasting zinc profiles in breast and prostate cancer cells are useful in understanding zinc homeostasis in cancer cells.

1.12 Aims

1 To investigate the involvement of CK2 in zinc homeostasis in two breast (MCF-7 and MDA-MB-231) and two prostate (DU145 and PC3) cancer cell lines.

2 To identify differentially expressed genes involved in zinc homeostasis in the MCF-7 breast cancer cell line through next-generation RNA sequencing.

3 To validate the differentially expressed genes identified in the above step using qRT-PCR in the six cell lines, including four cancer cells (breast cancer cell lines MCF-7 and MDA-MB-231 along with prostate cancer cell lines PC3 and DU145) and two control cell lines (MCF10A and RWPE-1).

2 MATERIALS AND METHODS

2.1 General materials

General reagents and consumables utilised in this study were sourced from Sigma-Aldrich (Sydney, Australia), Life Technologies (Australia), Lonza (Switzerland), Applied Biosystems (Australia), CHOICE Analytical (Australia), Labcon (North America) and Greiner Bio-One (Germany). Specific chemicals and solvents were obtained from commercial suppliers detailed in the methods below and they were of analytical grade or higher. Deionised water from a MilliQ^{TM} system (Millipore, Australia) was used in the preparation of buffers and stock solutions.

2.2 Modus operandi of general experimental practice throughout this study

General tissue culture practices, such as passaging cells, plating and treating cells, were carried out aseptically in a class II biological safety cabinet (Gelaire AS-2252.2). Tissue culture media and components of media (e.g., FBS, penicillin/streptomycin) were purchased in sterile form and maintained as such throughout experimental work. Tissue culture reagents, instruments, materials and necessary miscellaneous items were sterilised by autoclaving for 35 min at 121 °C (Tuttnauer 3150EL, Australia). Maintenance of a sterile working space within the class II biological safety cabinet was achieved through 45 minutes of UV exposure and cleaning with 70% (v/v) ethanol immediately before and post experimental work. The non-sterile exterior of all materials that entered the sterile space within the cell culture cabinet was thoroughly sterilised with 70% (v/v) ethanol. Experimental work was always methodically planned and conducted with great attention to detail to prevent any cross contaminations.

2.3 Growth and maintenance of mammalian cell lines

2.3.1 Maintaining and passaging conditions

Two cell lines for breast cancer (MCF-7 and MDA-MB-231) and one normal breast cell line (MCF10A), as shown in Table 2.1, were used herein. MCF-7 (human breast adenocarcinoma, Cat. No. ATCC® CRL HTB-22™) cells were cultured in Dulbecco's Modified Eagle's Medium (DMEM) (Life Technologies, Australia) supplemented with 10% (v/v) foetal bovine serum (FBS) (Life Technologies, Australia) and 1% (v/v) antibiotics (penicillin/streptomycin) (Life Technologies, Australia). MDA-MB-231 (human breast adenocarcinoma, Cat. No. ATCC® CRL HTB-26™) cells were cultured in Leibovitz's L-15 medium (Life Technologies, Australia) supplemented with 10% (v/v) FBS and 1% (v/v) antibiotics. MCF10A (human normal mammary gland epithelial cells, Cat. No. ATCC® CRL-10317™) were cultured in DMEM/F12 Ham's medium (Life Technologies, Australia) supplemented with 5% (v/v) horse serum (Life Technologies, Australia), SingleQuots™ kit (Cat: CC-4136), (Lonza, North America) containing Epidermal Growth Factor (EGF) (20 ng/mL), Insulin (10 µg/mL) 1% (v/v) antibiotics and cholera toxin (100 ng/mL) (Sigma-Aldrich Sydney, Australia).

Two cell lines for prostate cancer (PC3 and DU145) and one normal prostate cell line (RWPE-1), as shown in Table 2.1, were used in this study. PC3 (human prostate adenocarcinoma, Cat. No. ATCC® CRL-1435™) cells were cultured in RPMI 1640 (Life Technologies, Australia) supplemented with 10% (v/v) FBS and 1% (v/v) antibiotics. DU145 (human prostate carcinoma, Cat. No. ATCC® HTB-81™) cells were cultured in DMEM supplemented with 10% (v/v) FBS and 1% (v/v) antibiotics. RWPE-1 (human normal prostate epithelial cells, Cat. No. ATCC® CRL-11609™) were cultured in keratinocyte serum free medium (K-SFM) kit (Cat: 17005-042, Life Technologies,

Australia) supplemented with bovine pituitary extract (BPE) at 0.05 mg/mL, human recombinant epidermal growth factor (EGR) at 5 ng/mL and 1% (v/v) antibiotics. Cells were grown at 37 °C in 5% CO_2 incubator and observed daily until 80% confluence was achieved. The cells were then washed with 5 mL phosphate-buffered saline (PBS) (137 mM NaCl, 2.7 mM KCl, 10 mM Na_2HPO_4 and 2 mM KH_2PO_4 at pH 7.4), trypsinised with 1 mL trypsin (Life Technologies, Australia), counted using a haemocytometer (LW Scientific) and seeded into appropriate flasks or plates for experimentation.

Approximately 2.1×10^6 cells were seeded into a 75 cm^2 tissue culture flask (Greiner Bio-One, Germany) with 12 mL complete medium and incubated at 37 ^oC with 5% CO_2 (Thermo Scientific, HERA 150). The cells were examined regularly under an inverted microscope (Olympus CKX41) at 40x magnification to monitor the cell's health and confluence. When 80% confluency was reached, the cells were passaged into new flasks. The cells were first washed with 5 mL PBS then trypsinised with 1 mL of trypsin solution as previously described and incubated at 37 ^oC with 5% CO_2 for approximately 3 min and monitored every minute thereafter. Once all cells were detached, 12 mL complete medium was added and then cells were thoroughly re-suspended by pipetting up and down multiple times. Preparation of cells for experiments was accomplished by counting cells with a haemocytometer. The cells were then plated into new flasks at a ratio of 1 to 3.

Table 2.1 List of mammalian cell lines used in this study

Cell type	Organism	Source	Growth mode	Cell type
MCF-7	Homo sapiens (human)	Mammary gland; from metastatic site	Adherent	Epithelial
MDA-MB-231	Homo sapiens (human)	Mammary gland; from metastatic site	Adherent	Epithelial
MCF10A	Homo sapiens (human)	Mammary gland; Normal breast	Adherent	Epithelial
PC3	Homo sapiens (human)	Prostate; derived from metastatic site: bone	Adherent	Epithelial
DU145	Homo sapiens (human)	Prostate; derived from metastatic site: brain	Adherent	Epithelial
RWPE-1	Homo sapiens (human)	Normal prostate; epithelial	Adherent	Epithelial

2.3.2 Cryopreservation of mammalian cells

Frozen stocks of the cells for individual cell lines were prepared and stored for future experiments in cryovials (Greiner Bio-One, Germany) in liquid nitrogen storage at -196 ^{o}C. Cells were grown in 75 cm^2 tissue culture flasks in complete medium until reaching 80% confluency. Cells were then washed with 5 mL PBS and trypsinised with 1 mL of trypsin solution and incubated at 37 ^{o}C with 5% CO_2 for 3 min. Once the cells were detached, 12 mL of complete medium was added into the tissue culture flask and the cells were thoroughly resuspended by pipetting. The cell suspension was then transferred into a sterile 50 mL falcon tube and centrifuged (Allegra X-15R) at 900 g for 5 min. The supernatant was removed and cells were resuspended in 3 mL of freshly prepared freezing medium containing 70% (v/v) un-supplemented medium, 20% (v/v) FBS and 10% (v/v) dimethyl sulfoxide (DMSO). One millilitre of cell suspension was aliquoted per cryovial and placed in a rack in an insulated (Styrofoam) container. The cells were then gradually brought to -196 °C by first placing the insulated container in the -80 ^{o}C freezer (Thermo Scientific -80C ULT) overnight, then transferred to the liquid nitrogen tank at -196 ^{o}C for long term storage.

2.3.3 Thawing mammalian cells from cryopreservation

The cryovials were removed from liquid nitrogen storage and were immediately thawed in a 37 ^{o}C water bath (LAB-Tech, Australia). Caution was taken to ensure that the cryovial was not submerged in water to prevent any possible contamination. Once thawed, vials were taken into a clean class II biological safety cabinet, wiped with 70% (v/v) ethanol and cells were immediately pipetted into a sterile 50 mL falcon tube with 10 mL of complete medium and centrifuged at 900 g for 5 min. The supernatant was discarded and the cell pellet was re-suspended in 12 mL complete medium. The cell suspension was then

transferred into a 75 cm^2 sterile tissue culture flask and incubated at 37 ^oC with 5% CO_2 until cells reached to 80% confluency.

2.4 Experimental work using the mammalian cells

2.4.1 MTT assay and cell enumeration

Cells were seeded into 96-well plates (Greiner Bio-One, Germany) with 190 µL of complete medium containing 7,000 cells per well. The plates were then incubated at 37 °C and 5% CO_2 for 32 h before treatment with zinc sulfate ($ZnSO_4$). The stock solutions of $ZnSO_4$ were made at 20x concentrations and filter-sterilised by passing through a 0.22 µm filter. The cells were treated with 0, 20, 50, 100, 150, 200, 250, 300, 350, 400 and 500 µM concentration of $ZnSO_4$. After treatment, the plates were incubated for 6 h and then 50 µL of MTT [3-(4,5-dimethyliazol-2-yl)-2,5-diphenyl-2H-tetrazolium bromide, 5 mg/mL in PBS] was added per well, followed by further incubation for 2 h at 37 °C in 5% CO_2 incubator. The medium was aspirated and formazan crystals in each well were solubilised in 100 µL of DMSO. Plates were then mixed gently before the absorbance was measured at 600 nm (A_{600}) using a spectrophotometer (Multiskan EX, Thermo Electron). The cell viability was quantified from the collected data and the online AAT Bioquest tool (https://www.aatbio.com/tools/ic50-calculator) was used to generate the half-maximal inhibitory concentration (IC_{50}) values and further confirmed by plotting a graph using Excel.

For cell enumeration, the cells were grown, prepared and treated in the same way as described previously. Following the 6 h incubation of $ZnSO_4$ treatments, the medium from each 96-well plate was aspirated and wells were washed with 200 µL of PBS, trypsinised with 15 µL of trypsin and then incubated for 3 min at 37 °C in 5% CO_2 incubator. Then 185 µL of medium was pipetted into each well, cells were carefully re-suspended and

transferred to microfuge tubes. An equal volume of 0.4% (v/v) trypan blue dye (Life Technologies, Australia) was added to each tube and thoroughly mixed by pipetting prior to cell counting with a haemocytometer under a light microscope. Both live and dead cells were counted to calculate the percentage of viable cells. Cell viability was plotted using the Bioquest website for IC_{50} determination and further validated through plotting a graph in Excel.

2.4.2 Inhibition of CK2 activity and zinc treatment

Multiple 96-well plates were prepared by seeding 7,000 cells per well with 190 µL of complete medium and incubated for 32 h. Prior to the addition of $ZnSO_4$, the cells were treated with CK2 inhibitors TBB (4,5,6,7-tetrabromo-1H-benzotriazole) (Calbiochem-Millipore) or CX-4945 (Sigma-Aldrich, Australia) resuspended in DMSO. A final concentration of 20 µM TBB and 5 µM CX-4945 were used for CK2 inhibition. The dosage was chosen for these two inhibitors due to the lack of toxicity to the cells based on a titration I preformed and further supported by the literature (Cozza et al., 2009; Zwicker, Ebert, Huber, Debus, & Weber, 2011). After the addition of TBB or CX-4945, the cells were incubated at 37 °C with 5% CO_2 for 3 h. This was followed by 6 h incubation with $ZnSO_4$ at various IC_{50} concentration (MCF-7 320 µM, MDA-MB-231 350 µM, MCF10A 195.5 µM, PC3 110 µM, DU145 150 µM and RWPE-1 187 µM). At the end of the incubation, the plates were observed under an inverted microscope and the cell viability was measured by MTT assay as described earlier.

2.4.3 Knockdown of CK2 gene expression by siRNA

SMARTpool siRNA targeting each gene of CK2 subunits [*CSNK2A1* (CK2α), *CSNK2A2* (CK2α') and *CSNK2B* (CK2β)] were purchased from Dharmacon, USA (Table 2.2). The optimum concentration of each siRNA for the CK2 subunit gene knockdown study was determined by optimisation experiments in our laboratory (Zaman et al., 2019), in conjunction with the manufacturer's instructions (Dharmacon, USA) and the literature (Cannon et al., 2017). The efficiency of the knockdown was measured by qRT-PCR in Chapter 3. Each siRNA sequence is comprised of four targeting nucleotides for each gene of CK2 subunits. The targeting sequences for *CSNK2A1* encoding CK2α are UGAAUUAGAUCCACGUUUC, GCAAUUGUACCAGACGUUA, CAGAAAGCUUCGGCUAAUA, AGACUAUGACAUUCGAUUU. The targeting sequences for *CSNK2A2* encoding CK2α' are GCAAGUAUAGUGAAGUAUU, CAACAGAGAUUGACCGCCA, GGUGGAACAAAUAUCAUUA, GAACUAUAUGGUUAUCUGA. The targeting sequences for *CSNK2B* encoding CK2β are CAGCUGAGAUGCUUUAUGG, CCAAGUGCAUGGACGUGUA, GGUAAUGAAUUCUUCUGUG, GCAGGGAGACUUUGGCUAC. Each siRNA stock (10 µM) was prepared in siRNA buffer (pH 7.3) containing 300 mM potassium chloride, 31 mM HEPES and 2.1 mM magnesium chloride. For each siRNA transfection, two microfuge tubes were prepared, with tube 1 containing 20 µL of 10 µM siRNA and 480 µL OPTI-MEM (Life Technologies, Australia) and tube 2 containing 20 µL lipofectamine 2000 (Invitrogen, Australia) transfection reagent and 480 µL OPTI-MEM. After 5 min incubation at room temperature, the contents of tube 1 was pipetted into tube 2 for each siRNA and left at room temperature for 20 min. A mock tube with no siRNA containing 980 µL OPTI-MEM with 20 µL lipofectamine was also prepared as a control.

When cells reached 80% confluence, cells were washed with sterile PBS at room temperature, trypsinised (1 mL) and 5 mL of fresh complete medium was added. The cells were counted and 2×10^6 cells in 5 mL were prepared into each tube designated as tube 1 CK2α siRNA, tube 2 CK2α' siRNA, tube 3 CK2β siRNA, tube 4 mock control and tube 5 untreated control, respectively. After the incubation, the cells were centrifuged at 900 g for 5 min. The supernatant was removed, cells were then washed with 5 mL PBS and centrifuged again with the supernatant discarded. Each cell pellet was resuspended in 1 mL of each siRNA mixture which was resuspended and allowed to incubate at room temperature for 20 min. Afterwards, 9 mL of OPTI-MEM was added, the cells were thoroughly mixed and aliquoted 100 µL per well into 96-well plates. The plates were incubated for 72 h at 37 ^{o}C with 5% CO_2. To measure IC_{50} of $ZnSO_4$, 5 µL per well were used to treat the transfected cells in the plates and incubated at 37 ^{o}C with 5% CO_2 for 6 h. MTT assay was performed to measure cell viability as described above.

Table 2.2 siRNA targets and sequences for human CK2 subunits

Genes for human CK2 subunits	Target sequences
CSNK2A1 **CK2α**	GCAUUUAGGUGGAGACUUC, GGAAGUGUGUCUUAGUUAC, GCUGGUCGCUUACAUCACU, AACAUUGUCUGUACAGGUU
CSNK2A2 **CK2α'**	GAGUUUGGGCUGUAUGUUA, GGGACAACAUUCACGGAAA, GAUAGAUCACCAACAGAAA, UUAAGCAACUCUACCAGAU
CSNK2B **CK2β**	CCAAGUGCAUGGAUGUGUA, GCAAUGAAUUCUUCUGUGA, GCAAGGAGACUUUGGUUAC, CAACCAGAGUGACCUGAUU

2.4.4 Purification of RNA for quantitative reverse transcription-polymerase chain reaction (qRT-PCR)

Cells were grown in 75 cm^2 flasks for 32 h and then medium was aspirated and replaced with 11.9 mL of fresh complete medium. $ZnSO_4$ at 120x stock concentration was prepared and filter-sterilised through a 0.22 µm filter. Each flask was treated with 100 µL of the predetermined IC_{50} dose of $ZnSO_4$, or 100 µL of H_2O to serve as a control. Flasks were incubated at 37 °C with 5% CO_2 for three time points, i.e., T_0, T_{30} and T_{120} min respectively for each treatment. After the incubation, the medium was discarded, cells were washed with 5 mL PBS and 1 mL of TRIzol™ reagent (Thermofisher, Australia) added directly into the flasks. After gently mixing several times, the lysates were homogenised and transferred to 2 mL microfuge tubes. The resultant lysates were incubated for 5 min at room temperature to allow complete dissociation of the nucleoprotein complex. Then, 200 µL of chloroform (Sigma-Aldrich, Australia) was added, followed by a further 3 min incubation at room temperature. Samples were then centrifuged for 15 min at 12,000 g, 4 °C for 15 min to separate into three phases.

The RNA containing upper phase was transferred into a new tube and precipitated by adding 0.5 mL of isopropanol (Sigma-Aldrich, Australia). After 10 min incubation the sample was centrifuged for 10 min at 12,000 g, 4 ^oC. The supernatant was then discarded and the RNA pellet was washed in 1 mL 75% (v/v) ethanol (Sigma-Aldrich, Australia) by vortexing for 5 sec then centrifugation for 5 min at 7,500 g, 4 ^oC. The resultant pellet was allowed to air dry for about 20 min, then the RNA pellets were dissolved in 30 µL of diethylpyrocarbonate (DEPC) treated water (Sigma-Aldrich, Australia) and the RNA concentration was determined by measuring the UV absorbance (A_{260}/A_{280}) by Nanodrop spectrometer (Thermo Fisher Scientific, Australia).

2.4.5 cDNA synthesis by reverse transcriptase

cDNA was synthesised using high-capacity cDNA reverse transcription kits (Thermo Fisher Scientific, Australia) according to the manufacturer's instructions. First, in a clean PCR tube 10 µL of master mix was prepared with 2 µL 10x reverse transcription buffer, 0.8 µL 25x dNTP mix, 2 µL 10x reverse transcription random primers, 1 µL Multiscribe™ reverse transcriptase and 4.2 µL DEPC-treated water. Then, 10 µL of master mix was combined with 10 µL of 100 ng/µL total RNA from a given sample prepared in Section 2.4.4. The reaction tube was mixed and then run on a Veriti 96-well thermal cycler (Applied Biosystems) with the following setting: step 1 at 25 °C for 10 min, step 2 at 37 °C for 120 min, step 3 at 85 °C for 5 sec. cDNA synthesis was quantified by measuring the UV absorbance (A_{260}, A_{280}, A_{260}/A_{280}).

2.4.6 Real time quantitative reverse transcriptase polymerase chain reaction (qRT-PCR)

qRT-PCR was carried out using TaqMan real-time PCR reagents (Thermo Fisher Scientific, Australia) according to the manufacturer's instructions. Each 20 µL reaction mix contained 1 µL 20x TaqMan assay which includes specific primer/probe combination for a given gene, 10 µL master mix, 1 µL of cDNA synthesised previously for a given sample (500 ng/µL) prepared in Section 2.4.5 and 8 µL DEPC-treated water (9 µL for the no cDNA template control). Each cDNA of individual time points in the time course was run in triplicate. The reaction mix was heated at 95 °C for 10 min, then followed with each cycle at 95 °C for 15 sec and 60 °C for 1 min, for 40 cycles in total (Table 2.3). The relative expression of the differentially expressed genes of interest was quantified against the house keeping gene *GAPDH* (gene encoding glyceraldehyde-3-phosphate dehydrogenase as the endogenous control).

The qRT-PCR data were analysed by the $2^{-\Delta\Delta CT}$ method (Schmittgen and Livak, 2008). ΔCTc is calculated first, where the cycle threshold for the gene of interest in control condition was subtracted by the cycle threshold of the house-keeping gene *GAPDH* in control condition. ΔCTe is then calculated where the cycle threshold of the gene of interest under each treatment was subtracted by the cycle threshold of *GAPDH* under each experimental treatment. Finally, ΔΔCT is calculated by subtracting ΔCTc from ΔCTe. $2^{-\Delta\Delta CT}$ represents fold change of the gene expression relative to *GAPDH*.

Table 2.3 Run parameters for the qRT-PCR thermal cycler

Stage	Temp (°C)	Time (mm:ss)
Hold	50	2:00
Hold	95	10:00
Cycle	95	0:15
(40 cycles)	60	1:00

2.4.7 Comparison of gene expression in cancerous against normal cells via qRT-PCR

The differentially expressed genes discovered by RNA-seq was compared against their expression in cancer and normal cells, calculated according to the Schmittgen and Livak report (Schmittgen and Livak, 2008). Firstly, the CT values of *GAPDH* was subtracted from the CT value of each gene of interest in cancer and normal cells to get ΔCT for each gene separately. Then, $2^{-\Delta CT}$ values of each gene of interest were generated to achieve the mean ± SD of $2^{-\Delta CT}$. The mean of $2^{-\Delta CT}$ of each gene of interest in cancer cells was divided by the mean of $2^{-\Delta CT}$ of the same gene in normal cells to achieve fold change comparison of gene expression in cancerous against normal cells.

2.4.8 Next-generation RNA sequencing

MCF-7 cells were grown in 25 cm^2 flasks for 32 h at 80% confluency, then the medium was aspirated and replaced with 5.9 mL of fresh complete medium. $ZnSO_4$ at 60x stock concentration was prepared and filter-sterilised through a 0.22 µm filter. Each flask was treated with either 100 µL of the predetermined IC_{50} dose of $ZnSO_4$ (320 µM), or 100 µL of H_2O to serve as control (Zaman et al., 2019). Flasks were incubated at 37 °C with 5% CO_2 for T_0, T_{30} or T_{120} min respectively for each treatment. Immediately after incubation, medium was discarded, RNA was extracted as mentioned earlier and then RNA samples were prepared with DEPC-treated water to 100 ng/µL and sent to the Ramaciotti Centre for Genomics (University of New South Wales, Australia) for next-generation RNA sequencing.

At the University of New South Wales (UNSW), Ramaciotti Centre for Genomics, the quality of the RNA samples was further checked with the Tapestation (Agilent) for integrity and the Nanodrop for quantification and purity. Samples were then prepared

using the TruSeq Stranded mRNA-seq kit (Illumina) using 1 µg of total RNA as input. The number of PCR cycles was reduced from 15 to 12, to minimise PCR duplicates in the data. The generated libraries had a median insert size of 180bp (range 100-370bp) and were pooled in equal amounts for the sequencing run. Once sequencing run with NextSeq 500 was performed using a NextSeq 500/550 High Output v2 kit and sequenced to produce 75bp single reads. Fastq files were generated in Basespace using bcltofastq 2.18. The run generated over 450M reads (40-50M per sample) and quality specification Q30 was 93%.

2.4.9 Quantification of gene expression levels and differential expression analysis in MCF-7 breast cancer cells

Bioinformatic analysis to identify differentially expressed genes was performed at the systems biology Initiative (UNSW). The RNA reads were mapped to the Ensembl *Home sapiens* genome (GRCh38). The mapping was performed with Tophat2 (v 2.0.12) (Kim et al., 2013) and calling Bowtie2 (v 2.2.3) (Langmead and Salzberg, 2012). The featureCounts of Subread (v 1.4.6-p5) (Liao et al., 2014) was used to generate counts of reads uniquely mapped to annotated genes using the GRCh38 gtf file. Differential expression analysis was performed using the Bioconductor packages edgeR (v 3.18.1) (Robinson et al., 2010). Generalised linear models were used for differential expression analysis. In all cases, differentially expressed genes were defined as those genes with a Benjamini-Hochberg corrected *p*-value less than 0.05 (Benjamini and Hochberg, 1995). The fold change (FC) is expressed in Log_2FC. The genes with over 0.6 of Log_2FC are identified as the up-regulated genes, whilst the genes with lower than -0.6 of Log_2FC as the down-regulated genes. The advantage to use Log_2FC here rather than arithmetic fold change is its visualisation with respect to zero in plotting.

2.4.10 Imaging of intracellular zinc ion by confocal microscopy

During confocal imaging, all glass-bottom culture dishes (MatTek, USA) were treated with 20 µL of gelatin (Sigma-Aldrich, Australia) and allowed to dry for 2 h in a class II biological safety cabinet. Cells in complete medium with 25 mM HEPES buffer were seeded at 40, 000 cells per mL into each imaging dish at a final volume of 1 mL. Cells were incubated at 37 ºC with 5% CO_2 for 32 h. CK2 inhibitor TBB at 20 µM or CX4945 at 5 µM final concentration was added into all except the control dishes and allowed to incubate for 3 h. The metal treatment, using IC_{50} for $ZnSO_4$ were then added. After 1 h of exposure to the metal ion treatment, medium was removed and 1 mL fresh live cell imaging medium (Life Technologies) containing 140 mM NaCl, 2.5 mM KCl, 1.8 mM $CaCl_2$, 1 mM $MgCl_2$ in 20 mM HEPES buffer pH 7.4 was added. Then 100 µg of FluoZin-3 AM zinc probe (Life Technologies) was dissolved in 200 µL of DMSO and 2 µL of 50% (v/v) pluronic acid F127 (Life Technologies). The probe stocks were sonicated for 5 min and then 15 µL of FluoZin-3 AM stocks were applied to the imaging dishes. The confocal imaging dishes were further incubated at 37 °C with 5% CO_2 for 1 h. The medium was then replaced with 1 mL of fresh imaging medium and allowed to incubate at 37 °C with 5% CO_2 for 30 min before imaging was performed. Images were acquired using an LSM-5 Confocal Microscope system (Carl Zeiss Pty Ltd, North Ryde, Australia), with excitation at 488 nm and emission at 510-530 nm. Gain settings for fluorescence imaging were maintained constant to allow for quantification of intracellular fluorescence intensity through Image-J software.

Confocal imaging was also conducted for CK2 subunit knockdown using CK2α, CK2α' and CK2β siRNA. siRNA transfected cells were prepared as previously described and seeded into imaging dishes at a final volume of 1 mL. Cells were incubated at 37 ºC with

5% CO_2 for 32 h followed by a 1 h metal treatment of $ZnSO_4$ at IC_{50}. The medium was then removed, 1 mL of fresh imaging medium was added and FluoZin-3 AM was loaded into their respective dishes as described above.

2.4.11 Quantification of zinc ion content in mammalian cells by inductively coupled plasma-mass spectrometry (ICP-MS)

Cells were cultured in 25 cm^2 flasks at 37 °C with 5% CO_2 until 80% confluence. Aspiration of spent medium was conducted and 5.9 mL of complete medium was added. Post zinc treatments, flasks designated with CK2 inhibition were treated with 50 µL of TBB at a final concentration of 20 µM for a period of 3 h. For zinc treatments alone, 100 µL of 60x IC_{50} $ZnSO_4$ concentration was added, while 50 µL of 120x IC_{50} $ZnSO_4$ concentration for cells pre-treated with TBB. Control flasks were treated with H_2O. Three biological treatments were performed in the time course at the following time points: T_0, T_{30}, T_{120} h. Upon completion of treatments, medium was aspirated and cells were washed with 5 mL of PBS. Then 0.5 mL of trypsin was added, flasks were incubated for 3 min at 37 °C with 5% CO_2. Following trypsinisation, cells were resuspended in 3 mL of complete medium and counted using a haemocytometer. Once cell numbers were counted, the cells were centrifuged at 900 g for 5 min and medium was decanted. The cell pellet was washed once with 5 mL of 2 µM EDTA solution prepared in PBS by centrifugation at 900 g for 5 min and washed once in 1 mL of PBS in 1.5 mL microfuge tubes by centrifugation at 12, 000 g for 5 min. The supernatant was decanted and the cells were lyophilised using a SpeedVac Concentrator for 3-6 h.

Following lyophilisation, the cell pellets were acid-digested. Dried pellets were firstly suspended in 1 mL of 70% (v/v) ultra-pure nitric acid (CHOICE Analytical, Australia). The resultant suspensions were transferred to acid-washed glass tubes and placed in a

heating block (Perkin Elmer) at 120 ^{o}C for approximately 4 h. Acid alone and water alone controls were also included in each round of acid digestion, serving to identify residual metal contamination in glass tubes, if any. The acid digested samples were then re-suspended in 5 mL of 2% (v/v) ultra-pure nitric acid and analysed using a NexION 300X ICP-MS (Perkin Elmer).

2.4.12 Data analysis

Where statistical analysis was conducted, means were compared to identify significant differences using SPSS statistical software and Excel. When means of two different groups needed to be compared, a student t-test was performed; while comparing multiple groups, ANOVA was used.

3 PROTEIN KINASE CK2 IS INVOLVED IN ZINC HOMEOSTASIS IN BREAST AND PROSTATE CANCER CELLS

3.1 Introduction

As explained in Chapter 1.6, the ubiquitous and pleiotropic serine/threonine kinase CK2 plays roles in cell proliferation, differentiation and apoptosis, therefore it is implicated in diseases such as cancers (Guerra et al., 1999; Guerra and Issinger, 1999; Litchfield, 2003). CK2 has been regarded as the most pleiotropic kinase in eukaryotic organisms due to its numerous substrates which possibly make up one quarter of the eukaryotic phosphoproteome (Pinna, 1993; Meggio et al., 1994; Litchfield, 2003; Meggio and Pinna, 2003). Despite such enormous progress in the characterisation of CK2, many aspects of its function remain yet to be fully elucidated such as its role in regulating zinc homeostasis in cancer cells.

Previous studies utilising the model organism *S. cerevisiae*, discovered that the CK2α subunit is involved in Zn^{2+} sequestration (Johnson et al., 2017). I further demonstrated that CK2 plays a role in Zn^{2+} uptake and toxicity in neuronal cells (Zaman et al., 2016). Taylor et al. (2003) showed CK2 phosphorylates the zinc channel ZIP7 located in the membrane of endoplasmic reticulum, allowing Zn^{2+} to be released into the cytoplasm. The work in this chapter aims to investigate the role of CK2 in zinc homeostasis in breast and prostate cancer cells. My experimental approach is to target CK2 with its specific inhibitors at the protein level and its specific siRNA at the gene level in breast cancer cell lines (MCF-7 and MDA-MB-231) and prostate cancer cell lines (PC3 and DU145). The effects of such CK2 manipulation in combination of zinc exposure are then observed by MTT cell viability assay and confocal microscopy for intracellular zinc level quantification. As

mentioned in Section 2.4.2, the chosen concentration of TBB in this study is 20 μM, which had little effect on the cell viability of breast cancer cell lines (MCF-7 and MDA-MB-231) and the prostate cancer cell lines (PC3 and DU145). The findings reported below provide evidence for the involvement of CK2 in zinc homeostasis of breast and prostate cancer cells.

3.2 Results

3.2.1 IC_{50} of $ZnSO_4$ in the cancer cell lines

In order to measure the effect of zinc on the cancer cells, its IC_{50} for each cancer cell line was firstly determined by MTT assay. As shown in Fig. 3.1, the overall patterns for the breast cancer cell lines (MCF-7 and MDA-MB-231) and prostate cancer cell lines (PC3 and DU145) in response to the zinc exposure are divergent. The IC_{50} values of $ZnSO_4$ for MCF-7 (320 µM) and MDA-MB-231 (350 µM) are much higher than that of PC3 (110 µM) and DU145 (150 µM) (Fig. 3.1A). These IC_{50} values are used in the following experiments. For each cell line the IC_{50} of $ZnSO_4$ was also determined via cell counting, which confirms the trend observed by MTT assay as shown in Fig. 3.1B.

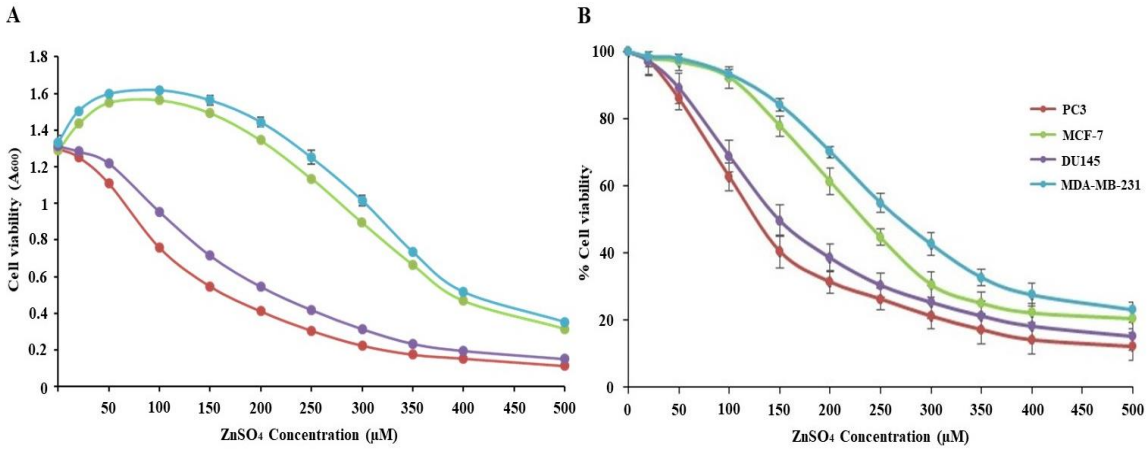

Fig 3.1 Determination of IC_{50} of $ZnSO_4$ by MTT assay

MTT cell viability assay is represented by (A) and cell viability determined by cell counting (B). IC_{50} of $ZnSO_4$ at 6 h for all four cancer cell lines was determined by MTT assay. IC_{50} for MCF-7 cells (green) is 320 µM, MDA-MB-231 cells (blue) 350 µM, PC3 cells (red) 110 µM and DU145 cells (purple) 150 µM. The trend observed by MTT assay (A) was confirmed by cell counting using trypan blue (B). Error bars denotes standard deviation of three biological replicates for each dose.

3.2.2 Effect of CK2 inhibitors on Zn^{2+} homeostasis under exposure of IC_{50} $ZnSO_4$

To uncover the role of protein kinase CK2 in regulating zinc homeostasis, the specific inhibitors TBB and CX-4945 were used. As shown in Fig. 3.2, CK2 inhibitor alone with TBB (20 μM) or CX-4945 (5 μM) had little effect on the cancer cell viability. The dosage was chosen for these two inhibitors due to their benign effect on the cells according to the titration in this study and the literature (Cozza et al., 2009; Zwicker et al., 2011; Zaman et al., 2019). The inhibitor plus IC_{50} of $ZnSO_4$ reduced the viability of both breast (MCF-7, MDA-MB-231) and prostate (PC3, DU145) cancer cells (P<0.001) and prostate cancer cells exhibited higher sensitivity to the treatment of CK2 inhibitor plus zinc exposure.

In this study, prostate cancer cells were found to be more sensitive to zinc exposure, compared to the breast cancer cells, following the inhibition of CK2 activity by TBB (20 μM) and CX-4945 (5 μM) coupled with IC_{50} zinc sulfate treatment (Fig. 3.2). This finding correlates well with the zinc sulfate IC_{50} values obtained by MTT cell viability assay. The IC_{50} values of zinc sulfate for PC3 (110 μM) and DU145 (150 μM) prostate cancer cells are much lower than the breast cancer cells MCF-7 (320 μM) and MDA-MB-231 (350 μM). The molecular mechanism for the higher sensitivity of prostate cancer cells is not clear. How CK2 regulates zinc transport proteins at either the gene or protein level remains to be further investigated. This is one reason as to why RNA-seq transcriptomic analysis was conducted in Chapter 4.

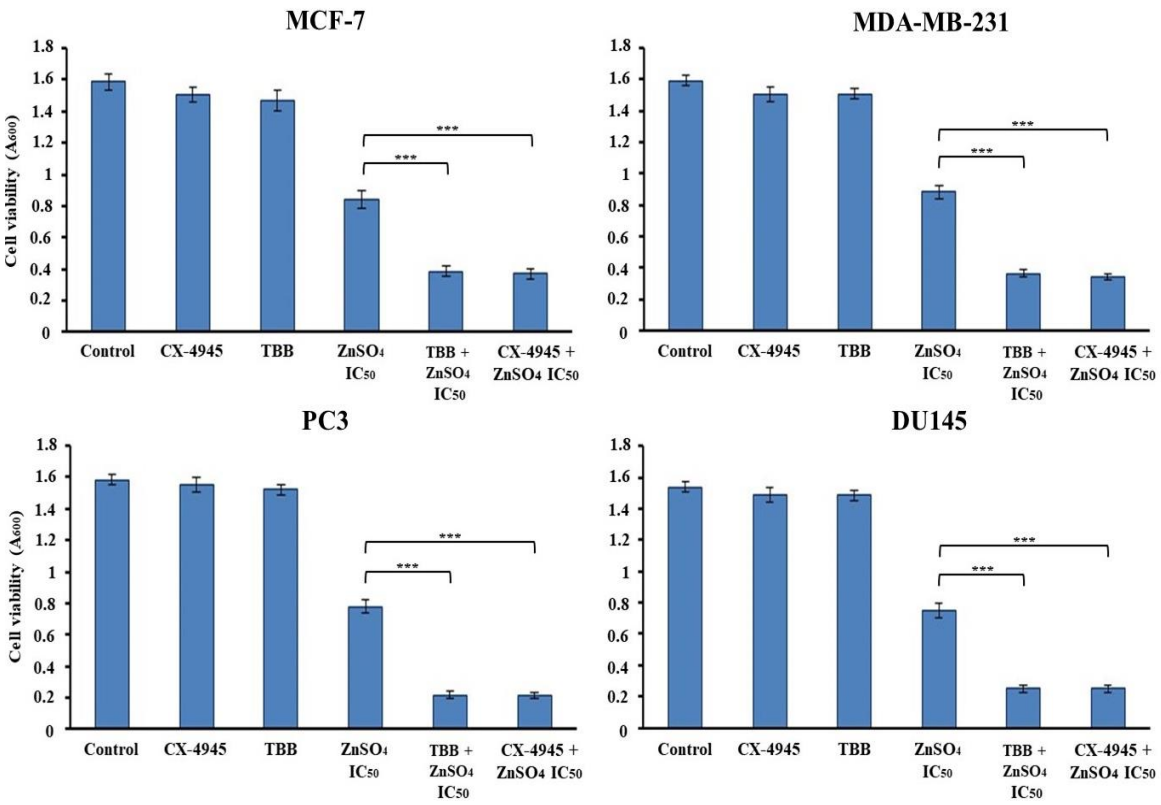

Fig 3.2 Effect of CK2 inhibitors on cancer cell viability under exposure of IC_{50} $ZnSO_4$

Cells were treated with 20 µM TBB or 5 µM CX-4945 inhibitor for 3 h and then incubated for 6 h with the IC_{50} of $ZnSO_4$. The cell viability was determined by MTT assay. Error bars denotes standard deviation of three biological replicates for each treatment and each biological replicate has three technical replicates. *P*-values were calculated by one-way ANOVA. *** denotes $P<0.001$.

3.2.3 Efficacy of CK2 gene expression knockdown by siRNA

Relative expression of CK2 subunit genes (*CSNK2A1*, *CSNK2A2* and *CSNK2B*) was determined with reference to the expression of housekeeping gene *GAPDH*. Fold change 1 means no change of the gene expression. Fold change >1 means increase of the gene expression whilst fold change <1 means decrease of the gene expression. Fig. 3.3 shows the percentage knockdown of *CSNK2A1* (encoding CK2α) is 80.7% for MCF-7, 59.4% for MDA-MB-231, 58.7% for PC3 and 65.7% for DU145 cells. The percentage knockdown of *CSNK2A2* (CK2α') is 70.5% for MCF-7, 67.1% for MDA-MB-231, 72.5% for PC3 and 61.4% for DU145 cells. The percentage knockdown of *CSNK2B* (CK2β) is 78.2% for MCF-7, 75.2% for MDA-MB-231, 76.4% for PC3 and 76% for DU145. In all the four cell lines, knockdown of one CK2 gene does not affect the other two, except in MCF-7 cells where knockdown CK2β leads to reduction in expression of CK2α and α' and knockdown α' leads to reduction in expression of β, as well as in DU145, knockdown of α' caused reduction in expression of α.

The possible explanation for the reduction of CK2α and CK2α' gene expression in MCF-7 breast cancer cells following knockdown of CK2β subunit may be due to the stoichiometry of CK2 holoenzyme. As is known, CK2 holoenzyme is a tetramer comprising two catalytic subunits and a CK2β dimer. The knockdown of CK2β subunit would disrupt the stoichiometry, less amount of CK2β might lead to lower requirement of CK2α and CK2α'. This notion could be supported by the finding by (Franchin et al., 2018), which showed that the knockout of CK2α and CK2α' resulted in a marked reduction of CK2β.

Similarly, the possible explanation for the reduction of CK2α gene expression in DU145 prostate cancer cells following knockdown of CK2α' subunit might also relate to the stoichiometry of CK2 holoenzyme.

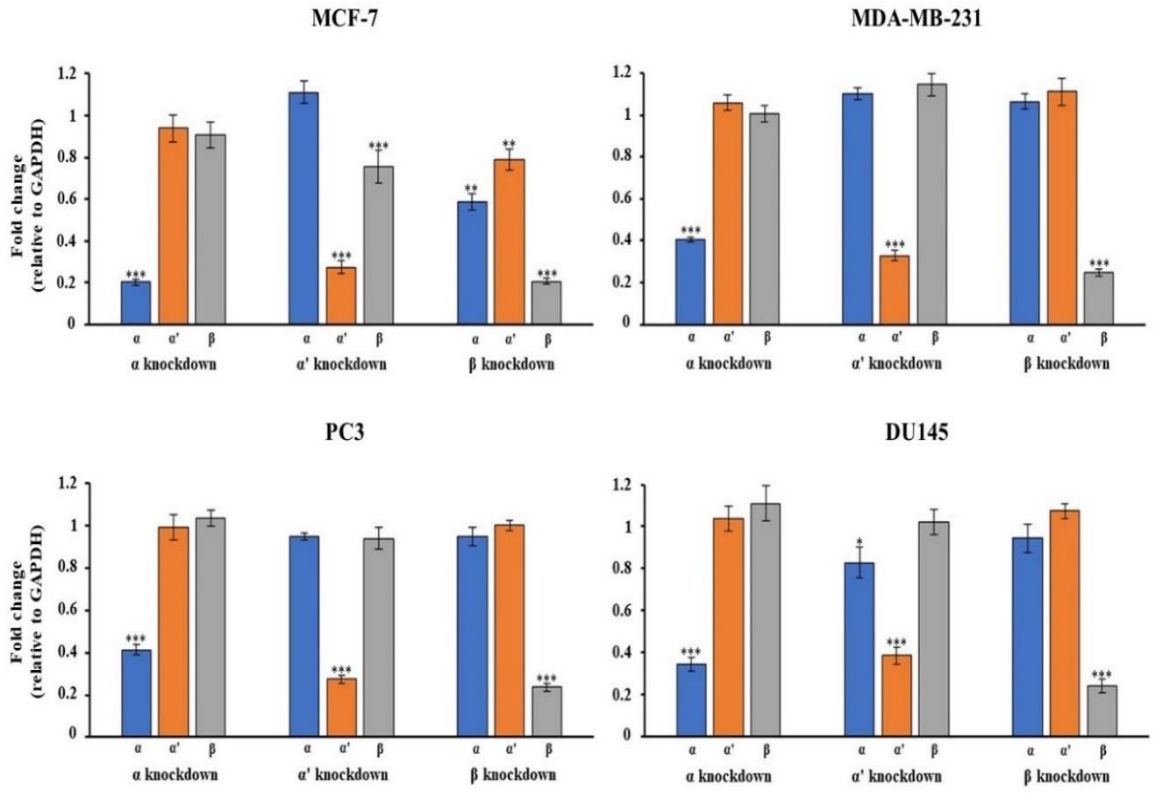

Fig 3.3 Efficacy of CK2 gene expression knockdown by the specific siRNA

Cells were transfected with CK2 subunit specific siRNA and incubated for 36 h. Total RNA was then prepared, cDNA synthesised and qRT-PCR performed. Relative expression of the subunit genes was quantified relative to *GAPDH*. * $P<0.05$, ** $P<0.01$ and *** $P<0.001$. Data represents the average of three biological replicates and each biological replicate has two technical replicates. Error bars represent SEM. *CSNK2A1* is denoted as α, *CSNK2A2* as α' and *CSNK2B* as β.

3.2.4 Effect of CK2 siRNA knockdown on cell viability under zinc exposure

The knockdown of individual CK2 subunit genes revealed their distinct involvements in regulating zinc homeostasis reflected by the cancer cell viability (Fig. 3.4). Compared to mock transfection plus $ZnSO_4$ IC_{50}, knockdown of CK2α increased cell viability of MDA-MB-231 cells (P<0.01) but decreased cell viability in MCF-7, PC3 and DU145 cells (P<0.001). Knockdown of CK2α' increased cell viability of MCF-7 and MDA-MB-231 cells (P<0.001) but decreased cell viability in PC3 and DU145 cells (P<0.001). Knockdown of CK2β decreased cell viability of MCF-7 and MDA-MB-231 cells (P<0.001) but increased cell viability in PC3 (P<0.01) and DU145 cells (P<0.001). Across all three knockdowns, the two prostate cancer cell lines showed consistent effects, the same is also true for the two breast cancer cell lines except the knockdown of CK2α. The discrepancy of the effect of CK2α knockdown is likely due to the lower knockdown efficacy in MDA-MB-231. It is possible that the effects of knockdown of CK2 subunits as observed in Fig. 3.4 are due to the involvement of different CK2 tetrameric isoforms with different combinations of catalytic subunits with the regulatory subunit such as ααββ, α'αββ, or α'α'ββ.

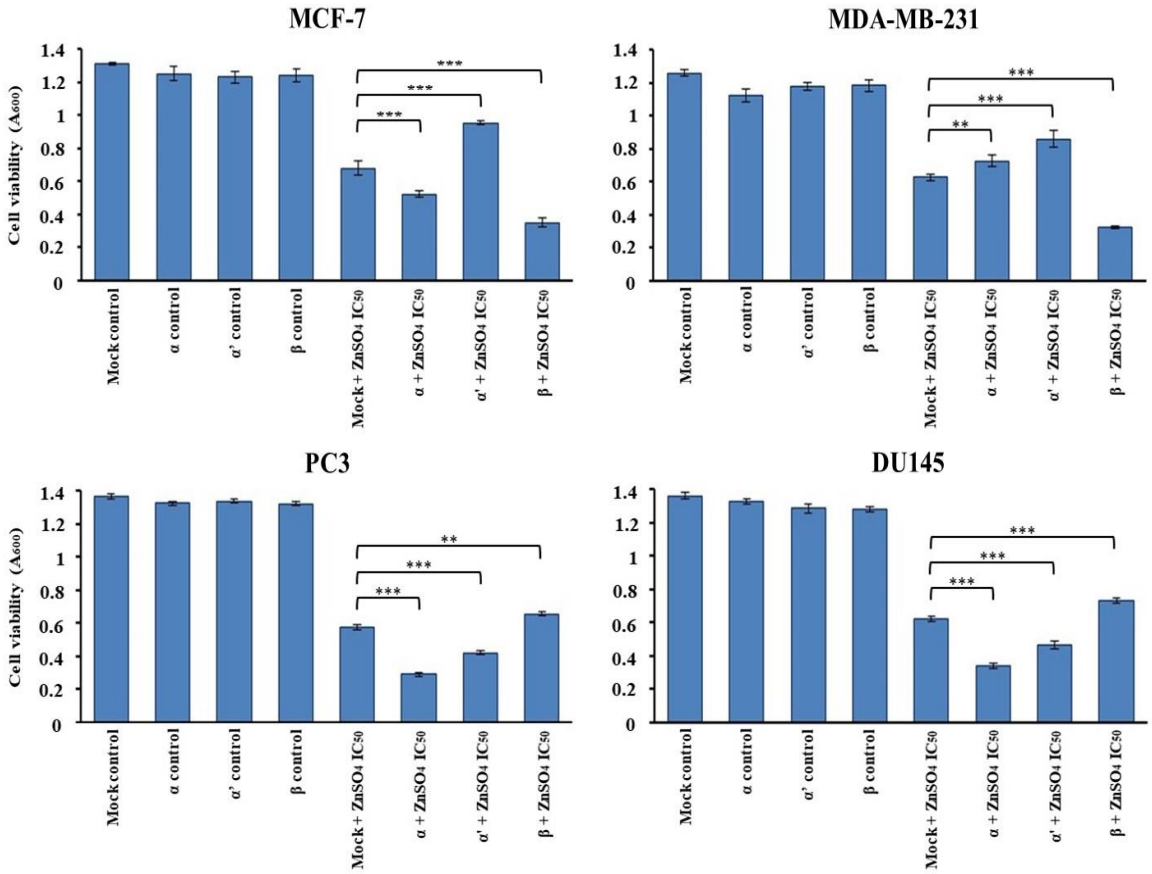

Fig 3.4 Effect of CK2 siRNA knockdown on cell viability under zinc exposure

Transfection of siRNA was carried out in MCF-7, MDA-MB-231, PC3 and DU145 cells, followed by treatment of $ZnSO_4$ IC_{50} and an MTT assay. Mock transfection as well as mock plus $ZnSO_4$ IC_{50} served as two controls. *P*-values were calculated by one-way ANOVA. ** denotes $P<0.01$ and *** $P<0.001$. Error bars denote standard deviation of three biological replicates for each treatment and each biological replicate has two technical replicates.

3.2.5 Visualisation of intracellular Zn^{2+} in $ZnSO_4$ treated cells under CK2 inhibition and siRNA knockdown

Apart from performing MTT assays, the effects of CK2 inhibitors and siRNA knockdown in MCF-7, MDA-MB-231, PC3 and DU145 cells were further studied by confocal imaging with the specific fluorophore (FluoZin-3 AM) for zinc visualisation and quantification (Fig. 3.5 and 3.6). Fig. 3.5 shows that zinc levels in all four cell lines were significantly increased by the inhibition of CK2 inhibitors TBB or CX-4945 in combination with IC_{50} zinc exposure compared to zinc IC_{50} treatment alone (P<0.001). The cells with inhibitor alone (Control panel) and the cells with $ZnSO_4$ only ($ZnSO_4$ panel) serve as controls. Notably, the zinc level in the controls of breast cancer cells is higher than the counterparts of prostate cancer cells, demonstrating the intrinsic characteristics of these two types of cancer cells.

Visualisation of zinc levels by confocal imaging in the cells transfected with CK2 specific siRNA reveals the distinct involvements between each CK2 subunit and intracellular zinc level (Fig. 3.6). Under $ZnSO_4$ IC_{50} treatment, knockdown of CK2β is detrimental to both breast cancer cell lines (P<0.001) but is beneficial to both prostate cancer cells (P<0.001), particularly PC3 cells. CK2α' knockdown reduced the zinc level significantly in MCF-7 and MDA-MB-231 cells (P<0.001), whereas no apparent effect was displayed by PC3 and DU145 cells. Knockdown of CK2α increased the zinc level in PC3 and DU145 cell lines (P<0.001), while such effect was not apparent for MCF-7 and MDA-MB-231 cells. Furthermore, the control images revealed that zinc ions are most likely localised surrounding the nuclei. Such a pattern was also obvious in the cells with CK2α' knockdown, particularly in MCF-7 and MDA-MB-231 cells.

CK2α' knockdown coupled with $ZnSO_4$ IC_{50} treatment in MCF-7 and MDA-MB-231 breast cancer cells results in increased cell survival, while the opposite effect was displayed in PC3 and DU145 prostate cancer cells (Fig. 3.4). The possible explanation for such a finding could be traced back to the intrinsic difference of these two types of cancer cells, that is, the cytoplasmic zinc level is much higher in breast cancer cells compared to the normal breast epithelial cells, whilst the cytoplasmic zinc level in prostate cancer cells is much lower than the normal prostate epithelial cells. The gene expression and regulation for zinc homeostasis in breast and prostate cancer cells must be different. More light could be shed on this front in the following Chapters 4 and 5.

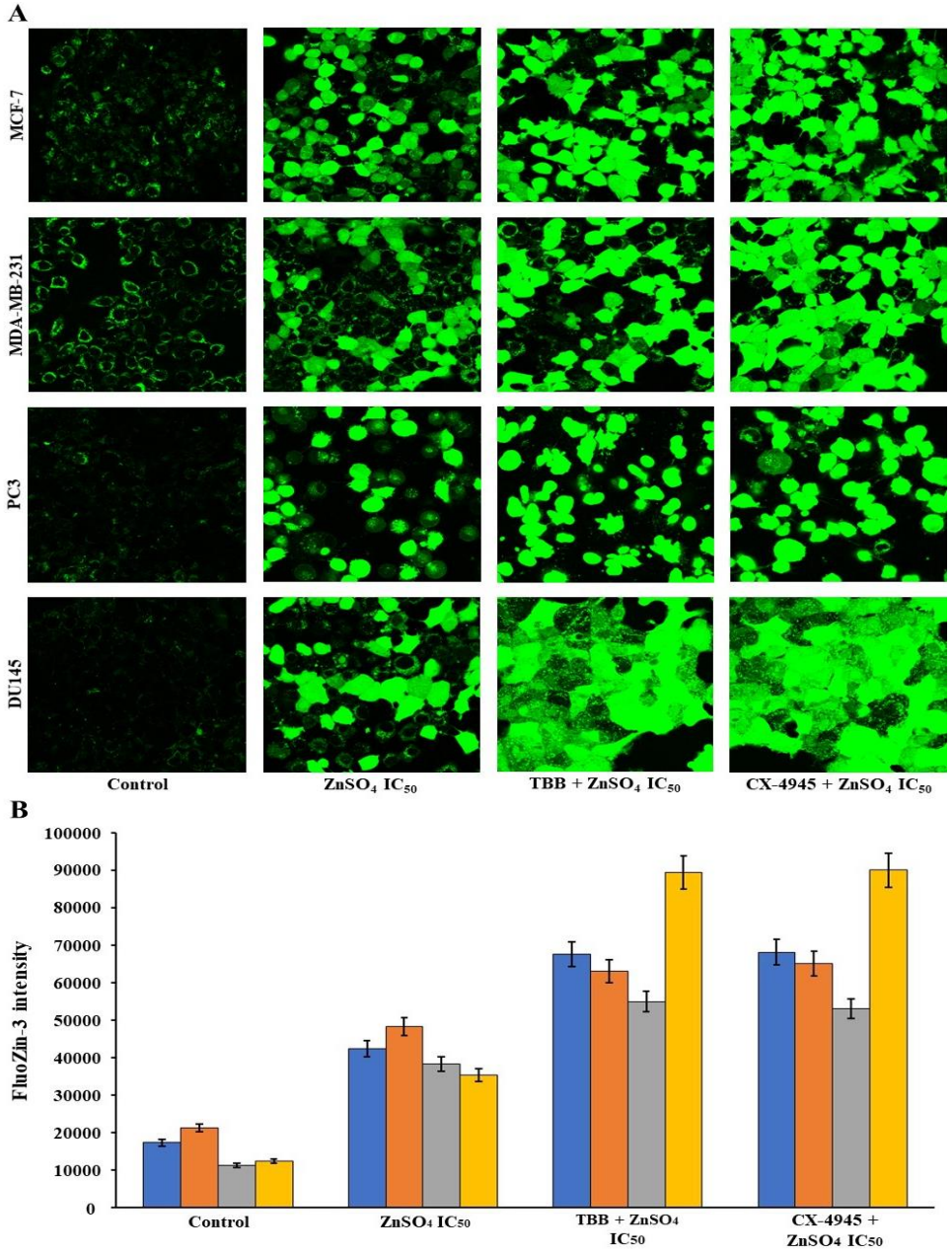

Fig 3.5 Visualisation of Zn^{2+} in $ZnSO_4$ treated cells under CK2 inhibition

Cells were grown in confocal imaging dishes for 32 h then treated with either TBB (20 µM) or CX-4945 (5 µM) for 3 h followed by $ZnSO_4$ IC_{50} treatment and incubation with the fluorescent probe FluoZin-3 AM. The confocal images (A) were taken at 40x magnification. The control panel represents the cells treated with the CK2 inhibitor alone (either TBB or CX-4945). Fluorescent intensity (B) was quantified for each treatment with confocal images at 40x magnification where blue indicates MCF-7 cells, orange MDA-MB-231 cells, grey PC3 cells and yellow DU145 cells. Error bars denote standard deviation of fluorescence intensity for each treatment.

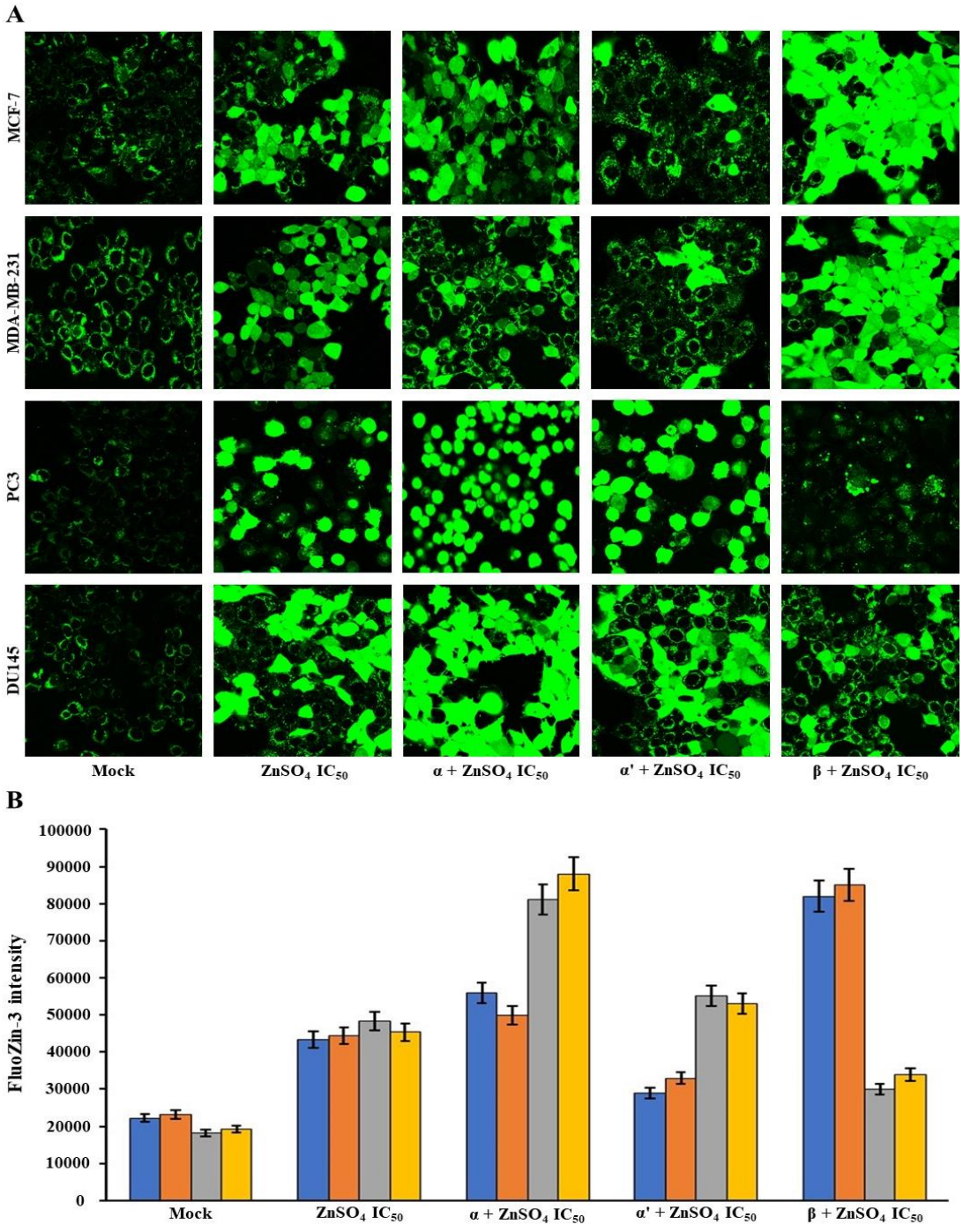

Fig 3.6 Visualisation of Zn^{2+} under siRNA knockdown of CK2 subunit genes

Cells were treated with each specific siRNA in confocal imaging dishes for 36 h prior to $ZnSO_4$ IC_{50} treatment and confocal imaging with fluorescent probe FluoZin-3 AM (A). Fluorescent intensity (B) was quantified for each treatment with confocal images at 40x magnification where blue indicates MCF-7 cells, orange MDA-MB-231 cells, grey PC3 cells and yellow DU145 cells. Error bars denote standard deviation of fluorescence intensity for each treatment.

3.3 Discussion

Zinc hyper-accumulates in breast cancer cells compared to normal mammary epithelial cells (Lopez et al., 2011; Chandler et al., 2016), while prostate cancer cells have much lower zinc content than normal prostate cells (Franklin et al., 2005; Song and Ho, 2009). Such phenomenon is poorly understood at a molecular level. By using breast and prostate cancer cells and manipulating protein kinase CK2 at protein and gene levels, this study acquired substantial evidence for the involvement of CK2 in zinc homeostasis of breast and prostate cancer cells.

From the response curves of breast and prostate cancer cells against zinc titration (Fig. 3.1A), a conspicuous divergence between the two types of cancer cells demonstrates that breast cancer cells are more capable of coping with acute zinc exposure than prostate cancer cells. No cytotoxicity is evident up to approximately 150 μM $ZnSO_4$ for breast cancer cells, whilst prostate cancer cells show little tolerance to 20 μM $ZnSO_4$. This is further confirmed by trypan blue staining and cell counting (Fig. 3.1B). Together with the control images in Fig. 3.5 and 3.6, the data supports the known phenomenon, that is, breast cancer cells have a higher zinc content than prostate cancer cells (Costello and Franklin, 2006; Alam and Kelleher, 2012). Further experiments done and their findings reported here provide some insights into this phenomenon in terms of the involvement of CK2.

The cancer cell's response to zinc exposure is underpinned by the regulation of uptake, sequestration and efflux of Zn^{2+}. As described at the outset, there are numerous membrane-bound transport proteins for Zn^{2+}, including 10 ZnT involved in decreasing cytoplasmic zinc level and 14 ZIP for increasing cytoplasmic zinc (Margalioth et al., 1983; Nelson, 1999; Yamasaki et al., 2007). These transporters are either present in the plasma membrane or in the membranes of subcellular organelles such as the endoplasmic reticulum (Cousins

et al., 2006; Yamasaki et al., 2007). Their regulation by other molecules such as CK2 (Guerra et al., 1999; Sekler et al., 2007; Taylor et al., 2008; Zaman et al., 2016) and metal regulatory transcription factor (Suhy et al., 1999; Lopez et al., 2011) is critical to maintain the homeostasis of cytoplasmic zinc, which is estimated to be at picomolar levels in eukarya (Outten and O'halloran, 2001; Bozym et al., 2006; Krężel and Maret, 2006; Vinkenborg et al., 2009).

The experiments using CK2 inhibitors demonstrate that CK2 function is required by both breast and prostate cancer cells to regulate zinc homeostasis under zinc exposure. The reason behind using two inhibitors, TBB and CX-4945, is to enhance the veracity of the findings since no inhibitor is absolutely specific against its target enzyme, although both TBB and CX-4945 are highly selective against CK2 (Lolli et al., 2012). Both TBB (20 µM) and CX-4945 (5 µM) showed the same effect, i.e., decreasing the cell viability of all four cancer cell lines under $ZnSO_4$ IC_{50} treatment (Fig. 3.2). Confocal imaging further demonstrates that reduction of cell viability was due to the increased accumulation of intracellular zinc (Fig. 3.5).

These findings together indicate CK2 is involved in zinc homeostasis, potentially through regulating zinc transport proteins associated with zinc uptake, sequestration, or efflux. It is well known that ZIP, ZnT and metallothioneins are the workhorses in zinc homeostasis. Zn^{2+} accumulation in breast cancer cells directly correlates with abnormal expression of ZIP6, ZIP7, ZIP10 and ZnT2 (Kagara et al., 2007; Taylor et al., 2008; Lopez et al., 2011), whilst decrease of cytoplasmic Zn^{2+} can be resulted from ZIP1 down-regulation in prostate cancer cells (Franklin et al., 2005; Prasad et al., 2009). It should be noted that since CK2 has many pleiotropic effects on various signal transduction pathways, simple interpretations about its role in zinc homeostasis, as stated above may not be the complete

picture. Further studies such as phosphoproteomics are needed to see if CK2 regulates the expression and/or activity of ZIP and ZnT.

siRNA mediated knockdown of individual CK2 subunit genes provide significant details on the involvement of CK2 in zinc homeostasis. Firstly, we analysed the efficacy of siRNA knockdown (Fig. 3.3). The average knockdown efficacy for all three CK2 subunit transcripts was 70.15%. Both MTT assay and confocal imaging demonstrate that CK2β knockdown is detrimental to both breast cancer cell lines whereas beneficial for both prostate cancer cell lines under IC_{50} Zn^{2+} (Fig. 3.4 and 3.6). Because CK2β is essential for the tetrameric holoenzyme CK2, these findings therefore suggest that the CK2 tetramer might be involved in up-regulating cytoplasmic zinc level in prostate cancer cells, while the opposite mode of action is likely the case for breast cancer cells. The varying behaviours of breast and prostate cancer cells are also evident in siRNA knockdown of CK2α' (Fig. 3.4 and 3.6). The cell viability was reduced, or zinc accumulation was elevated in PC3 and DU145 prostate cancer cells due to knockdown of CK2α', while the opposite was seen in MCF-7 and MDA-MB-231 breast cancer cells. Such opposite effect of CK2β and CK2α' demonstrates that CK2 is involved in zinc homeostasis, also that the CK2-related zinc homeostasis in breast and prostate cancer cells are divergent. Furthermore, siRNA knockdown of individual CK2 subunits shows that individual subunits of CK2 have distinct roles in zinc homeostasis in breast and prostate cancer cells.

3.4 Conclusion

In summary, the findings reported here demonstrate that CK2 is involved in zinc homeostasis in breast and prostate cancer cells and that individual CK2 subunits play distinct roles. The study provides a basis for future works on delineating the molecular network of zinc homeostasis involving CK2, zinc transport proteins (ZIP and ZnT),

metallothioneins and other players. The involvement of CK2 in zinc homeostasis may also have bearing in drug development for cancer treatment.

4 TRANSCRIPTOMIC INSIGHTS INTO THE ZINC HOMEOSTASIS IN MCF-7 BREAST CANCER CELLS VIA NEXT-GENERATION RNA SEQUENCING

4.1 Introduction

Zinc is one of the most abundant biometal ions in humans, because it is necessary for the structure and function of cellular proteins involved in multitudes of biological processes such as metabolism, proliferation and apoptosis (Vallee and Auld, 1990; Vallee and Auld, 1993; Franklin and Costello, 2007). There are at least 3000 zinc-binding proteins in the human proteome (Maret, 2003, 2012), many of which are enzymes and DNA-binding transcription factors (Vallee, 1983; Vallee and Auld, 1990; Vallee and Auld, 1993; Ebert and Altman, 2008). Zinc can also act as a second messenger in signal transduction cascades (Hershfinkel et al., 2001; Yamasaki et al., 2007; Maret, 2017). It is therefore plausible for the cell to maintain zinc homeostasis by tight control of zinc uptake, sequestration and export.

Impairment of cellular zinc homeostasis is linked to diseases such as breast cancer. It has been reported that breast cancer tissues accumulate zinc levels way beyond those observed in normal epithelial breast tissue (Ionescu et al., 2006). Such elevation in zinc level in cancerous breast tissue has been linked to cancer progression and malignancy (Ionescu et al., 2006; Cui et al., 2007; Alam and Kelleher, 2012). However, the molecular understanding underlying such a link is lacking. This transcriptomic study aims to fill this gap by gaining insights into zinc homeostasis of the luminal MCF-7 breast cancer cells.

Considerable progress has been made in the past decades on the membrane-bound proteins related to cellular zinc homeostasis, including 10 zinc exporting proteins (ZnT) in solute

carrier 30A (*SLC30A*) family for decreasing cytoplasmic concentration of zinc [Zn^{2+}] and 14 zinc importing proteins (ZIP) in SLC39A for increasing cytoplasmic [Zn^{2+}] (Nelson, 1999; Guerinot, 2000; Colvin et al., 2003; Kirschke and Huang, 2003; Maret, 2003; Desoize, 2004; Cousins et al., 2006; Kagara et al., 2007; Lopez et al., 2011; Choi and Bird, 2014). Recently, protein kinase CK2 in MCF-7 breast cancer cells was found to phosphorylate the zinc channel, ZIP7, which is located in the subcellular membrane of the ER (Taylor et al., 2012). The phosphorylation of ZIP7 by CK2 resulted in the release of zinc from the ER store to the cytoplasm, triggering a cascade of downstream signal transduction. In addition to zinc transport proteins, the cytoplasmic metallothioneins are involved in zinc sequestration, playing a critical role in cellular zinc homeostasis (Cousins et al., 2006; Vašák and Meloni, 2011; Kimura and Kambe, 2016).

In this study, we deployed a holistic approach by next-generation RNA sequencing to uncover genes involved in the cellular response to zinc exposure in MCF-7 breast cancer cells. It is anticipated that upon IC_{50} zinc exposure the breast cancer cells would up-regulate the genes related to intracellular zinc sequestration such as metallothionein genes. The family of ZIP transporters, responsible for zinc influx situated in the plasma membrane, are expected to be down-regulated in an attempt to reduce the influx of extracellular zinc. Similarly, ZIP transporters situated in organelles or subcellular compartments would likely be down-regulated in order to maintain the equilibrium of cytoplasmic zinc levels. Moreover, the gene expression of ZnT transporters would be up-regulated to efflux any excessive intracellular zinc. The most differentially expressed genes identified were then confirmed by quantitative reverse transcription polymerase chain reaction (qRT-PCR) and extended to the more malignant basal type of breast cancer cells (MDA-MB-231). Herein, we report the acquired dataset, the follow-up findings and the molecular insights gained from this study.

4.2 Results

4.2.1 Determination of IC_{50} of $ZnSO_4$ for MCF-7 and MDA-MB-231 breast cancer cells

IC_{50} values for MCF-7 and MDA-MB-231 breast cancer cells cultured in 96-well plates were firstly determined according to the dose response curves from the MTT assay (Fig. 4.1). The IC_{50} values of $ZnSO_4$ for MCF-7 and MDA-MB-231 cells were 320 µM and 350 µM, respectively. The cell enumeration by trypan blue staining further confirmed these IC_{50} values. The IC_{50} dose of $ZnSO_4$ for MCF-7 cells (320 µM) was applied to the cells at 80% confluency in 25 cm^2 flasks for RNA-seq transcriptomic analysis. The cells were morphologically healthy at T_{30} and T_{120} in the time course of treatment.

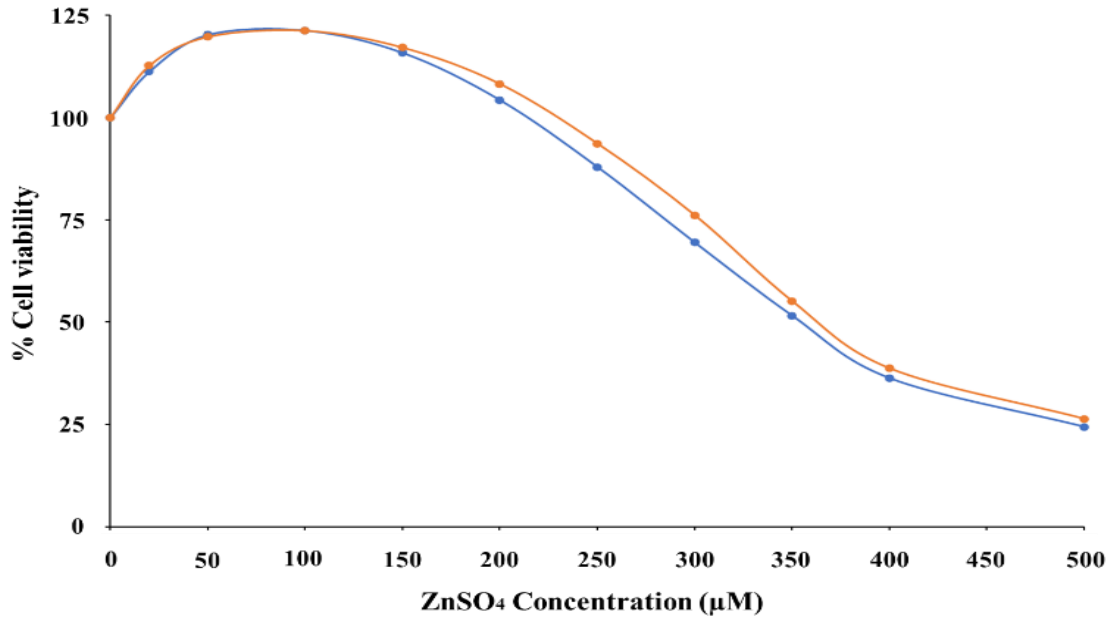

Fig 4.1 Zinc dose responsive curves of MCF-7 and MDA-MB-231 breast cancer cells Cells were grown for 32 h to reach 80% confluency and then treated with 0 to 500 µM of $ZnSO_4$. The viability of the cells was quantified by MTT assay at the end of 6 h treatment. Blue represents MCF-7 and orange represents MDA-MB-231. The IC_{50} for each cell line was determined according to their response curves. Error bars, too small to be seen, represent the standard deviation of six biological replicates.

4.2.2 Overview of differentially expressed genes in MCF-7 cells in the time course under zinc treatment

By comparing T_{30} zinc treatment against the control, 123 up-regulated and 8 down-regulated genes were identified (Appendices 1.1 and 1.2). At T_{120} zinc treatment against the control revealed 473 up-regulated and 123 down-regulated genes, using edgeR (Appendices 1.3 and 1.4). Differentially expressed genes were coloured in red (Log_2FC >0.6) and green (Log_2FC >1) with a Benjamini-Hochberg corrected *p*-value less than 0.05 (Benjamini and Hochberg, 1995). The synoptic overviews of the transcriptomic data for T_{30} and T_{120} zinc treatment in comparison to control are shown in Fig. 4.2 by differential expression analysis using the bioconductor packages edgeR (v 3.18.1).

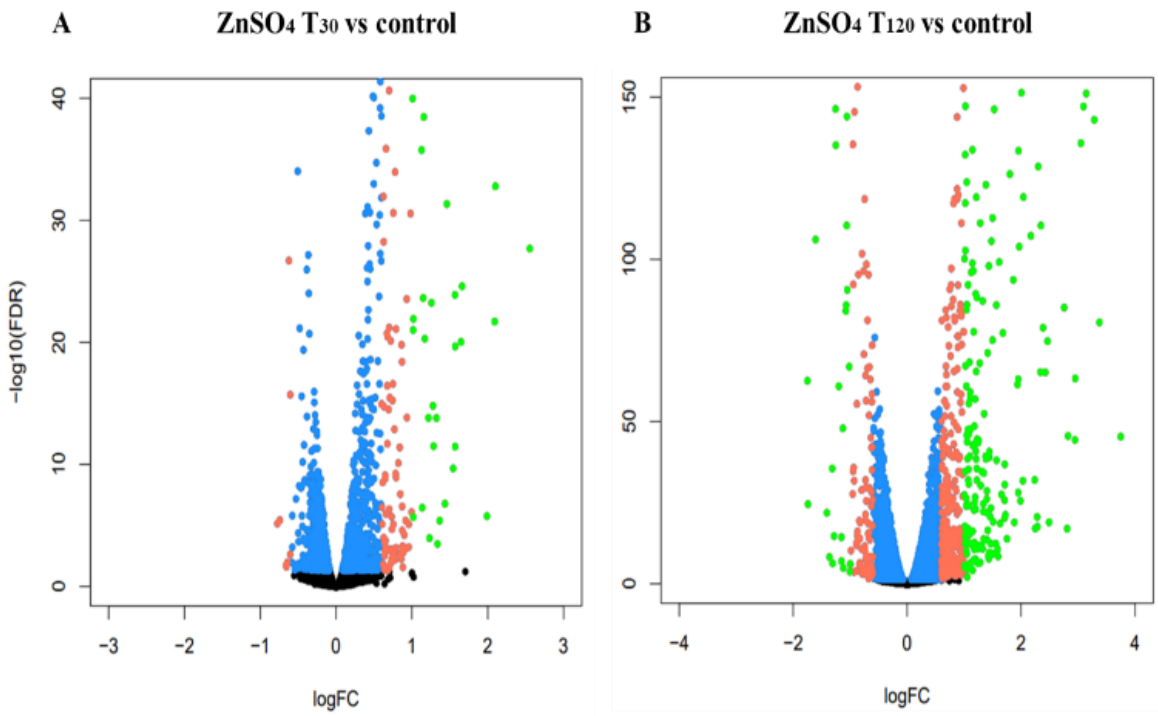

Fig 4.2 Volcano plots for T_{30} and T_{120} zinc treatment versus control

The volcano plots depict the gene expression profiles for T_{30} zinc treatment against control (A) and T_{120} zinc treatment against control (B). Genes in blue have Log_2FC between 0 and 0.6 or between 0 and -0.6, while genes in red and green are differentially expressed, with Log_2FC >0.6 for red and Log_2FC >1 for green.

4.2.3 Top differentially expressed genes in response to zinc exposure

Table 4.1 highlights the 19 up-regulated genes and 1 down-regulated gene for T_{30} against control. Metallothionein genes (*MT1B*, *MT1X*, *MT1F* and *MT2A*) and ZnT1 gene (*SLC30A1*) are prominent. The expression of *MT1B* was increased by 45-fold (Log_2FC = 5.4842) compared to the control. This finding suggests that metallothioneins and zinc exporter ZnT1 are the first line of response in dealing with extracellular zinc exposure, as their functions are to reduce intracellular free zinc by sequestration and export.

EGR1 and *EGR2*, encoding the early growth response proteins EGR1 and EGR2, were significantly up-regulated at both T_{30} and T_{120} zinc treatment shown in Table 4.1 and 4.2. EGR1 and EGR2 are zinc finger transcription factors and regulate the expression of numerous genes involved in response to extracellular stimuli and endoplasmic reticulum stress (Kumbrink et al., 2010). Their up-regulation indicates they are responsive to extracellular zinc. Similarly, many other zinc finger protein genes (*RNF165*, *SNAI1*, *ZNF442*, *ZNF365*, *ZNF547*, *ZNF563*, *ZNF296* and *ZBTB2*) were up-regulated at T_{30} and T_{120}, whereas *ZNF750* and *ZNF256* were only up-regulated at T_{30} zinc treatment. The up-regulation of *RGS16*, *RASD1*, *CTGF*, *NR4A3*, *NR4A1*, *TRIB1*, *NGFR* and *HES1* genes was also observed at T_{30} (Table 4.1). These genes are related to cell survival (*NGFR* and *TRIB1*), stress response (*HES1*, *RGS16*, *RASD1*, *NR4A3* and *NR4A1*) and cytoskeletal perturbation (*CTGF*). The increase of histone gene expression (*HIST1H4D*, *HIST1H1D* and *HIST1H2AD*) at T_{30} indicates that the excess of intracellular zinc affected genome stability in MCF-7 breast cancer cells.

The expression of metallothionein genes (*MT1B*, *MT1X*, *MT1F* and *MT2A*) and ZnT1 gene (*SLC30A1*) continues to increase at T_{120} (Table 4.2, Fig. 4.3). *MT1B* expression was

elevated dramatically by 869-fold ($Log_2FC = 9.7648$) against control. Fig. 4.3 shows the dynamic changes of expression for the 11 up-regulated genes shared by T_{30} and T_{120} as listed in Table 4.1 and 4.2, exhibiting the increased expression pattern for each of them. Furthermore, the genes for heat shock proteins were also significantly up-regulated at T_{120} (*HSPA6*, *HSPA1A*, *HSPA1B*, *HSPH1*, *HSPE1*, *HSP90AA1*, *HSPA8*, *HSPA1L*, *HSP90AB1*, *HSPA4L* and *HSPD1*) (Table 4.2). This demonstrates that heat shock proteins along with the other stress-responsive proteins are essential in dealing with extracellular zinc exposure.

PLK2, encoding Polo-like kinase 2, is a prominent down-regulated gene under zinc exposure, as its expression was decreased at both T_{30} (~1.5 arithmetic fold) and T_{120} (~4 arithmetic fold). qRT-PCR was used to validate the RNA-seq dataset. Nine genes (*MT1B*, *MT1X*, *MT1F*, *MT2A*, *SLC30A1*, *VMP1*, *ZNF850*, *HSP6* and *HSP90AA1*) were analysed and their expression pattern correlates with dynamic changes shown by RNA-seq (Fig. 4.4). These differentially expressed genes were further quantified in the basal-type breast cancer cells (MDA-MB-231) in the same zinc sulfate treatment condition. The result in Fig. 4.4 and 4.5 shows the similar pattern as the luminal-type MCF-7 cells, except *SLC30A1* which was expressed higher in MDA-MB-231 at both T_{30} and T_{120} in response to zinc exposure.

Table 4.1 Significantly up or down-regulated genes at T_{30} zinc treatment

Up-regulated Genes	Protein name	Log_2FC	*p*-value
MT1B	Metallothionein-1B	5.4842	1.3E-06
MT1X	Metallothionein-1X	4.9304	0
SLC30A1	Zinc transporter 1	4.2508	0
EGR2	Early growth response protein 2	3.8541	8.11E-52
MT1F	Metallothionein-1F	3.2883	0
RGS16	Regulator of G-protein signaling 16	2.9960	1.2E-271
RASD1	Dexamethasone-induced Ras-related protein 1	2.8272	5.94E-61
CTGF	Connective tissue growth factor	2.5543	1.11E-30
EGR1	Early growth response protein 1	2.1005	7.21E-36
NR4A3	Nuclear receptor subfamily 4 group A member 3	2.0909	1.35E-24
TRIB1	Tribbles homolog 1	1.7988	2.6E-244
NR4A1	Nuclear receptor subfamily 4 group A member 1	1.7706	4.11E-84
NGFR	Tumour necrosis factor receptor superfamily member 16	1.6617	1.54E-27
HES1	Transcription factor HES-1	1.6455	0

RNF165	E3 ubiquitin-protein ligase RNF165	1.5675	7.97E-27
HIST1H4D	Histone H4	1.5438	3.18E-12
HIST1H1D	Histone H1.3	1.5048	1.43E-51
HIST1H2AD	Histone H2A type 1-D	1.4599	2.14E-34
MT2A	Metallothionein-2A	1.4565	2.92E-160
Down-regulated Gene	**Protein name**	**Log_2FC**	***p*-value**
PLK2	Polo-like kinase 2	-0.6833	0

Table 4.2 Significantly up or down-regulated genes at T_{120} zinc treatment.

Up-regulated Genes	Protein name	Log_2FC	*p*-value
MT1B	Metallothionein-1B	9.7648	7.30E-82
HSPA6	Heat shock 70 kDa protein 6	8.1516	1.59E-123
MT1X	Metallothionein-1X	6.2610	0
MT1F	Metallothionein-1F	5.7923	0
SLC30A1	Zinc transporter 1	5.0368	0
CHRM4	Muscarinic acetylcholine receptor M4	4.9973	1.28E-35
RNF165	E3 ubiquitin-protein ligase RNF165	4.9857	0

HMOX1	Heme oxygenase 1	4.6412	2.41E-308
MT4	Metallothionein-4	4.5477	1.27E-29
RGS16	Regulator of G-protein signaling 16	3.8188	0
SLCO4A1	Solute carrier organic anion transporter family member 4A1	3.6227	0
EGR1	Early growth response protein 1	3.3742	2.48E-83
NGFR	Tumour necrosis factor receptor superfamily member 16	3.2832	3.74E-146
CNKSR3	Connector enhancer of kinase suppressor of ras 3	3.1801	3.82E-177
KBTBD11	Kelch repeat and BTB domain-containing protein 11	3.1410	2.39E-154
HSPA1A	Heat shock 70 kDa protein 1A	3.0934	2.53E-150
HSPA1B	Heat shock 70 kDa protein 1B	3.0474	5.99E-139
RASD1	Dexamethasone-induced Ras-related protein 1	2.9477	6.00E-66
SLC2A14	Solute carrier family 2, facilitated glucose transporter member 14	2.9443	7.79E-47
CLCF1	Cardiotrophin-like cytokine factor 1	2.8229	4.33E-48
EGR2	Early growth response protein 2	2.8057	5.36E-19
MT2A	Metallothionein-2A	2.5856	0

CHST3	Carbohydrate sulfotransferase 3	2.4900	4.99E-21
C17orf67	Uncharacterised protein C17orf67	2.4625	1.66E-77
RAB3A	Ras-related protein Rab-3A	2.3841	1.13E-81
NOTCH1	Neurogenic locus notch homolog protein 1	2.3543	0
DNAJB1	DnaJ homolog subfamily B member 1	2.3458	2.13E-113
TRIB1	Tribbles homolog 1	2.3407	0
SOCS2	Suppressor of cytokine signaling 2	2.3388	6.41E-68
HSPH1	Heat shock protein 105 kDa	2.2993	1.03E-131
CBARP	Voltage-dependent calcium channel beta subunit-associated regulatory protein	2.2869	1.31E-19
CSRP2	Cysteine and glycine-rich protein 2	2.2468	4.62E-19
ZNF365	Zinc Finger protein 365	2.2367	2.44E-34
NPL	N-acetylneuraminate lyase	2.1705	3.26E-110
MAP3K8	Mitogen-activated protein kinase kinase kinase 8	2.0395	3.14E-122
DUSP6	Dual specificity protein phosphatase 6	2.0303	4.37E-34
ZBTB2	Zinc finger and BTB domain-containing protein 2	2.0255	0

SPACA6	Sperm acrosome membrane-associated protein 6	2.0047	1.39E-154
SLC2A4	Solute carrier family 2, facilitated glucose transporter member 4	1.9872	8.77E-28
LRFN4	Leucine-rich repeat and fibronectin type-III domain-containing protein 4	1.9871	3.52E-229
DDIT4	DNA damage-inducible transcript 4 protein	1.9723	0
ZFP36	Zinc Finger protein 36	1.9661	7.37E-107
DUSP10	Dual specificity protein phosphatase 10	1.9529	1.41E-136
CREB5	Cyclic AMP-responsive element-binding protein 5	1.9478	1.01E-65
C2orf54	Chromosome 2 open reading frame 54, otherwise known as Mab21L4	1.9474	2.23E-30
POLH	DNA polymerase eta	1.9040	2.39E-305
CSRP1	Cysteine and glycine-rich protein 1	1.8985	0
C3orf80	Uncharacterised membrane protein C3orf80	1.8806	5.36E-21
SERPINE1	Plasminogen activator inhibitor 1	1.8622	1.43E-96
MCL1	Induced myeloid leukemia cell differentiation protein Mcl-1	1.8571	0

NR4A3	Nuclear receptor subfamily 4 group A member 3	1.7505	9.53E-16
PKDCC	Extracellular tyrosine-protein kinase PKDCC	1.7239	2.28E-23
SPRY4	Protein sprouty homolog 4	1.7115	7.13E-33
CALML5	Calmodulin-like protein 5	1.7113	3.12E-39
DNAJB5	DnaJ homolog subfamily B member 5	1.7084	5.57E-28
NUDT16L1	Tudor-interacting repair regulator protein	1.6808	0.00E+00
SERPINH1	Serpin H1	1.6788	4.78E-80
SNAI1	Zinc finger protein SNAI1	1.6551	9.37E-30
CEBPD	CCAAT/enhancer-binding protein delta	1.6142	4.45E-102
GBP1	Guanylate-binding protein 1	1.5968	4.28E-10
AKR1C2	Aldo-keto reductase family 1 member C2	1.5841	1.51E-12
DEDD2	DNA-binding death effector domain-containing protein 2	1.5648	9.95E-89
SKIL	Ski-like protein	1.5291	0
OSGIN1	Oxidative stress-induced growth inhibitor 1	1.5265	2.04E-149
NET1	Nucleolar protein NET1	1.5168	4.97E-261

FAM196A	Protein FAM196A	1.5037	7.13E-11
FAM189A2	Protein FAM189A2	1.4979	9.36E-116
C1orf132	Chromosome 1 open reading frame 132	1.4976	8.05E-78
SEMA3F	Semaphorin-3F	1.4797	0
INSIG1	Insulin-induced gene 1 protein	1.4780	1.40E-108
RND1	Rho-related GTP-binding protein Rho6	1.4688	1.61E-25
JUN	Transcription factor AP-1	1.4649	8.44E-238
Down-regulated Genes	**Protein name**	**Log_2FC**	***p*-value**
PLK2	Polo-like kinase 2	-2.0898	0
MAP10	Microtubule-associated protein 10	-1.7501	3.27E-65
ANKRD1	Ankyrin repeat domain-containing protein 1	-1.7400	1.01E-26
IRX5	Iroquois-class homeodomain protein IRX-5	-1.6967	0
BAMBI	BMP and activin membrane-bound inhibitor homolog	-1.6407	0
IL20	Interleukin-20	-1.6077	4.55E-109
DKK1	Dickkopf-related protein 1	-1.5413	0

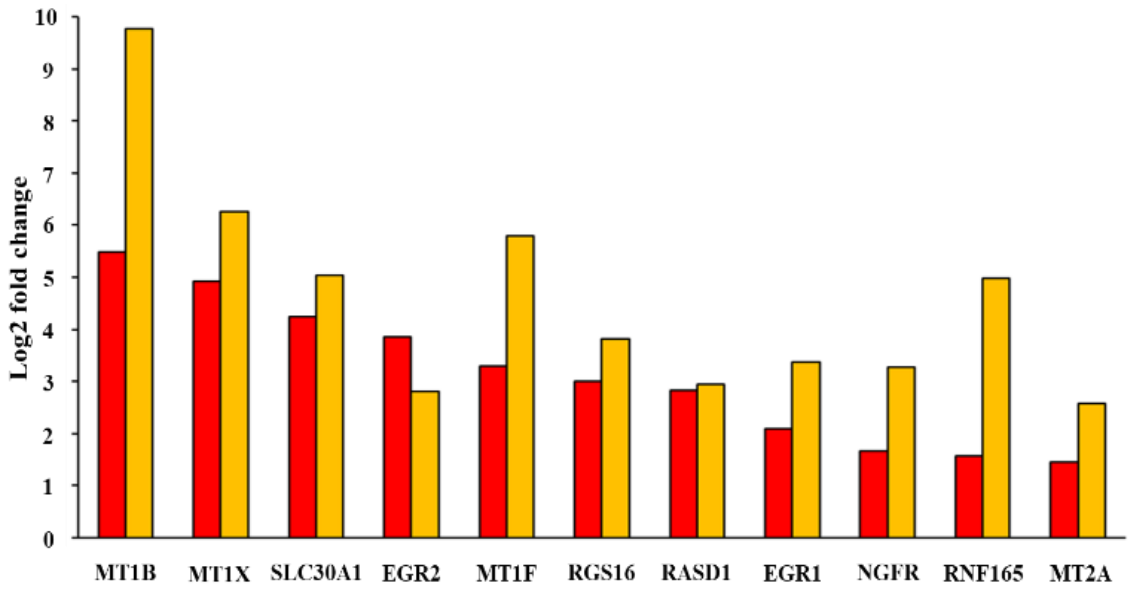

Fig 4.3 Log_2FC of differentially expressed genes shared by T_{30} and T_{120}

Summary of overlapping genes between T_{30} and T_{120} IC_{50} zinc treatment (320 µM) in MCF-7 breast cancer cells obtained via next-generation RNA sequencing. Red denotes Log_2FC for T_{30} zinc treatment while yellow represents Log_2FC for T_{120} zinc treatment. Data represents the average of three biological replicates.

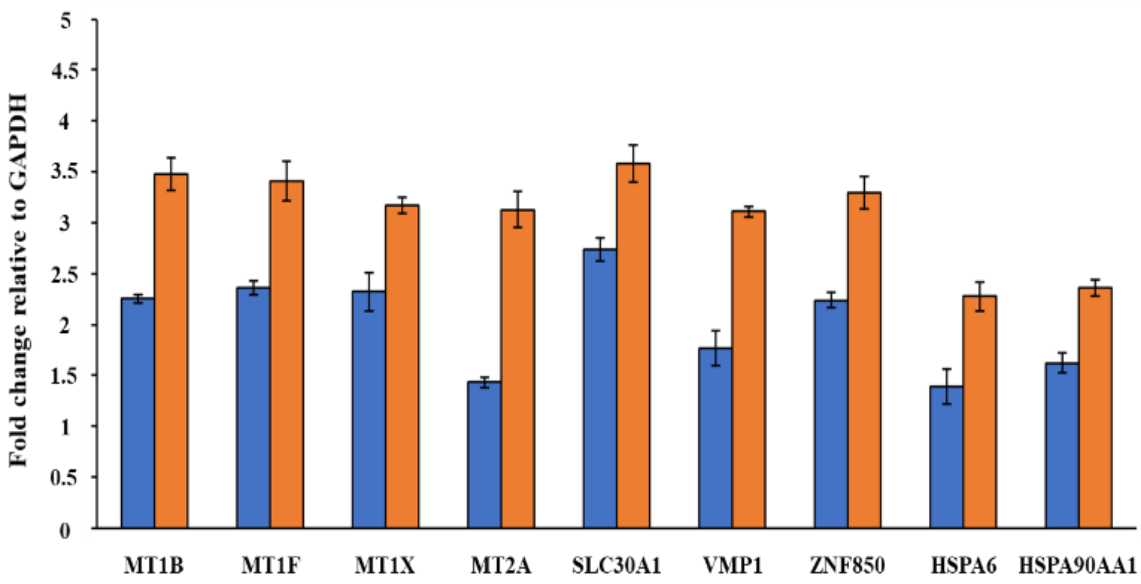

Fig 4.4 Quantification of gene expression in MCF-7 breast cancer cells by qRT-PCR
MCF-7 cells were grown for 32 h to reach 80% confluency and treated with IC_{50} $ZnSO_4$ (320 µM) for T_{30} and T_{120}. Total RNA was then prepared, cDNA synthesised and qRT-PCR performed. Relative expression of the genes *MT1B*, *MT1F*, *MT1X*, *MT2A*, *SLC30A1*, *VMP1*, *ZNF850*, *HSPA6* and *HSPA90AA1* was quantified relative to *GAPDH*. Blue represents MCF-7 cells treated with IC_{50} $ZnSO_4$ for T_{30} min and orange for T_{120} min. Data represents the average of three biological replicates and each biological replicate has three technical replicates. Error bars represent SEM of three biological replicates.

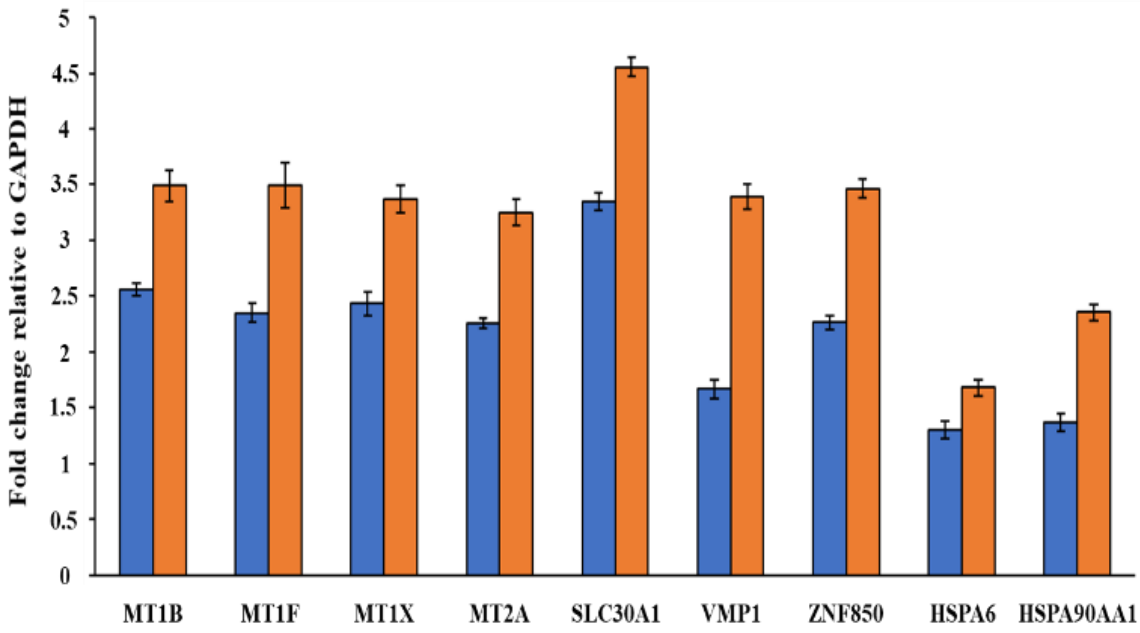

Fig 4.5 Quantification of gene expression in MDA-MB-231 breast cancer cells by qRT-PCR

MDA-MB-231 cells were grown for 32 h to reach 80% confluency and treated with IC_{50} $ZnSO_4$ (350 µM) for T_{30} and T_{120}. Total RNA was then prepared, cDNA synthesised and qRT-PCR performed. Relative expression of the genes *MT1B*, *MT1F*, *MT1X*, *MT2A*, *SLC30A1*, *VMP1*, *ZNF850*, *HSPA6* and *HSPA90AA1* was quantified relative to *GAPDH*. Blue represents MDA-MB-231 cells treated with IC_{50} $ZnSO_4$ for T_{30} min and orange for T_{120} min. Data represents the average of three biological replicates and each biological replicate has three technical replicates. Error bars represent SEM of three biological replicates.

4.3 Discussion

A pronounced feature of breast cancer cells is its high intracellular zinc level compared to normal breast epithelial cells (Margalioth et al., 1983; Franklin and Costello, 2007; Kagara et al., 2007; Franklin and Costello, 2009; Alam and Kelleher, 2012). For the first time, this study applies an all-inclusive approach by RNA-seq to explore the transcriptome of breast cancer cells in response to zinc exposure. An extensive literature survey indicates RNA-seq transcriptomic analysis has not been conducted for any cancer cell lines used in this study in response to zinc exposure. The dataset in triplicate reported above provides snapshots of the genes involved in zinc homeostasis, we see the dynamic changes in gene expression over time and further validation was carried out with qRT-PCR, performed in triplicate. The findings in MCF-7 breast cancer cells were further extended to the basal type of breast cancer cells (MDA-MB-231) through qRT-PCR.

The biological roles of metallothioneins are still under active research, although they were first isolated decades ago (Margoshes and Vallee, 1957). This study demonstrates that *MT1B*, *MT1F*, *MT1X* and *MT2A* are the initial response to zinc exposure. The finding agrees with the existing understanding for their role in zinc sequestration (Suhy et al., 1999; Adams et al., 2002; Coyle et al., 2002; Maret, 2003). Previous studies have reported on the involvement of metallothioneins in cancer cell survival and proliferation (Wu et al., 2016; Baltaci et al., 2018; Rahman and Karim, 2018; Si and Lang, 2018; Sinduja et al., 2020). However, the degree of the dramatic up-regulation, up to 869-fold, is not expected, which highlights the critical role of metallothioneins in zinc homeostasis of breast cancer cells. As is known, the zinc level in breast cancer cells is pronouncedly higher than the normal breast epithelial cells (Margalioth et al., 1983; Franklin and Costello, 2007; Kagara et al., 2007; Franklin and Costello, 2009; Alam and Kelleher, 2012) and the level of

expression for metallothioneins are also found to be increased in breast cancer cells (Meskel et al., 1993; Schmid et al., 1993; Goulding et al., 1995; Oyama et al., 1996; Suhy et al., 1999; Si and Lang, 2018). The notion that metallothioneins are involved in the proliferation of breast cancer cells is fascinating, particularly when we also consider the fact that breast cancer cells contain more zinc which incurs higher expression of metallothioneins as shown in this study. One might question whether there is a potential role of zinc in breast cancer development. It is no doubt that more research on the role of metallothioneins in zinc homeostasis and breast cancers will be carried out in the years to come.

Thus far, 11 functional metallothioneins are encoded by a family of genes located on chromosome 16q13 (*MT1A*, *MT1B*, *MT1E*, *MT1F*, *MT1G*, *MT1H*, *MT1M*, *MT1X*, *MT2A*, *MT3* and *MT4*). The pseudogenes (*MT1C*, *MT1D*, *MT1I*, *MT1J* and *MT1L*) cannot encode metallothionein (Si and Lang, 2018). While the expression of *MT1A*, *MT1B*, *MT1E*, *MT1F*, *MT1G*, *MT1H*, *MT1M*, *MT1X* and *MT2A* are ubiquitous, *MT3* and *MT4* are normally expressed in neurons of the brain and in stratified squamous epithelial cells of the skin (Vašák and Meloni, 2011). The significant up-regulation (24-fold) of MT4 upon zinc exposure in the breast cancer cells is a novel finding, which shows that MT4 is expressed in breast cancer cells and that it is involved in zinc homeostasis.

The gene for zinc exporter ZnT1 (*SLC30A1*) was prominently up-regulated in both T_{30} (19-fold) and T_{120} (32-fold). As the ZnT1 protein is a plasma membrane-bound transporter (Kambe et al., 2014; Kimura and Kambe, 2016), the finding indicates that ZnT1 is a key player in zinc homeostasis by exporting excess intracellular zinc out of the cell. This also means that the other nine members of *SLC30* family may not be prominent in response to extracellular zinc. Intriguingly, *SLC30A1* expression is higher in MDA-MB-231 cells than

MCF-7 cells according to the qRT-PCR data (Fig. 4.4 and 4.5). This finding shed light on the behaviour of these two types of breast cancer cells. The luminal MCF-7 cells are less malignant (Lee et al., 2015) and its IC_{50} of zinc sulfate (320 μM) is lower than the basal type MDA-MB-231 cells (350 μM). The IC_{50} values of zinc sulfate for basal MDA-MB-231 and luminal MCF-7 breast cancer cells demonstrate their robustness to extracellular zinc exposure. The basal MDA-MB-231 breast cancer cells showed greater tolerance to zinc exposure compared to luminal MCF-7 breast cancer cells, which may reflect the increased aggressiveness of basal type of breast cancer (Liu et al., 2003; Chavez et al., 2010). As is known, ZnT1 is the sole zinc efflux transporter residing in the plasma membrane and is functionally non-redundant in the maintenance of zinc homeostasis (Kambe et al., 2015). Its higher expression in MDA-MB-231 cells than MCF-7 explains the variation of zinc IC_{50} for the two cell lines, which may also relate to the degree of their malignancy because experimental evidence demonstrates that alterations in ZnT1 expression and the gene mutations of ZnT1 provide a molecular mechanism for impaired zinc homeostasis in cancer development and/or progression (Lehvy et al., 2019).

Furthermore, one would think that the effective way to control cytoplasmic zinc level is to regulate the import of extracellular zinc into the cell by either down-regulation of ZIP expression at the transcriptional level or reduction of functional ZIPs in the plasma membrane. Intriguingly, the dataset herein did not reveal any down-regulation of ZIP genes (*SLC39A*). The possible explanation for no alteration of ZIP gene expression in MCF-7 breast cancer cells following IC_{50} zinc exposure may be due to the propensity of breast cancer cells' zinc tolerance. MCF-7 cells would initially activate zinc sequestration and efflux mechanism to deal with an acute zinc exposure such as the experimental condition in this chapter. This notion is demonstrated true by the transcriptomic dataset reported in Section 4.2. This might be due to the inherent propensity of breast cancer cells

to import zinc via ZIPs at the beginning of the exposure and then there is a time lag for the cancer cells to mount a response to regulate ZIPs either at the transcriptomic or protein level.

It is puzzling to see that many zinc finger protein genes, such as *RNF165*, *SNAI1*, *ZNF442*, *ZNF365*, *ZNF547*, *ZNF563*, *ZNF296*, *ZBTB2*, *ZNF750* and *ZNF256*, were up-regulated in response to the increased extracellular zinc, for the roles of these genes in the cell have not yet been elucidated. But one obvious property shared by the zinc finger proteins is their ability to bind zinc. Hence, their sequestration of zinc could explain their up-regulation. Considering together with the increase of gene expression for metallothioneins and ZnT1 as discussed above, we can now visualise the all-hands-on-deck strategy adopted by the breast cancer cells in maintaining zinc homeostasis under the challenge of extracellular zinc exposure.

The up-regulation of the genes for heat shock proteins at T_{120} (*HSPA1A*, *HSPA1B*, *HSPA1L*, *HSPA4L*, *HSPA6*, *HSPA8*, *HSPH1*, *HSP90AA1* and *HSP90AB1*) along with the stress responsive gene *VMP1* demonstrates that the zinc exposure results in stress to the breast cancer cells and that these chaperone proteins are key responder molecules. The finding further points to the known fact that heat shock proteins are the bedrock for the robustness of cancer cells (Udono and Srivastava, 1993; Cornford et al., 2000; Isaacs et al., 2003; Calderwood et al., 2006). Therefore, they are increasingly targeted for anticancer drug development.

The gene for Polo-like kinase (*PLK2*) is a prominent down-regulated gene. It belongs to a family of genes encoding the structurally related serine/threonine protein kinases that are defined by the presence of C-terminal “polo box” domains and are best known as cell cycle regulators (Ma et al., 2003). Its significant decrease in gene expression against zinc

exposure is reported here for the first time. The underlining reason for this finding might be linked to its role in cell cycle regulation. It's down-regulation would lead to arrest of cell cycle progression, allowing the cancer cells to adapt to the stress incurred by zinc exposure. The finding could also be linked to zinc-related ER stress because a dramatic decrease in *PLK2* expression was also discovered in ER stress (Shen et al., 2017).

Surprisingly, the gene expression levels of protein kinase CK2 subunits (*CSNK2A1*, *CSNK2A2* and *CSNK2B*) were not changed. This suggests that the basal expression of CK2 subunits is sufficient for MCF-7 breast cancer cells to deal with the zinc exposure. Also unchanged is the *MTF-1* gene encoding metal response element binding transcription factor 1, also called metal regulatory transcription factor 1 (MTF-1), which is known to regulate metallothioneins and ZnT1 at the transcript level (Langmade et al., 2000; Andrews, 2001; Urani et al., 2010). MTF-1 has a serine and threonine rich region near its C-terminus (Potter et al., 2005). This leads to a possibility that it could be phosphorylated by protein kinases such as CK2 protein kinase. Indeed, it is found that the phosphorylation of MTF-1 plays a critical role in its activation by zinc, and protein kinase CK2 is one of the kinases which can phosphorylate MTF-1 (Saydam et al., 2002). The gene expression of both MTF-1 and CK2 subunits are not varied by the exposure to zinc in MCF-7 breast cancer cells, such a status quo belies their significance in regulating the zinc homeostasis of breast cancer cells.

Metal-responsive transcription factor 1 (MTF-1) is a highly conserved Cys_2-His_2 zinc finger protein that recognises and binds cis-acting DNA elements, termed metal response elements (MRE), to promote the transcription of genes that maintain metal ion homeostasis (Giedroc et al., 2001; Laity and Andrews, 2007; Lichten et al., 2011). Acting as a sensor for intracellular zinc level and a regulator of zinc homeostasis, MTF-1 translocates from

cytoplasm to nucleus in response to zinc overload, and activates the transcription of genes for zinc efflux transporter proteins and zinc sequestration proteins such as ZnT1 and metallothioneins (Hardyman et al., 2016). Consequently, it is certain for this study that MTF-1 is involved in the strong up-regulation of *SLC30A1* (ZnT1), *MT1B, MT1X*, *MT1F*, *MT2A* and *MT4* in MCF-7 breast cancer cells in response to zinc exposure. Jackson *et al*. (2020) identified a list of MTF-1 biomarker genes according to 10 microarray transcriptomic datasets representing diverse metal treatments and human cell types, 9 up-regulated genes (*AKR1C2*, *CLU*, *ATF3*, *GDF15*, *HMOX1*, *MAP1A*, *MAFG*, *SESN2* and *UBC*) of this study are on that list, apart from the common metallothionein genes and *SLC30A1*. *AKR1C2* (aldo-keto reductase family 1 member C2), *ATF3* (activating transcription factor 3), *CLU* (clusterin) and *HMOX1* (heme oxygenase 1) are involved in reducing the effects of oxidative stress (Schwochau et al., 1998; Hai et al., 1999; Hansen et al., 2000; Permenter et al., 2011; Shirato et al., 2014). *GDF15* (growth/differentiation factor 15), *MAP1A* (microtubule-associated protein 1A), *MAFG* (transcription factor MafG), *SESN2* (sestrin-2) and *UBC* (ubiquitin C) are associated with a range of cellular stress responses (Katsuoka et al., 2005; Parker et al., 2014; Wollert et al., 2017; Bianchi et al., 2018; Wang et al., 2020). The up-regulation of *AKR1C2*, *CLU*, *ATF3*, *GDF15*, *HMOX1*, *MAP1A*, *MAFG*, *SESN2* and *UBC*, together with the genes for heat shock proteins described previously, in MCF-7 breast cancer cells upon zinc exposure suggests that cell stress was incurred by the zinc overload, and the cancer cells mobilised their stress response machinery for survival. The up-regulation of *NOTCH1* (neurogenic locus notch homolog protein 1) in this study is also likely due to MTF-1 based on the previous study (Lichtlen et al., 2001). So is *PPP1R18* (protein phosphatase 1 regulatory subunit 18) since *PPP1R15A* is the biomarker gene of MTF-1 (Jackson et al., 2020).

Additionally, despite metallothionein genes and *SLC30A1* are common responsive genes to zinc exposure, the previous transcriptomic data demonstrated that the effects of zinc are cell-type specific (Haase et al., 2007; Lin et al., 2009; Ryu et al., 2011). Haase *et al*. compared the transcriptomic responses to zinc exposure of B cells, T cells and monocytes by the microarray analysis, only finding four common responsive genes (*SLCO1C1*, *SLC30A1*, *MT1L* and *MT1H*) amongst the three cell types in the immune system (Haase et al., 2007). Therefore, the RNA-seq dataset reported here is meaningful for MCF-7 breast cancer cells in response to zinc exposure, although *SLC30A1* and metallothionein genes are also present. A notion must be made that the exact genes for metallothionein isoforms in response to zinc exposure vary among cell types.

Imbalance of zinc homeostasis is harmful to the cell. A substantially greater zinc level has been discovered in breast cancer cells compared to normal breast epithelial cells (Alam and Kelleher, 2012). Higher intracellular zinc level has been associated with elevated malignancy for breast cancer (Margalioth et al., 1983; Rizk and Sky-Peck, 1984; Kagara et al., 2007). Its accumulation has been linked with aberrant expression of ZIP6, ZIP7, ZIP10, ZnT1 and ZnT2 (Kagara et al., 2007; Taylor et al., 2008; Lopez et al., 2011). In contrast, intracellular zinc level has been determined to be lower in prostate cancer cells when compared to normal prostate cells, and down-regulation of transporter expression such as ZIP1 in malignant prostate tissue correlates with a noticeable decrease of intracellular zinc level (Franklin et al., 2005; Song and Ho, 2009).

Finally, a notion must be made, that is, findings from a transcriptomic study might not always be replicated at the protein level. The change in gene expression at mRNA levels can be used as an indicator for proteins (Raghavan et al., 2002; Roux and Topisirovic, 2012; Liu et al., 2016). Regulation at mRNA level for various genes is essential for the

cell to respond to the flux of cytoplasmic zinc concentration (Liu et al., 2016). By studying mRNA levels, we can gain insight and knowledge into the mechanisms involved in the cell's reaction to zinc stress, thus providing clues into the molecular details of cellular zinc homeostasis. Previous studies demonstrated that increased gene expression of ZIP6, ZIP7 and ZIP10 is directly associated with elevated protein expression (Bafaro et al., 2017; Baltaci and Yuce, 2018). However, post-translational modifications such as phosphorylation is another regulatory mechanism for the activity of zinc transport proteins in the cell. For example, it has been demonstrated that protein kinase CK2 phosphorylates the zinc channel, ZIP7, situated in the membrane of the endoplasmic reticulum (Taylor et al., 2012). Phosphorylation of ZIP7 leads to the subsequent release of zinc ions in ER stores, resulting in elevated intracellular concentration of zinc, thereby sparking a surge of downstream signal transduction.

4.4 Conclusion

In conclusion, the significance of this study resides in the differentially expressed genes uncovered by RNA-seq in MCF-7 breast cancer cells in response to exogenous zinc. It is highly significant to discover that ZnT1 gene (*SLC30A1*) is differentially expressed in the aggressive MDA-MB-231 cells compared to MCF-7 cells. The dataset reported in this chapter contributes to our knowledge and understanding of zinc homeostasis in breast cancer cells. The role of zinc in breast cancer development and treatment is currently an area of active research worldwide. The molecular clues described here are a step forward in this endeavour.

5 VALIDATION OF THE DIFFERENTIALLY EXPRESSED GENES AND EXPLORATION OF THE ROLE OF CK2 IN ZINC HOMEOSTASIS VIA qRT-PCR AND ICP-MS ANALYSIS

5.1 Introduction

As described in Chapter 4, genes exhibiting differential expression in response to extracellular zinc exposure were revealed by RNA-seq. Nine genes at the top of the up-regulated gene list were further validated by qRT-PCR. The validation was carried out in six cell lines, including two breast cancer cell lines (MCF-7, MDA-MB-231) and a normal breast cell line (MCF10A), two prostate cancer cell lines (PC3, DU145) and a normal prostate cell line (RWPE-1). By using this expanded panel of cell lines, an in-depth understanding of those differentially expressed genes in zinc homeostasis of both breast and prostate cancer cells was gained. The gene expression of CK2 subunits (*CSNK2A1*, *CSNK2A2* and *CSNK2B*) was also analysed in these six cell lines by means of qRT-PCR to better understand the role of CK2 in zinc homeostasis. The cellular zinc content was quantified by ICP-MS and provides details of the cellular zinc level in the context of zinc exposure over time.

5.2 Results

5.2.1 Determination of inhibitory concentration IC_{50} of the six cell lines

The IC_{50} of $ZnSO_4$ for each cell line, MCF-7, MDA-MB-231, MCF10A, PC3, DU145 and RWPE-1 was determined according to the dose responsive curves in Fig. 5.1. The IC_{50} values of $ZnSO_4$ for MCF-7 and MDA-MB-231 cells were 320 µM and 350 µM, respectively. In contrast, the $ZnSO_4$ IC_{50} for the prostate cancer cells PC3 was 110 µM and 150 µM for DU145 cells. Additionally, the $ZnSO_4$ IC_{50} for MCF10A cells was 195.5 µM and 187 µM for the RWPE-1 cell line. By comparing the dose response curves of breast (Fig. 5.1A) and prostate cell lines (Fig. 5.1B), it is clear that breast and prostate cancer cells behave differently in terms of their tolerance to zinc exposure with the cancerous cells exhibiting markedly different IC_{50} values to control lines. Breast cancer cells tolerate higher zinc level (320 µM to 350 µM) shown in Fig. 5.1A as dark blue and orange line, whilst prostate cancer cells tolerate less (110 µM to 150 µM) represented as grey and yellow in Fig. 5.1B. Furthermore, the IC_{50} values of breast cancer cells are much higher than the normal breast cells (195.5 µM), while the IC_{50} values of prostate cancer cells are much lower than the normal prostate cells (187 µM).

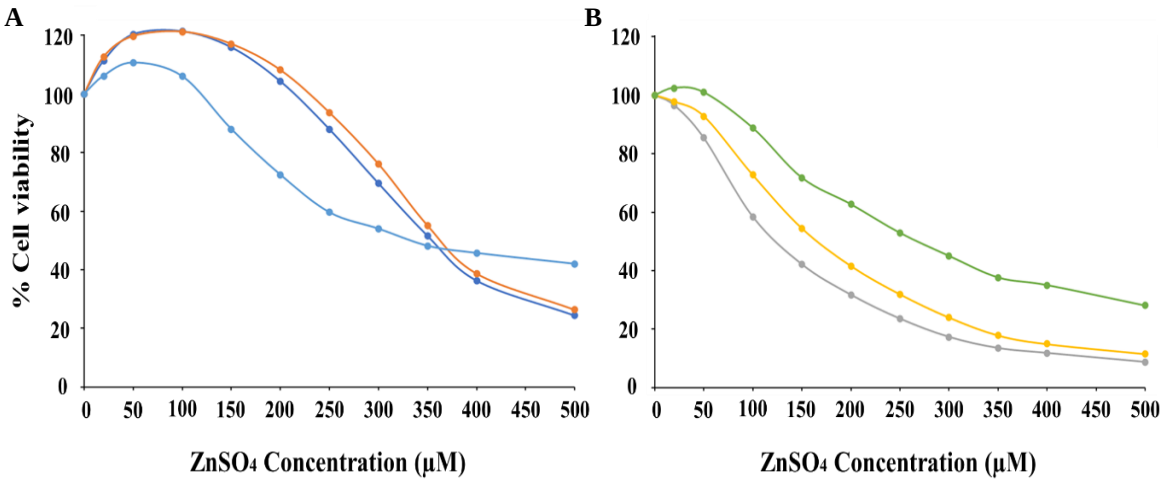

Fig 5.1 Zinc dose responsive curves of the six cell lines

Cells were grown for 32 h and treated with 0 to 500 µM of $ZnSO_4$ to determine IC_{50} for each cell line. Presented in panel (A) are MCF-7 cells (dark blue), MDA-MB-231 cells (red) and MCF10A cells (light blue). Displayed in panel (B) are PC3 cells (grey), DU145 cells (yellow) and RWPE-1 cells (green). Error bars represent standard deviation of three biological replicates.

5.2.2 Validation of the differentially expressed genes involved in zinc homeostasis by qRT-PCR

Relative expression of *MT1B*, *MT1F*, *MT1X*, *MT2A*, *SLC30A1*, *VMP1*, *ZNF850*, *HSPA6* and *HSPA90AA1* genes was firstly validated in MCF-7 breast cancer cells, in which the transcriptomic RNA-seq was carried out as described in Chapter 4. Herein, the expression analysis for these genes is expanded to MDA-MB-231 breast cancer cells, PC3 and DU145 prostate cancer cells, normal breast epithelial cells (MCF10A) and normal prostate epithelial cells (RWPE-1). As described in Chapter 2 Section 2.4.6, the gene expression was analysed relative to the expression of the housekeeping gene *GAPDH*. Fold change 1 means no change of the gene expression. Fold change >1 means increase of the gene expression whilst fold change <1 means decrease of the gene expression. Demonstrated in Fig. 5.2 are the expression of *GAPDH* in the cell lines of this study. As shown, *GAPDH* expression was consistent and similar throughout T_{30} and T_{120} IC_{50} $ZnSO_4$ treatment.

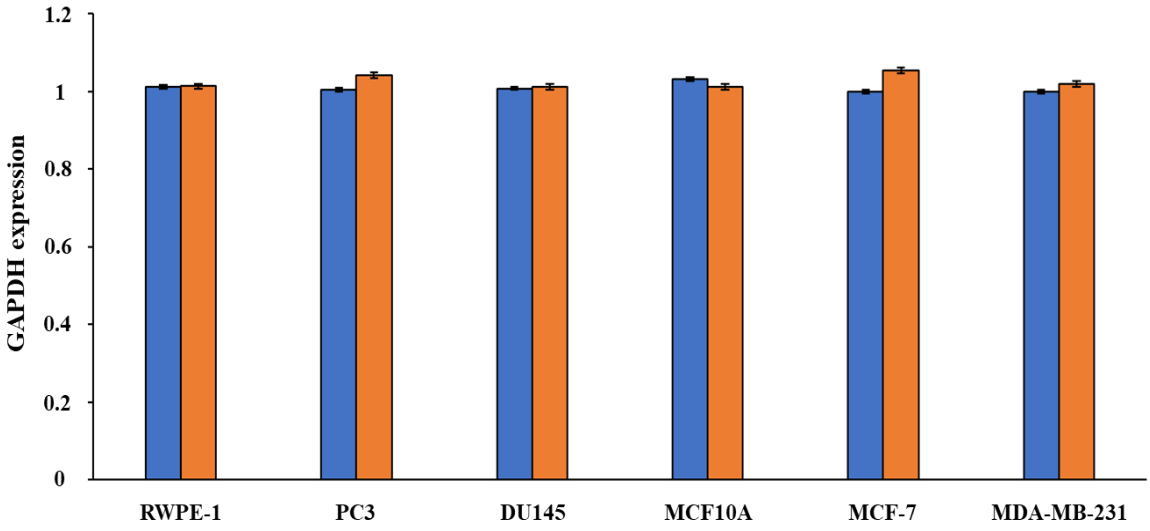

Fig 5.2 Validation of *GAPDH* expression in the cell lines of this study via qRT-PCR

Cells were grown for 32 h and treated with appropriate IC_{50} $ZnSO_4$ at T_{30} (blue) and T_{120} (orange). Total RNA was prepared, cDNA synthesised, qRT-PCR performed and expression of *GAPDH* quantified. Data represents the average of three biological replicates. Error bars represent SEM.

Fig. 5.3 reveals that exposure of MCF-7 cells to zinc IC_{50} at T_{30} resulted in increased gene expression of *MT1B, MT1F, MT1X, SLC30A1* and *ZNF850* (P<0.001); *MT2A* and *VMP1* (P<0.01); *HSPA6* and *HSPA90AA1* (P<0.05). Furthermore, exposure of MCF-7 cells to zinc IC_{50} at T_{120} resulted in a significant increase in gene expression of *MT1B, MT1F, MT1X, MT2A, SLC30A1, VMP1, ZNF850, HSPA2* and *HSPA90AA1* (P<0.001). The genes *MT1B, MT1F, MT2A, VMP1* and *ZNF850* showed substantial increase in expression from T_{30} to T_{120} in response to IC_{50} zinc treatment. These findings correlate with the RNA-seq dataset of Chapter 4.

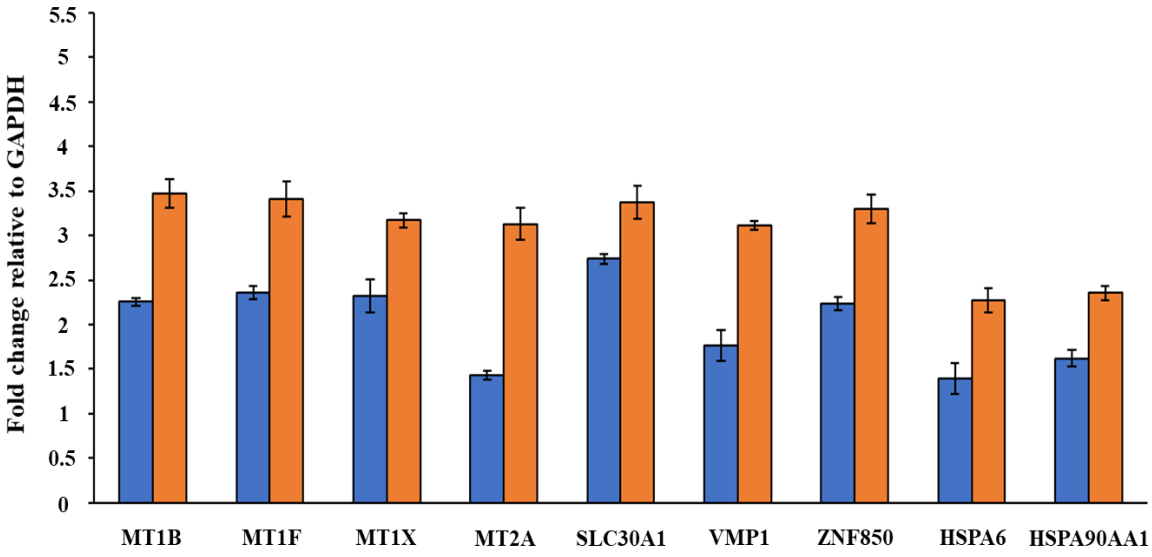

Fig 5.3 Validation of the differentially expressed genes in MCF-7 cells via qRT-PCR
MCF-7 cells were grown for 32 h and treated with IC_{50} $ZnSO_4$ (320 µM) at T_{30} (blue) and T_{120} (orange). Total RNA was prepared, cDNA synthesised and qRT-PCR performed. Relative expression of the genes *MT1B, MT1F, MT1X, MT2A, SLC30A1, VMP1, ZNF850, HSPA6* and *HSPA90AA1* was quantified relative to the housekeeping gene *GAPDH*. Data represents the average of three biological replicates. Error bars represent SEM.

Similarly, Fig. 5.4 shows that exposure of MDA-MB-231 cells to zinc IC_{50} at T_{30} resulted in increased gene expression of *MT1B*, *MT1F*, *MT1X*, *MT2A*, *SLC30A1* and *ZNF850* (P<0.001); *VMP1*, *HSPA* and *HSPA90AA1* (P<0.05). The exposure of MDA-MB-231 cells to zinc IC_{50} at T_{120} resulted in a major increase in gene expression of *MT1B*, *MT1F*, *MT1X*, *MT2A*, *SLC30A1*, *VMP1*, *ZNF850*, *HSPA6* and *HSPA90AA1* (P<0.001). The genes *MT1F*, *SLC30A1*, *VMP1* and *ZNF850* showed the largest increase in expression from T_{30} to T_{120} following IC_{50} $ZnSO_4$ treatment.

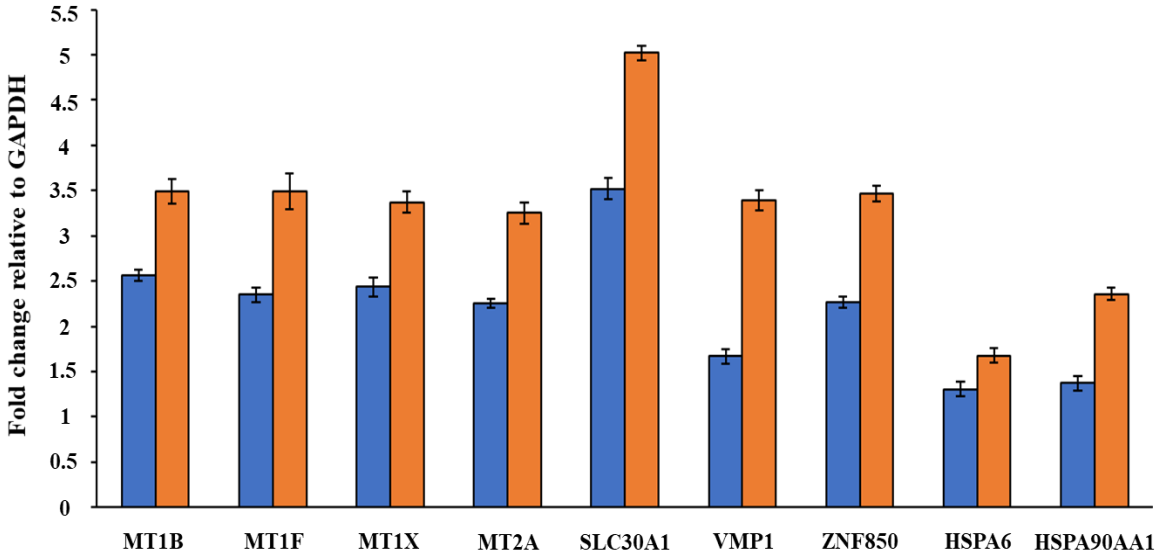

Fig 5.4 Quantification of the differentially expressed genes in MDA-MB-231 cells via qRT-PCR

MDA-MB-231 cells were grown for 32 h and treated with IC_{50} $ZnSO_4$ (350 µM) at T_{30} (blue) and T_{120} (orange). Total RNA was prepared, cDNA synthesised and qRT-PCR performed. Relative expression of the genes *MT1B*, *MT1F*, *MT1X*, *MT2A*, *SLC30A1*, *VMP1*, *ZNF850*, *HSPA6* and *HSPA90AA1* was quantified relative to the housekeeping gene *GAPDH*. Data represents the average of three biological replicates. Error bars represent SEM.

Fig. 5.5 illustrates that exposure of MCF10A cells to zinc IC_{50} at T_{30} resulted in increased gene expression of *MT2A* and *HSPA6* ($P<0.001$); *MT1B*, *MT1F*, *MT1X*, *SLC30A1*, *VMP1*, *ZNF850* and *HSPA90AA1* ($P<0.01$). The exposure of MCF10A cells to zinc IC_{50} at T_{120} resulted in a significant increase in gene expression of *MT1B*, *MT1F*, *MT1X*, *MT2A*, *SLC30A1*, *VMP1*, *ZNF850*, *HSPA6* and *HSPA90AA1* ($P<0.001$). Interestingly, *SLC30A1* gene expression in particular and *ZNF850* to a less degree demonstrated the most significant increase in gene expression from T_{30} to T_{120} following IC_{50} $ZnSO_4$ treatment.

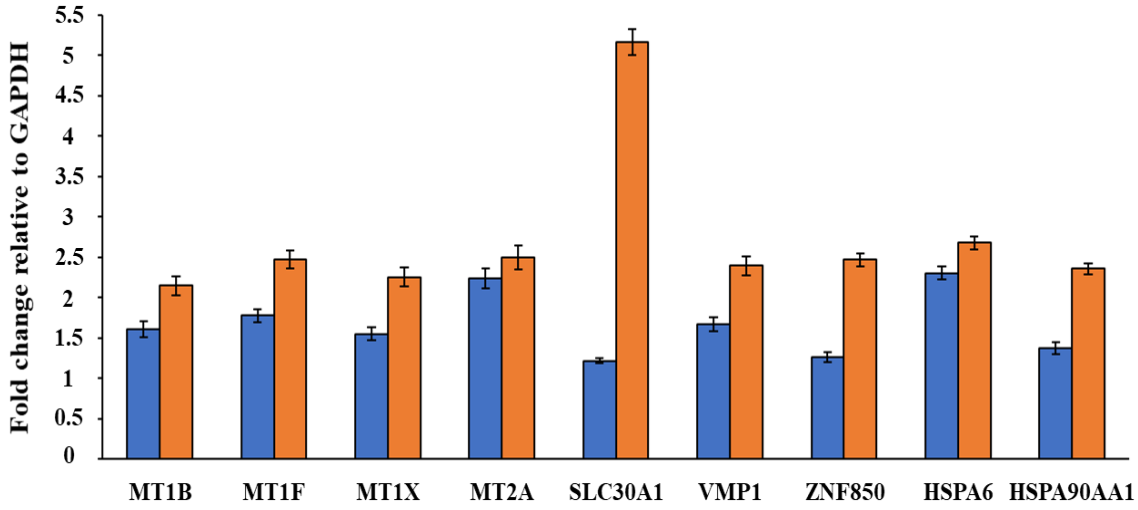

Fig 5.5 Quantification of the differentially expressed genes in MCF10A cells via qRT-PCR

MCF10A cells were grown for 32 h and treated with IC_{50} $ZnSO_4$ (195.5 µM) at T_{30} (blue) and T_{120} (orange). Total RNA was prepared, cDNA synthesised and qRT-PCR performed. Relative expression of the genes *MT1B*, *MT1F*, *MT1X*, *MT2A*, *SLC30A1*, *VMP1*, *ZNF850*, *HSPA6* and *HSPA90AA1* was quantified relative to the housekeeping gene *GAPDH*. Data represents the average of three biological replicates. Error bars represent SEM.

Fig. 5.6 shows the exposure of PC3 prostate cancer cells to zinc IC_{50} at T_{30} resulted in increased gene expression of *MT1X, SLC30A1, ZNF850* and *HSPA6* (P<0.001); *MT1B, MT1F, MT2A, VMP1* and *HSPA90AA1* (P<0.01). The exposure of PC3 cells to zinc IC_{50} at T_{120} resulted in a significant increase in gene expression of *MT1B, MT1X, SLC30A1, HSPA6* and *HSPA90AA1* (P<0.001). The genes *MT1B* and *HSPA6* showed the greatest increase in gene expression from T_{30} to T_{120} following IC_{50} $ZnSO_4$ treatment.

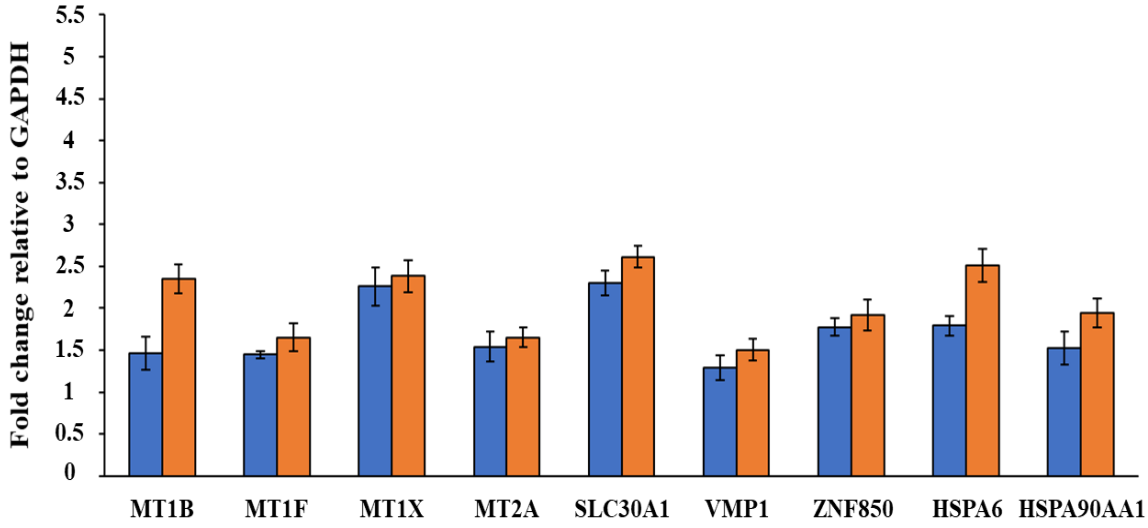

Fig 5.6 Quantification of the differentially expressed genes in PC3 cells via qRT-PCR
PC3 cells were grown for 32 h and treated with IC_{50} $ZnSO_4$ (110 µM) at T_{30} (blue) and T_{120} (orange). Total RNA was prepared, cDNA synthesised and qRT-PCR performed. Relative expression of the genes *MT1B, MT1F, MT1X, MT2A, SLC30A1, VMP1, ZNF850, HSPA6* and *HSPA90AA1* was quantified relative to the housekeeping gene *GAPDH*. Data represents the average of three biological replicates. Error bars represent SEM.

Fig. 5.7 reveals that exposure of DU145 prostate cancer cells to zinc IC_{50} at T_{30} resulted in increased gene expression of *MT1X*, *SLC30A1*, *ZNF850*, *HSPA6* and *HSPA90AA1* (P<0.001); *MT1B*, *MT1F*, *MT2A* and *VMP1* (P<0.01). The exposure of DU145 cells to zinc IC_{50} at T_{120} resulted in a significant increase in gene expression of *MT1B*, *MT1F*, *MT1X*, *MT2A*, *SLC30A1*, *VMP1*, *ZNF850*, *HSPA6* and *HSPA90AA1* (P<0.001). The genes *MT1F*, *MT2A* and *HSPA6* displayed the largest increase in gene expression from T_{30} to T_{120} following IC_{50} $ZnSO_4$ treatment.

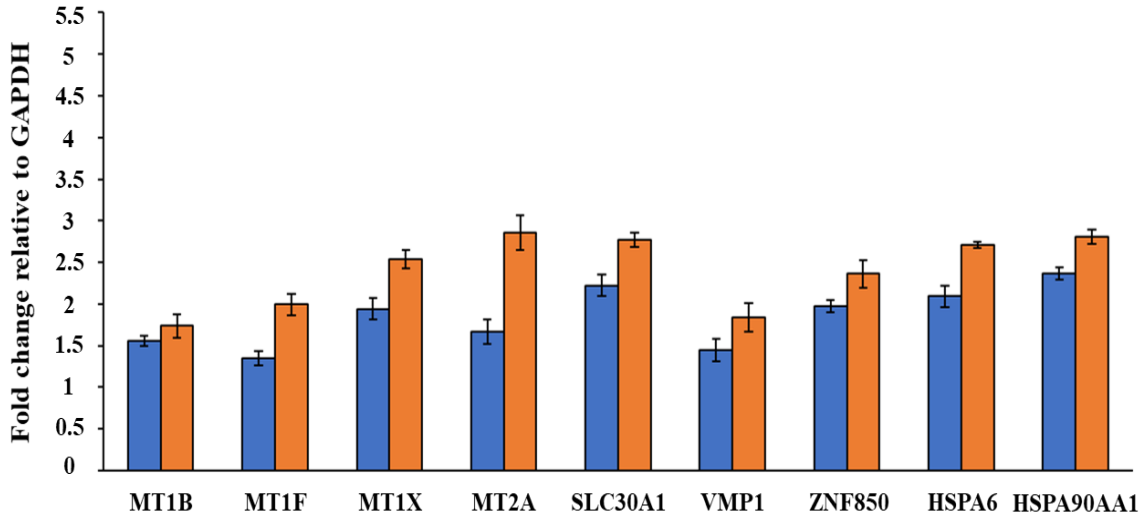

Fig 5.7 Quantification of the differentially expressed genes in DU145 cells via qRT-PCR

DU145 cells were grown for 32 h and treated with IC_{50} $ZnSO_4$ (150 µM) for T_{30} (blue) and T_{120} (orange). Total RNA was prepared, cDNA synthesised and qRT-PCR performed. Relative expression of the genes *MT1B*, *MT1F*, *MT1X*, *MT2A*, *SLC30A1*, *VMP1*, *ZNF850*, *HSPA6* and *HSPA90AA1* was quantified relative to the housekeeping gene *GAPDH*. Data represents the average of three biological replicates. Error bars represent SEM.

Fig. 5.8 uncovers that exposure of RWPE-1 normal prostate epithelial cells to zinc IC_{50} at T_{30} resulted in increased gene expression of *MT1B*, *MT1F*, *MT1X*, *MT2A*, *SLC30A1*, *VMP1*, *ZNF850*, *HSPA6* and *HSPA90AA1* (P<0.001). The exposure of RWPE-1 cells to zinc IC_{50} at T_{120} resulted in a significant increase in gene expression of *MT1B*, *MT1F*, *MT1X*, *MT2A*, *SLC30A1*, *VMP1*, *ZNF850*, *HSPA6* and *HSPA90AA1* (P<0.001). The genes *MT1F*, *MT1X*, *MT2A*, *SLC30A1* and *VMP1* showed the greatest increases in gene expression from T_{30} to T_{120} following IC_{50} $ZnSO_4$ treatment.

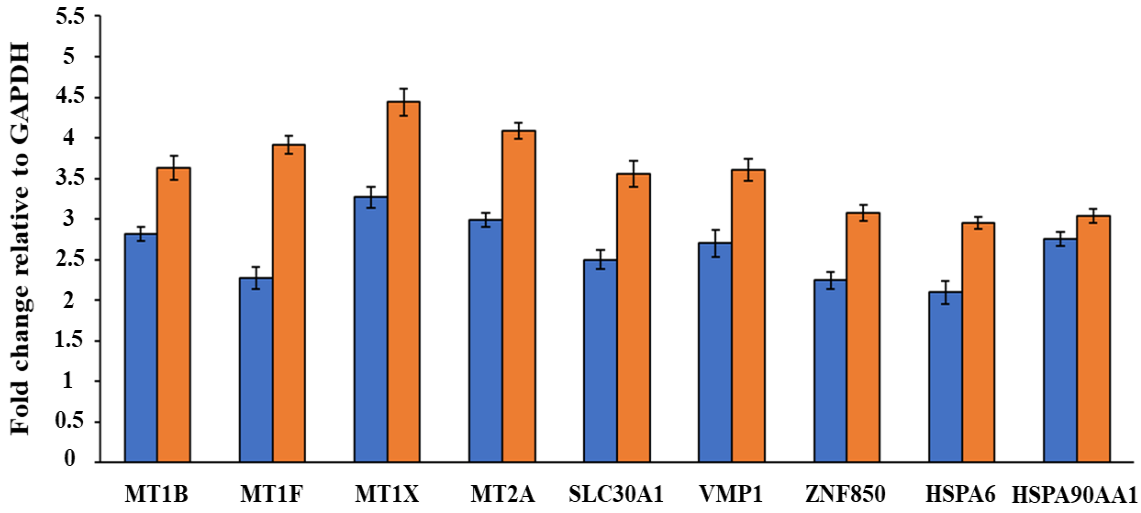

Fig 5.8 Quantification of the differentially expressed genes in RWPE-1 cells via qRT-PCR

RWPE-1 cells were grown for 32 h and treated with IC_{50} $ZnSO_4$ (186.88 µM) for T_{30} (blue) and T_{120} (orange). Total RNA was prepared, cDNA synthesised and qRT-PCR performed. Relative expression of the genes *MT1B*, *MT1F*, *MT1X*, *MT2A*, *SLC30A1*, *VMP1*, *ZNF850*, *HSPA6* and *HSPA90AA1* was quantified relative to the housekeeping gene *GAPDH*. Data represents the average of three biological replicates. Error bars represent SEM.

5.2.3 Comparison of the gene expression in cancerous and normal cells by qRT-PCR

The expression of the nine genes (*MT1B*, *MT1F*, *MT1X*, *MT2A*, *SLC30A1*, *VMP1*, *ZNF850*, *HSPA6* and *HSPA90AA1*) was quantified and compared as described in Section 2.4.7 between cancerous and normal cells by qRT-PCR. Fig. 5.9 compares the gene expression between MCF-7 breast cancer cells and MCF10A normal breast epithelial cells, which reveals a dramatic elevation in gene expression of *MT1B*, *MT1F*, *MT1X*, *MT2A*, *VMP1*, *ZNF850*, *HSPA6* and *HSPA90AA1* (P<0.001). While the gene *SLC30A1* has the least difference between cancerous and normal breast epithelial cells.

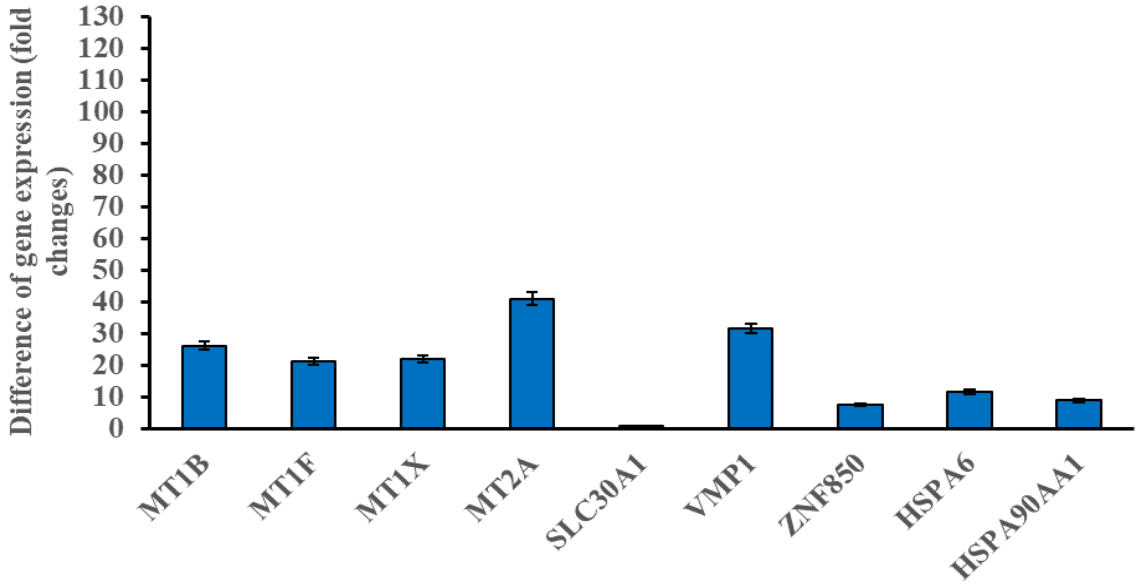

Fig 5.9 Comparison of gene expression in MCF-7 against MCF10A cells via qRT-PCR

MCF-7 breast cancer cells and MCF10A normal breast epithelial cells were grown for 32 h without any treatment for T_{120} to serve as control. Total RNA was prepared, cDNA synthesised and qRT-PCR performed. Expression of the genes *MT1B*, *MT1F*, *MT1X*, *MT2A*, *SLC30A1*, *VMP1*, *ZNF850*, *HSPA6* and *HSPA90AA1* under control conditions was quantified and compared between MCF-7 and MCF10A cells. Data represents the average of three biological replicates.

Fig. 5.10 shows comparison of the gene expression between MDA-MB-231 breast cancer cells and MCF10A normal breast epithelial cells demonstrated a spectacular rise in gene expression of *MT1B*, *MT1F*, *MT1X*, *MT2A*, *VMP1*, *ZNF850*, *HSPA6* and *HSPA90AA1* (P<0.001). While the gene *SLC30A1* alone revealed the lowest difference in gene expression between cancerous and normal breast epithelial cells.

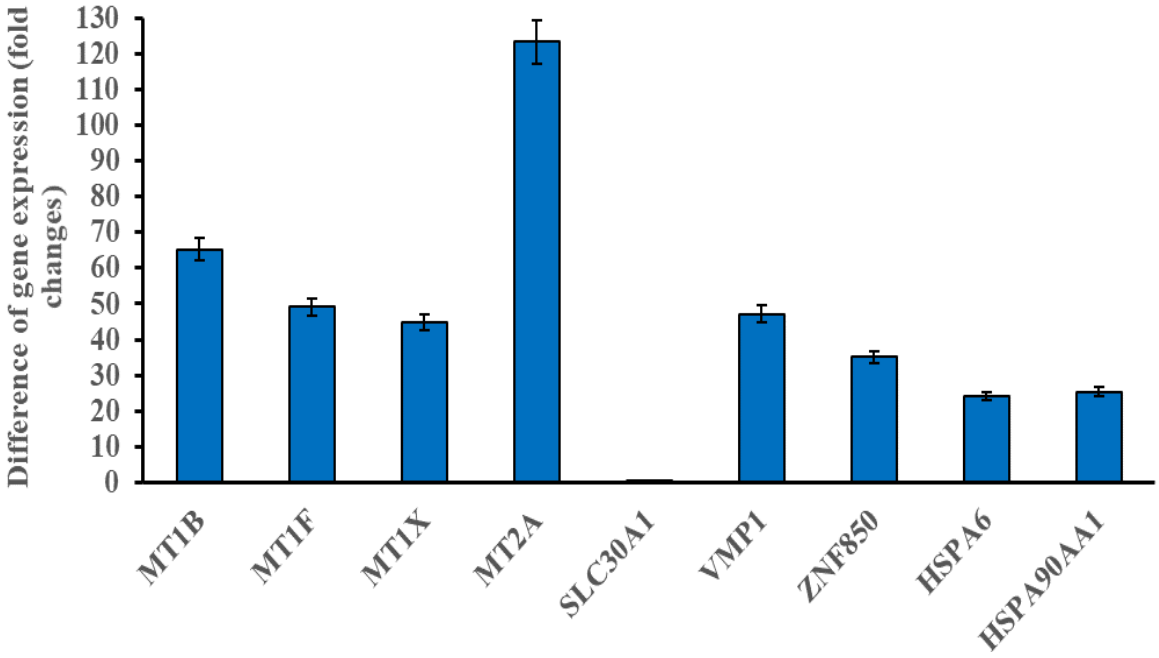

Fig 5.10 Comparison of gene expression MDA-MB-231 against MCF10A cells via qRT-PCR

MDA-MB-231 breast cancer cells and MCF10A normal breast epithelial cells were grown for 32 h without any treatment for T_{120} to serve as control. Total RNA was prepared, cDNA synthesised and qRT-PCR performed. Expression of the genes *MT1B*, *MT1F*, *MT1X*, *MT2A*, *SLC30A1*, *VMP1*, *ZNF850*, *HSPA6* and *HSPA90AA1* under control conditions was quantified and compared between MDA-MB-231 and MCF10A cells. Data represents the average of three biological replicates.

Fig. 5.11 illustrates comparison of the gene expression between PC3 prostate cancer cells and RWPE-1 normal prostate epithelial cells, demonstrating a spectacular rise in gene expression of *MT1B*, *MT1F*, *MT1X*, *MT2A*, *VMP1*, *ZNF850*, *HSPA6* and *HSPA90AA1* (P<0.001). Whilst the gene *SLC30A1* represented the smallest difference in comparison of gene expression between cancerous and normal prostate epithelial cells.

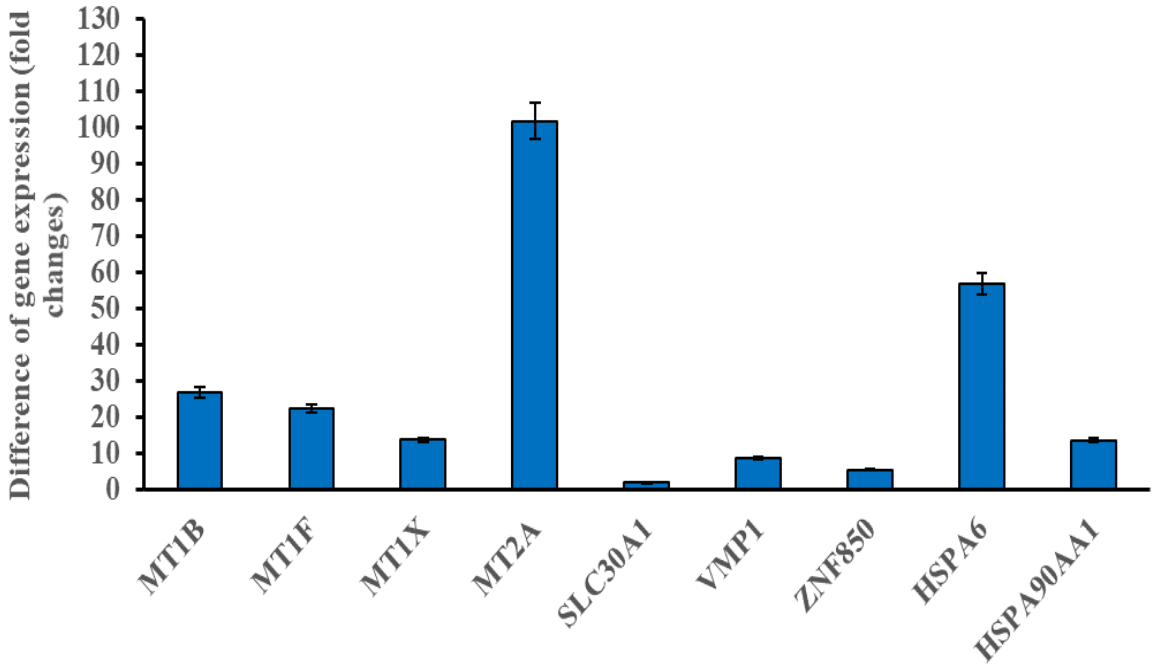

Fig 5.11 Comparison of gene expression in PC3 against RWPE-1 cells via qRT-PCR
PC3 prostate cancer cells and RWPE-1 normal prostate epithelial cells were grown for 32 h without any treatment for T_{120} to serve as control. Total RNA was prepared, cDNA synthesised and qRT-PCR performed. Expression of the genes *MT1B*, *MT1F*, *MT1X*, *MT2A*, *SLC30A1*, *VMP1*, *ZNF850*, *HSPA6* and *HSPA90AA1* under control conditions was quantified and compared between PC3 and RWPE-1 cells. Data represents the average of three biological replicates.

Fig. 5.12 compares the gene expression between DU145 prostate cancer cells and RWPE-1 normal prostate epithelial cells, showing a remarkable rise in gene expression of *MT1B*, *MT1F*, *MT1X*, *MT2A*, VMP1, *ZNF850*, *HSPA6* and *HSPA90AA1* (P<0.001). Whereas the genes *SLC30A1* suggested negligible difference in comparison of gene expression between cancerous and normal prostate epithelial cells.

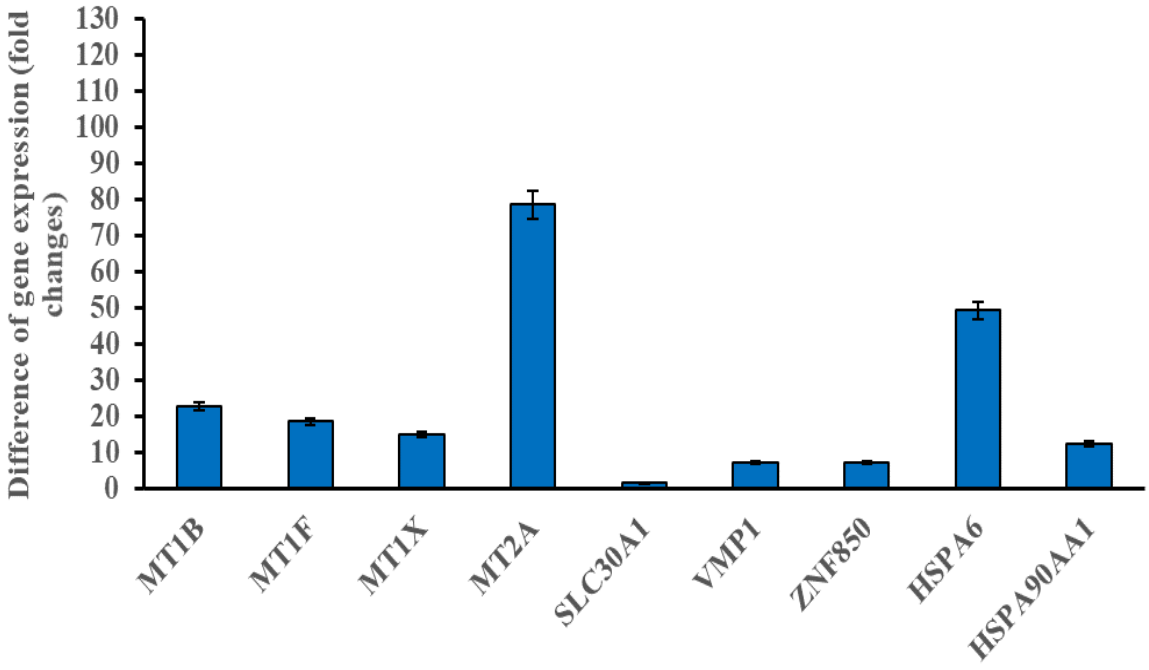

Fig 5.12 Comparison of gene expression in DU154 against RWPE-1 cells via qRT-PCR

DU145 prostate cancer cells and RWPE-1 normal prostate epithelial cells were grown for 32 h without any treatment for T_{120} to serve as control. Total RNA was prepared, cDNA synthesised and qRT-PCR performed. Expression of the genes *MT1B*, *MT1F*, *MT1X*, *MT2A*, *SLC30A1*, *VMP1*, *ZNF850*, *HSPA6* and *HSPA90AA1* under control conditions was quantified and compared between DU145 and RWPE-1 cells. Data represents the average of three biological replicates.

5.2.3 Quantification of the genes of CK2 subunits under zinc treatment by qRT-PCR expression

Fig. 5.13 reveals that *CSNK2A1*, *CSNK2A2* and *CSNK2B* genes which encode CK2α, CK2α' and CK2β subunits respectively, were up-regulated at T_{30} following zinc treatment for MCF-7 and MDA-MB-231 breast cancer cells (P<0.001) compared to normal breast epithelial cells (MCF10A). At T_{120} zinc exposure, the expression of *CSNK2A1*, *CSNK2A2* and *CSNK2B* genes was up-regulated in MDA-MB-231 breast cancer cells compared to normal breast epithelial cells (MCF10A) (P<0.01). The results demonstrated that the breast cancer cell line MDA-MB-231 requires the up-regulation of CK2 subunits to combat zinc exposure at T_{120} (P<0.01) compared to the normal breast cells, while the MCF-7 breast cancer cells tempered the level of *CSNK2A2* gene at T_{120} (P<0.05) albeit still significant compared to the normal breast cells, when *CSNK2A1* and *CSNK2B* genes returned to baseline or lower expression. Interestingly, the effect of zinc IC_{50} treatment at T_{30} and T_{120} for MCF10A, PC3, DU145 and RWPE-1 cells resulted in baseline expression or lower for CK2 subunits *CSNK2A1*, *CSNK2A2* and *CSNK2B* gene.

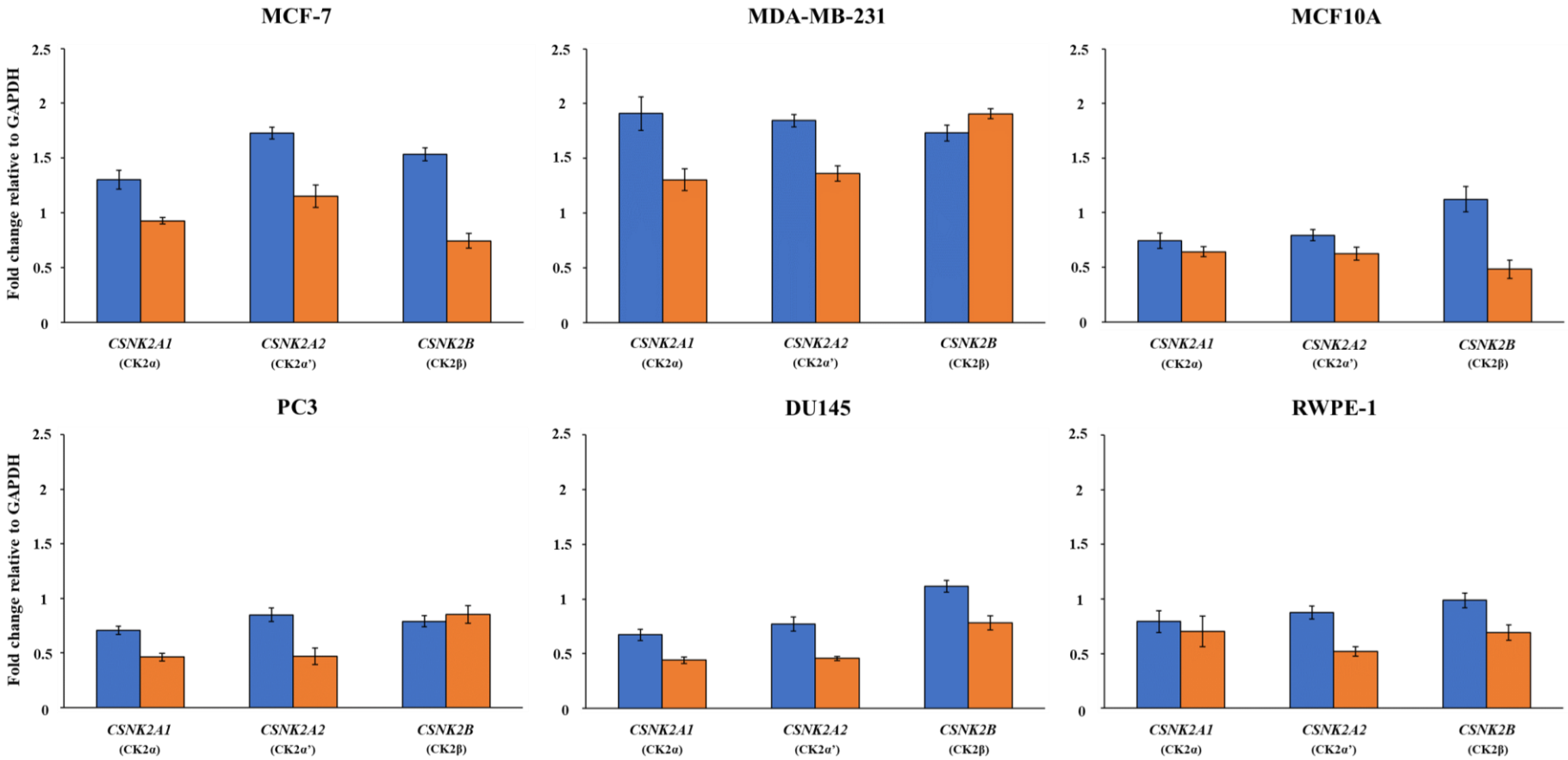

Fig 5.13 CK2 subunit expression profile under zinc IC_{50} treatment

Cells were grown for 32 h and treated with IC_{50} $ZnSO_4$ at T_{30} (blue) and T_{120} (orange). Total RNA was prepared, cDNA synthesised and qRT-PCR performed. Relative expression of *CSNK2A1*, *CSNK2A2* and *CSNK2B* gene expression was quantified relative to the housekeeping gene *GAPDH*. Data represents the average of three biological replicates. Error bars represent SEM.

5.2.4 Comparison of the genes of CK2 subunits without any treatment by qRT-PCR expression

The basal expression of *CSNK2A1, CSNK2A2* and *CSNK2B* genes was compared between the cancerous and normal cells. Fig. 5.14 reveals that *CSNK2A1, CSNK2A2* and *CSNK2B* genes which encode the CK2α, CK2α' and CK2β subunits was expressed higher in MCF-7, MDA-MB-231, PC3 and DU145 cancer cells compared to MCF10A and RWPE-1 normal cells. Interestingly, the expression of *CSNK2A1*, *CSNK2A2* and *CSNK2B* genes was substantially higher in breast cancer cells compared to prostate cancer cells ($P<0.001$). The results demonstrate that MCF-7 and MDA-MB-231 breast cancer cells possess a substantially higher expression of all three CK2 subunits compared to the MCF10A normal breast epithelial cells, with *CSNK2A1* and *CSNK2B* showing the highest difference ($P<0.001$). In contrast, PC3 and DU145 prostate cancer cells appear to have a higher expression of *CSNK2B* compared to normal prostate epithelial cells ($P<0.001$), with *CSNK2A1* and *CSNK2A2* also showing difference in expression ($P<0.01$).

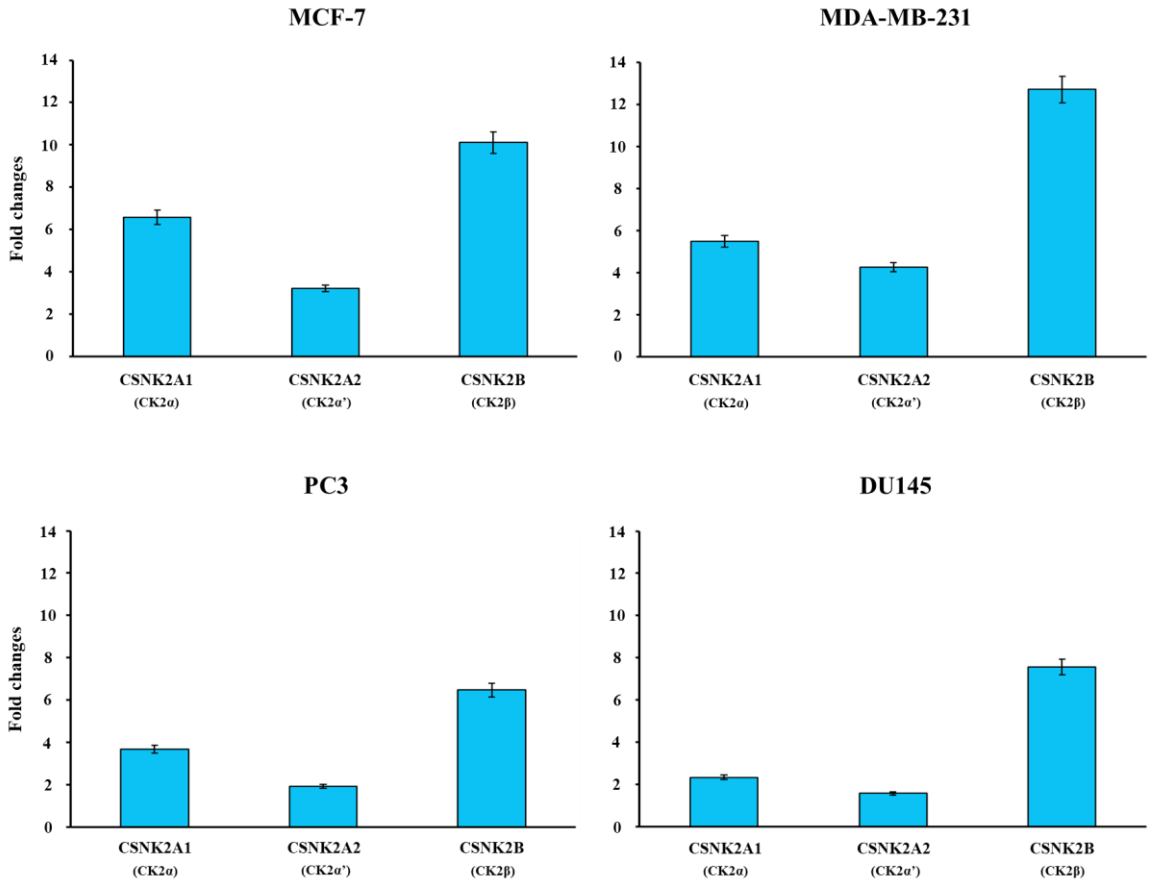

Fig 5.14 Comparison of CK2 subunit gene expression between cancerous and normal cells

Cells were grown without any treatment. Total RNA was prepared, cDNA synthesised and qRT-PCR performed. Expression of *CSNK2A1*, *CSNK2A2* and *CSNK2B* genes was quantified and compared between cancerous and normal cells. Data represents the average of three biological replicates.

5.2.5 Quantification of cellular zinc content under zinc IC_{50} treatment and CK2 inhibition by ICP-MS analysis

Cells were grown for 32 h and treated with IC_{50} $ZnSO_4$ for T_0, T_{30} and T_{120} (blue) and TBB (20 µM) plus IC_{50} $ZnSO_4$ for T_0, T_{30} and T_{120} (orange). The concentration of TBB (20 µM) utilised in this study had little effect on cell viability of all the six cell lines employed here (MCF-7, MDA-MB-231, MCF10A, PC3, DU145 and RWPE-1). The cells were then harvested, washed, digested and quantified by ICP-MS according to Chapter 2 Section 2.4.11. The result in Fig. 5.15 demonstrates that normal breast epithelial cells (MCF10A) accumulated a much higher level of cellular zinc than MCF-7 and MDA-MB-231 breast cancer cells. Inhibition of CK2 resulted in more zinc uptake in all cell lines except the normal breast cell line (MCF10A). It is also clear that prostate cancer cells (PC3 and DU145) accumulate more zinc than the normal prostate cells (RWPE-1) under zinc treatment.

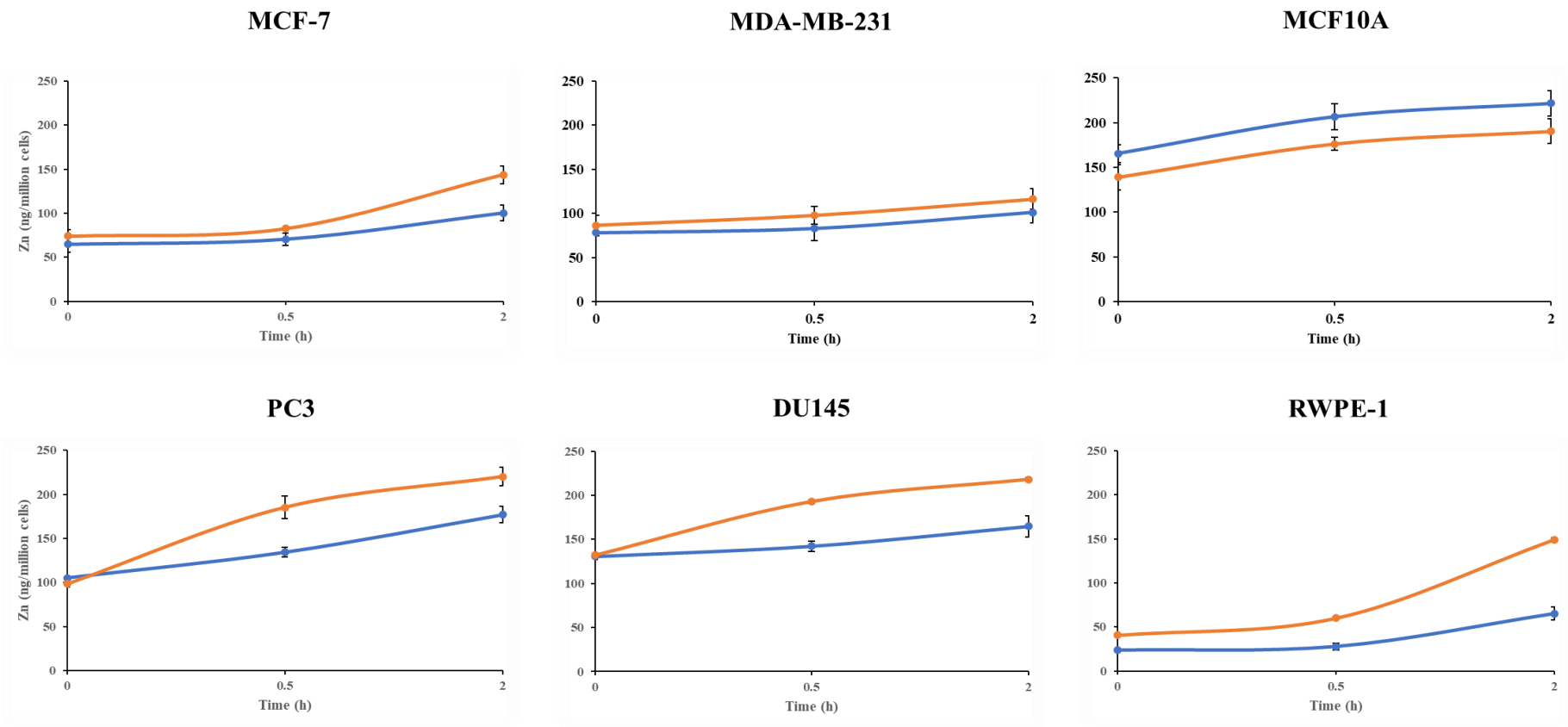

Fig 5.15 Determination of cellular zinc content through ICP-MS analysis

Cells were grown for 32 h and treated with IC_{50} $ZnSO_4$ for T_0, T_{30} and T_{120} (blue) and TBB (20 µM) plus IC_{50} $ZnSO_4$ for T_0, T_{30} and T_{120} (orange). The cells were then harvested, washed, digested and quantified by ICP-MS. Error bars represent standard deviation of three biological replicates.

5.3 Discussion

The findings described in this Chapter validated the RNA-seq data of Chapter 4 and extended further to the other breast and prostate cancer cells, as well as the normal breast and prostate epithelial cells. Such a sequence of experimental flow was designed from the outset because it is cost-efficient. With the constraint of budget, it was feasible to do transcriptomic RNA-seq analysis with MCF-7 breast cancer cells first, then validate the findings and extend to other normal and cancerous breast and prostate cells.

The gene expression profiles of, *SLC30A1*, *VMP1*, *ZNF850*, *HSPA6* and *HSPA90AA1* genes in all six cell lines showed a similar pattern, i.e., they were up-regulated at both T_{30} and T_{120} IC_{50} zinc exposure, suggesting that these genes are essential to maintain zinc ion homeostasis for both normal and cancerous breast and prostate cells. However, parsing the data carefully, some key findings become obvious.

The metallothionein genes in breast cancer cells were found to be markedly elevated in expression level compared to normal breast cells under IC_{50} zinc exposure which is not surprising as studies have determined that metallothionines genes play a role in zinc sequestration (Goulding et al., 1995; Coyle et al., 2002). What is extraordinary is the degree of basal expression of metallothionine genes, particularly the *MT2A* gene, in breast and prostate cancer cells compared to normal breast and prostate cells. Basal expression of metallothionine genes was greatest in the MDA-MB-231 breast cancer cells which might be one of the reasons why the basal type of breast cancer cells (MDA-MB-231) are much more tolerant to higher cellular zinc (Margalioth et al., 1983; Rizk and Sky-Peck, 1984; Goulding et al., 1995; Coyle et al., 2002; Kagara et al., 2007). Overall, breast cancer

cells (MCF-7 and MDA-MB-231) displayed higher basal expression of metallothionein genes compared to prostate cancer cells (PC3 and DU145) when compared to normal cells.

By comparing the fold changes of ZnT1 gene expression in breast cancer cell lines MCF-7 (3.58), MDA-MB-231 (4.55), prostate cancer cell lines PC3 (2.61), DU145 (2.76) and normal breast MCF10A (5.15) and prostate RWPE-1 (3.55) epithelial cells (Fig. 5.3-5.8), it is clear that the expression of ZnT1 (*SLC30A1*) is higher in normal breast and prostate epithelial cells. The elevated expression of ZnT1 expression in MCF10A normal breast epithelial cells is likely related to its low intracellular zinc level compared to breast cancer cells (Costello and Franklin, 2006; Cousins et al., 2006; Franklin and Costello, 2007; Franklin and Costello, 2009; Chandler et al., 2016; Reddy et al., 2018). Higher ZnT1 expression could mean higher zinc efflux, therefore low intracellular zinc level. However, it is intriguing for the higher expression of ZnT1 in the MDA-MB-231 breast cancer cells when compared to MCF-7 breast cancer cells. One possible underlying reason for this could be that such a higher gene expression of ZnT1 might not be translated to higher functional ZnT1 protein transporters, because (Lehvy et al., 2019) found that ZnT1 displays a markedly increased frequency of loss of function mutations in malignant tumours, as compared to a healthy population (Lehvy et al., 2019).

The lower expression of ZnT1 (*SLC30A1*) in prostate cancer cells, compared to the normal prostate epithelial cells, is rather expected due to the lower zinc level in prostate cancer cells (Franklin et al., 2005; Song and Ho, 2009). Since prostate cancer cells have a reduced requirement for zinc, the expression of ZnT1 transporter is anticipated to be lower accordingly. The findings here confirm that the heat shock protein gene *HSPA6* was elevated in response to zinc exposure in both normal and cancerous breast cells. This suggests that the degree to which *HSPA6* is expressed under zinc exposure can potentially

be used as a stress indicator. The fact that breast cancer cells have a higher zinc IC_{50} compared to normal breast cells, indicates that they can handle much higher zinc stress. This notion can be explained by the data in this Chapter and Chapter 4, that is, the breast cancer cells are more inherently capable at responding to zinc stress because they depend on a broader spectrum of genes from metallothioneins to heat shock proteins compared to normal breast cells, which appears to be significantly dependant on ZnT1 efflux.

Since the next-generation RNA-seq results in Chapter 4 demonstrate that the expression levels for CK2 subunits genes (*CSNK2A1*, *CSNK2A2* and *CSNK2B*) were basically unchanged under IC_{50} zinc exposure at T_{30} and T_{120} in the MCF-7 breast cancer cells. By the means of qRT-PCR, I explored in this chapter the expression profile of all CK2 subunits under zinc exposure for all six cell lines (Fig. 5.13) and basal expression of CK2 subunits in the cells without any treatment (Fig. 5.14). The results demonstrated that the expression of CK2 subunits were significantly up-regulated at both T_{30} and T_{120} IC_{50} zinc exposure in MDA-MB-231 breast cancer cells. A similar pattern was found at T_{30} zinc exposure for the MCF-7 breast cancer cells, compared to normal breast epithelial cells. Taking the findings here together with the data of Chapter 4, the RNA-seq transcriptomic finding that the gene expression of CK2 was unchanged in response to zinc exposure (T_{30} vs T_0 and T_{120} vs T_0) is explicable, when considering the qRT-PCR finding in this Chapter that the breast cancer cells have higher gene expression of CK2 than the normal breast epithelial cells with no treatment (Fig. 5.14). Such elevated basal level of CK2 subunit expression in cancer cells compared to normal cells is therefore likely to be sufficient in maintaining zinc homeostasis.

The findings of this chapter and the previous experimental Chapters 3 and 4 can be related to clinical cancer tissues from breast and prostate cancer patients. Studies have determined

that breast cancer tumours express higher expression levels of metallothioneins, *ZIP4*, *ZIP14* genes and lower levels of *ZIP6*, *ZIP9*, *ZIP11* compared to normal breast tissue (Coyle et al., 2002; Chandler et al., 2016; Kimura and Kambe, 2016; Si and Lang, 2018). The luminal subtype of breast cancer tissue has been shown to display higher expression of *ZIP6* than basal and HER2 over-expression tumours (Coyle et al., 2002; Chandler et al., 2016; Kimura and Kambe, 2016; Si and Lang, 2018). In comparison, studies have established that prostate cancer tumours show down-regulation of *ZIP1* gene expression which coincides with marked depletion of intracellular zinc levels (Franklin et al., 2005; Song and Ho, 2009). Likewise, it has been revealed that *ZIP2*, *ZIP3*, *ZIP4* and *ZIP9* genes are also down-regulated in prostate cancer tissue, while up-regulated in normal prostate epithelial tissue (Rishi et al., 2003; Franklin et al., 2005; Costello and Franklin, 2006; Franklin and Costello, 2009; Huang and Tepaamorndech, 2013). Interestingly, studies have established that CK2 expression is up-regulated in all cancers examined, and this correlation has prompted studies on CK2's role in oncogenesis (Trembley et al., 2009). Dysregulation of CK2 invokes unwarranted oncogenic capability on cells even though CK2 is not formally classed as an oncogene (Trembley et al., 2009).

The finding described above is in correlation with the findings of this chapter, where CK2 expression in breast (MCF-7 and MDA-MB-231) and prostate (PC3 and DU145) cancer cells is substantially higher compared to the normal breast (MCF10A) and prostate (RWPE-1) epithelial cells. The findings described in this chapter could be potentially helpful for cancer prognosis and treatment. For example, by decreasing intracellular zinc levels the growth of breast cancer cells might be tempered. Such a strategy could be implemented through down-regulation of ZIP gene expression (*ZIP4*, *ZIP6* and *ZIP14*) in breast cancer cells. In contrast, the strategy of increasing intracellular zinc level in prostate

cancer cells could be achieved by up-regulation of ZIP gene expression (*ZIP1*, *ZIP2*, *ZIP3*, *ZIP4* and *ZIP9*) which could benefit prostate cancer patients.

5.4 Conclusion

In summary, the work in this chapter validated, by means of qRT-PCR, the nine top differentially expressed genes uncovered by RNA-seq, further extension of this discovery to the other cancer cells, the normal breast and prostate epithelial cells. By using this expanded panel of cell lines, an in-depth understanding of those differentially expressed genes in zinc homeostasis of both breast and prostate cancer cells was gained. The gene expression of CK2 subunits (*CSNK2A1*, *CSNK2A2* and *CSNK2B*) was also analysed in these six cell lines by the means of qRT-PCR to better understand the role of CK2 in zinc homeostasis. The cellular zinc content was quantified by ICP-MS in this chapter, the data provides details of the cellular zinc level in the context of zinc exposure and time course, which is helpful in the overall data analysis of this chapter. The data here adds to our understanding of CK2's role in zinc homeostasis of breast and prostate cancer cells.

6 FINAL DISCUSSION

This study investigates the role of CK2 subunits in zinc homeostasis of breast and prostate cancer cells and applied a holistic transcriptomic analysis via RNA-seq for uncovering the genes involved in zinc homeostasis. The findings described in Chapters 3 to 5 demonstrate that protein kinase CK2 is indeed involved in zinc homeostasis of breast and prostate cancer cells. To be precise, CK2 plays a role in the impaired zinc homeostasis of the cancer cells. This novel discovery adds to the previously known biological functions of CK2 described in Chapter 1, such as regulating cell proliferation and anti-apoptosis (Guerra and Issinger, 1999; Litchfield, 2003; Meggio and Pinna, 2003; Kappes et al., 2004). Revelation of the differentially expressed genes in MCF-7 breast cancer cells by RNA-seq is highly significant. In-depth understanding of zinc homeostasis in the cancer cells is further gained through the extension of these genes to the other breast and prostate cancer cells as well as the normal breast and prostate epithelial cells.

6.1 Involvement of CK2 in zinc homeostasis of breast and prostate cancer cells

Protein kinase CK2 has been regarded as one of the most ubiquitous and pleiotropic enzymes in biological systems (Guerra et al., 1999; Litchfield, 2003; Filhol et al., 2004; Costello and Franklin, 2006). By employing the experimental approaches of CK2 inhibition with its specific inhibitors, subunit-specific siRNA-mediated knockdown, confocal imaging by zinc specific fluorophores, RNA-seq, ICP-MS analysis and qRT-PCR, the distinctive details of CK2's involvement in zinc ion homeostasis were elucidated. Inhibition of CK2 activity coupled with IC_{50} zinc exposure in breast and prostate cancer cells revealed reduction in cell viability, which was accompanied with the elevated

intracellular zinc accumulation as shown by confocal imaging. Furthermore, I discovered that zinc accumulation was heightened in prostate cancer cells (PC3 and DU145 cell lines) due to knockdown of the gene expression for CK2α', whilst the contrary was true for breast cancer cells. This finding reflects the intrinsic difference between breast and prostate cancer cells in terms of cellular zinc accumulation and the expression of CK2α' gene (*CSNK2A2*) is one factor related to such a difference. Thus, siRNA mediated knockdown of specific CK2 subunits demonstrates that individual subunits of CK2 have unique roles in zinc homeostasis in breast and prostate cancer cells, providing evidence for the involvement of CK2 in zinc homeostasis of breast and prostate cancer cells.

These discoveries were achieved by using the appropriate dosage of CK2 inhibition via TBB (20 μM) and CX-4945 (5 μM) and CK2 subunit knockdown for their gene expression with the average knockdown efficiency for all three CK2 subunit transcripts at approximately 70.15%. Little effect on the cell viability was observed in the above-mentioned conditions for CK2 inhibition or knockdown, according to Fig. 3.2, 3.4 and Fig. 5.14. Such findings could be due to the fact that the CK2 inhibition or its subunit knockdown is only partial, the functional portion of CK2 is sufficient for maintaining the cell viability.Following on the discovery reported in Chapter 3, I carried out transcriptomic analysis by RNA-seq, in order to uncover the genes involved in zinc homeostasis of breast cancer cells and to see if the genes of CK2 subunits are differentially expressed in response to zinc exposure. Remarkably the expression of CK2 subunit genes (*CSNK2A1*, *CSNK2A2* and *CSNK2B*) is basically unchanged, as described in Chapter 4. This suggests that the basal expression at the gene level of CK2 is sufficient to sustain the cell's response to zinc challenge. As CK2 is a constitutively active kinase (Litchfield and Luscher, 1993; Blanquet, 2000; Litchfield, 2003; Meggio and Pinna, 2003), it is understandable that its

basal expression and activity is enough for the cell to handle the IC_{50} of zinc sulfate. This finding also revealed that any perturbation of the basal CK2 expression or activity should affect zinc homeostasis. Such a notion is exactly demonstrated by the findings of Chapter 3 where CK2 inhibitors and the specific siRNA were used to inhibit CK2 activity and its gene expression.

By looking at the difference of CK2 gene expression level between the cancer cells and normal epithelial cells in Chapter 5, I found that the gene expression for CK2 subunits varies. CK2 subunit expression appears to be elevated in both breast and prostate cancer cells compared to normal breast and prostate cells. This implies that cancer cells of the breast and prostate require a higher expression of CK2 subunits at the basal level. The finding is in agreement with the published data that CK2 gene expression is up-regulated in cancer cells (Faust et al., 1999; Guerra and Issinger, 1999; Faust and Montenarh, 2000; Trembley et al., 2009). The higher expression of CK2 subunit genes implies that more CK2 is required in cancer cells for growth and perhaps for response to zinc exposure.

6.2 Holistic view of zinc homeostasis in MCF-7 breast cancer cells

The RNA-seq findings described in Chapter 4 reveals the prominent genes involved in response to zinc exposure in the MCF-7 breast cancer cells. Differential gene expression for metallothioneins (*MT1B*, *MT1F*, *MT1X* and *MT2A*) was observed throughout the time course of RNA-seq, implying the reliance of breast cancer cells on metallothioneins in response to extracellular zinc challenge. This is understandable because metallothioneins are the key players in sequestrating free zinc in cytoplasm (Suhy et al., 1999; Thirumoorthy et al., 2011; Kimura and Kambe, 2016). However, the degree of the dramatic up-regulation, up to 869-fold for *MT1B*, is a great surprise. The elevated expression of

metallothionein genes highlights not only the significance of their role in zinc homeostasis, but also their potential role in response to any other environmental stressors such as anti-cancer drugs as previous research demonstrates that metallothioneins are involved in drug resistance (Goulding et al., 1995; Coyle et al., 2002; Thirumoorthy et al., 2011; Vašák and Meloni, 2011; Si and Lang, 2018).

Since the only zinc exporter ZnT1 (*SLC30A1*), amongst 10 ZnTs, was differentially expressed in MCF-7 breast cancer cells as revealed by RNA-seq, one could question why the other nine zinc efflux transporters (ZnT2-10) were not differentially expressed. The fact that ZnT1 is the only ZnT present in plasma membrane could explain the finding. By being the plasma membrane zinc exporter, ZnT1 is the main workhorse to get the intracellular zinc out of the cell.

One would think that the effective way to control cytoplasmic zinc level is to regulate the import of extracellular zinc into the cell by either down-regulation of ZIP expression at the transcriptional level or reduction of functional ZIP in the plasma membrane. Intriguingly, the RNA-seq dataset from this study did not reveal any down-regulation of ZIP genes (*SLC39A*). This might be due to the inherent propensity of breast cancer cells to import zinc via ZIPs at the beginning of the exposure followed by a time lag where the cancer cells mount a response to regulate ZIPs either at the transcriptomic or protein level. The finding might point to the regulation of ZIPs at the protein level in response to zinc exposure. Indeed, phosphorylation of ZIPs and ZnTs is an important mode of post-transcriptional modification (Taylor et al., 2008; Taylor et al., 2012; Johnson and Wu, 2016; Thingholm et al., 2020). Degradation of membrane-bound ZIPs is also demonstrated in the previous studies (Sekler et al., 2007; Kambe, 2011; Kambe et al., 2014; Thingholm et al., 2020).

It seems that breast cancer cells also depend on the up-regulation of zinc-binding proteins such as zinc finger proteins (*RNF165*, *ZNF365*, *ZBTB2*, *SNAI1*, *ZNF442*, *ZNF547*, *ZNF563* and *ZNF296*) and vacuolar membrane protein gene *VMP1*, in order to lower the intracellular free zinc level, ultimately preventing cellular toxicity and damage. This finding, together with the up-regulation of metallothioneins and ZnT1, provides us insights into the all-hands-on-deck response strategy of the MCF-7 cancer cells.

6.3 Understanding zinc homeostasis in breast cancer cells

The differentially expressed genes uncovered by transcriptomic RNA-seq analysis in luminal MCF-7 breast cancer cells were extended to the more aggressive MDA-MB-231 basal type breast cancer cells and normal breast epithelial cells (MCF10A). The findings from qRT-PCR analysis provide us an insightful understanding between luminal (MCF-7) and basal (MDA-MB-231) breast cancer cells. The gene expression of *MT1B*, *MT1F*, *MT1X*, *MT2A*, *VMP1*, *ZNF850*, *HSPA6* and *HSPA90AA1* is higher in the MDA-MB-231 cells compared to MCF-7 cells. Their differential expression in response to zinc exposure reveals the different behaviour between luminal and basal breast cancer cells. The higher expression in MDA-MB-231 provides evidence to explain the higher IC_{50} of zinc sulfate in MDA-MB-231 cells (350 μM) against MCF-7 (320 μM). As metallothioneins and heat shock proteins play key roles in stress response, their high expression in basal MDA-MB-231 cells may underpin the malignancy of basal breast cancers. Indeed, previous publications demonstrate that basal breast cancers have much higher expression of metallothioneins (Ionescu et al., 2006; Cui et al., 2007; Chavez et al., 2010; Chandler et al., 2016).

The ZnT1 gene *SLC30A1*, is expressed higher in MDA-MB-231 cells than MCF-7 cells according to the qRT-PCR data (Fig. 5.3 and 5.4). This feature again highlights the difference between the luminal MCF-7 cells which are less malignant and MDA-MB-231 cells which are more aggressive (Franklin and Costello, 2007; Lee et al., 2015). As mentioned previously, ZnT1 is the sole zinc efflux transporter residing in the plasma membrane and is functionally non-redundant in the maintenance of zinc homeostasis (Kambe et al., 2015). The higher expression of ZnT1 in MCF-7 cells than MDA-MB-231 cells could be related to the degree of their malignancy because experimental evidence demonstrates that alterations in ZnT1 expression and the gene mutations of ZnT1 provide a molecular mechanism for impaired zinc homeostasis in cancer development and/or progression (Lehvy et al., 2019).

What is interesting is the degree of ZnT1 up-regulation in MCF10A normal breast epithelial cells in response to extracellular zinc exposure, which is comparable to MDA-MB-231 breast cancer cells. This suggests that ZnT1 is a key player in zinc homeostasis of both cancerous and normal breast cells. Considering that the differentially expressed genes uncovered by RNA-seq such as *MT1B, MT1F, MT1X, MT2A, VMP1, ZNF850, HSPA6* and *HSPA90AA1* are expressed higher in MCF-7 and MDA-MB-231 breast cancer cells, compared to MCF10A normal breast epithelial cells, we can conclude that zinc homeostasis involves a bevy of molecules related to zinc sequestration, efflux and stress response.

6.4 Understanding zinc homeostasis in prostate cancer cells

The findings in Chapter 3 demonstrates that PC3 and DU145 prostate cancer cells were less tolerant to zinc exposure compared to MCF-7 and MDA-MB-231 breast cancer cells.

The determined IC_{50} values for PC3 and DU145 cells were 110 µM and 150 µM, respectively. This provides a characteristic feature of prostate cancer cells on zinc exposure. The differentially expressed genes revealed by transcriptomic RNA-seq analysis in luminal MCF-7 breast cancer cells were extended to the PC3 and DU145 prostate cancer cells and normal prostate epithelial cells (RWPE-1). The discoveries from qRT-PCR analysis provides an understanding of PC3 and DU145 prostate cancer cells in response to zinc exposure. The gene expression of *MT2A*, *VMP1*, *ZNF850*, *HSPA6* and *HSPA90AA1* is higher in the DU145 cells compared to PC3 prostate cancer cells. This might reflect the malignancy of these two types of prostate cancer cells, that is, PC3 cells are more metastatic than DU145 cells.

It is important to recall that metallothioneins genes are responsible for buffering excessive cytoplasmic zinc, whereas zinc-finger protein (*ZNF850*) genes are known to be associated with zinc-binding, the genes for vacuolar membrane protein (*VMP1*) and heat shock protein (*HSPA6* and *HSPA90AA1*) genes are involved in zinc stress response. Collectively, it seems that up-regulation of *MT2A*, *VMP1*, *ZNF850*, *HSPA6* and *HSPA90AA1* genes are essential in response to elevated cytoplasmic zinc in prostate cancer cells. In contrast with the breast cancer cells, the gene expression of prostate cancer cells related to zinc exposure is not as robust. This implies that prostate cancer cells are naturally programmed to inhabit in low-zinc environments compared to breast cancer cells. Intriguingly, up-regulation of ZnT1 (*SLC30A1*) coupled with *MT1B*, *MT1F*, *MT1X*, *MT2A*, *VMP1*, *ZNF850*, *HSPA6* and *HSPA90AA1* gene expression was observed in the normal prostate cells (RWPE-1) compared to cancerous prostate cells. This suggests that non-cancerous prostate cells are more effective in dealing with zinc exposure.

6.5 Proposed molecular mechanisms of zinc homeostasis

Based on the results reported in this thesis, zinc homeostasis involves a network of molecules responsible for zinc uptake, sequestration, efflux and stress response. The mechanism by which zinc ion homeostasis is maintained is illustrated in Fig. 6.1. Zinc ions enter the cell via zinc importers such as ZIP1. While the intracellular zinc level gradually rises, the cell responds by coordinating the expression of numerous genes involved in zinc sequestration and efflux. It is proposed that elevated intracellular zinc level is sensed by the cell through the transcription factor MTF-1. As discussed in Chapter 4, RNA-seq demonstrated that the expression level of MTF-1 is not changed in MCF-7 cells upon zinc exposure. Such a status quo is important for MTF-1 to regulate zinc homeostasis. CK2 could be involved in this as well, for, MTF-1 has been demonstrated to be phosphorylated by CK2. Once MTF-1 is phosphorylated by CK2, cytoplasmic MTF-1 translocates to the nucleus where it binds metal responsive elements of the genes such as *SLC30A1* and metallothionein genes, leading to the activation of transcription of ZnT1 and metallothioneins.

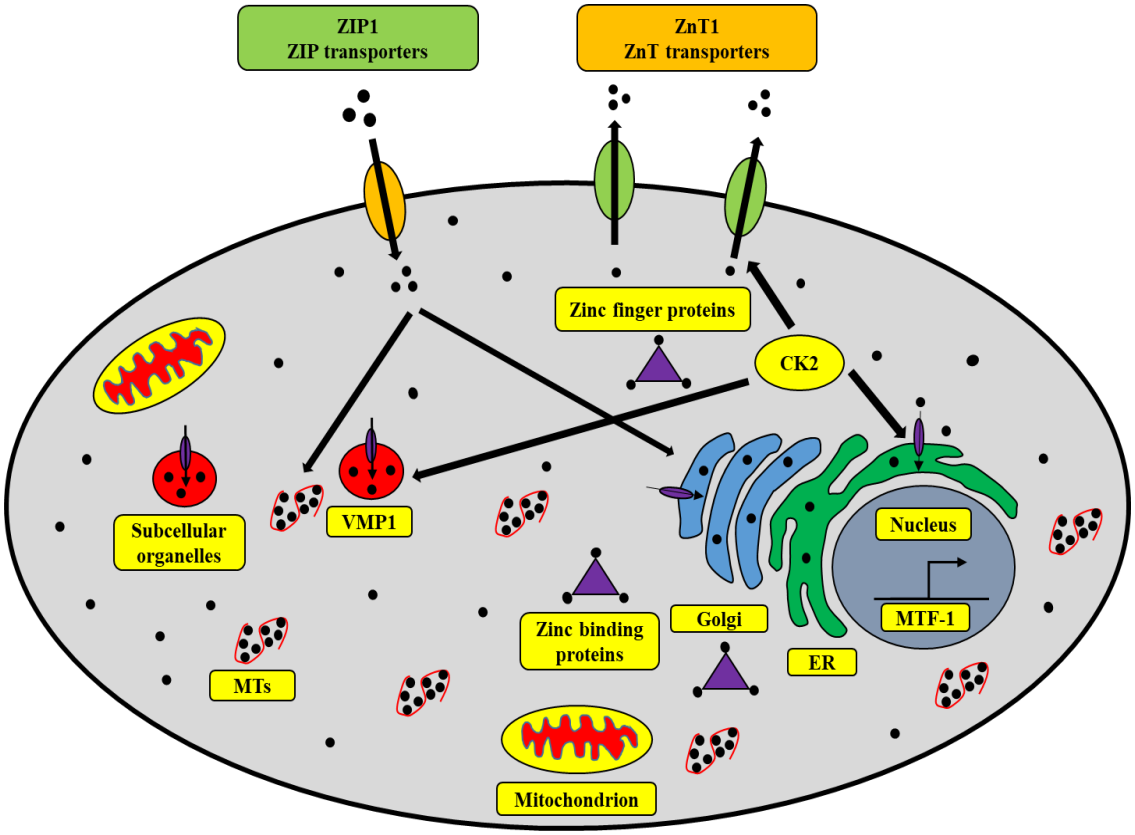

Fig 6.1 Schematic description for molecular details in zinc homeostasis

Zinc ions enter the cell through zinc importers such as ZIP1. The increase of cytoplasmic zinc concentration is sensed by MTF-1, which is then translocated into nucleus, triggering expression of a range of genes involved in zinc sequestration and export. These genes, as uncovered by RNA-seq, include *MT1B*, *MT1F*, *MT1X*, *MT2A*, *SLC30A1*, *VMP1* and *ZNF850*. Excess zinc in cytoplasm causes cellular stress and the heat shock protein genes such as *HSPA6* and *HSPA90AA1* are up-regulated in dealing with this stress.

Up-regulation of ZnT1 and metallothionine genes consequently results in increased zinc efflux and sequestration. This is supported by my RNA-seq findings represented in Chapter 4, where I identified that ZnT1 gene (*SLC30A1*) and metallothionein genes *MT1B, MT1F, MT1X* and *MT2A* in MCF-7 breast cancer cells were significantly up-regulated at both T_{30} and T_{120} zinc exposure. Apart from phosphorylating MTF-1, CK2 may be directly involved in the activation of zinc transporters (ZIPs and ZnTs), similar to CK2's role in the phosphorylation of endoplasmic reticulum zinc channel ZIP7 which results in the gated release of Zn^{2+} from intracellular stores (Taylor et al., 2012).

The findings in Chapters 3-5 reveal that breast cancer cells (MCF-7 and MDA-MB-231) have a higher tolerance to zinc exposure compared to normal breast (MCF10A) epithelial cells as manifested by their IC_{50} values for zinc sulfate. This phenotypic observation is likely due to the increase of gene expression in breast cancer cells (*MT1B, MT1F, MT1X, MT2A, SLC30A1, VMP1, ZNF850, HSPA6* and *HSPA90AA1*) as described in the results of Chapter 4. In comparison, prostate cancer cells (PC3 and DU145) exhibit lower tolerance to zinc exposure compared to normal prostate epithelial cells (RWPE-1). The decreased expression level of the genes (*MT1B, MT1F, MT1X, MT2A, SLC30A1, VMP1, ZNF850, HSPA6* and *HSPA90AA1*) in these two prostate cancer cells was observed, which lends support to the above explanation for the zinc tolerance of breast cancer cells. The findings demonstrate that breast cancer cells are better equipped at responding to high cytoplasmic zinc level whilst prostate cancer cells are not.

6.6 The significance of this study and future work

In summary, the findings described in this thesis demonstrate that CK2 is engaged in zinc ion homeostasis in breast and prostate cancer cells. Individual CK2 subunits play distinctive roles in response to zinc exposure. The uncovered differentially expressed genes of the cancer cells in response to zinc exposure provide us insightful knowledge and understanding of zinc homeostasis in breast and prostate cancer cells. The employment of two cancerous and one normal breast epithelial cell line, and two cancerous and one normal prostate epithelial cell line, is strategically important for this study.

The role of zinc in breast and prostate cancer development and treatment is currently an area of active research worldwide. The molecular clues described in this thesis are a step forward in this endeavour. For example, this project as well as the previous studies demonstrated that the cellular zinc level in breast cancer cells is elevated in comparison to the normal breast epithelial cells (Costello and Franklin, 2006; Cousins et al., 2006; Franklin and Costello, 2007; Franklin and Costello, 2009; Chandler et al., 2016; Reddy et al., 2018), and the zinc level is considerably lower in prostate cancer cells compared to their normal prostate epithelial cells (Rishi et al., 2003; Franklin et al., 2005; Costello and Franklin, 2006; Franklin and Costello, 2009; Huang and Tepaamorndech, 2013). It could be a viable treatment strategy if one could lower the intracellular zinc level of breast cancer cells or elevate the intracellular zinc level of prostate cancer cells. The findings of this study could contribute to making such a treatment strategy a reality. When targeting breast cancer cells such a strategic treatment approach would entail down-regulation of ZIP (*ZIP4*, *ZIP6* and *ZIP14*) and ZnT1 gene expression in breast cancer cells. Contrastingly, the up-regulation of ZIP gene expression (*ZIP1*, *ZIP2*, *ZIP3*, *ZIP4* and *ZIP9*) would make prostate cancer cells less viable.

The discoveries of this thesis open a new avenue for cancer research. Future studies should focus on the molecular details between CK2 and zinc transport proteins (ZIP and ZnT). The interaction between CK2 and MTF-1 should also be investigated. The breast and prostate cancers should be studied together for zinc homeostasis, because of their contrasting cellular profiles.

7 REFERENCES

Aagaard. L JJR (2007) siRNA therapeutics: principle, prospects & challenges. RNA Technologies **3:** 75-86

Achary MP, Jaggernauth W, Gross E, Alfieri A, Klinger H, Vikram B (2001) Cell lines from the same cervical carcinomabut with different radiosensitivities exhibit different cDNA microarray patterns of gene expression. Cytogenetic & Genome Research **91:** 39-43

Adams TK, Saydam N, Steiner F, Schaffner W, Freedman JH (2002) Activation of gene expression by metal-responsive signal transduction pathways. Environmental Health Perspectives **110:** 813

Alam S, Kelleher SL (2012) Cellular mechanisms of zinc dysregulation: a perspective on zinc homeostasis as an etiological factor in the development and progression of breast cancer. Nutrients **4:** 875-903

Allende JE, Allende CC (1995) Protein kinases. 4. Protein kinase CK2: an enzyme with multiple substrates and a puzzling regulation. The FASEB Journal **9:** 313-323

Almedia. R ARC (2005) RNA silencing and genome regulation. Trends in Cell Biology **15:** 251-228

Ambion RNA Interference Research Guide - Applied Biosystems. *In* AA Biosystems, ed. Ambion Austin

Andreini C, Banci L, Bertini I, Rosato A (2006) Counting the zinc-proteins encoded in the human genome. Journal of Proteome Research **5:** 196-201

Andrews GK (2001) Cellular zinc sensors: MTF-1 regulation of gene expression. *In* Zinc Biochemistry, Physiology, & Homeostasis. Springer, pp 37-51

Bafaro E, Liu Y, Xu Y, Dempski RE (2017) The emerging role of zinc transporters in cellular homeostasis and cancer. Signal transduction and targeted therapy **2:** 1-12

Baguley BC, Leung E (2011) Heterogeneity of phenotype in breast cancer cell lines. Breast Cancer Research**:** 245-256

Baltaci AK, Yuce K (2018) Zinc transporter proteins. Neurochemical research **43:** 517-530

Baltaci AK, Yuce K, Mogulkoc R (2018) Zinc metabolism and metallothioneins. Biological trace element research **183:** 22-31

Bastide C, Bagnis C, Mannoni P, Hassoun J, Bladou F (2002) A Nod Scid mouse model to study human prostate cancer. Prostate Cancer & Prostatic Diseases **5:** 311-315

Becaria, Campbell A, Bondy SC (2002) Aluminum as a toxicant. Toxicology & Industrial Health **18:** 309-320

Bello D, Webber M, Kleinman H, Wartinger D, Rhim J (1997) Androgen responsive adult human prostatic epithelial cell lines immortalized by human papillomavirus 18. Carcinogenesis **18:** 1215-1223

Benjamini Y, Hochberg Y (1995) Controlling the False Discovery Rate - a Practical and Powerful Approach to Multiple Testing. Journal of the Royal Statistical Society Series B-Methodological **57:** 289-300

Beveridge R, Pintos J, Parent M, Asselin J, Siemiatycki J (2010) Lung cancer risk associated with occupational exposure to nickel, chromium VI, and cadmium in two population-based case–control studies in Montreal. American Journal of Industrial Medicine **53:** 476-485

Bianchi M, Crinelli R, Arbore V, Magnani M (2018) Induction of ubiquitin C (UBC) gene transcription is mediated by HSF 1: role of proteotoxic and oxidative stress. FEBS Open Bio **8:** 1471-1485

Bischoff N, Olsen B, Raaf J, Bretner M, Issinger O-G, Niefind K (2011) Structure of the Human Protein Kinase CK2 Catalytic Subunit CK2α′ and Interaction Thermodynamics with the Regulatory Subunit CK2β. Journal of Molecular Biology **407:** 1-12

Blanquet PR (2000) Casein kinase 2 as a potentially important enzyme in the nervous system. Progress in Neurobiology **60:** 211-246

Bozym RA, Thompson RB, Stoddard AK, Fierke CA (2006) Measuring picomolar intracellular exchangeable zinc in PC-12 cells using a ratiometric fluorescence biosensor. ACS Chemical Biology **1:** 103-111

Bray F, Ferlay J, Soerjomataram I, Siegel RL, Torre LA, Jemal A (2018) Global cancer statistics 2018: GLOBOCAN estimates of incidence and mortality worldwide for 36 cancers in 185 countries. CA: A Cancer Journal for Clinicians **68:** 394-424

Brelje TC, Sorenson RL (1992) Chapter 4 Multicolor Laser Scanning Confocal Immunofluorescence Microscopy: Practical Application and Limitations. Methods in Cell Biology

Bustin S (2002) INVITED REVIEW Quantification of mRNA using real-time reverse transcription PCR (RT-PCR): trends and problems. Journal of Molecular Endocrinology **29:** 23-39

Cailleau R, Cruciger Q, Hokanson K, Olive M, Blumenschein G (1976) Morphological, biochemical and chromosomal characterization of breast tumor lines from pleural effusions. *In* IN VITRO-JOURNAL OF THE TISSUE CULTURE ASSOCIATION, Vol 12. SOC IN VITRO BIOLOGY 9315 LARGO DR WEST, STE 25, LARGO, MD 20774, pp 331-331

Cailleau R, Olive M, Cruciger QV (1978) Long-term human breast carcinoma cell lines of metastatic origin: preliminary characterization. In vitro **14:** 911-915

Calderwood SK, Khaleque MA, Sawyer DB, Ciocca DR (2006) Heat shock proteins in cancer: chaperones of tumorigenesis. Trends in Biochemical Sciences **31:** 164-172

Cannon CM, Trembley JH, Kren BT, Unger GM, O'Sullivan MG, Cornax I, Modiano JF, Ahmed K (2017) Evaluation of protein kinase CK2 as a therapeutic target for squamous cell carcinoma of cats. American Journal of Veterinary Research **78:** 946-953

Chabosseau P, Tuncay E, Meur G, Bellomo EA, Hessels A, Hughes S, Johnson PR, Bugliani M, Marchetti P, Turan B (2014) Mitochondrial and ER-targeted eCALWY probes reveal high levels of free Zn2+. ACS Chemical Biology **9:** 2111-2120

Chandler P, Kochupurakkal BS, Alam S, Richardson AL, Soybel DI, Kelleher SL (2016) Subtype-specific accumulation of intracellular zinc pools is associated with the malignant phenotype in breast cancer. Mol Cancer **15:** 2

Chandler P, Kochupurakkal BS, Alam S, Richardson AL, Soybel DI, Kelleher SL (2016) Subtype-specific accumulation of intracellular zinc pools is associated with the malignant phenotype in breast cancer. Molecular Cancer **15:** 2

Chantalat L, Leroy D, Filhol O, Nueda A, Benitez MJ, Chambaz EM, Cochet C, Dideberg O (1999) Crystal structure of the human protein kinase CK2 regulatory subunit reveals its zinc finger-mediated dimerization. The EMBO Journal **18:** 2930-2940

Chasapis CT, Ntoupa P-SA, Spiliopoulou CA, Stefanidou ME (2020) Recent aspects of the effects of zinc on human health. Archives of Toxicology **94:** 1443-1460

Chavez KJ, Garimella SV, Lipkowitz S (2010) Triple negative breast cancer cell lines: one tool in the search for better treatment of triple negative breast cancer. Breast Disease **32:** 35

Chen T (1993) Chromosome identity of human prostate cancer cell lines, PC-3 and PPC-1. Cytogenetic and Genome Research **62:** 183-184

Ching KZ, Ramsey E, Pettigrew N, D'cunha R, Jason M, Dodd JG (1993) Expression of mRNA for epidermal growth factor, transforming growth factor-alpha and their receptor in human prostate tissue and cell lines. Molecular & Cellular Biochemistry **126:** 151-158

Choi S, Bird AJ (2014) Zinc'ing sensibly: controlling zinc homeostasis at the transcriptional level. Metallomics **6:** 1198-1215

Chyan W, Zhang DY, Lippard SJ, Radford RJ (2014) Reaction-based fluorescent sensor for investigating mobile Zn^{2+} in mitochondria of healthy versus cancerous prostate cells. Proceedings of the National Academy of Sciences of the United States of America **111:** 143-148

Clemons M, Danson S, Howell A (2002) Tamoxifen ('Nolvadex'): a review: Antitumour treatment. Cancer treatment reviews **28:** 165-180

Colvin RA, Fontaine CP, Laskowski M, Thomas D (2003) Zn2+ transporters and Zn^{2+} homeostasis in neurons. European Journal of Pharmacology **479:** 171-185

Colvin. R, Laskowski. M, Fontaine. C (2006) Zinquin identifies subcellular compartmentalization of zinc in cortical neurons. Relation to the trafficking of zinc and the mitochondrial compartment. Brain Research **1085:** 1-10

Cornford PA, Dodson AR, Parsons KF, Desmond AD, Woolfenden A, Fordham M, Neoptolemos JP, Ke Y, Foster CS (2000) Heat shock protein expression independently predicts clinical outcome in prostate cancer. Cancer Research **60:** 7099-7105

Costello LC, Franklin RB (2006) The clinical relevance of the metabolism of prostate cancer; zinc and tumor suppression: connecting the dots. Molecular Cancer **5:** 17

Cousins RJ, Liuzzi JP, Lichten LA (2006) Mammalian Zinc Transport, Trafficking, and Signals. Journal of Biological Chemistry **281:** 24085-24089

Coyle P, Philcox JC, Carey LC, Rofe AM (2002) Metallothionein: the multipurpose protein. Cellular & Molecular Life Sciences **59:** 627-647

Coyle YM, Minahjuddin AT, Hynan LS, Minna JD (2006) An ecological study of the association of metal air pollutants with lung cancer incidence in Texas. Journal of Thoracic Oncology **1:** 654-661

Cozza G, Mazzorana M, Papinutto E, Bain J, Elliott M, Di Maira G, Gianoncelli A, Pagano M, Sarno S, Ruzzene M (2009) Quinalizarin as a potent, selective and cell-permeable inhibitor of protein kinase CK2. Biochemical Journal **421:** 387-395

Cui Y, Vogt S, Olson N, Glass AG, Rohan TE (2007) Levels of zinc, selenium, calcium, and iron in benign breast tissue and risk of subsequent breast cancer. Cancer Epidemiology & Prevention Biomarkers **16:** 1682-1685

de Paiva EL, Medeiros C, Fioravanti MIA, Milani RF, Morgano MA, Pallone JAL, Arisseto-Bragotto AP (2020) Aluminium in infant foods: Total content, effect of in vitro digestion on bioaccessible fraction and preliminary exposure assessment. Journal of Food Composition and Analysis **90:** 103493

Desoize B (2004) Metals and metal compounds in cancer treatment. Anticancer Research **24:** 1529-1544

Duncan JS, Gyenis L, Lenehan J, Bretner M, Graves LM, Haystead TA, Litchfield DW (2008) An unbiased evaluation of CK2 inhibitors by chemoproteomics: characterization of inhibitor effects on CK2 and identification of novel inhibitor targets. Molecular & Cellular Proteomics **2008 Jun;7(6):1077-88. doi:** 10.1074/mcp.M700559-MCP700200

Duncan JS, Litchfield DW (2008) Too much of a good thing: the role of protein kinase CK2 in tumorigenesis and prospects for therapeutic inhibition of CK2. Biochimica et Biophysica Acta **1784:** 33-47

Ebara M, Fukuda H, Hatano R, Saisho H, Nagato Y, Suzuki K, Nakajima K, Yukawa M, Kondo F, Nakayama A, Sakurai H (2000) Relationship between copper, zinc and metallothionein in hepatocellular carcinoma and its surrounding liver parenchyma. Journal of Hepatology **33:** 415-422

Ebert JC, Altman RB (2008) Robust recognition of zinc binding sites in proteins. Protein Science **17:** 54-65

Edzwald JK (2020) Aluminum in Drinking Water: Occurrence, Effects, and Control. Journal: American Water Works Association **112**

Eide DJ (1998) The molecular biology of metal ion transport in *Saccharomyces cerevisiae*. Annu Rev Nutr **18:** 441-469

Exley C, Clarkson E (2020) Aluminium in human brain tissue from donors without neurodegenerative disease: A comparison with Alzheimer's disease, multiple sclerosis and autism. Scientific reports **10:** 1-7

Faust M, Montenarh M (2000) Subcellular localization of protein kinase CK2. A key to its function? Cell & Tissue Research **301:** 329-340

Faust RA, Niehans G, Gapany M, Hoistad D, Knapp D, Cherwitz D, Davis A, Adams GL, Ahmed K (1999) Subcellular immunolocalization of protein kinase CK2 in normal and carcinoma cells. The International Journal of Biochemistry & Cell Biology **31:** 941-949

Ferlay J, Colombet M, Soerjomataram I, Dyba T, Randi G, Bettio M, Gavin A, Visser O, Bray F (2018) Cancer incidence and mortality patterns in Europe: Estimates for 40 countries and 25 major cancers in 2018. European Journal of Cancer **103:** 356-387

Filhol O, Martiel J-L, Cochet C (2004) Protein kinase CK2: a new view of an old molecular complex. EMBO Reports **5:** 351-355

Fleige S, Pfaffl MW (2006) RNA integrity and the effect on the real-time qRT-PCR performance. Molecular Aspects of Medicine **27:** 126-139

Foulkes WD, Smith IE, Reis-Filho JS (2010) Triple-negative breast cancer. New England journal of medicine **363:** 1938-1948

Franchin C, Borgo C, Cesaro L, Zaramella S, Vilardell J, Salvi M, Arrigoni G, Pinna LA (2018) Re-evaluation of protein kinase CK2 pleiotropy: new insights provided by a phosphoproteomics analysis of CK2 knockout cells. Cellular and Molecular Life Sciences **75:** 2011-2026

Franklin RB, Costello LC (2007) Zinc as an anti-tumor agent in prostate cancer and in other cancers. Archives of Biochemistry and Biophysics **463:** 211-217

Franklin RB, Costello LC (2009) The important role of the apoptotic effects of zinc in the development of cancers. Journal of Cellular Biochemistry **106:** 750-757

Franklin RB, Feng P, Milon B, Desouki MM, Singh KK, Kajdacsy-Balla A, Bagasra O, Costello LC (2005) hZIP1 zinc uptake transporter down regulation and zinc depletion in prostate cancer. Molecular cancer **4:** 32

Franklin RB, Feng P, Milon B, Desouki MM, Singh KK, Kajdacsy-Balla A, Bagasra O, Costello LC (2005) hZIP1 zinc uptake transporter down regulation and zinc depletion in prostate cancer. Molecular Cancer **4:** 32

Freeman WM, Walker SJ, Vrana KE (1999) Quantitative RT-PCR: pitfalls and potential. BioTechniques **26:** 112-125

Frezza M, Hindo S, Chen D, Davenport A, Schmitt S, Tomco D, Ping Dou Q (2010) Novel metals and metal complexes as platforms for cancer therapy. Current pharmaceutical design **16:** 1813-1825

Garrido-Castro AC, Lin NU, Polyak K (2019) Insights into molecular classifications of triple-negative breast cancer: improving patient selection for treatment. Cancer discovery **9:** 176-198

Geddes DT (2007) Inside the lactating breast: the latest anatomy research. Journal of Midwifery & Women's Health **52:** 556-563

Geldmacher-von Mallinckrodt M, Meissner D (1994) General aspects of the role of metals in clinical chemistry. *In*. Marcel Dekker, New York, pp 13-29

Giedroc DP, Chen X, Apuy JL (2001) Metal response element (MRE)-binding transcription factor-1 (MTF-1): structure, function, and regulation. Antioxidants & Redox Signaling **3:** 577-596

Goulding H, Jasani B, Pereira H, Reid A, Galea M, Bell J, Elston C, Robertson J, Blamey R, Nicholson R (1995) Metallothionein expression in human breast cancer. British Journal of Cancer **72:** 968-972

Grattan BJ, Freake HC (2012) Zinc and cancer: implications for LIV-1 in breast cancer. Nutrients **4:** 648-675

Grummt F, Weinmann-Dorsch C, Schneider-Schaulies J, Lux A (1986) Zinc as a second messenger of mitogenic induction: Effects on diadenosine tetraphosphate (Ap4A) and DNA synthesis. Experimental Cell Research **163:** 191-200

Guerinot ML (2000) The ZIP family of metal transporters. Biochimica et Biophysica Acta **1465:** 190-198

Guerra B, Boldyreff B, Sarno S, Cesaro L, Issinger OG, Pinna LA (1999) CK2: A Protein Kinase in Need of Control. Pharmacology & Therapeutics **82:** 303-313

Guerra B, Boldyreff B, Sarno S, Cesaro L, Issinger OG, Pinna LA (1999) CK2: A protein kinase in need of control. Pharmacol Therapeut **82:** 303-313

Guerra B, Issinger OG (1999) Protein kinase CK2 and its role in cellular proliferation, development and pathology. Electrophoresis **20:** 391-408

Haase H, Mazzatti DJ, White A, Ibs KH, Engelhardt G, Hebel S, Powell JR, Rink L (2007) Differential gene expression after zinc supplementation and deprivation in human leukocyte subsets. Molecular Medicine **13:** 362-370

Hai T, Wolfgang CD, Marsee DK, Allen AE, Sivaprasad U (1999) ATF3 and stress responses. Gene Expression The Journal of Liver Research **7:** 321-335

Hansen RJ, Friedberg EC, Reagan MS (2000) Sensitivity of a *S. cerevisiae RAD27* deletion mutant to DNA-damaging agents and in vivo complementation by the human *FEN-1* gene. Mutation Research **461:** 243-248

Hardyman JEJ, Tyson J, Jackson KA, Aldridge C, Cockell SJ, Wakeling LA, Valentine RA, Ford D (2016) Zinc sensing by metal-responsive transcription factor 1 (MTF1) controls metallothionein and ZnT1 expression to buffer the sensitivity of the transcriptome response to zinc. Metallomics **8:** 337-343

He X, Wang X, Zhang L, Fang G, Liu J, Wang S (2018) Sensing and intracellular imaging of Zn2+ based on affinity peptide using an aggregation induced emission fluorescence "switch-on" probe. Sensors and actuators B: chemical **271:** 289-299

Hershfinkel M, Moran A, Grossman N, Sekler I (2001) A zinc-sensing receptor triggers the release of intracellular Ca^{2+} and regulates ion transport. Proceedings of the National Academy of Sciences of the United States of America **98:** 11749-11754

Ho E, Ames BN (2002) Low intracellular zinc induces oxidative DNA damage, disrupts p53, NFκB, and AP1 DNA binding, and affects DNA repair in a rat glioma cell line. Proceedings of the National Academy of Sciences **99:** 16770-16775

Holliday DL, Speirs V (2011) Choosing the right cell line for breast cancer research. Breast Cancer Research **13:** 1-7

Houk RS, Fassel VA, Flesch GD, Svec HJ, Gray AL, Taylor CE (1980) Inductively coupled argon plasma as an ion source for mass spectrometric determination of trace elements. Analytical Chemistry **52:** 2283-2289

Huang L, Tepaamorndech S (2013) The SLC30 family of zinc transporters – a review of current understanding of their biological and pathophysiological roles. Molecular Aspects of Medicine **34:** 548-560

Ionescu JG, Novotny J, Stejskal V, Lätsch A, Blaurock-Busch E, Eisenmann-Klein M (2006) Increased levels of transition metals in breast cancer tissue. Neuroendocrinology Letters **27:** 36-39

Isaacs JS, Xu W, Neckers L (2003) Heat shock protein 90 as a molecular target for cancer therapeutics. Cancer Cell **3:** 213-217

Jackson AC, Liu J, Vallanat B, Jones C, Nelms MD, Patlewicz G, Corton JC (2020) Identification of novel activators of the metal responsive transcription factor (MTF-1) using a gene expression biomarker in a microarray compendium. Metallomics **12:** 1400-1415

Jacob P. T. GV, Michelle. G, and Litchfield. D. W (2013) Characterizing the convergence of protein kinase CK2 and caspase-3 reveals isoform-specific phosphorylation of caspase-3 by CK2α′: implications for pathological roles of CK2 in promoting cancer cell survival. Oncotarget**:** 560-571

Johnson AJ, Veljanoski F, O'Doherty PJ, Zaman MS, Petersingham G, Bailey TD, Munch G, Kersaitis C, Wu MJ (2016) Molecular insight into arsenic toxicity via the genome-wide deletion mutant screening of *Saccharomyces cerevisiae*. Metallomics **8:** 228-235

Johnson AJ, Veljanoski F, O'Doherty PJ, Zaman MS, Petersingham G, Bailey TD, Munch G, Kersaitis C, Wu MJ (2016) Revelation of molecular basis for chromium toxicity by phenotypes of *Saccharomyces cerevisiae* gene deletion mutants. Metallomics **8:** 542-550

Johnson AJ, Veljanoski F, O'Doherty PJ, Zaman MS, Petersingham G, Bailey TD, Münch G, Kersaitis C, Wu MJ (2016) Molecular insight into arsenic toxicity via the genome-wide deletion mutant screening of Saccharomyces cerevisiae. Metallomics **8:** 228-235

Johnson AJ, Wu MJ (2016) The new role for an old kinase: Protein kinase CK2 regulates metal ion transport. Pharmaceuticals **9:** 80

Johnson AJ, Zaman MS, Veljanoski F, Phrakaysone AA, Li S, O'Doherty PJ, Petersingham G, Perrone GG, Molloy MP, Wu MJ (2017) Unravelling the role of protein kinase CK2 in metal toxicity using gene deletion mutants. Metallomics **9:** 301-308

Johnson FV, Patrick. J. O'Doherty, Mohammad S. Zaman, Gayani Petersingham, Trevor D. Bailey, Gerald Münch, Cindy Kersaitisa and Ming J. Wu (2016) Revelation of molecular basis for chromium toxicity by phenotypes of Saccharomyces cerevisiae gene deletion mutants. Metallomics **8:** 542-550

Jordan VC (2003) Tamoxifen: a most unlikely pioneering medicine. Nature reviews Drug discovery **2:** 205-213

Kagara N, Tanaka N, Noguchi S, Hirano T (2007) Zinc and its transporter ZIP10 are involved in invasive behavior of breast cancer cells. Cancer Science **98:** 692-697

Kaighn M, Narayan KS, Ohnuki Y, Lechner J, Jones L (1979) Establishment and characterization of a human prostatic carcinoma cell line (PC-3). Investigative Urology **17:** 16

Kambe T (2011) An overview of a wide range of functions of ZnT and Zip zinc transporters in the secretory pathway. Bioscience, Biotechnology & Biochemistry **75:** 1036-1043

Kambe T, Hashimoto A, Fujimoto S (2014) Current understanding of ZIP and ZnT zinc transporters in human health and diseases. Cellular and molecular life sciences **71:** 3281-3295

Kambe T, Tsuji T, Hashimoto A, Itsumura N (2015) The physiological, biochemical, and molecular roles of zinc transporters in zinc homeostasis and metabolism. Physiological Reviews **95:** 749-784

Kappes F, Damoc C, Knippers R, Przybylski M, Pinna LA, Gruss C (2004) Phosphorylation by protein kinase CK2 changes the DNA binding properties of the human chromatin protein DEK. Molecular & Cellular Biology **24:** 6011-6020

Katsuoka F, Motohashi H, Engel JD, Yamamoto M (2005) Nrf2 transcriptionally activates the mafG gene through an antioxidant response element. Journal of Biological Chemistry **280:** 4483-4490

Keilin D, Mann T (1940) Carbonic anhydrase. Purification and nature of the enzyme. Biochemical Journal **34:** 1163-1176

Kelland L (2007) The resurgence of platinum-based cancer chemotherapy. Nature Reviews Cancer **7:** 573-584

Kelleher SL, Lönnerdal B (2003) Zn transporter levels and localization change throughout lactation in rat mammary gland and are regulated by Zn in mammary cells. The Journal of Nutrition **133:** 3378-3385

Keller PJ, Lin AF, Arendt LM, Klebba I, Jones AD, Rudnick JA, DiMeo TA, Gilmore H, Jefferson DM, Graham RA (2010) Mapping the cellular and molecular heterogeneity of normal and malignant breast tissues and cultured cell lines. Breast Cancer Research **12:** R87

Kelliher MA, Seldin DC, Leder P (1996) Tal-1 induces T cell acute lymphoblastic leukemia accelerated by casein kinase IIalpha. The EMBO Journal **15:** 5160-5166

Kelsey JL, Gammon MD, John EM (1993) Reproductive factors and breast cancer. Epidemiologic Reviews **15:** 36

Kim D, Pertea G, Trapnell C, Pimentel H, Kelley R, Salzberg SL (2013) TopHat2: accurate alignment of transcriptomes in the presence of insertions, deletions and gene fusions. Genome Biol **14:** R36

Kim U, Kim C-Y, Lee JM, Oh H, Ryu B, Kim J, Park J-H (2020) Phloretin inhibits the human prostate cancer cells through the generation of reactive oxygen species. Pathology & Oncology Research **26:** 977-984

Kimura T, Kambe T (2016) The functions of metallothionein and ZIP and ZnT transporters: an overview and perspective. International Journal of Molecular Sciences **17:** 336

Kirschke CP, Huang L (2003) ZnT7, a Novel Mammalian Zinc Transporter, Accumulates Zinc in the Golgi Apparatus. Journal of Biological Chemistry **278:** 4096-4102

Koh JY, Choi DW (1994) Zinc toxicity on cultured cortical neurons: Involvement of N-methyl-D-aspartate receptors. Neuroscience **60:** 1049-1057

Krężel A, Maret W (2006) Zinc-buffering capacity of a eukaryotic cell at physiological pZn. Journal of Biological Inorganic Chemistry **11:** 1049-1062

Kumar V, Majumder P (1995) Prostate gland: structure, functions and regulation. International Urology & Nephrology **27:** 231-243

Kumar. D. L aCRA (2007) Gene manipulation through the use of small interfering RNA (siRNA): From in vitro to in vivo applications. RNA Technologies **2:** 87-100

Kumbrink J, Kirsch KH, Johnson JP (2010) EGR1, EGR2, and EGR3 activate the expression of their coregulator NAB2 establishing a negative feedback loop in cells of neuroectodermal and epithelial origin. Journal of Cellular Biochemistry **111:** 207-217

Laity JH, Andrews GK (2007) Understanding the mechanisms of zinc-sensing by metal-response element binding transcription factor-1 (MTF-1). Archives of Biochemistry and Biophysics **463:** 201-210

Laity JH, Lee BM, Wright PE (2001) Zinc finger proteins: new insights into structural and functional diversity. Current Opinion in Structural Biology **11:** 39-46

Landesman-Bollag E, Channavajhala PL, Cardiff RD, Seldin DC (1998) p53 deficiency and misexpression of protein kinase CK2α collaborate in the development of thymic lymphomas in mice. Oncogene **16**

Landesman-Bollag E, Song DH, Mourez RR, Sussman DJ, Cardiff RD, Sonenshein GE, Seldin DC (2001) Protein kinase CK2: signaling and tumorigenesis in the mammary gland. *In* Protein Kinase CK2—From Structure to Regulation. Springer, pp 153-165

Langmade SJ, Ravindra R, Daniels PJ, Andrews GK (2000) The transcription factor MTF-1 mediates metal regulation of the mouse ZnT1 gene. Journal of Biological Chemistry **275:** 34803-34809

Langmead B, Salzberg SL (2012) Fast gapped-read alignment with Bowtie 2. Nat Methods **9:** 357-359

Lee AV, Oesterreich S, Davidson NE (2015) MCF-7 cells—changing the course of breast cancer research and care for 45 years. Journal of the National Cancer Institute **107**

Lehvy AI, Horev G, Golan Y, Glaser F, Shammai Y, Assaraf YG (2019) Alterations in ZnT1 expression and function lead to impaired intracellular zinc homeostasis in cancer. Cell death discovery **5:** 1-12

Levenson AS, Jordan VC (1997) MCF-7: the first hormone-responsive breast cancer cell line. Cancer Research **57:** 3071-3078

Levoy M, Chen B, Vaish V, Horowitz M, McDowall I, Bolas M (2004) Synthetic aperture confocal imaging. ACM Transactions on Graphics **23:** 825-834

Li M, Zhang Y, Liu Z, Bharadwaj U, Wang H, Wang X, Zhang SW, Liuzzi JP, Chang S, Cousins RJ, Fisher WE, Brunicardi FC, Logsdon CD, Chen C, Yao Q (2007) Aberrant expression of zinc transporter ZIP4 (SLC39A4) significantly contributes to human pancreatic cancer pathogenesis and progression. Proceedings of the National Academy of Sciences of the United States of America **104:** 18636-18641

Liang JY, Liu YY, Zou J, Franklin RB, Costello LC, Feng P (1999) Inhibitory effect of zinc on human prostatic carcinoma cell growth. The Prostate **40:** 200-207

Liao Y, Smyth GK, Shi W (2014) featureCounts: an efficient general purpose program for assigning sequence reads to genomic features. Bioinformatics **30:** 923-930

Lichten LA, Ryu M-S, Guo L, Embury J, Cousins RJ (2011) MTF-1-mediated repression of the zinc transporter Zip10 is alleviated by zinc restriction. PLOS One **6:** e21526

Lichtlen P, Wang Y, Belser T, Georgiev O, Certa U, Sack R, Schaffner W (2001) Target gene search for the metal-responsive transcription factor MTF-1. Nucleic Acids Research **29:** 1514-1523

Lin S-f, Wei H, Maeder D, Franklin RB, Feng P (2009) Profiling of zinc-altered gene expression in human prostate normal vs. cancer cells: a time course study. The Journal of Nutritional Biochemistry **20:** 1000-1012

Litchfield DW (2003) Protein kinase CK2: structure, regulation and role in cellular decisions of life and death. Biochem. J. **369:** 1-15

Litchfield DW, Luscher B (1993) Casein kinase II in signal transduction and cell cycle regulation. Molecular & Cellular Biochemistry **127-128:** 187-199

Liu H, Zang C, Fenner M, Possinger K, Elstner E (2003) PPARγ ligands and ATRA inhibit the invasion of human breast cancer cells in vitro. Breast Cancer Research **79:** 63-74

Liu L, Cui WM, Zhang SW, Kong FH, Pedersen MA, Wen Y, Lv JP (2015) Effect of glucose tolerance factor (GTF) from high chromium yeast on glucose metabolism in insulin-resistant 3T3-L1 adipocytes. RSC Advances **5:** 3482-3490

Liu Y, Beyer A, Aebersold R (2016) On the dependency of cellular protein levels on mRNA abundance. Cell **165:** 535-550

Lolli G, Cozza G, Mazzorana M, Tibaldi E, Cesaro L, Donella-Deana A, Meggio F, Venerando A, Franchin C, Sarno S (2012) Inhibition of protein kinase CK2 by flavonoids and tyrphostins. A structural insight. Biochemistry **51:** 6097-6107

Lopez V, Foolad F, Kelleher SL (2011) ZnT2-overexpression represses the cytotoxic effects of zinc hyper-accumulation in malignant metallothionein-null T47D breast tumor cells. Cancer Letters **304:** 41-51

Ma S, Charron J, Erikson RL (2003) Role of Plk2 (Snk) in mouse development and cell proliferation. Molecular & Cellular Biology **23:** 6936-6943

Mackay JP, Crossley M (1998) Zinc fingers are sticking together. Trends in Biochemical Sciences **23:** 1-4

Maret W (2001) Crosstalk of the group IIa and IIb metals calcium and zinc in cellular signaling. Proceedings of the National Academy of Sciences of the United States of America **98:** 12325-12327

Maret W (2003) Cellular zinc and redox states converge in the metallothionein/thionein pair. The Journal of Nutrition **133:** 1460S-1462S

Maret W (2012) New perspectives of zinc coordination environments in proteins. Journal of Inorganic Biochemistry **111:** 110-116

Maret W (2012) New perspectives of zinc coordination environments in proteins. J Inorg Biochem **111:** 110-116

Maret W (2017) Zinc in cellular regulation: The nature and significance of "zinc signals". International Journal of Molecular Sciences **18:** 2285

Margalioth EJ, Schenker JG, Chevion M (1983) Copper and zinc levels in normal and malignant tissues. Cancer **52:** 868-872

Margoshes M, Vallee BL (1957) A cadmium protein from equine kidney cortex. Journal of the American Chemical Society **79:** 4813-4814

McCarty KM, Hanh HT, Kim K (2011) Arsenic geochemistry and human health in South East Asia. Reviews on Environmental Health **26:** 71-78

McNeal JE, Redwine EA, Freiha FS, Stamey TA (1988) Zonal distribution of prostatic adenocarcinoma: correlation with histologic pattern and direction of spread. The American Journal of Surgical Pathology **12:** 897-906

Medunić G, Fiket Ž, Ivanić M (2020) Arsenic contamination status in Europe, Australia, and other parts of the world. *In* Arsenic in Drinking Water and Food. Springer, pp 183-233

Meggio F, Marin O, Pinna L (1994) Substrate specificity of protein kinase CK2. Cellular & Molecular Biology Research **40:** 401-409

Meggio F, Pinna LA (2003) One-thousand-and-one substrates of protein kinase CK2? The FASEB Journal **17:** 349-368

Meiser B, Wong WT, Peate M, Julian-Reynier C, Kirk J, Mitchell G (2017) Motivators and barriers of tamoxifen use as risk-reducing medication amongst women at increased breast cancer risk: a systematic literature review. Hereditary cancer in clinical practice **15:** 1-9

Mello. C aCD (2004) Revealing the world of RNA interference. Nature**:** 338-343

Meskel HH, Cherian M, Martinez V, Veinot L, Frei J (1993) Metallothionein as an epithelial proliferative compartment marker for DNA flow cytometry. Modern Pathology **6:** 755-760

Mickey DD, Stone KR, Wunderli H, Mickey GH, Vollmer RT, Paulson DF (1977) Heterotransplantation of a human prostatic adenocarcinoma cell line in nude mice. Cancer Research **37:** 4049-4058

Montaser A (1998) Inductively coupled plasma mass spectrometry. John Wiley & Sons

Nelson N (1999) Metal ion transporters and homeostasis. The EMBO Journal **18:** 4361-4371

Neve RM, Chin K, Fridlyand J, Yeh J, Baehner FL, Fevr T, Clark L, Bayani N, Coppe J-P, Tong F (2006) A collection of breast cancer cell lines for the study of functionally distinct cancer subtypes. Cancer Cell **10:** 515-527

Nguyen NNT, Le PN, Nguyen TBT, Nguyen NH, Bach LG, Doan VN, Tran HLB, Le VT, Tran NQ (2018) Synergic activity against MCF-7 breast cancer cell growth of nanocurcumin-encapsulated and cisplatin-complexed nanogels. Molecules **23:** 3347

Ohnuki Y, Marnell MM, Babcock MS, Lechner JF, Kaighn ME (1980) Chromosomal analysis of human prostatic adenocarcinoma cell lines. Cancer Research **40:** 524-534

Outten CE, O'halloran TV (2001) Femtomolar sensitivity of metalloregulatory proteins controlling zinc homeostasis. Science **292:** 2488-2492

Oyama T, Takei H, Hikino T, Iino Y, Nakajima T (1996) Immunohistochemical expression of metallothionein in invasive breast cancer in relation to proliferative activity, histology and prognosis. Oncology **53:** 112-117

Ozsolak F, Milos PM (2011) RNA sequencing: advances, challenges and opportunities. Nature Reviews Genetics **12:** 87-98

Pan Y, Kytölä S, Farnebo F, Wang N, Lui WO, Nupponen N, Isola J, Visakorpi T, Bergerheim U, Larsson C (1999) Characterization of chromosomal abnormalities in prostate cancer cell lines by spectral karyotyping. Cytogenetic and Genome Research **87:** 225-232

Parker AL, Kavallaris M, McCarroll JA (2014) Microtubules and their role in cellular stress in cancer. Frontiers in Oncology **4:** 153

Patel DV, McGhee CN (2007) Contemporary in vivo confocal microscopy of the living human cornea using white light and laser scanning techniques: a major review. Clinical & Experimental Ophthalmology **35:** 71-88

Pechkova E, Zanotti G, Nicolini C (2003) Three-dimensional atomic structure of a catalytic subunit mutant of human protein kinase CK2. Acta Crystallographica**:** 2003 Dec;2059(Pt 2012):2133-2009

Permenter MG, Lewis JA, Jackson DA (2011) Exposure to nickel, chromium, or cadmium causes distinct changes in the gene expression patterns of a rat liver derived cell line. PLOS One **6:** e27730

Pinna LA (1990) Casein kinase 2: an 'eminence grise' in cellular regulation? Biochimica et Biophysica Acta **24:** 267-284

Pinna LA (1993) A historical view of protein kinase CK2. Cellular & Molecular Biology Research **40:** 383-390

Poonia T, Singh N, Garg M (2021) Contamination of Arsenic, Chromium and Fluoride in the Indian groundwater: a review, meta-analysis and cancer risk assessment. International Journal of Environmental Science and Technology**:** 1-12

Potter BM, Feng LS, Parasuram P, Matskevich VA, Wilson JA, Andrews GK, Laity JH (2005) The six zinc fingers of metal-responsive element binding transcription factor-1 form stable and quasi-ordered structures with relatively small differences in zinc affinities. Journal of Biological Chemistry **280:** 28529-28540

Prasad A, Beck F, Snell D, Kucuk O (2009) Zinc in Cancer Prevention. Nutrition & Cancer **61:** 879

Prasad A, Beck F, Snell D, Kucuk O (2009) Zinc in cancer prevention. Nutrition and cancer **61:** 879

Pulukuri SM, Gondi CS, Lakka SS, Jutla A, Estes N, Gujrati M, Rao JS (2005) RNA interference-directed knockdown of urokinase plasminogen activator and urokinase plasminogen activator receptor inhibits prostate cancer cell invasion, survival, and tumorigenicity in vivo. Journal of biological chemistry **280:** 36529-36540

Qin Y, Miranda JG, Stoddard CI, Dean KM, Galati DF, Palmer AE (2013) Direct comparison of a genetically encoded sensor and small molecule indicator: implications for quantification of cytosolic Zn2+. ACS Chemical Biology **8:** 2366-2371

Raghavan A, Ogilvie RL, Reilly C, Abelson ML, Raghavan S, Vasdewani J, Krathwohl M, Bohjanen PR (2002) Genome-wide analysis of mRNA decay in resting and activated primary human T lymphocytes. Nucleic acids research **30:** 5529-5538

Rahman MT, Karim MM (2018) Metallothionein: a potential link in the regulation of zinc in nutritional immunity. Biological trace element research **182:** 1-13

Raulin J (1869) Etudes chimiques sur la vegetation. Annales des Sciences Naturelles. Botanique et Biologie Vegetale **11:** 92-299

Reddy S, Barcenas C, Sinha A, Hsu L, Moulder S, Tripathy D, Hortobagyi G, Valero V (2018) Long-term survival outcomes of triple-receptor negative breast cancer survivors who are disease free at 5 years and relationship with low hormone receptor positivity. British Journal of Cancer **118:** 17-23

Rishi I, Baidouri H, Abbasi JA, Bullard-Dillard R, Pestaner JP, Skacel M, Tubbs R, Bagasra O (2003) Prostate cancer in African American men is associated with downregulation of zinc transporters. Applied Immunohistochemistry & Molecular Morphology **11:** 253-260

Rizk SL, Sky-Peck HH (1984) Comparison between concentrations of trace elements in normal and neoplastic human breast tissue. Cancer Research **44:** 5390-5394

Robinson MD, McCarthy DJ, Smyth GK (2010) edgeR: a Bioconductor package for differential expression analysis of digital gene expression data. Bioinformatics **26:** 139-140

Rondón-Lagos M, Di Cantogno LV, Marchiò C, Rangel N, Payan-Gomez C, Gugliotta P, Botta C, Bussolati G, Ramírez-Clavijo SR, Pasini B (2014) Differences and homologies of chromosomal alterations within and between breast cancer cell lines: a clustering analysis. Molecular cytogenetics **7:** 1-14

Roux PP, Topisirovic I (2012) Regulation of mRNA translation by signaling pathways. Cold Spring Harbor perspectives in biology **4:** a012252

Rutherford JC, Bird AJ (2004) Metal-responsive transcription factors that regulate iron, zinc, and copper homeostasis in eukaryotic cells. Eukaryotic Cell **3:** 1-13

Ryu M-S, Langkamp-Henken B, Chang S-M, Shankar MN, Cousins RJ (2011) Genomic analysis, cytokine expression, and microRNA profiling reveal biomarkers of human dietary zinc depletion and homeostasis. Proceedings of the National Academy of Sciences of the United States of America **108:** 20970-20975

Sakallı Çetin E, Nazıroğlu M, Çiğ B, Övey İS, Aslan Koşar P (2017) Selenium potentiates the anticancer effect of cisplatin against oxidative stress and calcium ion signaling-induced intracellular toxicity in MCF-7 breast cancer cells: involvement of the TRPV1 channel. Journal of Receptors and Signal Transduction **37:** 84-93

Saydam N, Adams TK, Steiner F, Schaffner W, Freedman JH (2002) Regulation of metallothionein transcription by the metal-responsive transcription factor MTF-1: identification of signal transduction cascades that control metal-inducible transcription. Journal of Biological Chemistry **277:** 20438-20445

Schmid K, Ellis I, Gee JM, Darke BM, Lees WE, Kay J, Cryer A, Stark J, Hittmair A, Öfner D (1993) Presence and possible significance of immunocytochemically demonstrable metallothionein over-expression in primary invasive ductal carcinoma of the breast. European Journal of Pathology **422:** 153-159

Schmittgen TD, Livak KJ (2008) Analyzing real-time PCR data by the comparative C T method. Nature Protocols **3:** 1101

Schmittgen TD, Livak KJ (2008) Analyzing real-time PCR data by the comparative C(T) method. Nat Protoc **3:** 1101-1108

Schnitzler A, Olsen B, Issinger O-G, Niefind K (2014) The protein kinase CK2Andante holoenzyme structure supports proposed models of autoregulation and trans-autophosphorylation. Journal of Molecular Biology

Schwochau GB, Nath KA, Rosenberg ME (1998) Clusterin protects against oxidative stress in vitro through aggregative and nonaggregative properties. Kidney international **53:** 1647-1653

Sekler I, Sensi SL, Hershfinkel M, Silverman WF (2007) Mechanism and regulation of cellular zinc transport. Molecular Medicine **13:** 337

Seldin DC, Landesman-Bollag E, Farago M, Currier N, Lou D, Dominguez I (2005) CK2 as a positive regulator of Wnt signalling and tumourigenesis. Molecular & Cellular Biochemistry **274:** 63-67

Seldin DC, Leder P (1995) Casein kinase II alpha transgene-induced murine lymphoma: relation to theileriosis in cattle. Science **267:** 894-897

Shen T, Li Y, Chen Z, Liang S, Guo Z, Wang P, Wu Q, Ba G, Fu Q (2017) CHOP negatively regulates Polo-like kinase 2 expression via recruiting C/EBPα to the upstream-promoter in human osteosarcoma cell line during ER stress. The International Journal of Biochemistry & Cell Biology **89:** 207-215

Sherwood ER, Berg LA, Mitchell NJ, McNeal JE, Kozlowski JM, Lee C (1990) Differential cytokeratin expression in normal, hyperplastic and malignant epithelial cells from human prostate. The Journal of Urology **143:** 167-171

Shirato A, Kikugawa T, Miura N, Tanji N, Takemori N, Higashiyama S, Yokoyama M (2014) Cisplatin resistance by induction of aldo-keto reductase family 1 member C2 in human bladder cancer cells. Oncology Letters **7:** 674-678

Shirazi FH, Zarghi A, Ashtarinezhad A, Kobarfard F, Nakhjavani M, Anjidani N, Zendehdel R, Arfaiee S, Shoeibi S, Mohebi S (2011) Remarks in successful cellular investigations for fighting breast cancer using novel synthetic compounds. INTECH Open Access Publisher Croatia

Si M, Lang J (2018) The roles of metallothioneins in carcinogenesis. Journal of Hematology & Oncology **11:** 107

Si M, Lang J (2018) The roles of metallothioneins in carcinogenesis. Journal of hematology & oncology **11:** 1-20

Sinduja P, Ramani P, Gheena S, Ramasubramanian A (2020) Expression of metallothionein in oral squamous cell carcinoma: A systematic review. Journal of Oral and Maxillofacial Pathology: JOMFP **24:** 143

Sohn E (2014) Contamination: The toxic side of rice. Nature **514:** S62-S63

Song Y, Ho E (2009) Zinc and prostatic cancer. Current Opinion in Clinical Nutrition & Metabolic Care **12:** 640-645

Soule H, Vazquez J, Long A, Albert S, Brennan M (1973) A human cell line from a pleural effusion derived from a breast carcinoma. Journal of the National Cancer Institute **51:** 1409-1416

Soule HD, Maloney TM, Wolman SR, Peterson WD, Brenz R, McGrath CM, Russo J, Pauley RJ, Jones RF, Brooks S (1990) Isolation and characterization of a spontaneously immortalized human breast epithelial cell line, MCF-10. Cancer Research **50:** 6075-6086

Stephens PJ, Tarpey PS, Davies H, Van Loo P, Greenman C, Wedge DC, Nik-Zainal S, Martin S, Varela I, Bignell GR (2012) The landscape of cancer genes and mutational processes in breast cancer. Nature **486:** 400-404

Stone K, Wheeler A (2015) A review of anatomy, physiology, and benign pathology of the nipple. Annals of Surgical Oncology **22:** 3236-3240

Stone KR, Mickey DD, Wunderli H, Mickey GH, Paulson DF (1978) Isolation of a human prostate carcinoma cell line (DU 145). International Journal of Cancer **21:** 274-281

Suhy DA, Simon KD, Linzer DI, O'Halloran TV (1999) Metallothionein is part of a zinc-scavenging mechanism for cell survival under conditions of extreme zinc deprivation. Journal of Biological Chemistry **274:** 9183-9192

Sun S, Gong F, Liu P, Miao Q (2018) Metformin combined with quercetin synergistically repressed prostate cancer cells via inhibition of VEGF/PI3K/Akt signaling pathway. Gene **664:** 50-57

Tai S, Sun Y, Squires JM, Zhang H, Oh WK, Liang CZ, Huang J (2011) PC3 is a cell line characteristic of prostatic small cell carcinoma. The Prostate **71:** 1668-1679

Tait L, Soule HD, Russo J (1990) Ultrastructural and immunocytochemical characterization of an immortalized human breast epithelial cell line, MCF-10. Cancer Research **50:** 6087-6094

Tang X, Han J, Wang Y, Ni L, Bao X, Wang L, Zhang W (2017) A multifunctional Schiff base as a fluorescence sensor for Fe3+ and Zn2+ ions, and a colorimetric sensor for Cu2+ and applications. Spectrochimica Acta Part A: Molecular and Biomolecular Spectroscopy **173:** 721-726

Taylor KM, Hiscox S, Nicholson RI, Hogstrand C, Kille P (2012) Protein Kinase CK2 Triggers Cytosolic Zinc Signaling Pathways by Phosphorylation of Zinc Channel ZIP7. Sci. Signal. **5:** ra11-

Taylor KM, Hiscox S, Nicholson RI, Hogstrand C, Kille P (2012) Protein kinase CK2 triggers cytosolic zinc signaling pathways by phosphorylation of zinc channel ZIP7. Science Signaling **5:** ra11-

Taylor KM, Hiscox S, Nicholson RI, Hogstrand C, Kille P (2012) Protein kinase CK2 triggers cytosolic zinc signaling pathways by phosphorylation of zinc channel ZIP7. Sci. Signal. **5:** ra11

Taylor KM, Morgan HE, Smart K, Zahari NM, Pumford S, Ellis IO, Robertson JFR, Nicholson RI (2007) The emerging role of the LIV-1 subfamily of zinc transporters in breast cancer. Molecular Medicine **13:** 396

Taylor KM, Muraina IA, Brethour D, Schmitt-Ulms G, Nimmanon T, Ziliotto S, Kille P, Hogstrand C (2016) Zinc transporter ZIP10 forms a heteromer with ZIP6 which regulates embryonic development and cell migration. Biochemical Journal **473:** 2531-2544

Taylor KM, Vichova P, Jordan N, Hiscox S, Hendley R, Nicholson RI (2008) ZIP7-mediated intracellular zinc transport contributes to aberrant growth factor signaling in antihormone-resistant breast cancer cells. Endocrinology **149:** 4912-4920

Thingholm T, Rönnstrand L, Rosenberg P (2020) Why and how to investigate the role of protein phosphorylation in ZIP and ZnT zinc transporter activity and regulation. Cellular & Molecular Life Sciences 1-18

Thirumoorthy N, Sunder AS, Kumar KM, Ganesh G, Chatterjee M (2011) A review of metallothionein isoforms and their role in pathophysiology. World Journal of Surgical Oncology **9:** 54

Torre LA, Bray F, Siegel RL, Ferlay J, Lortet-Tieulent J, Jemal A (2015) Global cancer statistics, 2012. CA: A Cancer Journal for Clinicians **65:** 87-108

Trembley JH, Wang G, Unger G, Slaton J, Ahmed K (2009) Protein kinase CK2 in health and disease: CK2: a key player in cancer biology. Cellular & Molecular Life Sciences **66:** 1858-1867

Tun NM, O'Doherty PJ, Chen Z-H, Wu X-Y, Bailey TD, Kersaitis C, Wu MJ (2014) Identification of aluminium transport-related genes via genome-wide phenotypic screening of Saccharomyces cerevisiae. Metallomics

Udono H, Srivastava PK (1993) Heat shock protein 70-associated peptides elicit specific cancer immunity. The Journal of Experimental Medicine **178:** 1391-1396

Urani C, Melchioretto P, Gribaldo L (2010) Regulation of metallothioneins and ZnT-1 transporter expression in human hepatoma cells HepG2 exposed to zinc and cadmium. Toxicology in Vitro **24:** 370-374

Urbano AM, Ferreira LMR, Alpoim MC (2012) Molecular and cellular mechanisms of hexavalent chromium-induced lung cancer: an updated perspective. Current Drug Metabolism **13:** 284-305

Vallee BL (1983) A role for zinc in gene expression. Journal of Inherited Metabolic Disease **6:** 31-33

Vallee BL, Auld DS (1990) Zinc coordination, function, and structure of zinc enzymes and other proteins. Biochemistry **29:** 5647-5659

Vallee BL, Auld DS (1993) Zinc: biological functions and coordination motifs. Accounts of Chemical Research **26:** 543-551

Van Dyke N, Yenugadhati N, Birkett NJ, Lindsay J, Turner MC, Willhite CC, Krewski D (2021) Association between aluminum in drinking water and incident Alzheimer's disease in the Canadian Study of Health and Aging cohort. Neurotoxicology **83:** 157-165

Vašák M, Meloni G (2011) Chemistry and biology of mammalian metallothioneins. Journal of Biological Inorganic Chemistry **16:** 1067

Vinkenborg JL, Nicolson TJ, Bellomo EA, Koay MS, Rutter GA, Merkx M (2009) Genetically encoded FRET sensors to monitor intracellular Zn 2+ homeostasis. Nature Methods **6:** 737-740

Wang L-X, Zhu X-M, Luo Y-N, Wu Y, Dong N, Tong Y-l, Yao Y-M (2020) Sestrin2 protects dendritic cells against endoplasmic reticulum stress-related apoptosis induced by high mobility group box-1 protein. Cell Death & Disease **11:** 1-17

Webber MM (1979) Normal and benign human prostatic epithelium in culture. In vitro **15:** 967-982

Webber MM, Trakul N, Thraves PS, Bello-DeOcampo D, Chu WW, Storto PD, Huard TK, Rhim JS, Williams DE (1999) A human prostatic stromal myofibroblast cell line WPMY-1: a model for stromal–epithelial interactions in prostatic neoplasia. Carcinogenesis **20:** 1185-1192

Werynska B, Pula B, Muszczynska-Bernhard B, Gomulkiewicz A, Piotrowska A, Prus R, Podhorska-Okolow M, Jankowska R, Dziegiel P (2013) Metallothionein 1F and 2A overexpression predicts poor outcome of non-small cell lung cancer patients. Experimental and Molecular Pathology **94:** 301-308

White J, Amos W, Fordham M (1987) An evaluation of confocal versus conventional imaging of biological structures by fluorescence light microscopy. The Journal of Cell Biology **105:** 41-48

Wilschefski SC, Baxter MR (2019) Inductively coupled plasma mass spectrometry: introduction to analytical aspects. The Clinical Biochemist Reviews **40:** 115

Wollert KC, Kempf T, Wallentin L (2017) Growth differentiation factor 15 as a biomarker in cardiovascular disease. Clinical chemistry **63:** 140-151

Wu LE, Levina A, Harris HH, Cai Z, Lai B, Vogt S, James DE, Lay PA (2016) Carcinogenic chromium(VI) compounds formed by intracellular oxidation of chromium(III) dietary supplements by adipocytes. Angewandte Chemie International Edition **55:** 1742-1745

Wu S, Powers S, Zhu W, Hannun YA (2016) Substantial contribution of extrinsic risk factors to cancer development. Nature **529:** 43-47

Yamane K, Kinsella TJ (2005) CK2 Inhibits Apoptosis and Changes Its Cellular Localization Following Ionizing Radiation. Cancer Research **65:** 4362-4367

Yamasaki S, Sakata-Sogawa K, Hasegawa A, Suzuki T, Kabu K, Sato E, Kurosaki T, Yamashita S, Tokunaga M, Nishida K (2007) Zinc is a novel intracellular second messenger. The Journal of Cell Biology **177:** 637-645

Yamasaki S, Sakata-Sogawa K, Hasegawa A, Suzuki T, Kabu K, Sato E, Kurosaki T, Yamashita S, Tokunaga M, Nishida K, Hirano T (2007) Zinc is a novel intracellular second messenger. The Journal of Cell Biology **177:** 637-645

Yoon D-S, Wersto RP, Zhou W, Chrest FJ, Garrett ES, Kwon TK, Gabrielson E (2002) Variable levels of chromosomal instability and mitotic spindle checkpoint defects in breast cancer. The American Journal of Pathology **161:** 391-397

Zaman MS, Johnson AJ, Bobek G, Kueh S, Kersaitis C, Bailey TD, Buskila Y, Wu MJ (2016) Protein kinase CK2 regulates metal toxicity in neuronal cells. Metallomics **8:** 82-90

Zaman MS, Johnson AJ, Petersingham G, Muench GW, Dong Q, Wu MJ (2019) Protein kinase CK2 is involved in zinc homeostasis in breast and prostate cancer cells. BioMetals **32:** 861-873

Zatta P, Drago D, Bolognin S, Sensi SL (2009) Alzheimer's disease, metal ions and metal homeostatic therapy. Trends in Pharmacological Sciences **2009 Jul;30(7):346-55. doi:** 10.1016/j.tips.2009.1005.1002

Zeng X, Du Z, Sheng Z, Jiang W (2019) Characterization of the interactions between banana condensed tannins and biologically important metal ions (Cu2+, Zn2+ and Fe2+). Food Research International **123:** 518-528

Zhu Y, Liu Y, Zhang C, Chu J, Wu Y, Li Y, Liu J, Li Q, Li S, Shi Q (2018) Tamoxifen-resistant breast cancer cells are resistant to DNA-damaging chemotherapy because of upregulated BARD1 and BRCA1. Nature communications **9:** 1-11

Zou J, Milon BC, Desouki MM, Costello LC, Franklin RB (2011) hZIP1 zinc transporter down-regulation in prostate cancer involves the overexpression of ras responsive element binding protein-1 (RREB-1). The Prostate **71:** 1518-1524

Zwicker F, Ebert M, Huber PE, Debus J, Weber K-J (2011) A specific inhibitor of protein kinase CK2 delays gamma-H2Ax foci removal and reduces clonogenic survival of irradiated mammalian cells. Radiation Oncology **6:** 15

8 APPENDICES

8.1 Up-regulated genes at T_{30} zinc treatment

Up-regulated genes	Protein name	Entrez	Log_2FC	Log CPM	*p-value*
MT1B	Metallothionein-1B	4490	5.484	-0.102	1.3E-06
MT1X	Metallothionein-1X	4501	4.930	8.448	0
SLC30A1	Zinc transporter 1	7779	4.250	8.997	0
EGR2	Early growth response protein 2	1959	3.854	0.037	8.11E-52
MT1F	Metallothionein-1F	4494	3.288	7.202	0
RGS16	Glycerophosphodiester phosphodiesterase 1	6004	2.996	5.252	1.2E-271
RASD1	Dexamethasone-induced Ras-related protein 1	51655	2.827	2.275	5.94E-61
CTGF	Connective tissue growth factor	1490	2.554	0.657	1.11E-30
EGR1	Early growth response protein 1	1958	2.100	5.174	7.21E-36
NR4A3	Nuclear receptor subfamily 4 group A member 3	8013	2.090	0.506	1.35E-24
TRIB1	Tribbles homolog 1	10221	1.798	6.625	2.6E-244
NR4A1	Nuclear receptor subfamily 4 group A member 1	3164	1.770	4.365	4.11E-84
NGFR	Tumour necrosis factor receptor superfamily member 16	4804	1.661	2.122	1.54E-27
HES1	Transcription factor HES-1	3280	1.645	6.317	0
RNF165	E3 ubiquitin-protein ligase RNF165	4944	1.567	3.637	7.97E-27
HIST1H4D	Histone H4	8360	1.543	0.485	3.18E-12
HIST1H1D	Histone H1.3	3007	1.504	2.303	1.43E-51
HIST1H2AD	Histone H2A type 1-D	3013	1.459	2.762	2.14E-34
MT2A	Metallothionein-2	4502	1.456	9.290	2.92E-160
GBP1	Guanylate-binding protein 1	2633	1.366	-0.021	1.17E-07
CHST3	Carbohydrate sulfotransferase 3	9469	1.337	-0.440	1.52E-05
DUSP6	Dual specificity protein phosphatase 6	1848	1.284	2.289	4.05E-14
SNAI1	Zinc finger protein SNAI1	6615	1.277	1.486	1.6E-17
HIST4H4	Histone H4	1215	1.249	2.726	8.67E-56
SPRY4	Protein sprouty homolog 4	8184	1.218	1.785	1.69E-16
DUSP1	Dual specificity protein phosphatase 1	1843	1.217	5.219	1.3E-159
HIST1H2BF	Histone H2B type 1-C/E/F/G/I	8343	1.169	2.290	3.78E-23
DUSP10	Dual specificity protein phosphatase 10	1122	1.155	3.107	1.31E-41
MAFF	Transcription factor MafF	2376	1.148	2.933	1.48E-26
FOSB	Protein fosB	2354	1.136	0.193	8.21E-09
ZNF442	Zinc finger protein 442	7997	1.128	3.360	7.11E-39
ID1	DNA-binding protein inhibitor ID-1	3397	1.118	3.244	3.39E-57
MYC	Myc proto-oncogene protein	4609	1.091	7.799	1.5E-127
EGR3	Early growth response protein 3	1960	1.036	6.095	3.61E-74
HIST2H2BF	Histone H2B type 2-F	4406	1.032	5.463	1.14E-89
ARRDC3	Arrestin domain-containing protein 3	5756	1.030	7.806	1.8E-145
DLL4	Delta-like protein 4	5456	1.017	0.564	5.59E-08
DUSP4	Dual specificity protein phosphatase 4	1846	1.009	4.231	3.86E-43
HIST1H3B	Histone H3.1	8358	0.995	0.909	2.02E-08
JUN	Transcription factor AP-1	3725	0.990	7.381	2.5E-110
HIST1H2BG	Histone H2B type 1-C/E/F/G/I	8339	0.983	4.507	1.46E-64
CSRP1	Cysteine and glycine-rich protein 1	1465	0.971	8.698	4.2E-171
EPPK1	Epiplakin	8348	0.940	6.460	2.28E-62
ATOH8	Protein atonal homolog 8	8491	0.916	1.019	1.13E-07

ZNF365	Protein ZNF365	2289	0.914	0.316	4.45E-05
VMP1	Vacuole membrane protein 1	8167	0.908	9.771	1.75E-76
ID2	DNA-binding protein inhibitor ID-2	3398	0.889	6.473	6.55E-72
SLC2A4	SLC2A4 regulator	6517	0.879	0.527	2.58E-05
HIST1H2BL	Histone H2B type 1-L	8340	0.871	0.500	8.73E-07
HIST1H4E	Histone H4	8367	0.870	1.347	6.38E-09
MCL1	Induced myeloid leukemia cell differentiation protein Mcl-1	4170	0.870	9.618	4.3E-153
GEM	GTP-binding protein GEM	2669	0.868	2.586	3.26E-21
ZFP36	mRNA decay activator protein ZFP36	7538	0.863	6.389	1.24E-22
CALML5	Calmodulin-like protein 5	5180	0.846	2.440	5.29E-10
ATF3	Cyclic AMP-dependent transcription factor ATF-3	4670	0.837	4.588	2.38E-51
HIST1H3J	Histone H3.1	8356	0.820	1.557	1.14E-12
GADD45B	Growth arrest and DNA damage-inducible protein GADD45 beta	4616	0.809	6.746	7.1E-111
EDN1	Endothelin-1	1906	0.791	2.664	1.9E-11
ZNF750	Zinc finger protein 750	7975	0.790	2.701	5.72E-24
IER5L	Immediate early response gene 5-like protein	3897	0.785	5.900	2.93E-79
HIST1H2AK	Histone H2A type 1	8330	0.785	1.570	8.81E-12
IER3	Radiation-inducible immediate-early gene IEX-1	8870	0.778	4.819	4.75E-37
DUSP5	Dual specificity protein phosphatase 5	1847	0.772	4.968	9.33E-47
MAP3K8	Mitogen-activated protein kinase kinase kinase 8	1326	0.769	3.157	1.54E-15
ID3	DNA-binding protein inhibitor ID-3	3399	0.756	5.241	7.01E-47
RND1	Rho-related GTP-binding protein Rho6	2728	0.755	1.990	2.49E-07
C1GALT1C1L	C1GALT1-specific chaperone 1-like protein	7288	0.744	0.214	7.79E-05
PLK3	Serine/threonine-protein kinase PLK3	1263	0.743	2.691	5.54E-18
RAB3A	Ras-related protein Rab-3A	5864	0.735	1.938	6.69E-07
ELF3	ETS-related transcription factor Elf-3	1999	0.734	5.449	1.42E-55
PCDH8	Protocadherin-8	5100	0.731	-0.021	0.003
PRICKLE2	Prickle-like protein 2	1663	0.728	5.253	1.06E-53
NEDD9	Enhancer of filamentation 1	4739	0.721	4.794	5.84E-63
ITPRIP	Inositol 1,4,5-trisphosphate receptor-interacting protein	8545	0.721	3.584	5.76E-23
CLDN23	Claudin-23	1370	0.708	2.751	3.28E-18
ZNF547	Zinc finger protein 547	2843	0.704	-0.168	0.003
HMOX1	Heme oxygenase 1	3162	0.701	5.512	1.13E-08
HIST1H2BD	Histone H2B type 1-D	3017	0.699	5.177	8E-44
HIST1H2AG	Histone H2A type 1	8969	0.699	5.001	4.26E-24
CEBPD	CCAAT/enhancer-binding protein delta	1052	0.693	3.278	3.29E-17
HIST1H2BN	Histone H2B type 1-N	8341	0.677	3.536	2.53E-23
ZNF563	Zinc finger protein 563	1478	0.676	2.482	2.54E-14
TLR2	Toll-like receptor 2	7097	0.676	1.146	6.57E-05
GADD45G	Growth arrest and DNA damage-inducible protein GADD45 gamma	1091	0.674	3.317	3.24E-19
ZNF256	Zinc finger protein 256	1017	0.671	3.106	1.35E-23
NET1	Neuroepithelial cell-transforming gene 1 protein	1027	0.670	9.251	8.1E-54
EPHA2	Ephrin type-A receptor 2	1969	0.658	4.090	5.47E-39
OR2B6	Olfactory receptor 2B6	2621	0.657	1.590	2.98E-08
VPS37D	Vacuolar protein sorting-associated protein 37D	1553	0.653	0.799	7.15E-06

ZBTB2	Zinc finger and BTB domain-containing protein 2	5762	0.650	6.622	2.14E-63
HIST1H3G	Histone H3.1	8355	0.648	3.257	2.36E-11
HAP1	Huntingtin-associated protein 1	9001	0.642	-0.005	0.002
SOCS2	Suppressor of cytokine signaling 2	8835	0.641	2.376	1.64E-05
C3orf80	Uncharacterised membrane protein C3orf80	4010	0.638	0.371	0.005
PXDC1	Plexin domain-containing protein 1	2217	0.635	0.076	0.005
ZNF296	Zinc finger protein 296	1629	0.633	2.188	1.08E-05
FAM43A	Protein FAM43A	1315	0.630	3.743	1.86E-17
C2orf54	Uncharacterised protein C2orf54	7991	0.629	0.404	0.002
VASN	Vasorin	1149	0.627	5.140	3.01E-31
SGK1	Serine/threonine-protein kinase Sgk1	6446	0.627	1.195	4.01E-06
HIST1H3H	Histone H3.1	8357	0.624	6.134	5.1E-35
KLF6	Krueppel-like factor 6	1316	0.622	6.141	1.16E-55
HIST3H2BB	Histone H2B type 3-B	1283	0.614	2.184	5.06E-11
CBX4	E3 SUMO-protein ligase CBX4	8535	0.607	7.026	1.84E-53
ARC	Activity-regulated cytoskeleton-associated protein	2323	0.607	3.280	7.56E-09
GPRC5A	Retinoic acid-induced protein 3	9052	0.606	6.341	2.14E-46
HIST1H2AI	Histone H2A type 1	8329	0.600	4.013	1.12E-17

8.2 Down-regulated genes in T_{30} zinc treatment

Down-regulated genes	Protein name	Entrez	Log_2FC	Log CPM	*p-value*
CCDC17	Coiled-coil domain-containing protein 17	1494	-0.774	0.584	2.11E-07
FBXO48	S-phase kinase-associated protein 1	5542	-0.741	0.842	1.04E-07
HERC2P3	Putative HERC2-like protein 3	2837	-0.660	0.049	0.001
NFKBIZ	NF-kappa-B inhibitor zeta	6433	-0.604	3.680	1.79E-18
PLK2	Serine/threonine-protein kinase PLK2	1076	-0.683	6.380	1.83E-93
PPP1R3C	Protein phosphatase 1 regulatory subunit 3C	5507	-0.622	4.773	1.12E-29
SNX15	Sorting nexin-15	2990	-0.640	-0.002	0.009

8.3 Up-regulated genes at T_{120} zinc treatment

Up-regulated genes	Protein name	Entrez	Log_2FC	Log CPM	*p-value*
MT1B	Metallothionein-1B	4490	9.764	-0.102	7.30E-82
HSPA6	Heat shock 70 kDa protein 6	3310	8.151	3.536	1.59E-123
MT1X	Metallothionein-1X	4501	6.261	8.448	0
MT1F	Metallothionein-1F	4494	5.792	7.202	0
SLC30A1	Zinc transporter 1	7779	5.036	8.997	0
CHRM4	Muscarinic acetylcholine receptor M4	1132	4.997	-0.914	1.28E-35
RNF165	E3 ubiquitin-protein ligase RNF165	4944	4.985	3.637	0
HMOX1	Heme oxygenase 1	3162	4.641	5.512	2.41E-308
MT4	Matrix metalloproteinase-17	8456	4.547	-0.944	1.27E-29
RGS16	Regulator of G-protein signaling 16	6004	3.818	5.252	0
SLCO4A1	Solute carrier organic anion transporter family member 4A1	2823	3.622	6.131	0
EGR1	Early growth response protein 1	1958	3.374	5.174	2.48E-83
NGFR	Tumour necrosis factor receptor superfamily member 16	4804	3.283	2.122	3.74E-146
CNKSR3	Connector enhancer of kinase suppressor of ras 3	1540	3.180	2.528	3.82E-177
KBTBD11	Kelch repeat and BTB domain-containing protein 11	9920	3.141	1.969	2.39E-154
HSPA1A	Heat shock 70 kDa protein 1A	3303	3.093	7.487	2.53E-150
HSPA1B	Heat shock 70 kDa protein 1B	3304	3.047	6.522	5.99E-139
RASD1	Dexamethasone-induced Ras-related protein 1	5165	2.947	2.275	6.00E-66
SLC2A14	Solute carrier family 2, facilitated glucose transporter member 14	1441	2.944	0.268	7.79E-47
CLCF1	Cardiotrophin-like cytokine factor 1	2352	2.822	0.990	4.33E-48
EGR2	Early growth response protein 2	1959	2.805	0.037	5.36E-19
MT2A	Metallothionein-2	4502	2.585	9.290	0
CHST3	Carbohydrate sulfotransferase 3	9469	2.490	-0.440	4.99E-21
C17orf67	Uncharacterised protein C17orf67	3392	2.462	2.177	1.66E-77
RAB3A	Ras-related protein Rab-3A	5864	2.384	1.938	1.13E-81
NOTCH1	Neurogenic locus notch homolog protein 1	4851	2.354	6.307	0
DNAJB1	DnaJ homolog subfamily B member 1	3337	2.345	7.280	2.13E-113
TRIB1	Tribbles homolog 1	1022	2.340	6.625	0
SOCS2	Suppressor of cytokine signaling 2	8835	2.338	2.376	6.41E-68
HSPH1	Heat shock protein 105 kDa	1080	2.299	8.864	1.03E-131
CBARP	Voltage-dependent calcium channel beta subunit-associated regulatory protein	2550	2.286	-0.028	1.31E-19
CSRP2	Cysteine-rich protein 2-binding protein	1466	2.246	0.514	4.62E-19
ZNF365	Protein ZNF365	2289	2.236	0.316	2.44E-34
NPL	Nuclear protein localisation protein 4 homolog	8089	2.170	2.584	3.26E-110
MAP3K8	Mitogen-activated protein kinase kinase kinase 8	1326	2.039	3.157	3.14E-122
DUSP6	Dual specificity protein phosphatase 6	1848	2.030	2.289	4.37E-34
ZBTB2	Zinc finger and BTB domain-containing protein 2	5762	2.025	6.622	0
SPACA6	Sperm acrosome membrane-associated protein 6	1476	2.004	3.419	1.39E-154

SLC2A4	Solute carrier family 2, facilitated glucose transporter member 4	6517	1.987	0.527	8.77E-28
LRFN4	Leucine-rich repeat and fibronectin type-III domain-containing protein 4	7899	1.987	5.449	3.52E-229
DDIT4	DNA damage-inducible transcript 4 protein	5454	1.972	7.635	0
ZFP36	mRNA decay activator protein ZFP36	7538	1.966	6.389	7.37E-107
DUSP10	Dual specificity protein phosphatase 10	1122	1.952	3.107	1.41E-136
CREB5	Cyclic AMP-responsive element-binding protein 5	9586	1.947	1.760	1.01E-65
C2orf54	Uncharacterised protein C2orf54	7991	1.947	0.404	2.23E-30
POLH	DNA polymerase eta	5429	1.904	5.254	2.39E-305
CSRP1	Cysteine and glycine-rich protein 1	1465	1.898	8.693	0
C3orf80	Uncharacterised membrane protein C3orf80	4010	1.880	0.371	5.36E-21
SERPINE1	Plasminogen activator inhibitor 1	5054	1.862	2.216	1.43E-96
MCL1	Induced myeloid leukemia cell differentiation protein Mcl-1	4170	1.857	9.618	0
NR4A3	Nuclear receptor subfamily 4 group A member 3	8013	1.750	0.506	9.53E-16
PKDCC	Extracellular tyrosine-protein kinase PKDCC	9146	1.723	0.527	2.28E-23
SPRY4	Protein sprouty homolog 4	8184	1.711	1.785	7.13E-33
CALML5	Calmodulin-like protein 5	5180	1.711	2.440	3.12E-39
DNAJB5	DnaJ homolog subfamily B member 5	2582	1.708	1.870	5.57E-28
NUDT16L1	Tudor-interacting repair regulator protein	8430	1.680	5.381	0.00E+00
SERPINH1	Serpin H1	8710	1.678	6.999	4.78E-80
SNAI1	Zinc finger protein SNAI1	6615	1.655	1.486	9.37E-30
CEBPD	CCAAT/enhancer-binding protein delta	1052	1.614	3.278	4.45E-102
GBP1	Guanylate-binding protein 1	2633	1.596	-0.021	4.28E-10
AKR1C2	Aldo-keto reductase family 1 member C2	1646	1.584	-0.127	1.51E-12
DEDD2	DNA-binding death effector domain-containing protein 2	1629	1.564	4.882	9.95E-89
SKIL	Ski-like protein	6498	1.529	7.177	0
OSGIN1	Oxidative stress-induced growth inhibitor 1	2994	1.526	5.578	2.04E-149
NET1	Neuroepithelial cell-transforming gene 1 protein	1027	1.516	9.251	4.97E-261
FAM196A	Protein FAM196A	6429	1.503	-0.222	7.13E-11
FAM189A2	Protein FAM189A2	9413	1.497	3.457	9.36E-116
SEMA3F	Semaphorin-3F	6405	1.479	7.629	0
INSIG1	Insulin-induced gene 1 protein	3638	1.478	7.645	1.40E-108
RND1	Rho-related GTP-binding protein Rho6	2728	1.468	1.990	1.61E-25
JUN	Transcription factor AP-1	3725	1.464	7.381	8.44E-238
WNT6	Protein Wnt-6	7475	1.442	-0.118	2.38E-11
BDKRB2	B2 bradykinin receptor	6241	1.440	2.170	3.56E-43
MAFF	Transcription factor MafF	2376	1.440	2.933	1.96E-41
SH2D5	SH2 domain-containing protein 5	4007	1.433	-0.419	2.31E-09
KLHL23	Kelch-like protein 23	1512	1.433	3.671	7.38E-101
SLC16A6	Monocarboxylate transporter 7	9120	1.420	6.217	1.91E-302
SEMA7A	Semaphorin-7A	8482	1.412	1.022	1.83E-18
WNT9A	Protein Wnt-9a	7483	1.412	2.897	7.36E-74
DUSP1	Dual specificity protein phosphatase 1	1843	1.411	5.219	7.10E-215
HIST1H2AD	Histone H2A type 1-D	3013	1.398	2.762	6.90E-31

ITGB8	Integrin beta-8	3696	1.395	1.448	2.44E-28
DNAJB4	DnaJ homolog subfamily B member 4	1108	1.382	2.637	6.33E-41
LPAR2	Lysophosphatidic acid receptor 2	9170	1.380	4.318	4.99E-126
ARC	Activity-regulated cytoskeleton-associated protein	2323	1.377	3.280	1.11E-41
DNAJA4	DnaJ homolog subfamily A member 4	5546	1.349	5.231	5.64E-55
ENTPD8	Ectonucleoside triphosphate diphosphohydrolase 8	3778	1.344	2.314	1.69E-36
ATOH8	Protein atonal homolog 8	8491	1.342	1.019	1.11E-15
FJX1	Four-jointed box protein 1	2414	1.335	1.242	8.81E-27
PLEKHO2	Pleckstrin homology domain-containing family O member 2	8030	1.334	1.792	2.09E-24
GPANK1	G patch domain and ankyrin repeat-containing protein 1	7918	1.325	4.463	5.22E-90
CSF1	Macrophage colony-stimulating factor 1 receptor	1435	1.324	0.484	1.60E-12
KCNF1	Potassium voltage-gated channel subfamily F member 1	3754	1.308	0.605	1.80E-13
HSPE1	10 kDa heat shock protein, mitochondrial	3336	1.290	4.304	1.48E-32
NAB2	NGFI-A-binding protein 2	4665	1.283	7.365	9.54E-270
EPPK1	Epiplakin	8348	1.282	6.460	3.71E-114
TMEM37	Voltage-dependent calcium channel gamma-like subunit	1407	1.281	0.13	4.29E-08
FOSL2	Fos-related antigen 2	2355	1.280	8.011	0
DNAJA1	DnaJ homolog subfamily A member 1	3301	1.273	7.679	1.08E-70
KCNN4	Intermediate conductance calcium-activated potassium channel protein 4	3783	1.273	0.537	1.38E-13
HSP90AA1	Heat shock protein HSP 90-alpha	3320	1.252	10.636	1.14E-46
SOX12	Protein SOX-15	6666	1.250	6.113	1.38E-255
HIST1H4D	Histone H4	8360	1.244	0.485	7.46E-08
CHORDC1	Cysteine and histidine-rich domain-containing protein 1	2697	1.244	4.918	5.82E-46
PTHLH	Parathyroid hormone-related protein	5744	1.243	0.675	1.11E-12
ODC1	Ornithine decarboxylase	4953	1.229	6.584	2.03E-304
RNF125	E3 ubiquitin-protein ligase RNF125	5494	1.227	2.423	4.57E-47
ARVCF	Armadillo repeat protein deleted in velo-cardio-facial syndrome	4212	1.225	4.757	4.55E-91
IL15RA	Interleukin-15 receptor subunit alpha	3601	1.222	2.189	2.96E-34
PHLDA2	Pleckstrin homology-like domain family A member 2	7262	1.221	4.284	6.50E-38
MACC1	Metastasis-associated in colon cancer protein 1	3463	1.213	4.241	3.50E-122
SERTAD4	Putative uncharacterised protein SERTAD4-AS1	5625	1.213	6.365	1.82E-247
VEGFA	Vascular endothelial growth factor A	7422	1.204	8.346	1.31E-179
ZNF442	Zinc finger protein 442	7997	1.202	3.360	2.28E-43
EDN1	Endothelin-1	1906	1.202	2.664	4.02E-25
FAM212B	PAK4-inhibitor INKA2	5592	1.201	3.922	3.36E-92
HBEGF	Proheparin-binding EGF-like growth factor	1839	1.197	-0.092	3.39E-09
RIMS3	Regulating synaptic membrane exocytosis protein 3	9783	1.192	3.948	1.57E-59
MGAT5B	Alpha-1,6-mannosylglycoprotein 6-beta-N-acetylglucosaminyltransferase B	1466	1.190	2.172	6.23E-29

SCNN1G	Amiloride-sensitive sodium channel subunit gamma	6340	1.182	0.475	2.45E-13
POLR3G	DNA-directed RNA polymerase III subunit RPC7	1062	1.179	2.701	1.59E-45
SGMS2	Phosphatidylcholine:ceramide cholinephosphotransferase 2	1669	1.178	2.724	4.02E-51
CCNE1	G1/S-specific cyclin-E1	8981	1.177	1.758	2.09E-12
BAG2	BAG family molecular chaperone regulator 2	9532	1.172	2.239	6.81E-25
HAP1	Huntingtin-associated protein 1	9001	1.168	-0.051	5.56E-09
ATF3	Cyclic AMP-dependent transcription factor ATF-3	4673	1.160	4.588	2.57E-99
JMJD6	Bifunctional arginine demethylase and lysyl-hydroxylase JMJD6	2321	1.149	3.842	3.65E-45
TPST1	Protein-tyrosine sulfotransferase 1	8460	1.148	1.743	3.63E-18
ENC1	Ectoderm-neural cortex protein 1	8507	1.145	4.854	7.19E-137
DDIT3	DNA damage-inducible transcript 3 protein	1649	1.144	6.451	1.05E-101
DUSP5	Dual specificity protein phosphatase 5	1847	1.123	4.968	6.78E-99
TRIM16L	Tripartite motif-containing protein 16-like protein	1471	1.117	1.906	4.88E-14
LIF	Leukemia inhibitory factor receptor	3976	1.115	0.329	2.06E-06
SPSB2	SPRY domain-containing SOCS box protein 2	8472	1.110	3.232	3.67E-50
GFOD1	Glucose-fructose oxidoreductase domain-containing protein 1	5443	1.106	3.696	1.01E-61
C11orf95	Uncharacterised protein C11orf95	6599	1.106	3.047	4.14E-60
ZNF547	Zinc finger protein 547	2843	1.102	-0.161	2.86E-06
SH2B3	SH2B adapter protein 3	1001	1.100	0.475	7.76E-08
FERMT1	Fermitin family homolog 1	5561	1.098	1.636	3.46E-18
NRARP	Notch-regulated ankyrin repeat-containing protein	4414	1.098	3.872	9.55E-42
RIPOR3	RIPOR family member 3	1408	1.092	4.368	5.69E-71
NREP	Neuronal regeneration-related protein	9315	1.081	3.674	3.23E-58
ZNF296	Zinc finger protein 296	1629	1.081	2.188	2.15E-14
NAT8L	N-acetylaspartate synthetase	3399	1.078	2.276	3.76E-33
SLC5A3	Sodium/myo-inositol cotransporter	6526	1.076	5.238	1.69E-48
PLK3	Serine/threonine-protein kinase PLK3	1263	1.076	2.691	1.20E-37
HIST1H2BF	Histone H2B type 1-C/E/F/G/I	8343	1.072	2.290	6.96E-19
DUSP8	Dual specificity protein phosphatase 8	1850	1.068	5.033	5.21E-95
HSPA8	Heat shock cognate 71 kDa protein	3312	1.066	10.860	5.21E-50
PDE4A	cAMP-specific 3',5'-cyclic phosphodiesterase 4A	5141	1.059	-0.366	2.10E-06
FAM167A	Protein FAM167A	8364	1.059	3.834	5.64E-41
KREMEN2	Kremen protein 2	7941	1.058	0.263	2.64E-06
SNX32	Sorting nexin-32	2541	1.054	0.129	0.003
FAM46A	Terminal nucleotidyltransferase 5A	5560	1.052	5.662	2.79E-46
PAIP2B	Polyadenylate-binding protein-interacting protein 2B	4009	1.048	4.383	7.74E-89
MAP1A	Microtubule-associated protein 1A	4130	1.045	0.929	6.11E-11
OVOL1	Putative transcription factor Ovo-like 1	5017	1.044	5.792	6.95E-127
IER5	Immediate early response gene 5 protein	5127	1.044	5.961	2.63E-48
CHAC1	Glutathione-specific gamma-glutamylcyclotransferase 1	7909	1.041	4.662	2.70E-87
GLI1	Zinc finger protein GLI1	2735	1.040	-0.062	1.29E-06
DLX3	Homeobox protein DLX-3	1747	1.039	2.038	1.85E-28

MXD1	Max dimerization protein 1	4084	1.037	5.276	1.55E-63
HIST1H4E	Histone H4	8367	1.033	1.347	5.31E-12
TRIM16	Tripartite motif-containing protein 16	1062	1.033	3.289	3.58E-26
ZNF460	Zinc finger protein 460	1079	1.026	2.418	2.04E-18
ERF	Eukaryotic peptide chain release factor GTP-binding subunit ERF3A	2077	1.021	6.673	2.05E-150
FKBP4	Peptidyl-prolyl cis-trans isomerase FKBP4	2288	1.020	9.819	1.11E-105
AKR7A3	Aflatoxin B1 aldehyde reductase member 3	2297	1.019	0.010	9.03E-07
LFNG	Beta-1,3-N-acetylglucosaminyltransferase lunatic fringe	3955	1.018	5.458	2.45E-120
MAFK	Transcription factor MafK	7975	1.017	5.521	2.33E-135
DUSP15	Dual specificity protein phosphatase 15	1288	1.007	0.096	3.00E-07
PCDH8	Protocadherin-8	5100	1.006	-0.021	6.40E-07
UBC	SUMO-conjugating enzyme UBC9	7316	1.005	10.351	4.06E-103
MB21D1	Cyclic GMP-AMP synthase	1150	1.005	3.032	1.41E-29
DGKE	Diacylglycerol kinase epsilon	8526	0.992	5.942	2.33E-80
HIST2H2BF	Histone H2B type 2-F	4406	0.987	5.463	1.87E-80
DOK7	Protein Dok-7	2854	0.986	6.482	4.81E-156
TLR2	Toll-like receptor 2	7097	0.983	1.146	3.83E-09
MYEOV	COP9 signalosome complex subunit 9	2657	0.981	0.712	2.96E-09
GCAT	2-amino-3-ketobutyrate coenzyme A ligase, mitochondrial	2346	0.973	3.090	3.13E-29
CYR61	Protein CYR61	3491	0.971	3.943	4.17E-36
VMP1	Vacuole membrane protein 1	8167	0.970	9.771	8.69E-87
TFEB	Transcription factor EB	7942	0.966	1.015	9.45E-10
RELT	Tumour necrosis factor receptor superfamily member 19L	8495	0.962	2.879	3.52E-18
SERTAD1	SERTA domain-containing protein 1	2995	0.959	4.028	1.87E-76
ELK3	ETS domain-containing protein Elk-3	2004	0.959	4.476	1.62E-55
ZNF483	Zinc finger protein 483	1583	0.954	0.832	4.88E-10
MAFG	Transcription factor MafG	4097	0.951	5.086	3.68E-114
SELENOW	Selenoprotein N	6415	0.951	6.430	2.33E-85
DPF1	Zinc finger protein neuro-d4	8193	0.950	-0.001	1.94E-06
HSPA1L	Heat shock 70 kDa protein 1-like	3305	0.947	0.892	4.04E-12
ZNF408	Zinc finger protein 408	7979	0.945	4.700	5.34E-61
KCTD12	BTB/POZ domain-containing protein KCTD12	1152	0.940	1.334	8.58E-15
ERRFI1	ERBB receptor feedback inhibitor 1	5420	0.936	4.831	1.75E-58
SH2B2	SH2B adapter protein 2	1060	0.934	0.180	9.39E-08
PFKFB3	6-phosphofructo-2-kinase/fructose-2,6-bisphosphatase 3	5209	0.932	5.910	6.78E-89
SMTNL2	Smoothelin-like protein 2	3425	0.931	1.507	2.24E-12
LRP8	Low-density lipoprotein receptor-related protein 8	7804	0.926	4.209	3.19E-08
NOL4L	Nucleolar protein 4-like	1406	0.925	4.139	1.38E-41
ITPRIP	Inositol 1,4,5-trisphosphate receptor-interacting protein	8545	0.924	3.584	5.94E-37
ETS2	Protein C-ets-2	2114	0.924	5.313	6.58E-87
DLL4	Delta-like protein 4	5456	0.918	0.564	2.08E-06
ZNF682	Zinc finger protein 682	9112	0.914	3.315	1.07E-24
SLC38A3	Sodium-coupled neutral amino acid transporter 3	1099	0.907	-0.097	2.37E-05
ZNF324	Zinc finger protein 324A	2579	0.907	3.463	5.98E-41

KCNQ4	Potassium voltage-gated channel subfamily KQT member 4	9132	0.906	0.685	1.66E-07
HCN4	Potassium/sodium hyperpolarisation-activated cyclic nucleotide-gated channel 4	1002	0.903	0.850	1.07E-08
HRK	Activator of apoptosis harakiri	8739	0.903	3.470	9.43E-37
TRIM47	Tripartite motif-containing protein 47	9110	0.898	0.868	1.09E-07
RHOBTB1	Rho-related BTB domain-containing protein 1	9886	0.898	3.709	6.17E-37
TP53RK	EKC/KEOPS complex subunit TP53RK	1128	0.897	5.486	5.53E-79
ZBTB21	Zinc finger and BTB domain-containing protein 21	4985	0.897	5.719	7.26E-123
LDLR	Sortilin-related receptor	3949	0.897	7.009	4.04E-50
SYNGR3	Synaptogyrin-3	9143	0.894	2.323	2.32E-16
PITPNM2	Membrane-associated phosphatidylinositol transfer protein 2	5760	0.892	5.176	6.96E-95
CRYBG2	Beta/gamma crystallin domain-containing protein 2	5505	0.891	0.534	1.52E-08
ARID3A	AT-rich interactive domain-containing protein 3A	1820	0.888	4.642	1.40E-75
FGFR3	Fibroblast growth factor receptor 3	2261	0.888	1.963	7.09E-09
GPRC5C	G-protein coupled receptor family C group 5 member C	5589	0.882	4.792	4.95E-79
ZNF346-IT1	N/A	NA	0.881	0.176	5.30E-05
MAPRE2	Microtubule-associated protein RP/EB family member 2	1098	0.881	1.518	4.46E-15
ISL2	Insulin gene enhancer protein ISL-2	6484	0.883	1.021	2.48E-08
DAGLB	Sn1-specific diacylglycerol lipase beta	2219	0.880	4.496	1.04E-61
MAFA	Transcription factor MafA	3896	0.881	1.318	2.32E-13
STBD1	Starch-binding domain-containing protein 1	8987	0.880	0.454	1.90E-07
ZNF16	Zinc finger protein 16	7564	0.879	4.318	6.36E-69
SESN2	Sestrin-2	8366	0.877	6.246	1.27E-121
OSER1	Oxidative stress-responsive serine-rich protein 1	5152	0.876	6.664	5.04E-147
SPRED2	Sprouty-related, EVH1 domain-containing protein 2	2007	0.876	6.354	9.22E-125
ZNF555	Zinc finger protein 555	1482	0.875	2.344	3.24E-18
DUSP7	Dual specificity protein phosphatase 7	1849	0.875	2.974	1.22E-23
S100P	Protein S100-P	6286	0.868	0.523	8.42E-06
TUBA4A	Tubulin alpha-4A chain	7277	0.866	0.022	0.008
BMP7	Bone morphogenetic protein 7	6552	0.866	4.597	5.21E-51
HIST1H2BL	Histone H2B type 1-L	8340	0.862	0.500	2.09E-06
B4GALNT1	Beta-1,4 N-acetylgalactosaminyltransferase 1	2583	0.859	3.376	2.28E-08
ZC3H12A	Endoribonuclease ZC3H12A	8014	0.859	4.443	6.09E-31
KLHL25	Kelch-like protein 25	6441	0.859	4.129	3.93E-26
AHDC1	AT-hook DNA-binding motif-containing protein 1	2724	0.858	4.343	5.43E-43
CELF5	CUGBP Elav-like family member 5	6068	0.856	0.006	2.00E-05
HIST1H2AK	Histone H2A type 1	8330	0.852	1.570	3.11E-13
SCD	Stearoyl-CoA desaturase 5	6319	0.852	10.487	1.38E-31
CTGF	Connective tissue growth factor	1490	0.848	0.657	0.001
C1GALT1C1L	C1GALT1-specific chaperone 1-like protein	7288	0.844	0.214	9.39E-06

MBLAC2	Metallo-beta-lactamase domain-containing protein 2	1533	0.842	5.123	9.59E-85
CAVIN1	Caveolae-associated protein 1	2841	0.842	1.558	6.51E-14
CLCN2	Chloride channel protein 2	1181	0.838	3.515	3.84E-34
CAMTA1	Calmodulin-binding transcription activator 1	2326	0.834	4.923	9.43E-42
ASB13	Ankyrin repeat and SOCS box protein 13	7975	0.832	5.373	6.63E-84
BCOR	BCL-6 corepressor	5488	0.823	6.659	1.40E-121
GZF1	GDNF-inducible zinc finger protein 1	6441	0.827	5.741	6.29E-85
LRRC10B	Leucine-rich repeat-containing protein 10B	3902	0.826	1.259	7.43E-08
MCAM	Cell surface glycoprotein MUC18	4162	0.824	0.781	2.89E-07
HIST1H3B	Histone H3.1	8358	0.822	0.909	7.81E-06
NSMF	NMDA receptor synaptonuclear signaling and neuronal migration factor	2601	0.822	5.914	3.47E-68
FBXL18	F-box/LRR-repeat protein 18	8002	0.822	4.475	3.12E-52
DIXDC1	Dixin	8545	0.817	3.515	1.75E-45
PCDH1	Protocadherin-1	5097	0.813	6.368	3.11E-120
MEX3B	RNA-binding protein MEX3B	8420	0.813	3.173	1.99E-26
FHL3	Four and a half LIM domains protein 3	2275	0.812	1.372	2.70E-10
TP53INP2	Tumour protein p53-inducible nuclear protein 2	5847	0.809	1.166	8.93E-08
C11orf84	SPIN1-docking protein	1440	0.807	5.579	1.47E-28
FAM105A	Inactive ubiquitin thioesterase FAM105A	5449	0.809	0.803	9.23E-07
THEG	Testicular haploid expressed gene protein	5129	0.805	0.821	5.57E-06
SERTAD3	SERTA domain-containing protein 3	2994	0.806	5.440	2.14E-90
HIST1H2BG	Histone H2B type 1-C/E/F/G/I	8339	0.803	4.507	1.55E-41
ABCB6	ATP-binding cassette sub-family B member 6, mitochondrial	1005	0.794	0.212	1.55E-06
NES	Nestin	1076	0.793	1.819	1.06E-05
LY6G5B	Lymphocyte antigen 6 complex locus protein G5b	5849	0.792	1.005	9.58E-10
SLC16A9	Monocarboxylate transporter 9	2209	0.788	3.739	7.79E-28
EN2	Homeobox protein engrailed-2	2020	0.784	0.397	9.95E-06
WNT3	Proto-oncogene Wnt-3	7473	0.787	0.604	5.67E-06
SYNM	Synemin	2333	0.783	3.128	1.61E-16
GRHL3	Grainyhead-like protein 3 homolog	5782	0.782	2.696	1.13E-14
ID1	DNA-binding protein inhibitor ID-1	3397	0.781	3.244	2.56E-25
AP3B2	AP-3 complex subunit beta-2	8120	0.778	0.770	3.20E-08
TMEM121	Transmembrane protein 121	8075	0.777	0.739	0.001
HSP90AB1	Heat shock protein HSP 90-beta	3326	0.776	9.994	1.70E-27
F2RL1	Proteinase-activated receptor 2	2150	0.774	3.419	7.67E-13
GADD45B	Growth arrest and DNA damage-inducible protein GADD45 beta	4616	0.774	6.746	4.42E-100
HCFC1	Host cell factor 1	3054	0.774	7.683	2.43E-88
FHL2	Four and a half LIM domains protein 2	2274	0.770	5.017	3.20E-54
TNFRSF12A	Tumour necrosis factor receptor superfamily member 12A	5131	0.769	7.602	6.18E-95
HIST1H2AG	Histone H2A type 1	8969	0.769	5.001	1.35E-28
CCDC117	Coiled-coil domain-containing protein 117	1502	0.768	2.297	1.21E-11
FSTL3	Follistatin-related protein 3	1027	0.766	4.499	7.72E-49
IER5L	Immediate early response gene 5-like protein	3897	0.761	5.900	6.34E-73

HIST4H4	Histone H4	1215	0.759	2.726	4.89E-18
ZNF488	Zinc finger protein 488	1187	0.757	1.414	2.57E-08
PPP1R18	Phostensin	1709	0.757	2.991	3.27E-16
ZC3HAV1L	Zinc finger CCCH-type antiviral protein 1-like	9209	0.753	3.253	1.45E-32
PRSS53	Serine protease 53	3391	0.751	2.145	1.50E-14
TCTE3	Tctex1 domain-containing protein 3	6991	0.751	3.320	8.53E-26
HEY1	Hairy/enhancer-of-split related with YRPW motif protein 1	2346	0.749	0.588	2.89E-06
HPCAL1	Hippocalcin-like protein 1	3241	0.747	6.443	1.21E-93
PADI3	Protein-arginine deiminase type-3	5170	0.747	0.706	3.77E-05
SAMD10	Sterile alpha motif domain-containing protein 10	1407	0.746	4.574	2.15E-42
PPP4R4	Serine/threonine-protein phosphatase 4 regulatory subunit 4	5771	0.744	0.289	0.001
NR4A1	Nuclear receptor subfamily 4 group A member 1	3164	0.736	4.365	4.95E-15
UBALD1	UBA-like domain-containing protein 1	1244	0.731	6.036	7.97E-44
CBX4	E3 SUMO-protein ligase CBX4	8535	0.730	7.026	4.61E-76
SYPL2	Synaptophysin-like protein 2	2846	0.729	0.514	0.001
PLEKHH2	Pleckstrin homology domain-containing family H member 2	1302	0.723	0.872	7.62E-08
HSH2D	Hematopoietic SH2 domain-containing protein	8494	0.722	3.358	2.99E-29
HSPA4L	Heat shock 70 kDa protein 4L	2282	0.719	5.130	2.56E-24
SP6	Transcription factor Sp6	8032	0.713	1.187	2.16E-06
RAPGEFL1	Rap guanine nucleotide exchange factor-like 1	5119	0.718	5.567	6.96E-82
CACYBP	Calcyclin-binding protein	2710	0.719	6.951	5.68E-31
TNS4	Tensin-4	8495	0.717	3.139	1.12E-17
HIST1H3G	Histone H3.1	8355	0.716	3.257	2.23E-13
ZYX	Zyxin	7791	0.712	6.691	3.46E-31
ZNF181	Zinc finger protein 181	3393	0.718	3.753	2.08E-33
IFFO2	Intermediate filament family orphan 2	1269	0.714	3.773	2.53E-30
TUBB2A	Tubulin beta-2A chain	7280	0.713	1.722	1.57E-07
JUNB	Transcription factor jun-B	3726	0.712	5.378	3.54E-33
KLF16	Krueppel-like factor 16	8385	0.718	4.217	2.73E-35
MLLT11	Protein AF1q	1096	0.711	2.864	4.05E-15
C16orf71	Uncharacterised protein C16orf71	1465	0.709	1.334	1.83E-09
TIMP3	Metalloproteinase inhibitor 3	7078	0.707	0.654	0.006
KRT81	Keratin, type II cuticular Hb1	3887	0.707	0.666	5.91E-06
SLC29A4	Equilibrative nucleoside transporter 4	2229	0.706	1.356	1.11E-07
EGLN2	Egl nine homolog 2	1123	0.700	3.801	1.23E-28
HOXB9	Homeobox protein Hox-B9	3219	0.699	1.102	4.74E-08
SLC2A6	Solute carrier family 2, facilitated glucose transporter member 6	1118	0.698	-0.001	0.003
FAM214B	Protein FAM214B	8025	0.697	2.687	2.77E-15
KRT80	Keratin, type II cytoskeletal 80	1445	0.697	7.807	1.83E-63
ZNF548	Zinc finger protein 548	1476	0.695	3.529	2.98E-21
MYADM	Myeloid-associated differentiation marker	9166	0.694	6.941	1.83E-57
FZD5	Frizzled-5	7855	0.692	3.968	1.40E-32
TMEM50B	Transmembrane protein 50B	7576	0.687	5.711	3.98E-67
ZIC5	Zinc finger protein ZIC 5	8541	0.687	1.258	1.16E-06
FAM169A	Soluble lamin-associated protein of 75 kDa	2604	0.687	3.952	9.53E-35
CNBP	Cellular nucleic acid-binding protein	7555	0.687	8.819	8.98E-85

FUT1	Galactoside 2-alpha-L-fucosyltransferase 1	2523	0.686	3.801	1.80E-31
C5orf56	Uncharacterised protein C5orf56	NA	0.685	0.071	0.004
PLD6	Mitochondrial cardiolipin hydrolase	2011	0.684	3.379	1.62E-24
S1PR2	Sphingosine 1-phosphate receptor 2	9294	0.682	1.011	2.56E-05
MKNK2	MAP kinase-interacting serine/threonine-protein kinase 2	2872	0.682	6.830	1.02E-69
ZNF616	Zinc finger protein 616	9031	0.680	4.119	3.16E-27
ENGASE	Cytosolic endo-beta-N-acetylglucosaminidase	6477	0.680	3.016	8.58E-11
C8orf58	Uncharacterised protein C8orf58	5415	0.679	0.809	2.54E-06
CLU	Clusterin	1191	0.679	7.923	2.83E-44
ASCL2	Achaete-scute homolog 2	4304	0.678	4.899	2.71E-34
ZNF354A	Zinc finger protein 354A	6940	0.677	5.517	2.04E-63
MAT2A	S-adenosylmethionine synthase isoform type-2	4144	0.676	8.958	3.73E-87
ZNF563	Zinc finger protein 563	1478	0.669	2.482	1.96E-13
SCN1B	Sodium channel subunit beta-1	6324	0.668	3.125	1.63E-19
GPR153	Probable G-protein coupled receptor 153	3875	0.667	1.195	2.58E-05
PPFIA4	Liprin-alpha-4	8497	0.661	2.510	2.85E-14
STARD4	StAR-related lipid transfer protein 4	1344	0.666	2.703	1.13E-12
ZNF416	Zinc finger protein 416	5565	0.664	2.035	6.66E-11
SLC4A11	Sodium bicarbonate transporter-like protein 11	8395	0.662	-0.005	0.006
MTURN	Maturin	2221	0.662	0.816	4.82E-06
RHEBL1	GTPase RhebL1	1212	0.662	0.672	7.33E-06
AZGP1	Zinc-alpha-2-glycoprotein	5637	0.661	0.128	0.002
RTL5	Retrotransposon Gag-like protein 5	3405	0.660	0.580	3.93E-05
NBL1	Neuroblastoma suppressor of tumourigenicity 1	4681	0.660	0.409	0.002
OR2B6	Olfactory receptor 2B6	2621	0.659	1.590	6.10E-08
HIST1H2BN	Histone H2B type 1-N	8341	0.659	3.536	2.72E-21
SRF	Serum response factor	6722	0.658	6.302	3.27E-54
ZBTB7A	Zinc finger and BTB domain-containing protein 7A	5134	0.657	6.864	5.90E-59
OASL	2'-5'-oligoadenylate synthase-like protein	8638	0.657	1.048	9.07E-05
ADAMTSL5	ADAMTS-like protein 5	3393	0.653	3.318	2.05E-20
ARRDC3	Arrestin domain-containing protein 3	5756	0.652	7.806	6.73E-59
TAP1	Antigen peptide transporter 1	6890	0.650	3.466	2.93E-18
CDC42EP2	Cdc42 effector protein 2	1043	0.649	3.072	9.67E-16
UNC5B	Netrin receptor UNC5B	2196	0.649	4.568	2.76E-19
ZSCAN21	Zinc finger and SCAN domain-containing protein 21	7589	0.648	2.756	8.53E-16
SLC6A8	Sodium- and chloride-dependent creatine transporter 1	6535	0.646	2.851	2.99E-14
GDF15	Growth/differentiation factor 15	9518	0.646	4.567	1.20E-23
ZNF44	Zinc finger protein 44	5171	0.646	4.475	5.53E-29
ZNF275	Zinc finger protein 275	1083	0.645	4.880	8.05E-45
GABARAPL1	Gamma-aminobutyric acid receptor-associated protein-like 1	2371	0.6453	0.308	0.003
ARSJ	Arylsulfatase J	7964	0.643	0.679	8.62E-05
VCL	Vinculin	7414	0.642	6.837	9.32E-50
PLEKHO1	Pleckstrin homology domain-containing family O member 1	5117	0.642	1.598	0.006

EEPD1	Endonuclease/exonuclease/phosphatase family domain-containing protein 1	8082	0.638	0.238	0.002
LPAR5	Lysophosphatidic acid receptor 5	5712	0.635	1.701	4.38E-06
PRR5	Proline-rich protein 5	5561	0.635	2.354	1.17E-07
AQP3	Aquaporin-3	3606	0.633	1.495	4.27E-08
KLB	Beta-klotho	1528	0.632	1.778	2.59E-09
ZNF160	Zinc finger protein 160	9033	0.631	5.672	3.41E-47
HSPD1	60 kDa heat shock protein, mitochondrial	3329	0.631	9.090	2.57E-30
DSC2	Desmocollin-2	1824	0.628	0.726	1.28E-05
PRODH	Proline dehydrogenase 1, mitochondrial	5625	0.628	2.278	1.33E-11
ZNF696	Zinc finger protein 696	7994	0.626	2.979	5.63E-12
SCNN1A	Amiloride-sensitive sodium channel subunit alpha	6337	0.626	2.875	2.00E-16
EIF1AD	Probable RNA-binding protein EIF1AD	8428	0.625	5.303	1.46E-41
HIST1H3J	Histone H3.1	8356	0.625	1.557	3.11E-07
NUMBL	Numb-like protein	9253	0.624	3.544	6.43E-16
PTCH1	Protein patched homolog 1	5727	0.624	2.416	3.80E-12
EPDR1	Mammalian ependymin-related protein 1	5474	0.623	1.051	1.00E-05
ZBTB46	Zinc finger and BTB domain-containing protein 46	1406	0.621	3.672	2.52E-21
KLHL31	Kelch-like protein 31	4012	0.621	2.081	4.59E-09
HES1	Transcription factor HES-1	3280	0.618	6.317	1.02E-44
BCL3	B-cell lymphoma 3 protein	6023	0.618	4.823	3.55E-30
INHBE	Inhibin beta E chain	8372	0.617	1.995	2.95E-08
ZNF473	Zinc finger protein 473	2588	0.616	4.485	5.39E-28
RGPD5	RANBP2-like and GRIP domain-containing protein 5/6	8422	0.615	0.088	0.002
ZNF574	Zinc finger protein 574	6476	0.615	5.267	6.20E-29
ZNF134	Zinc finger protein 134	7693	0.614	4.412	2.58E-30
PXDC1	Plexin domain-containing protein 1	2217	0.613	0.076	0.009
ORAI1	Calcium release-activated calcium channel protein 1	NA	0.613	5.116	2.11E-27
CPEB2	Cytoplasmic polyadenylation element-binding protein 2	1328	0.611	4.536	5.20E-27
RASSF3	Ras association domain-containing protein 3	2833	0.608	5.450	5.01E-39
RPS6KL1	Ribosomal protein S6 kinase-like 1	8369	0.608	3.331	4.26E-17
ZNF850	Zinc finger protein 850	3428	0.608	3.355	3.39E-19
PRELID3B	PRELI domain containing protein 3B	5101	0.608	8.175	6.05E-84
CNN2	Calponin-2	1265	0.608	5.938	8.76E-38
MAG	Glycerol-3-phosphate acyltransferase 3	4099	0.607	0.762	0.002
FLT4	Vascular endothelial growth factor receptor 3	2324	0.606	0.572	0.007
PDGFA	Platelet-derived growth factor subunit A	5154	0.605	4.324	3.04E-32
HIST1H1D	Histone H1.3	3007	0.604	2.303	1.16E-07
FOXO1	Forkhead box protein O1	2308	0.604	3.755	4.12E-24
NOTCH3	Neurogenic locus notch homolog protein 3	4854	0.603	6.334	1.10E-52
PLEKHG2	Pleckstrin homology domain-containing family G member 2	6485	0.603	3.606	9.76E-09

PPRC1	Peroxisome proliferator-activated receptor gamma coactivator-related protein 1	2308	0.603	5.827	1.24E-46
PTK6	Protein-tyrosine kinase 6	5753	0.602	0.988	9.99E-06
MOB3C	MOB kinase activator 3C	1489	0.602	2.931	7.91E-14
SPATA2L	Spermatogenesis-associated protein 2-like protein	1240	0.601	4.497	7.30E-27
ARHGAP45	Rho GTPase-activating protein 45	2352	0.600	2.278	2.35E-08

8.4 Down-regulated genes in T_{120} zinc treatment

Down-regulated genes	Protein name	Entrez	Log_2FC	Log CPM	*p-value*
PLK2	Serine/threonine-protein kinase PLK2	1076	-2.089	6.380	0
MAP10	Microtubule-associated protein 10	5462	-1.750	2.372	3.27E-65
ANKRD1	Ankyrin repeat domain-containing protein 1	2703	-1.740	1.331	1.01E-26
IRX5	Iroquois-class homeodomain protein IRX-5	1026	-1.696	6.176	0
BAMBI	BMP and activin membrane-bound inhibitor homolog	2580	-1.640	6.964	0
IL20	Interleukin-20 receptor subunit beta	5060	-1.607	4.355	4.55E-109
DKK1	Dickkopf-related protein 1	2294	-1.541	5.741	0
ZNF703	Zinc finger protein 703	8013	-1.435	7.558	8.90E-274
ASCL1	Achaete-scute homolog 1	4293	-1.409	1.726	5.28E-24
OTUB2	Ubiquitin thioesterase OTUB2	7899	-1.363	0.480	6.62E-10
IRX3	Iroquois-class homeodomain protein IRX-3	7919	-1.349	6.640	2.08E-241
FBXO32	F-box only protein 32	1149	-1.314	2.359	6.64E-38
NHLRC1	E3 ubiquitin-protein ligase NHLRC1	3788	-1.283	1.152	1.26E-16
GATA3	Trans-acting T-cell-specific transcription factor GATA-3	2625	-1.257	9.916	1.52E-149
IRS1	Insulin receptor substrate 1	3667	-1.252	6.526	2.61E-138
AKAP5	A-kinase anchor protein 5	9495	-1.200	3.419	1.65E-63
FILIP1L	Filamin A-interacting protein 1-like	1125	-1.153	1.748	2.76E-16
HTR1E	5-hydroxytryptamine receptor 1E	3354	-1.153	0.484	1.60E-08
KCNK5	Potassium channel subfamily K member 5	8645	-1.127	3.363	1.81E-50
ARHGAP20	Rho GTPase-activating protein 20	5756	-1.120	0.277	2.93E-06
PARD6B	Partitioning defective 6 homolog beta	8461	-1.078	8.748	5.39E-225
AMOTL2	Angiomotin-like protein 2	5142	-1.075	7.017	6.40E-87
NEDD9	Enhancer of filamentation 1	4739	-1.070	4.794	1.06E-88
CITED2	Cbp/p300-interacting transactivator 2	1037	-1.062	6.319	2.05E-113
PGR	Progesterone receptor	5241	-1.057	9.017	3.45E-147
FAM83B	Protein FAM83B	2225	-1.051	4.881	1.92E-93
RHOB	Rho-related GTP-binding protein RhoB	3881	-1.034	7.995	3.15E-195
PPP1R3C	Protein phosphatase 1 regulatory subunit 3C	5507	-1.016	4.773	1.38E-69
NRIP1	Nuclear receptor-interacting protein 1	8204	-0.986	8.171	3.06E-171
RNF152	E3 ubiquitin-protein ligase RNF152	2204	-0.955	2.949	6.44E-30
RAB30	Ras-related protein Rab-30	2731	-0.951	6.584	1.52E-138
REL	Proto-oncogene c-Rel	5966	-0.944	5.455	3.87E-95
ARHGAP32	Rho GTPase-activating protein 32	9743	-0.944	7.011	1.02E-189
TSPYL5	Testis-specific Y-encoded-like protein 5	8545	-0.939	3.330	3.68E-38
SHISA2	Protein shisa-2 homolog	3879	-0.929	3.461	4.29E-34
NR2F2	COUP transcription factor 2	7026	-0.925	6.598	1.29E-148
KITLG	Kit ligand	4254	-0.914	7.354	3.88E-162
KLHDC7A	Kelch domain-containing protein 7A	1277	-0.895	0.157	3.06E-05
AVIL	Advillin	1067	-0.894	2.660	2.85E-14
DLC1	Rho GTPase-activating protein 7	1039	-0.893	7.140	5.90E-170
RUSC2	Iporin	9853	-0.883	4.278	4.96E-58
SLITRK6	SLIT and NTRK-like protein 6	8418	-0.872	2.675	5.79E-17
PCDH19	Protocadherin-19	5752	-0.872	2.163	1.10E-14

PIK3R1	Phosphatidylinositol 3-kinase regulatory subunit alpha	5295	-0.869	8.240	2.08E-156
TTC30B	Tetratricopeptide repeat protein 30B	1506	-0.868	2.353	3.35E-16
IRF2BPL	Interferon regulatory factor 2-binding protein-like	6420	-0.855	6.313	3.37E-98
SLFN5	Schlafen family member 5	1623	-0.840	3.343	1.73E-21
SOCS1	Suppressor of cytokine signaling 1	8651	-0.832	0.955	6.61E-08
MAFB	Transcription factor MafB	9935	-0.829	2.698	7.64E-16
NAT1	Arylamine N-acetyltransferase 1	9235	-0.826	2.782	5.96E-21
ZNF614	Zinc finger protein 614	8011	-0.799	3.712	3.74E-31
GEM	GTP-binding protein GEM	2669	-0.796	2.586	1.97E-12
DNMBP	Dynamin-binding protein	2326	-0.792	5.933	1.16E-104
ANKRD50	Ankyrin repeat domain-containing protein 50	5718	-0.765	6.211	2.85E-99
GRPR	Gastrin-releasing peptide receptor	2925	-0.761	0.333	0.001
CDV3	Protein CDV3 homolog	5557	-0.759	10.073	1.93E-73
CYS1	Cystin-1	1926	-0.750	0.267	5.58E-05
SNX15	Sorting nexin-15	2990	-0.749	-0.002	0.002
TPBG	Trophoblast glycoprotein	7162	-0.747	8.405	1.44E-121
SEMA6D	Semaphorin-6D	8003	-0.747	0.258	0.001
DISP1	Protein dispatched homolog 1	8496	-0.744	2.487	2.21E-13
FKBPL	FK506-binding protein-like	6394	-0.739	2.499	8.25E-12
FBN2	Fibrillin-2	2201	-0.733	1.432	4.50E-09
ARL4A	ADP-ribosylation factor-like protein 4A	1012	-0.732	3.261	1.96E-23
CENPQ	Centromere protein Q	5516	-0.731	3.535	1.10E-21
ARID5B	AT-rich interactive domain-containing protein 5B	8415	-0.730	5.665	7.00E-67
BCAR3	Breast cancer anti-estrogen resistance protein 3	8412	-0.730	4.246	2.62E-34
ACTRT3	Actin-related protein T3	8451	-0.729	1.079	7.52E-06
ZNF552	Zinc finger protein 552	7981	-0.721	5.337	4.78E-59
INSIG2	Insulin-induced gene 2 protein	5114	-0.721	3.999	5.92E-32
COX10	Protoheme IX farnesyltransferase, mitochondrial	1352	-0.716	3.639	9.27E-28
TET2	Methylcytosine dioxygenase TET2	5479	-0.715	6.731	2.26E-101
BNC1	Zinc finger protein basonuclin-1	6461	-0.711	0.175	0.002
CCDC17	Coiled-coil domain-containing protein 17	1494	-0.704	0.584	3.86E-06
CTSK	Cathepsin K	1513	-0.697	1.660	4.77E-09
TOB1	Protein Tob1	1014	-0.696	7.963	4.05E-69
MEGF9	Multiple epidermal growth factor-like domains protein 9	1955	-0.695	6.278	5.51E-84
NAPSA	Napsin-A	9476	-0.694	0.217	0.002
LRRK2	Leucine-rich repeat serine/threonine-protein kinase 2	1208	-0.687	1.826	2.59E-09
GCNA	Acidic repeat-containing protein	9395	-0.685	0.142	0.001
SOCS3	Suppressor of cytokine signaling 3	9021	-0.683	2.996	2.07E-17
STON1	Stonin-1	1103	-0.680	3.088	1.18E-20
KCNJ14	ATP-sensitive inward rectifier potassium channel 15	3770	-0.679	0.131	0.002
ARHGAP35	Rho GTPase-activating protein 35	2909	-0.677	8.204	3.88E-98
ACOT1	Acyl-coenzyme A thioesterase 1	6413	-0.677	-0.052	0.008
HCAR3	Hydroxycarboxylic acid receptor 3	8843	-0.675	2.037	5.70E-10
DRG1	Developmentally-regulated GTP-binding protein 1	4733	-0.668	5.489	1.78E-54
FRAT1	Proto-oncogene FRAT1	1002	-0.668	2.988	6.63E-16

MSS51	Putative protein MSS51 homolog, mitochondrial	1184	-0.666	0.199	0.007
BHLHB9	Protein BHLHb9	8082	-0.664	2.819	8.03E-18
WNT5B	Protein Wnt-5b	8102	-0.662	0.527	0.005
SOX4	Transcription factor SOX-4	6659	-0.662	7.241	1.72E-69
DHFR2	Dihydrofolate reductase 2, mitochondrial	2008	-0.658	4.173	9.03E-32
ARRDC4	Arrestin domain-containing protein 4	9194	-0.654	5.468	1.88E-15
MYB	Transcriptional activator Myb	4602	-0.645	7.781	1.33E-65
CDH18	Cadherin-18	1016	-0.640	1.000	0.001
ASNSD1	Asparagine synthetase domain-containing protein 1	5452	-0.638	5.566	1.58E-47
C2orf82	Protein SNORC	3890	-0.637	-0.031	0.004
TNFSF10	Tumour necrosis factor ligand superfamily member 10	8743	-0.636	0.899	6.14E-05
INAVA	Innate immunity activator protein	5576	-0.635	1.406	6.55E-07
KLF5	Krueppel-like factor 5	6881	-0.626	4.701	4.33E-26
TIAM2	T-lymphoma invasion and metastasis-inducing protein 2	2623	-0.626	1.871	2.80E-07
FRAT2	GSK-3-binding protein FRAT2	2340	-0.626	5.114	1.95E-44
GRB7	Growth factor receptor-bound protein 7	2886	-0.625	4.496	1.52E-30
TSNAXIP1	Translin-associated factor X-interacting protein 1	5581	-0.624	0.579	0.001
LRFN3	Leucine-rich repeat and fibronectin type-III domain-containing protein 3	7941	-0.622	2.080	7.60E-10
STC1	Stanniocalcin-1	6781	-0.620	7.513	1.03E-58
DOK3	Docking protein 3	7993	-0.620	1.550	2.49E-06
CENPC	Centromere protein C	1060	-0.618	5.015	1.98E-37
RNF43	E3 ubiquitin-protein ligase RNF43	5489	-0.617	6.286	4.28E-61
PPP1R10	Serine/threonine-protein phosphatase 1 regulatory subunit 10	5514	-0.615	6.238	3.17E-76
TP53INP1	Tumour protein p53-inducible nuclear protein 1	9424	-0.614	5.770	1.26E-44
RIN2	Ras and Rab interactor 2	5445	-0.605	4.000	5.86E-20
DBR1	Lariat debranching enzyme	5116	-0.603	4.547	3.89E-28
KIAA1683	IQ domain-containing protein N	8072	-0.600	2.535	5.70E-10